



National Library  
of Canada

Bibliothèque nationale  
du Canada

Canadian Theses Service Service des thèses canadiennes

Ottawa, Canada  
K1A 0N4

## NOTICE

The quality of this microform is heavily dependent upon the quality of the original thesis submitted for microfilming. Every effort has been made to ensure the highest quality of reproduction possible.

If pages are missing, contact the university which granted the degree.

Some pages may have indistinct print especially if the original pages were typed with a poor typewriter ribbon or if the university sent us an inferior photocopy.

Previously copyrighted materials (journal articles, published tests, etc.) are not filmed.

Reproduction in full or in part of this microform is governed by the Canadian Copyright Act, R.S.C. 1970, c. C-30.

## AVIS

La qualité de cette microforme dépend grandement de la qualité de la thèse soumise au microfilmage. Nous avons tout fait pour assurer une qualité supérieure de reproduction.

S'il manque des pages, veuillez communiquer avec l'université qui a conféré le grade.

La qualité d'impression de certaines pages peut laisser à désirer, surtout si les pages originales ont été dactylographiées à l'aide d'un ruban usé ou si l'université nous a fait parvenir une photocopie de qualité inférieure.

Les documents qui font déjà l'objet d'un droit d'auteur (articles de revue, tests publiés, etc.) ne sont pas microfilmés.

La reproduction, même partielle, de cette microforme est soumise à la Loi canadienne sur le droit d'auteur, SRC 1970, c. C-30.

THE UNIVERSITY OF ALBERTA

Solvent Extraction - Flow Injection Analysis: Application and Speed of Analysis

by

Charles A. Lucy

A Thesis

Submitted To The Faculty Of Graduate Studies And Research

In Partial Fulfillment Of The Requirements For The Degree

Of Doctor Of Philosophy

The Department of Chemistry

Edmonton, Alberta

Fall, 1988

Permission has been granted to the National Library of Canada to microfilm this thesis and to lend or sell copies of the film.

The author (copyright owner) has reserved other publication rights, and neither the thesis nor extensive extracts from it may be printed or otherwise reproduced without his/her written permission.

L'autorisation a été accordée à la Bibliothèque nationale du Canada de microfilmer cette thèse et de prêter ou de vendre des exemplaires du film.

L'auteur (titulaire du droit d'auteur) se réserve les autres droits de publication; ni la thèse ni de longs extraits de celle-ci ne doivent être imprimés ou autrement reproduits sans son autorisation écrite.

ISBN 0-315-45688-4

**THE UNIVERSITY OF ALBERTA**  
**RELEASE FORM**

NAME OF AUTHOR: Charles A. Lucy

TITLE OF THESIS: Solvent Extraction - Flow Injection Analysis: Application  
and Speed of Analysis

DEGREE FOR WHICH THESIS WAS PRESENTED: Ph.D.

YEAR THIS DEGREE GRANTED: 1988

Permission is hereby granted to THE UNIVERSITY OF ALBERTA LIBRARY to reproduce single copies of this thesis and to lend or sell such copies for private, scholarly or scientific research purposes only.

The author reserves other publication rights, and neither the thesis nor extensive extracts from it may be printed or otherwise reproduced without the author's written permission.

*Charles Lucy*  
.....  
(signed)

PERMANENT ADDRESS:  
5240 Keith Street  
Burnaby, British Columbia  
V5J 3C5


Date: 14 June 1988



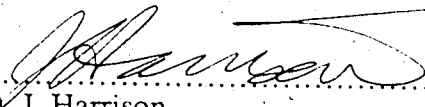
THE UNIVERSITY OF ALBERTA

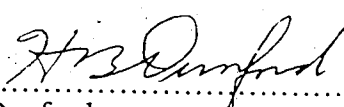
FACULTY OF GRADUATE STUDIES AND RESEARCH

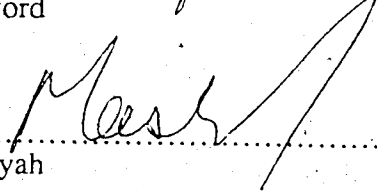
The undersigned certify that they have read, and recommend to the Faculty of Graduate Studies and Research for acceptance, a thesis entitled SOLVENT EXTRACTION - FLOW INJECTION ANALYSIS: APPLICATION AND SPEED OF ANALYSIS submitted by CHARLES A. LUCY in partial fulfillment of the requirements for the degree of Doctor of Philosophy in Analytical Chemistry.


  
F. F. Cantwell, Supervisor

  
N. Dovichi

  
D. J. Harrison

  
B. Dunford

  
J. Masliyah

  
J. Ružička, External Examiner

Date: 14 June 1988.

This thesis is dedicated to Bridget for her support and understanding, and to my parents and brother for their encouragement during my student years.

## Abstract

A solvent extraction-flow injection analysis (SE-FIA) apparatus with two membrane phase separators arranged in series was used to simultaneously monitor both the organic and aqueous phases. Detector electronics were modified to yield positive signals from both flow cells. This instrument was used to analyze pheniramine maleate and phenylephrine hydrochloride in a commercial nasal spray with a precision and accuracy of 1-2% and a sampling frequency of 30 inj/h. Miniature ion-exchange columns remove interfering species on-line. Band broadening was characterized using statistical moment analysis, and the phase separators and connecting tubing were the major contributors.

In straight tubes, the extraction rate increases rapidly with decreasing segment length for short segments and is approximately constant for longer segments. The segment ends interact hydrodynamically to enhance radial convection when the segment length is decreased below ~3 times the tube diameter, which leads to a dramatic increase in extraction rate. The interfacial area was also a strong determinant of the extraction rate. In coiled tubes, the extraction rates are much higher than in straight tubes due to the generation of secondary flow within the segments.

The mechanism of extraction and band broadening within segmented flow were studied by monitoring the absorbance of each chloroform segment as it passed through an on-tube photometer located at various distances along the Teflon extraction tube. Band broadening, studied by injecting iodine into a single chloroform segment, is intermediate in magnitude between that predicted using a mixing chamber model and that predicted by assuming only diffusional mixing between the segments and the wetting-film of chloroform on the tube wall. Extraction from aqueous into chloroform segments was studied by generating iodine within a single aqueous segment using the "iodine clock" reaction. Application of a "successive reaction" model to the axial extraction from the front of the aqueous segment

reveals that, in straight tubes, solute extracts at the same rate per unit area across all of the interface, both that at the segment ends and side.

## Acknowledgements

My most sincere thanks go to Dr. F. F. Cantwell for his patient guidance throughout the course of this work and for his helpful suggestions in the preparation of this manuscript.

Thanks are also extended to Lynne Fossey for her tutorage on the experimental aspects of solvent extraction-flow injection analysis and to Dr. J. Masliyah for his sage advice on the relevant chemical engineering literature.

I would like to acknowledge the Chemistry Department Machine Shop and Electronic Shop without whose expertise and eager assistance this work would not have been possible.

Financial support from the University of Alberta and the National Sciences and Engineering Research Council is gratefully acknowledged.

## Table of Contents

Chapter 1 Introduction .....	1
Chapter 2 Solvent Extraction / FIA Analysis of a Commercial Nasal Spray.....	15
2.1 Introduction .....	15
2.2 Experimental .....	16
2.2.1 Chemicals and Solvents .....	16
2.2.2 Apparatus.....	19
2.2.2.1 Nasal Spray Apparatus .....	19
2.2.2.2 Single Phase FIA System .....	26
2.2.3 Detector Modification .....	26
2.2.4 Calibration Curves .....	28
2.2.5 Nasal Spray Assay.....	28
2.3 Results and Discussion .....	29
2.3.1 Detector Modification .....	29
2.3.2 Extraction coil length.....	32
2.3.3 Extraction pH .....	34
2.3.4 Interferences .....	38
2.3.4.1 Cation Column .....	39
2.3.4.2 Anion column .....	41
2.3.5 Calibration Curves .....	44
2.3.6 Nasal Spray Assay .....	44
2.4 Conclusions .....	48
Chapter 3 Instrumental Band Broadening in a Solvent Extraction-FIA Instrument .....	49
3.1 Introduction .....	49

3.2 Background and Data Analysis .....	49
3.3 Experimental .....	54
3.3.1 Chemicals and Solvents .....	54
3.3.2 Apparatus.....	54
3.3.3 Data analysis.....	59
3.3.4 Procedure.....	59
3.4 Results and Discussion .....	62
3.4.1 Pheniramine Band Broadening .....	65
3.4.2 Phenylephrine Band Broadening .....	67
3.4.3 Phase Separator.....	68
3.4.4 Injector/Detector Variance .....	70
3.4.5 Ion Exchange Columns .....	72
3.5 Conclusions .....	73
Chapter 4 Kinetics of Extraction in Solvent Extraction - Flow Injection Analysis .....	74
4.1 Introduction .....	74
4.2 Theory .....	75
4.2.1 Flow hydrodynamics .....	75
4.2.1.1 Segmented Flow .....	75
4.2.1.2 Secondary Flow .....	80
4.2.2 Wetting Film Formation .....	83
4.2.3 Extraction model.....	85
4.3 Experimental .....	87
4.3.1 Chemicals, Solvents and Reagents.....	87
4.3.2 Apparatus.....	88
4.3.3 Measurement of extraction rates .....	93
4.4 Results and Discussion .....	95

4.4.1 Instrumental considerations .....	95
4.4.2 Extra-tube extraction .....	96
4.4.3 Extraction rate .....	100
4.4.4 Phase ratio .....	103
4.4.5 Segmentor Type .....	105
4.4.6 Segment length .....	105
4.4.7 Flow rate .....	109
4.4.8 Tube diameter .....	111
4.4.9 Coiling .....	114
4.5 Conclusions .....	118
Chapter 5 Mechanism of Solvent Extraction and Band Broadening within	
Segmented Two Phase Flow .....	120
5.1 Introduction .....	120
5.2 Experimental .....	121
5.2.1 Chemicals and Solvents .....	121
5.2.2 Iodine Clock Reaction .....	122
5.2.3 Apparatus .....	122
5.2.4 Extraction Studies .....	129
5.2.5 Band Broadening Studies .....	131
5.2.6 Measurement of Segment Shape .....	131
5.3 Results and Discussion .....	133
5.3.1 On-Tube Detection .....	134
5.3.2 Band Broadening .....	135
5.3.3 Iodine Clock Reaction .....	149
5.3.4 Iodine Extraction .....	157
5.3.4.1 Extraction Profiles .....	157



5.3.4.2 Overall extraction rates .....	157
5.3.5 Successive Reaction Approximation .....	167
5.4 Conclusions .....	174
Chapter 6 Future Studies .....	176
6.1 On-Tube Detection .....	176
6.2 Further Studies of Extraction Rate in SE-FIA .....	179
References .....	183
Appendix A Moment Analysis Program .....	199
Appendix B Data Acquisition Program .....	217
Appendix C Segment Analysis Program .....	228
Appendix D Nonsteady State Extraction .....	238

## List of Tables

### TABLE

2-1	Acid Dissociation Behavior of Components of Nasal Spray.....	40
2-2	Determination of Active Ingredients in a Commercial Nasal Spray based on the use of Peak Area and Peak Height.....	47
3-1	Comparison of Variances calculated for Synthetic Peaks using Various Measurement Techniques .....	52
3-2	Validation of Moment Analysis Program using Known Statistical Distributions as Simulated Peaks .....	60
3-3	Comparison of Variances for Peaks calculated using the Sternberg Graphical Method and by Moment Analysis.....	61
3-4	Statistical Moments for Pheniramine Peaks Observed in the Band Broadening Studies of the Nasal Spray SE-FIA Instrument.....	63
3-5	Statistical Moments for Phenylephrine HCl Peaks Observed in the Band Broadening Studies of the Nasal Spray SE-FIA Instrument.....	64
3-6	Contributions to Band Broadening in the Nasal Spray SE-FIA Instrument.....	66
4-1	Specifications of the Phase Separators .....	99
4-2	Rate constants for the extraction of caffeine using continuous sample feed ....	102
4-3	Effect of phase ratio on extraction rate constant .....	104
4-4	Extraction rate constants observed in Segmented Flow formed by the "Tee" and Technicon A-8 Segmentors at two Aqueous Segment Lengths .....	106
4-5	Dependence of extraction rate constant and mass transfer coefficient on Segment Length in Straight and Tightly Coiled Extraction Tube .....	116
5-1	Rate Constants Observed and Predicted by the Ideal Model for Iodine leaving the Injection Segment .....	148
5-2	Dependence of the Iodine Clock Reaction on pH .....	152

TABLE

5-3	Observed Rate Constants for Extraction of Iodine formed within the Segmented Flow .....	168
5-4	Estimates of the Extraction Rate through the Front End of a Segment and the Band Broadening based on Nonlinear Least Squares Fitting of Segment -1 Absorbance Data to the Successive Reaction Model.....	173

## List of Figures

FIGURE	
1-1	Analogy between a manual classical chemical assay and an automated analysis using flow injection analysis (FIA)..... 2
1-2	FIA signal for successive injections of increasing concentrations of caffeine..... 4
1-3	Simple solvent extraction - flow injection analysis manifold showing an expanded section of the segmented flow ..... 6
1-4	Various designs of instruments to perform automated extraction using segmented flow ..... 9-10
2-1	Schematic diagram of SE-FIA instrument used for nasal spray analysis..... 20
2-2	Schematic diagram of a miniature ion exchange column ..... 22
2-3	A three-dimensional view of the membrane phase separator..... 23
2-4	Instrumental response for a nasal spray injection at time zero. Baseline shift is due to switching of the flow cell designation. .... 25
2-5	Modification to detector electronics to allow switching of the sample/reference flow cell designation. .... 27
2-6	Detector response to caffeine injections into the sample and reference flow cells in a single phase FIA instrument. .... 31
2-7	Inverter circuit for dual photodiode spectrometer ..... 33
2-8	Peak area in the organic phase versus the extraction coil length for pheniramine..... 35
2-9	Peak area in the organic phase versus aqueous phase pH for pheniramine and phenylephrine ..... 37
2-10	Typical chart tracing for regeneration testing of Amberlyst 26 anion exchange column..... 43

## FIGURE

2-11	Calibration curves for phenylephrine hydrochloride in the aqueous phase.....	45
2-12	Calibration curves for pheniramine in the organic phase.....	46
3-1	Instrumental arrangements for measuring the band broadening due to the components of nasal spray SE-FIA apparatus.....	55-56
3-2	Effect of percentage of organic phase passing through the membrane on the total peak variance .....	69
4-1	Plots of the streamlines within segments of various lengths from the Navier Stokes hydrodynamic solution of the flow in the plasmatic gaps between red blood cells flowing through narrow capillaries.....	79
4-2	Mid-segment axial velocity profiles for the flow within the plasmatic fluid between red blood cells in narrow capillaries for various segment aspect ratios.....	81
4-3	Secondary flow patterns and velocity profiles for single phase flow through coiled tubing.....	82
4-4	Schematic diagram of SE-FIA instrument used for kinetic studies.....	89
4-5	Segmentors used in the kinetic experiments .....	90
4-6	Frei type membrane phase separator.....	92
4-7	Extraction occurring in the phase separator measured as the percentage of caffeine extracted into the organic phase versus the proportion of the organic phase flowing through the porous Teflon membrane .....	98
4-8	Extraction of caffeine into chloroform.....	101
4-9	Effect of segment length on the observed extraction rate constants and mass transfer coefficients for segments between 0.7 and 8 mm in length at three total flow rates .....	107
4-10	Double logarithmic plots of $k_{obs}$ as a function of flow rate for three segment lengths .....	110

# FIGURE

4-11	Observed extraction rate constants and the mass transfer coefficients in four different diameter extraction tubes at a constant linear velocity .....	112
4-12	Mass transfer coefficients vs segment aspect ratios for data from extraction tubes of varying diameter .....	113
4-13	Observed extraction rate constant for various degrees of coiling at three different segment lengths .....	115
5-1	Schematic diagram of the SE-FLA instrument .....	123
5-2	Single segment injection valve .....	125
5-3	Electronic circuit of the on-tube photometric detector.....	127
5-4	Absorbance versus time profile obtained after iodine injection with injector V <sub>2</sub> into a single chloroform segment, with the on-tube photometric detector positioned some distance downstream of the injector.....	128
5-5	Photograph of 5.4 mm long aqueous segment flowing through the 3.0 mm i.d. Teflon tubing at a linear velocity of 3.5 cm/s.....	132
5-6	Linearity of iodine absorbance at 10 cm in chloroform-injection segment measured by the On-tube Photometric Detector for Single Segment Injection.....	136
5-7	Segment profiles due to band broadening of iodine originally in a single 14.3 mm organic segment .....	137-138
5-8	Segment profiles due to band broadening of iodine originally in a single 9.6 mm organic segment.....	139-140
5-9	Segment profiles due to band broadening of iodine originally in a single 5.4 mm organic segment.....	141-142
5-10	Observed variance resulting from band broadening in segmented flow for extraction tube lengths of 10 to 200 cm for three segment lengths.....	145

## FIGURE

5-11	Normalized absorbances of iodine in the injection segment 0 as it travels through the extraction coil for three segment lengths .....	147
5-12	Reaction sequence of the Iodine Clock reaction.....	151
5-13	Iodine formation via the Iodine Clock reaction under the conditions used in the extraction studies .....	153
5-14	Acid catalysis of the delay period of the Iodine Clock reaction.....	154
5-15	Dependence of iodine formation rate of the Iodine Clock reaction on the pH.....	155
5-16	Segment profiles for iodine extracted from a single 14.3 mm aqueous segment .....	158-160
5-17	Segment profiles for iodine extracted from a single 9.6 mm aqueous segment .....	161-163
5-18	Segment profiles for iodine extracted from a single 5.4 mm aqueous segment .....	164-166
5-19	Absorbance of segment -1 observed after iodine formation within a single aqueous segment compared with the Successive Reaction Model.....	172
6-1	On-tube detector signal of iodine injected into a single organic segment displayed as the raw data and smoothed using a digital filter .....	177
6-2	Electronics diagram of an on-tube photometer for routine used in a SE-FIA instrument .....	178
D-1	Approach to steady state diffusion through a plane sheet .....	240

## List of Symbols

- a      interfacial area,  $\text{cm}^2$ .
  - $A_{\text{eq},\text{o}}$    organic phase intensity at equilibrium measured as absorbance or peak area.
  - $A_{\text{t},\text{o}}$    organic phase intensity at time t measured as absorbance or peak area.
  - $A_{\text{o}}$    peak area in organic phase, arbitrary units.
  - b      pathlength of spectrometer flow cell, cm.
  - b      minor axis of ellipsoid; equations 5.2 to 5.4.
  - $c(t)$    concentration at time t.
  - $d_{\text{c}}$    coil diameter measured from the central axis of the tube, cm.
  - $d_{\text{f}}$    wetting film thickness, cm.
  - $d_{\text{t}}$    inner diameter of tube, cm.
  - De      Dean number,  $\text{Re } (d_{\text{t}}/d_{\text{c}})^{1/2}$ , dimensionless.
  - $D_{\text{m}}$    molecular diffusion coefficient,  $\text{cm}^2/\text{s}$ .
  - E      Excess of a peak. Defined by equation 3.5; dimensionless.
  - f      response factor relating the absorbance to an integrator count rate.
  - $F_{\text{a}}$    total aqueous flow rate,  $\text{mL}/\text{min}$ .
  - $F_{\text{m},\text{a}}$    aqueous flow through membrane of phase separator,  $\text{mL}/\text{min}$ .
  - $F_{\text{m},\text{o}}$    organic flow through membrane of phase separator,  $\text{mL}/\text{min}$ .
  - $F_{\text{o}}$    total organic flow rate,  $\text{mL}/\text{min}$ .
  - g      acceleration due to gravity.
  - $k_{\text{bb}}$    observed band broadening rate constant,  $\text{s}^{-1}$ .
  - $k_{\text{I}_2}$    initial reaction rate constant for iodine formation after the delay,  $\text{s}^{-1}$ .
  - $k_{\text{obs}}$    observed extraction rate constant,  $\text{s}^{-1}$ .
  - $k_1$    extraction rate constant into the forward organic segment (segment -1),  $\text{s}^{-1}$ .
- Determined using the Successive Reaction Model.



$k_2$	band broadening rate constant from segment -1, $s^{-1}$ . Determined using the Successive Reaction Model.
$k_3$	extraction rate constant into the organic film at the side of the aqueous segment and into the backward organic segment (segment +1), $s^{-1}$ .
$K$	proportionality constant (equation 2.1).
$K_a$	acid dissociation constant.
$K_D$	distribution constant of compound, $C_O/C_a$ .
$L$	length of tubing, cm.
$L_s$	length of segment, cm.
$L_{aq}$	aqueous segment length, cm. Defined in equation 4.13.
$m_k$	$k^{th}$ ordinary statistical moment. Defined by equation 3.2.
$\overline{m}_k$	$k^{th}$ central statistical moment. Defined by equation 3.3.
$n$	number of moles injected into the instrument.
$n$	Statistical number of degrees of freedom.
$N$	number of segment pairs measured, equation 4-13.
$P$	total pressure.
$r_t$	inner radius of tube, cm.
$Re$	Reynolds number, $d_t v \rho / \eta$ , dimensionless.
$S$	Skewness of a peak. Defined in equation 3.4; dimensionless.
$Sc$	Schmidt number, $v/D_m$ , dimensionless.
$t$	time, s.
$X$	total distance in measurement of segment lengths, equation 4.13, cm.
$V$	volume, $cm^3$ .
$V_f$	total volume of film wetting the walls of a tube, $cm^3$ .
$\alpha$	Parameter pertaining to the dependence of the mass transfer coefficient on the linear velocity.
$\overline{\beta}$	overall mass transfer coefficient for extraction, $cm^2/s$ .

- $\beta_{aq}$  mass transfer coefficient in aqueous phase,  $\text{cm}^2/\text{s}$ .
- $\beta_{axial}$  axial mass transfer coefficient at the ends of an aqueous segment,  $\text{cm}^2/\text{s}$ .
- $\beta_i$  mass transfer coefficient across interface,  $\text{cm}^2/\text{s}$ .
- $\beta_{org}$  mass transfer coefficient in organic phase,  $\text{cm}^2/\text{s}$ .
- $\beta_{radial}$  radial mass transfer coefficient through the side of an aqueous segment,  $\text{cm}^2/\text{s}$ .
- $\epsilon$  Eccentricity of an ellipsoid. Defined by equation 5.4.
- $\epsilon_o$  molar absorptivity of the neutral form of the sample species in the organic phase.
- $\gamma$  surface tension of liquid,  $\text{dyn/cm}$ .
- $\eta$  viscosity, poise.
- $\eta_c$  viscosity of the continuous phase which wets the walls of the tubing, poise.
- $\rho$  fluid density,  $\text{g/cm}^3$ .
- $\sigma_x^2$  variance associated with instrument component  $x$ .
- $\tau$  time constant associated with an exponential process.
- $v$  mean linear velocity,  $\text{cm/s}$ .
- $v_\theta$  azimuthal velocity,  $\text{cm/s}$ .
- $v_r$  radial velocity,  $\text{cm/s}$ .
- $v_z$  axial velocity,  $\text{cm/s}$ .
- $\Psi$  stream function, see equation 4.5.
- $\nu$  kinematic viscosity,  $\text{cm}^2/\text{s}$ .

## Chapter 1

### Introduction

Chemical analyses have become an integral part of almost all facets of our modern society, from our health care to industrial process control. In order to meet the demand of the ever increasing number of samples, analytical laboratories have turned to automated methods of analysis. The goals of automation are to speed up the analyses, to reduce the manpower costs and to improve the reproducibility.

Since its introduction in the early 1970's, flow injection analysis (FIA) has rapidly gained acceptance as an automation technique, and has been the subject of numerous books and reviews [1-13]. The popularity of this technique stems largely from its instrumental simplicity and the ease by which classical chemical methods can be automated using it. The analogy between a classical analytical procedure and the FIA method is shown in Figure 1-1. The steps performed in a manual chemical analysis (A) are: (i) A measured quantity of the sample is introduced into a reagent solution; (ii) The solution is mixed and the sample and reagent are allowed to react for a fixed length of time; and (iii) A portion of the solution is removed to a detector to determine the concentration of product in solution.

In the FIA instrument (B), reagent solution is pumped through narrow tubing ( $< 0.8$  mm i.d.) at a constant rate using a peristaltic, constant pressure, long stroke piston or reciprocating pump. A precise volume of sample is introduced into the reagent stream via an injection valve in the form of a discrete plug, *a*. As the sample is carried along through the tubing by the reagent, it develops a parabolic distribution (*b,c*) as a result of the viscous drag of the solution along the walls of the tubing. This parabolic profile is relaxed by diffusion of sample from the sample band (high concentration) to the surrounding reagent solution (low concentration), and of reagent in the opposite direction. In this manner the sample and reagent are mixed by diffusional relaxation of the laminar flow.

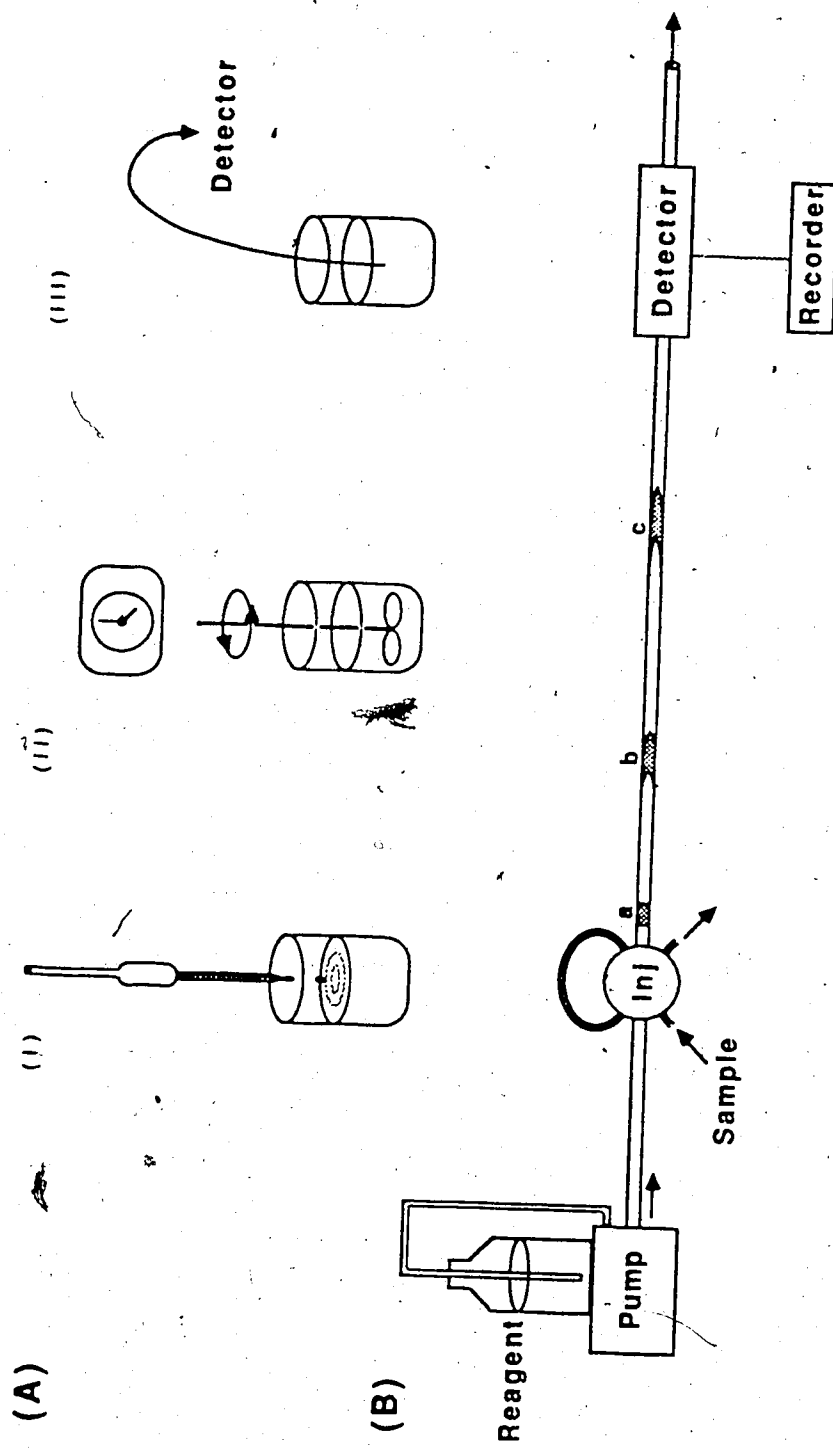


**Figure 1-1** Analogy between (A) a manual classical chemical assay and (B) an automated analysis using flow injection analysis (FLA). The manual steps of (i) adding a precise volume of sample to a reagent solution, (ii) mixing the reactant solution for a given length of time and (iii) measuring the product with a detector are performed automatically by the injector, the laminar flow in the reaction tube which disperses the sample into the reagent (a  $\rightarrow$  c) and the flow-through detector.

Alternatively, this mixing can be performed by injecting the sample into a solvent carrier stream which then merges with a reagent stream [1]. In either case a product is formed within the flowing stream which is monitored by a flow-through detector as a sharp peak. For example, Figure 1-2 shows the response for injections of five caffeine samples of linearly increasing concentration into a simple FIA manifold, such as shown in Figure 1-1. The area or height of the peaks can be directly related to the concentration in the original sample solution. The detector is typically a uv/vis spectrometer, although electrochemical, atomic absorption and emission, chemiluminescence and fluorimetric detectors are seeing increased use [6].

For a discrete analyzer such as FIA, the measurement criteria of the speed of analysis are the dead time and the sampling frequency [14]. The *dead time* is defined as the time interval, after injection of the sample, during which no signal is observed at the detector, and in FIA results solely from the pumping speed. By adjusting this speed, the dead time can be adjusted to give the required mixing, as well as sufficient time for the reaction to proceed to a detectable level. However since this timing can be controlled with a high degree of precision, it is not necessary to wait for the reaction to proceed to completion before making measurements, and so the dead times associated with FIA are typically only 3 to 30 s. The second measure of the analysis speed, the *sampling frequency*, is a function of the broadening which the sample plug experiences due to the injection, the tubing and the detector. Thus if the injector and detector volumes are small and the dead time of the detector is of the order mentioned above, sampling frequencies of > 120 samples/h are attained.

FIA has been used in a wide variety of applications [1,6], including agricultural, biochemical, clinical [11,12], environmental, food, industrial [13] and pharmaceutical analyses. Owing to the complexity of samples in these areas, it is often necessary to incorporate a separation step in the automated analysis. To date, gas diffusion, distillation, hydride generation, ion exchange, adsorption, precipitation, chromatography,

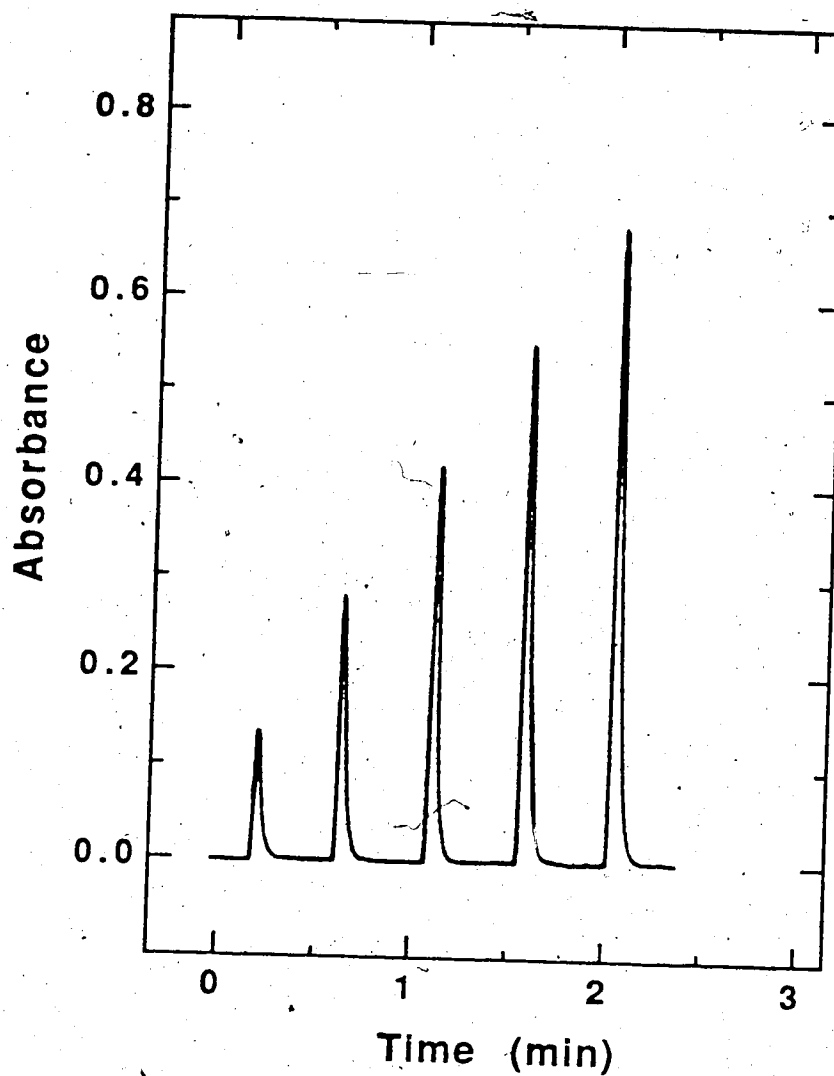
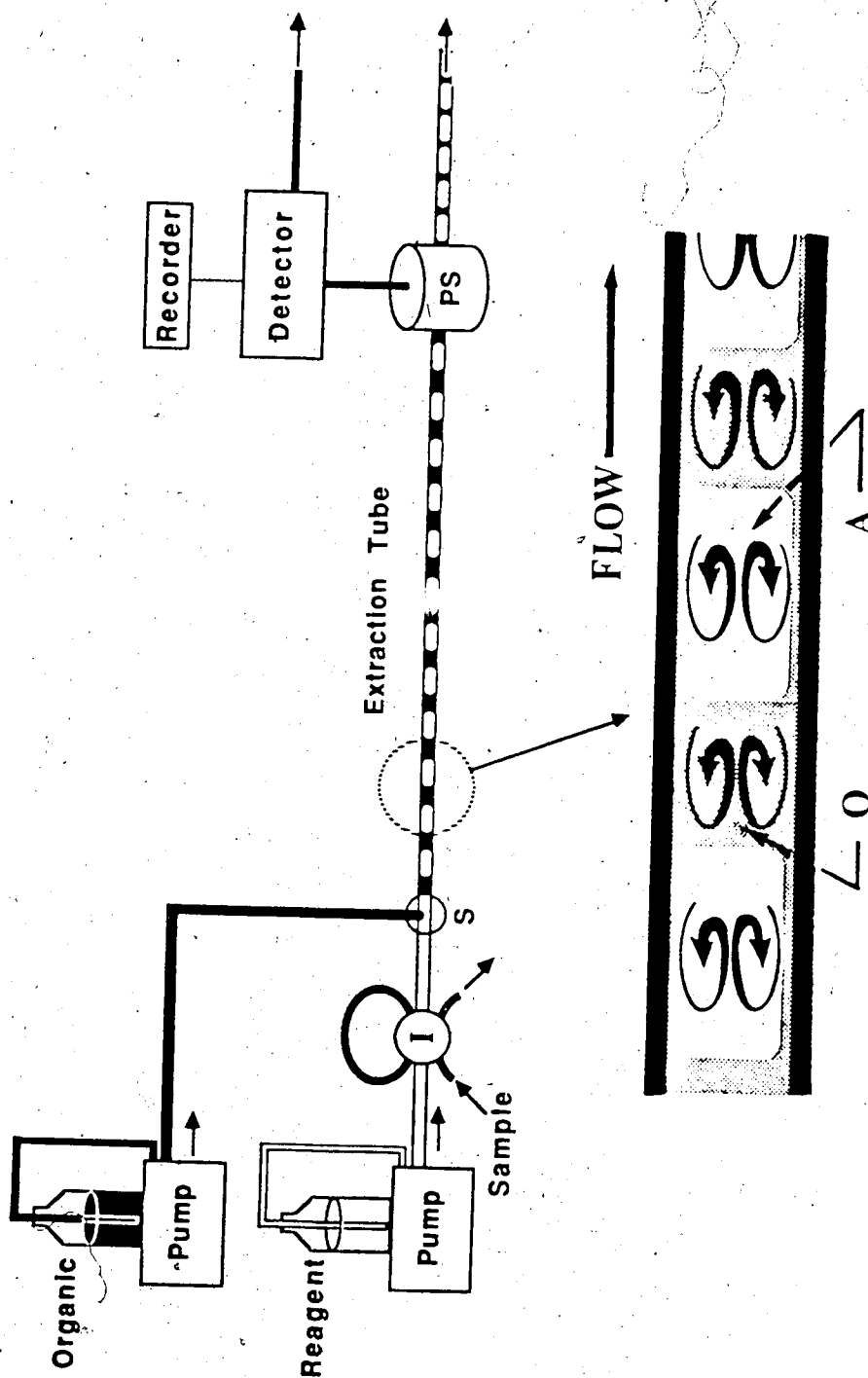


Figure 1-2 FIA signal for successive injections of increasing concentrations of caffeine.

dialysis and liquid-liquid extraction have all been used as separation methods in FIA [15]. However, since its simultaneous introduction by Karlberg and Thelander [16] and Bergamin *et al* [17] in 1978, solvent extraction/flow injection analysis (SE-FIA) has become the most common FIA separation technique [15,18]. A schematic diagram of a simple SE-FIA manifold is shown in Figure 1-3. As in the regular FIA instrument, sample is injected into a flowing reagent stream using a valve, I. Subsequent introduction of an immiscible fluid to the aqueous reagent stream downstream of the injector produces a *segmented* two phase flow, so called because it is comprised of discrete alternating segments of the two immiscible solvents. The sample plug is distributed over many of the aqueous segments and as it flows through the Extraction Tube sample will extract from these segments into the adjacent organic phase segments. The two phase flow then enters a phase separator, PS, which separates a portion of one phase from the segmented flow stream and directs it to the flow-through detector. As in normal FIA, this detector can be of many different types, but in all cases the signal is a single sharp peak for each injection. The effect of experimental parameters on the height [19] and area [20] of this peak have been studied for SE-FIA.

In the enlarged section of the Extraction Tube shown in Figure 1-3, it can be seen that one solvent segment is excluded from the tubing surface, while the other solvent freely wets the tubing inner wall. If the tube is made of Teflon, as is the case in all work discussed herein, the organic phase preferentially wets the tube walls [21-23]. The excluded segment thus forms a slug or bolus which is completely surrounded by the other solvent, giving rise to the alternate terms of *slug* [24] and *bolus flow* [25] for the flow through the Extraction Tube. Viscous drag along the walls of the tubing will induce a circulatory flow within the segments in the general shape of a toroid [22,24-28]. If the Extraction Tube is wrapped in a coil, as it normally is, then a "secondary" radial circulation, in addition to the toroidal circulation, would develop within the segments [24,26-28]. The rate at which material extracts within the Extraction Tube will govern the



**Figure 1-3** Simple solvent extraction - flow injection analysis (SE-FIA) manifold, showing an expanded section of the segmented flow. I is the injection valve, S is the segmentor and PS is the phase separator. See text for details.



dead time of SE-FIA. Since extraction is a mass transfer process, factors affecting the interfacial area and the convection within the segments will control the dead time. Such factors are the length of the segments, the diameter of the tube, linear velocity of the liquid [24,29], coiling of the tubing [24] and the presence of surface active compounds [30]. Typically the dead time of SE-FIA instruments is 15-60 s.

The device in which the two immiscible solvents meet to form the segmented flow is known as the *segmentor*. The simplest segmentor is a three-way T connector, such as shown in the expanded portion of Figure 1-3. The size of segment produced by such a segmentor results from the balancing of hydrodynamic and interfacial forces [31]. A growing "drop" of one phase, the organic in Figure 1-3, is dislodged to produce a segment when the hydrodynamic force exerted on it as a result of the aqueous flow is equal to the interfacial force holding it in place. Kawase [32] observed that the geometry of the confluence point affects the segment length. A W shaped segmentor, with the segmented flow exiting the central channel, formed shorter segments than T and Y configurations of the same channel diameter. Similar results were observed by Apffel *et al* [33]. The shortest segment length possible is approximately equal to the tube diameter [33]. In early SE/FIA instruments, a modified A-8 Technicon connector was used as an adjustable segmentor [16,18,23,34]. However the segments produced by this segmentor are typically >5 mm in 0.8 mm i.d. tubing, and so this segmentor is seeing decreasing usage as the technique follows a movement towards miniaturization.

Several types of phase separators have been used in SE-FIA. The earliest designs depended on gravity [17,35,36] or gravity plus a phase guide [18,23,37]. These phase separators however had large dead volumes, which resulted in large amounts of band broadening and consequently lower sampling frequencies. Currently, membrane phase separators [20,33,38-40] are most popular. These are based on the selective permeability of a membrane towards the phase which wets the membrane material. For instance, a Teflon membrane is preferentially wet by solvents such as pentanol, chloroform, methyl-

isobutyl ketone, toluene and cyclohexane and so a Teflon membrane phase separator can be used to separate these solvents from water [41]. In addition to having a smaller inner volume than gravity based separators, membrane phase separators are more reliable for separating the phases when high flow rates are used, do not require density differences between the solvents and can produce almost quantitative separation efficiencies if microporous membranes (pore size  $< 1\mu\text{m}$ ) are used. Dual membrane phase separators with both a hydrophobic (Teflon) and a hydrophilic (paper) membrane have been used to simultaneously generate clean streams of both the organic and aqueous phase [42,43]. However, despite great effort to characterize and minimize the band broadening of the membrane phase separator [44], this device is still one of the major factors contributing to the band broadening and, therefore, limiting the sampling frequency of SE-FIA, which is typically 20-60 injections/h.

The applications and various manifold designs of instruments using segmented flow extraction have recently been reviewed [15,18,45]. The simple manifold design for SE-FIA shown in Figure 1-4a has been used for analysis of pharmaceuticals [16,20,34,42,46-49], natural products [50-52], surfactants [32,36,53-55] and metals [17,35,56-64]. This technique has also been used for measurements of distribution constants [65] and the acid dissociation constants of sparingly soluble compounds [43], as well as an investigation of "phase transfer catalysis" [66].

In an alternative design of the segmented flow extractor, generally referred to as "continuous liquid-liquid extraction" and shown in Figure 1-4b, the sample is fed into the instrument as a constant stream rather than via injection. This procedure has been used to automate extraction steps prior to off-line analysis by infrared spectroscopy [67] and gas and high performance liquid chromatography [23,68,69]. Generally, if multiple extractions are being performed [23,69-71], continuous liquid-liquid extraction is used rather than SE-FIA because passage through multiple phase separators would result in unacceptably large band broadening and consequently low sensitivity.

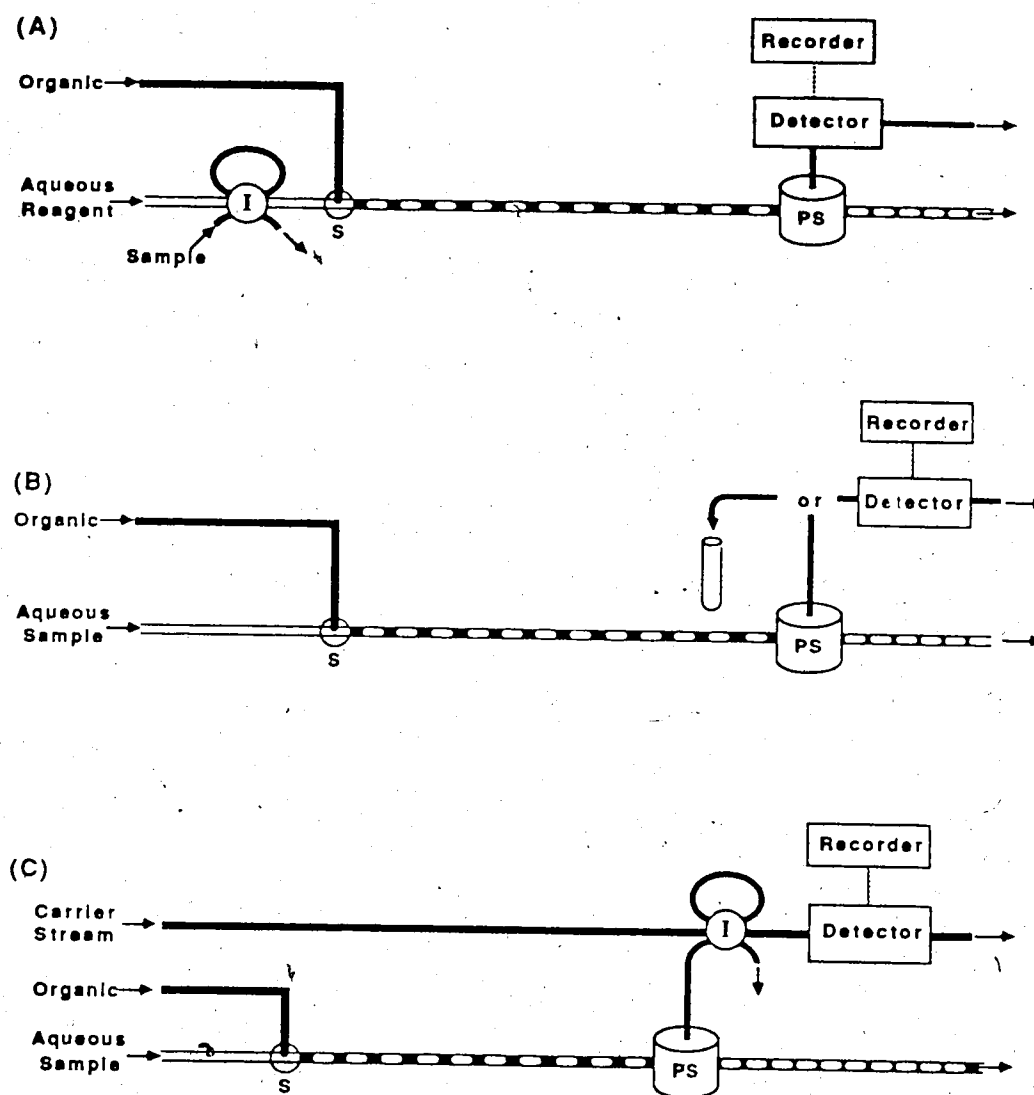


**Figure 1-4** Various designs of instruments to perform automated extraction using segmented flow. (A) Typical Solvent Extraction-Flow Injection Analysis (SE-FIA) manifold. (B) Continuous liquid-liquid extraction connected either to a batch collector or directly to a detector. (C) Continuous liquid-liquid extraction to fill the injection loop of a discrete analyzer. (continued on next page.)

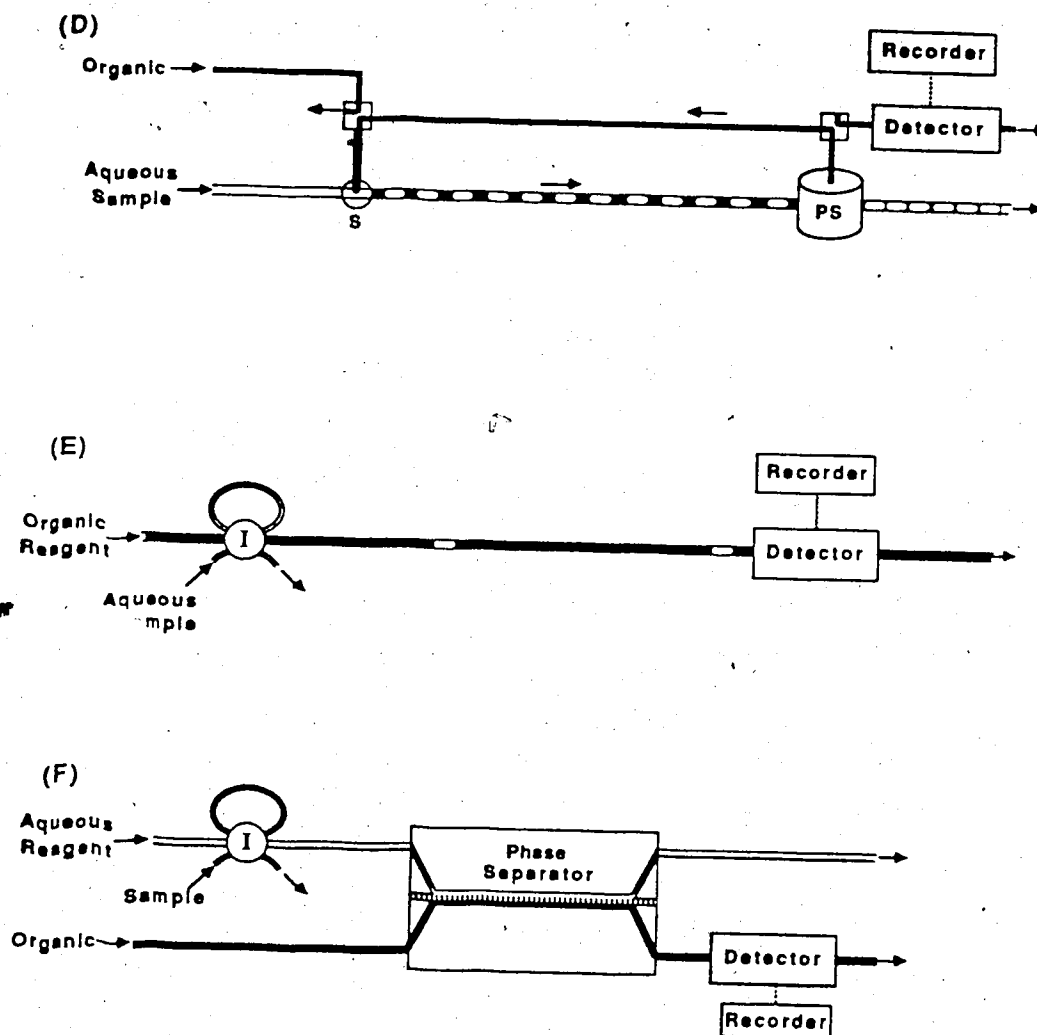


**Figure 1-4** Various designs of instruments to perform automated extraction using segmented flow - continued. (D) Continuous closed loop solvent extraction system (CLSES) shown in recirculation setting. Both valves must be turned 90° clockwise to direct the organic phase to the detector. (E) On-tube detection of the segmented flow. (F) Unsegmented extraction flow injection analysis apparatus.

Alternately if on-line detection is used and the sample feed is the effluent from a liquid chromatograph, then this system acts as a postcolumn reaction detector [33,72-83]. Due to the low band broadening in the segmented flow, this type of postcolumn detector is preferred over open-tubular or packed bed reactors when the reaction times are greater than 15-20 s [79]. In fact, analytically useful results have been obtained for reactions requiring up to 23 min residence times [83].

A second form of the continuous liquid-liquid extraction technique, shown in Figure 1-4c, involves an injection loop filled with the phase separated from the segmented flow. This injector is then connected to an atomic spectroscopy-FIA [84-90] or gas chromatograph [91,92]. This procedure is favored in atomic spectroscopic SE-FIA methods because of incompatibilities between the flow through the membrane of the phase separator and the nebulization rates of the spectrometers.

Preconcentration using the instruments described above can only be accomplished by varying the aqueous-to-organic phase ratio in the segmented flow, which generally cannot be increased above five if reproducible results are to be obtained [93]. Recently, enrichment factors of approximately 20 were obtained using a continuous closed loop solvent extraction system (CLSES) [57,94], which is shown in Figure 1-4d. In this method, the organic phase and the aqueous sample solution flow through the extraction coil, achieve equilibrium and then pass through a phase separator which separates a portion of the organic phase and the spent aqueous phase is discarded, just as in the previously discussed instrument. The difference is that this separated organic phase is directed back to the segmentor where it merges with fresh sample solution. This recirculation results in the extraction of more sample by a given volume of organic phase than is possible in a single pass extraction technique, such as in a to c in Figure 1-4. After sample loading, the loop is opened (both valves V in Figure 1-4d turn 90° clockwise) and the concentrated organic solution of sample flows through a detector.

In the progression from the typical SE-FIA to the closed loop design, the manifold has become steadily more complex. Two simplified SE-FIA manifolds which have been reported are shown in Figure 1-4e and 1-4f. In the first of these instruments the need for the segmentor and phase separator was eliminated by use of an on-tube fluorimetric detector [95]. Aqueous sample was injected into an organic stream containing reagent. The resultant product extracted into the organic phase in which it was fluorescent. In the second instrument, shown in Figure 1-4f [96], the aqueous and organic phases pass through opposite sides of the membrane in a phase separator. This extraction cell acts much as does a dialysis cell, and eliminates the need for the segmentor and extraction coil of a SE-FIA instrument. However, due to the small contact area and short contact time between the two phases, the extraction efficiencies were only in the range of 8-18% for compounds which are quantitatively extracted at equilibrium.

While the manifold designs shown in Figure 1-4 appear quite different, each has the primary goal of automating a chemical analysis - i.e. to make the analyses faster, to reduce the manpower costs and to improve the reproducibility. In all of the manifolds, except that in Figure 1-4f, the extraction kinetics determines the dead time, and in the unsegmented extraction FIA instrument (Fig. 1-4f) the extraction kinetics will still be important, in that it dictates the sensitivity of the technique. The band broadening will also be an important determinant of the speed of each of these instruments. For the discrete analysis instruments, the band broadening limits the sampling frequency, as has been discussed earlier for FIA. For the continuous extraction, however, the band broadening is still of importance in the speed of analysis because it controls the response time of the instrument [14].

Thus, the speed of analysis of SE-FIA, in all its forms, is a function of the band broadening occurring within the instrumental components and of the kinetics of extraction within the segmented flow. The focus of this work is to study these two factors, in order

to characterize their influence on the speed of analysis. A secondary goal is to simplify the SE-FIA instrument.

In Chapter 2 of this work, an SE-FIA apparatus which can monitor both the organic and aqueous phases using a single photometric detector is discussed. After solvent extraction via segmented flow, a porous membrane separates a portion of the chloroform phase and directs it to the sample flow cell of the photometer. A paper membrane located farther downstream in the segmented flow separates a portion of the aqueous phase and directs it to the reference flow cell. The detector electronics are modified to allow reassignment of the sample/reference designation of the flow cells, so that positive signals can be obtained from both. To demonstrate the utility of this instrument it is applied to the analysis of the two active ingredients of a commercial nasal spray, phenylephrine hydrochloride and pheniramine maleate. At pH 13 pheniramine is quantitatively extracted into the chloroform phase and phenylephrine remains in the aqueous phase. Interfering species - thimerosal, maleate and benzalkonium chloride - present in the nasal spray are removed from the injected sample using miniature in-line ion exchange columns. Injections are made at a rate of 30 samples/h, with a precision and accuracy of quantification of 1-2% based on both peak height and area.

Chapter 3 describes the characterization of the band broadening occurring within the components of the extraction/FIA instrument introduced above. Variance determined using statistical moment analysis is used to describe the broadening of the sample plug as it passes through the instrument. The phase separators and the combination of the injector, detector and connecting tubing are the primary devices giving rise to the peak width.

In Chapter 4, the effect of instrumental parameters on the rate of extraction in SE/FIA is studied. In straight tubes, the extraction rate is dependent on the length of the segment relative to the tube diameter, on the linear velocity of flow and on the ratio of interfacial area to volume. The results obtained are interpreted in light of hydrodynamic studies of

the "toroidal" flow within each of the segments as it flows through straight tubing, which indicate that the convection within long segments is laminar-like, whereas that in short segments is more turbulent in nature. Coiling of the extraction tubing results in much higher extraction rates than in comparable straight tubes. This enhancement is due to the generation of secondary flow within the segments and is greater for long segments than short.

In Chapter 5, studies of the extraction from a single aqueous segment and the subsequent band broadening occurring in chloroform/water segmented flow are presented. The absorbance of each chloroform segment is measured as it passes through an on-tube photometer located at various distances along the Teflon extraction tube. Band broadening, which is studied by injecting iodine into a single chloroform segment, results from combined effects of the segment acting as a mixing chamber and also slow mixing between the bulk chloroform and the quasi-static wetting film of chloroform on the walls of the tube. Extraction from aqueous into organic segments is studied by generating iodine within a single aqueous segment using the bisulfite/iodate clock reaction. Application of a "successive reaction" model to the axial extraction through the front interface of the aqueous segment reveals that, in straight extraction tubes, solute extracts at the same rate across all of its interface, both at the segment ends and side.

Finally in Chapter 6, a number of areas of future study in solvent extraction/flow injection analysis are discussed. Firstly, the use of an on-tube detector greatly reduces the overall band broadening of the instrument. Use of a simple low pass filter should allow the on-tube photometer to produce an analytically useful signal on a chart recorder. Secondly, a number of studies still remain with regard to the kinetics of extraction. Paramount of these are further work on the effect of surface active compounds on the extraction rate and a study of the factors which would affect the extraction from the film-forming phase into the dispersed phase, i.e. from organic into aqueous phase in Teflon tubing.



## Chapter 2

### Solvent Extraction / FIA Analysis of a Commercial Nasal Spray

#### 2.1 Introduction

Simultaneous monitoring of both the aqueous and organic phases in solvent extraction/flow injection analysis has been used to analyze diphenhydramine and 8-chlorotheophylline in Dramamine tablets [42] and for the determination of acidity constants [43]. In both of these applications two detectors were used, one to monitor the absorbance of the aqueous phase and the other for the organic phase. The use of two detectors increases the cost of such an instrument. It would therefore be advantageous if only a single detector were needed to monitor the two sample streams.

In this chapter, an extraction-FIA system is presented in which both the organic and aqueous phases are monitored using a single photometric detector. A portion of the organic phase is first separated from the segmented flow by a porous Teflon membrane and passes through the sample flow cell of the detector. Farther downstream a portion of the aqueous phase is separated from the segmented flow by a paper membrane and directed to the reference flow cell. The detector electronics are modified to obtain analytically useful signals from both flow cells of the photometric detector.

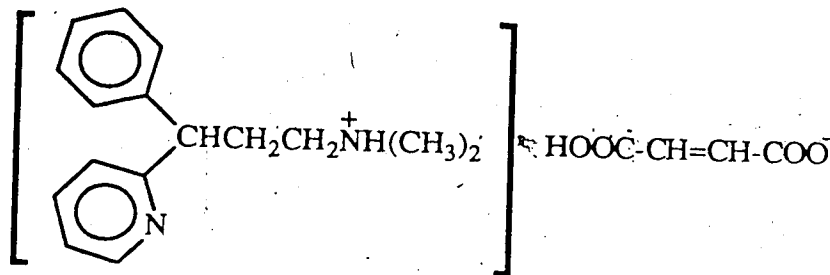
The instrument is used for the assay of phenylephrine hydrochloride and pheniramine maleate, the active components of a commercial nasal spray. Under alkaline conditions, pheniramine quantitatively extracts into chloroform as the neutral free-base, while phenylephrine remains unextracted in the phenolate form. To avoid both spectral and chemical interferences from minor components of the nasal spray, miniature on-line ion exchange columns are included in the instrument manifold.

## 2.2 Experimental

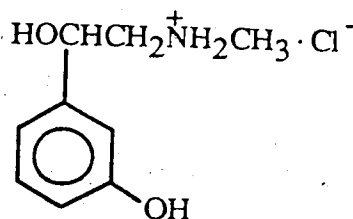
16

### 2.2.1 Chemicals and Solvents

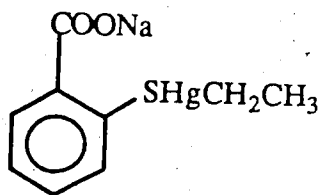
Pheniramine Maleate was U.S.P. grade and was used as received from the manufacturer. Its chemical assay was 99.77%. Its structure is:



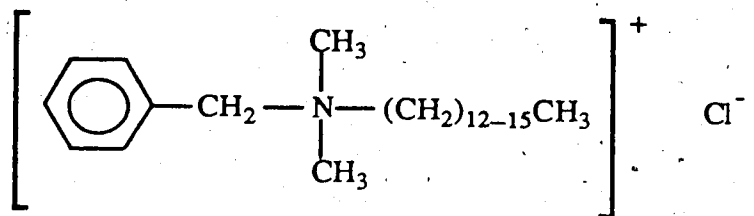
Phenylephrine Hydrochloride was U.S.P. grade and was used as received from the manufacturer. Its chemical assay was 98.45%. Its structure is:



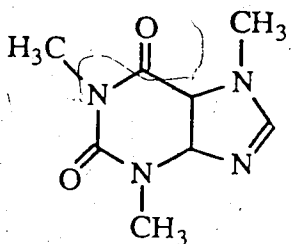
Thimerosal (Sodium ethylmercurithiosalicylate) (reagent grade) was used as received from Sigma, St. Louis, Missouri. Its structure is:



Benzalkonium chloride (reagent grade) was used as received from Sigma, St. Louis, Missouri. Its structure is:



Caffeine was analytical reagent grade and was used as received from the Aldrich Chemical Company (Milwaukee, Wisconsin). Its structure is:



Double Distilled Water was prepared by distilling the laboratory distilled water from alkaline permanganate in an all-glass still. The first 20% of the distillate was discarded and the middle fraction was collected. This water was used to prepare all aqueous solutions referred to in this work.

Chloroform was reagent grade (Caledon Laboratories Ltd.) and was distilled and extracted with distilled water shortly before use to remove uv-absorbing impurities and the ethanol additive respectively.

Methanol was reagent grade (Caledon Laboratories Ltd.) and was used as received.

Other chemicals including sodium hydrogen phosphate, citric acid, boric acid, sodium hydroxide, sodium borate and potassium chloride were all analytical reagent grade.

Reagent buffers between pH 2.6 and 7.6 were prepared by combining the appropriate volumes of 0.2 M  $\text{Na}_2\text{HPO}_4$  and 0.1 M citric acid to give a final volume of 500 mL; pH 8.0 and 9.1 buffers were prepared from 0.1 M  $\text{H}_3\text{BO}_3$  and 0.1 M NaOH; pH 9.5 and 10.1 buffer were made from 0.025 M  $\text{Na}_2\text{B}_4\text{O}_7$  and 0.1 M NaOH; pH 11.3 buffer was prepared from 0.05 M  $\text{Na}_2\text{HPO}_4$  and 0.1 M NaOH; buffers with pH >12 were prepared

from 0.2 M KCl and 0.2 M NaOH [97]. The ionic strength of these buffers was not constant, and varied from 0.044 to 0.49.

Commercial buffers (Fisher Scientific Co.) of  $\text{pH} = 4.00 \pm 0.01$ ,  $\text{pH} = 7.00 \pm 0.01$  and  $\text{pH} = 10.00 \pm 0.01$  and were used for calibration of the pH meter.

Amberlyst 15 strong acid cation exchange resin (Rohm and Haas Co.), with an exchange capacity of 4.6 meq/g, was ground in a clean, dry mortar and pestle, and sieved to obtain the 60-80, 80-100, 100-140, 140-200, 200-325 and >325 Mesh fractions. The fines were removed from the resin by repeated suspension and decantation in three bed volumes of distilled water until the supernatant was clear. Approximately 1 gram of resin was then placed in a borosilicate glass column and washed with 1 M HCl until the effluent was colorless (~10 mL). The resin was converted into the sodium form by washing with 1 M NaOH until the effluent had the same pH as the influent. This was followed by a water wash to constant pH. Finally the resin was washed with 50 mL of ethanol, followed by a water wash and then dried in a convection oven at 45°C for 18 hours. The dry resin was stored in a tightly closed bottle.

Amberlyst A-26 anion exchange resin (Rohm and Haas Co.), with an exchange capacity of 4.2 meq/g, was treated in a similar manner to the cation exchange resin. The resin was dry ground and the various fractions were collected. The material was de-fined by repeated suspension/decantation, washed with 1 M NaOH and converted to the chloride form using 1 M HCl. Finally, the resin was washed successively with distilled water, ethanol and then water again, and dried in a convection oven at 45°C for 18 hours. The dry resin was stored in a tightly closed bottle.

Carboxymethyl cellulose (Fibrous form, medium mesh, Sigma), with an ion exchange capacity of 0.6 meq/g, was used as received.

## 2.2.2.1 Nasal Spray Apparatus

A schematic diagram of the extraction/FIA instrument used to analyze a commercial nasal spray is shown in Figure 2-1. Its design was based on an instrument previously described [42] with the main differences being the sequential arrangement of the phase separators and the use of only one detector. The chloroform to be pumped is held in a 1700 mL glass bottle, while the water, aqueous reagent and methanol are held in 2 liter polyethylene bottles. These bottles are placed inside aluminum cylinders which are pressurized with nitrogen to produce solvent flow. All tubing is made of Teflon, with 0.3 mm i.d. tubing being used whenever it is desirable to minimize sample band broadening or to provide increased resistance to flow. Wider 0.8 mm i.d. tubing is used in the rest of the system.

The solvent flow can be turned on or off using valves  $V_1$  (part no. CAV2031, Laboratory Data Control (LDC), Riviera Beach, FL). Valve  $V_2$  (part no. R6031 V6, LDC) is a six-port rotary valve which allows selection of any of a number of solutions contained in 400 mL glass bottles within the multi-reagent cylinder [42]. In experiments in which the pH was varied, the multi-reagent cylinder contained six buffer solutions and distilled water, while for the nasal spray analysis it contained only distilled water and 0.1 M HCl. The sample is injected into a carrier stream of distilled water via a 10  $\mu$ L slider injection valve,  $V_4$ , (part no. CSVA-10, LDC). Valve  $V_4$  is actuated by an air solenoid valve (part no. SOL-3-24-VDC, LDC) controlled by an electrical timer which allows variation of fill and injection times.

The sample stream flows through a miniature anion exchange column,  $C_a$ , based on a design previously described [98] and shown in Figure 2-2. The 10 mm long bed of 100-140 Mesh Amberlyst A-26 macroporous anion exchange resin is packed within a 50 mm long piece of 1.5 mm i.d. Teflon tubing, and held in place by a sinter glass outlet frit.

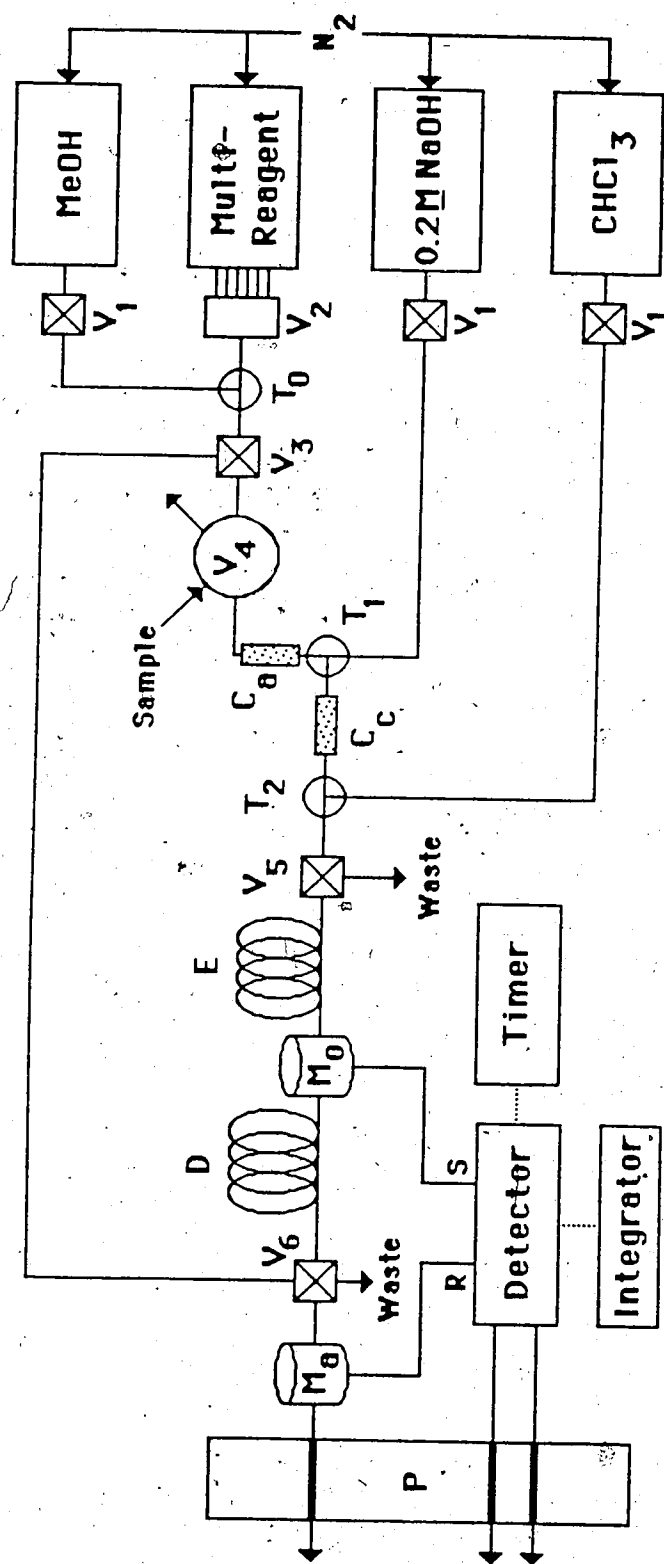


**Figure 2-1** Schematic diagram of the SE-FIA instrument used for the nasal spray analysis. Methanol, reagent and chloroform are in pressure cylinders. Distilled water and 0.1 M HCl are in the multi-reagent cylinder. V<sub>1</sub> are 2-way valves; V<sub>2</sub> is a 6-way valve; V<sub>3</sub> and V<sub>5</sub> are 3-way valves; V<sub>4</sub> is a slider injection valve; V<sub>6</sub> is a 4-way valve; T<sub>0</sub>, T<sub>1</sub> and T<sub>2</sub> are tee-fittings; C<sub>a</sub> and C<sub>c</sub> are miniature anion and cation exchange columns; E and D are the extraction and delay coils; M<sub>0</sub> and M<sub>a</sub> are the organic and aqueous membrane phase separators; R and S are the two flow cells of the photometer whose sample/reference designation is timer controlled and P is the peristaltic pump. See Section 2.2.2.1 for further details.

This frit is made from a 1.5 mm diameter core drilled through a sinter glass plate (nominal pore size 50  $\mu\text{m}$ ). The extra length of the column, beyond the bed and frit, was necessary to accommodate the two end fittings. The dead volume of the column was reduced by inserting tight fitting Teflon tubing (1.58 mm o.d. and 0.3 mm i.d.) into each end.

The sample stream then merges with the reagent stream, 0.2 M NaOH, at tee-fitting  $T_1$  and flows through a miniature cation exchange column,  $C_C$ , consisting of a 10 mm long bed of 100-140 Mesh Amberlyst 15 macroporous cation exchange resin and constructed as shown in Figure 2-2. The combined aqueous stream joins the chloroform stream at the segmentor, tee-fitting  $T_2$ , and the resulting segmented flow stream passes through the extraction coil, E, in which the solvent extraction occurs between the aqueous and the organic phases, and equilibrium is achieved. Various lengths of 0.8 mm i.d. Teflon tubing were used as the extraction coil depending on the experiment. After exiting coil E the stream enters the first membrane phase separator,  $M_O$ , where a portion of the organic phase is separated.

The porous membrane phase separator is similar to one previously described [20]. Figure 2-3 shows an expanded view of the membrane phase separator. The membrane is comprised of two layers of 4 mil, 10-20  $\mu\text{m}$  pore size Teflon membrane (Zitex, No. E249-122, Chemplast Inc., Wayne, NJ) and is sandwiched between two Kel-F body pieces. The main body pieces are pressed together with four screws and two stainless steel end plates. The volume of the membrane chamber is about 0.05 mL. The three threaded holes accept standard polypropylene pieces (part no. TEF 107, LDC) and flared Teflon tubing.

The portion of the chloroform phase which passes through this membrane flows through the 8  $\mu\text{L}$  sample flow cell of the uv-vis absorbance detector (SF770 Spectroflow, Schoeffel Instrument Corp.). The remainder of the chloroform, and all of the aqueous phase, pass through a delay coil, D, to the second phase separator,  $M_a$ . This phase separator is similar to  $M_O$  except that it contains a hydrophilic membrane consisting of two

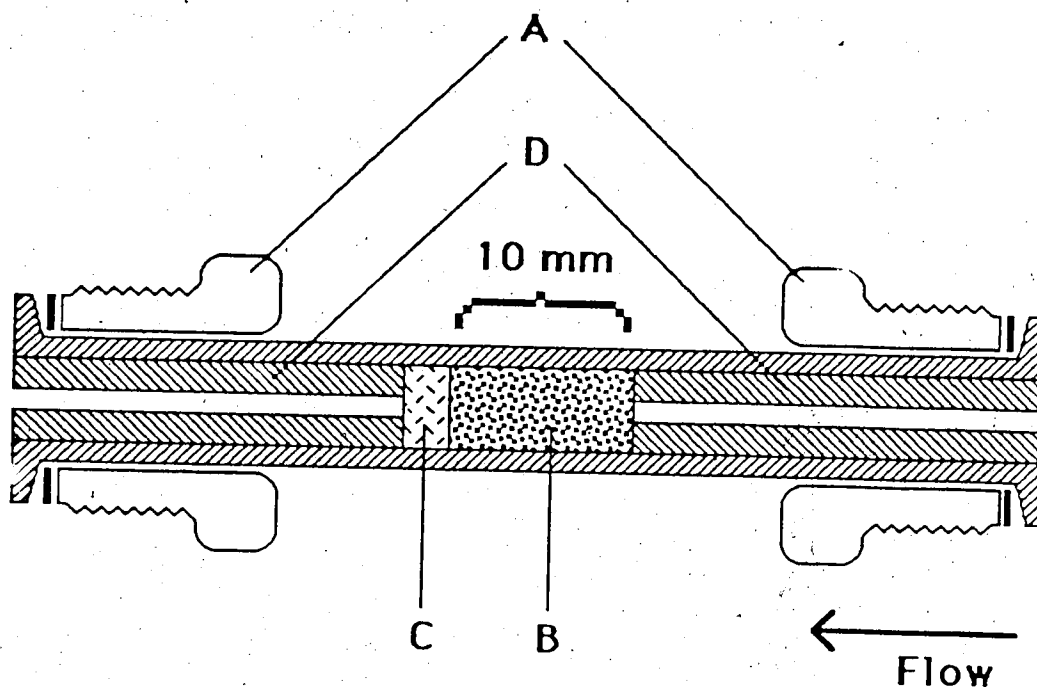


**Figure 2-2** Schematic diagram of miniature ion exchange column; A are two connectors (including two stainless steel washers). The resin particles, B, are held in place by a porous silica outlet frit, C, within a 1.5 mm i.d. Teflon tube (shown in right hand thatch). Two Teflon tubes (0.3 mm i.d.), D, are inserted from both ends to reduce the dead volume. Flow through the column would be from right to left. Length of the resin bed is 10 mm and the overall column 50 mm. The width of the column is exaggerated  $2\frac{1}{2}$  times to display the column features.



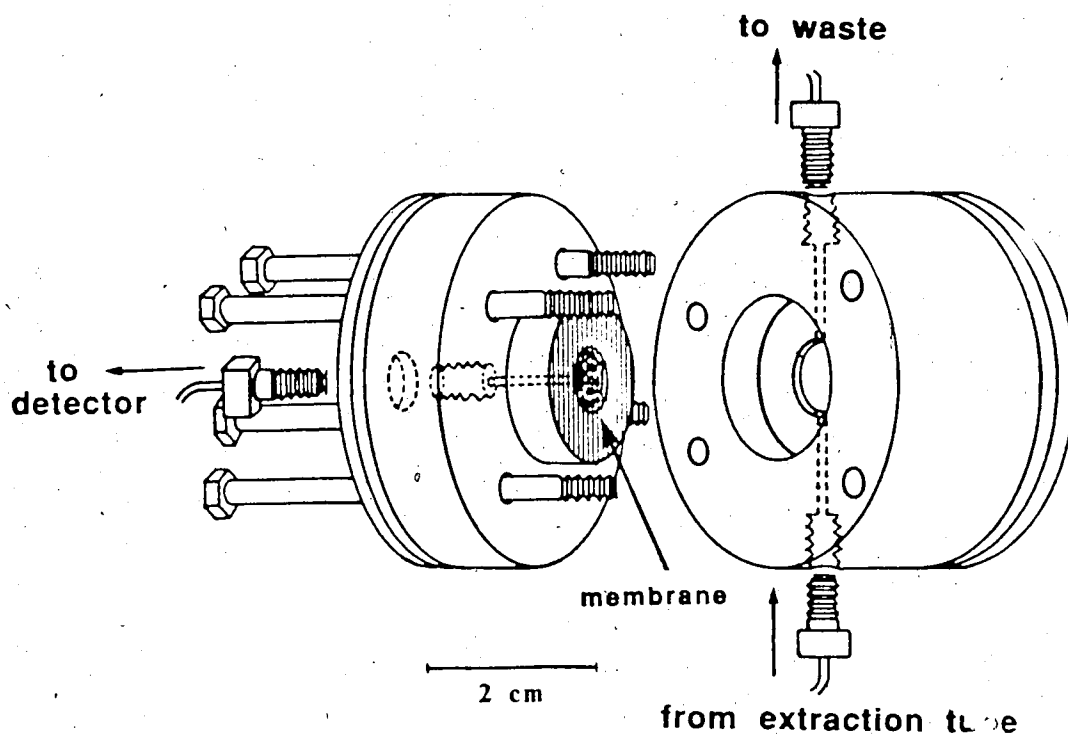


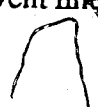
**Figure 2-3** A three-dimensional view of the membrane phase separator design used in this work. The membrane is sandwiched between two Kel-F blocks thus partitioning the outlet to the detector from the internal separation chamber. The two blocks are pressed together with four screws and two metal end plates. The radial and circular grooves in the left hand membrane support direct the filtrate to the outlet hole. (Figure drawn by Jamal Sweileh).

pieces of Whatman No. 5 filter paper, rather than the hydrophobic Teflon membrane.

This paper membrane separates a portion of the aqueous phase and passes it through the 8  $\mu\text{L}$  reference flow cell of the detector.

The delay coil, D, is 0.8 mm i.d. Teflon tubing of a sufficient length to allow the attainment of baseline absorbance between the signals from the two flow cells of the detector, as can be seen in Figure 2-4. The signals from the two channels are integrated using a digital integrator, I, (Model 3390A, Hewlett Packard) to obtain peak areas and heights. The chloroform exiting the sample flow cell, the aqueous solution exiting the reference flow cell, and the combined  $\text{CHCl}_3$ /aqueous stream leaving the second phase separator all pass through Acidflex pump tubes (Technicon Corp.) in a Minipuls variable speed peristaltic pump, P, (Gilson Instruments, Ville-le-Belle, France) which is used to provide accurate flow control [20]. Acidflex tubes used were: organic filtrate, red-red; aqueous filtrate, white-white; two phase flow, purple-purple.

At the time of start-up the need to wet each membrane with the appropriate solvent requires the inclusion of some additional plumbing. The system is initially flushed with methanol from the "rinse" cylinder. Then the three-port valve  $V_3$  (part no. CAV3031, LDC) and the four-port valve  $V_6$  (part no. CAV4031, LDC) are switched to their start-up positions and the chloroform and distilled water streams are turned on. The chloroform flow passes through the extraction coil E and wets the Teflon membrane in phase separator  $M_0$ , but is diverted to waste by valve  $V_6$  before reaching phase separator  $M_a$ . The water stream from the multi-reagent cylinder bypasses the extraction and delay coils and is directed by  $V_6$  into  $M_a$  where it wets the paper membrane. Next the reagent flow is initiated by opening the appropriate valve  $V_1$ . The reagent establishes the segmented flow in the extraction coil. After the segmented flow has reached valve  $V_6$ , switching of valves  $V_3$  and  $V_6$  restores the instrument to its normal operating mode. The three-port valve  $V_5$  is included in the system to allow the flushing of air bubbles which may form in the solvent lines when the instrument is idle.



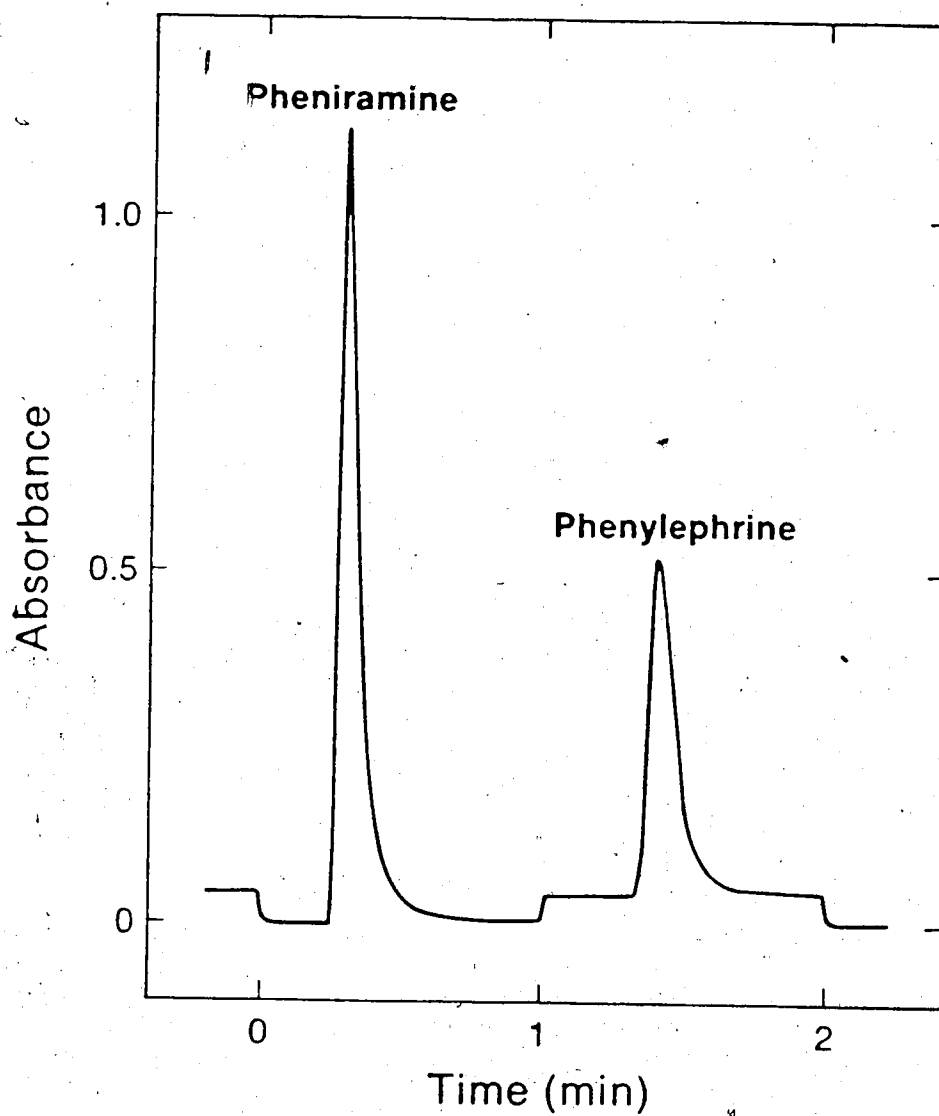


**Figure 2-4** Instrumental response for a nasal spray injection at time zero. Baseline shift is due to switching of the flow cell designation.

The shut-down procedure at the end of the day consists of a 10 minute flush with 0.1 M HCl from the multi-reagent cylinder to regenerate the anion exchange column, followed by a 5 minute methanol rinse of the full instrument.

#### 2.2.2.2 Single Phase FIA System

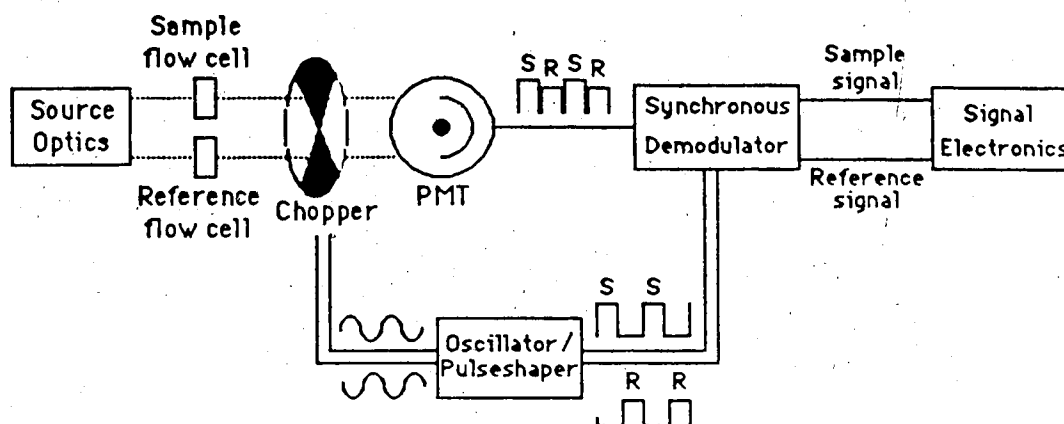
During the construction of the nasal spray assay instrument it was often necessary to study individual components of the system. To simplify these studies a single phase apparatus was constructed from that shown in Figure 2-1 by disconnecting the anion exchange column,  $C_a$ , from the injector,  $V_4$ , and the sample flow cell of the detector,  $S$ , from the organic phase separator,  $M_O$ . The injector was then connected directly to the flow cell of the detector by a short piece of Teflon tubing. The peristaltic pump was used to control the flow.

#### 2.2.3 Detector Modification

The photometer (Schoeffel SF770) was modified to allow electronic switching of the sample/reference designation of its two flow cells. This was done by placing a double-pole double-throw relay (part no. RA30572051, Elec-Trol) across the two control lines from the chopper to the synchronous demodulator, as is shown in Figure 2-5. These lines were used to define the signal coming from the photomultiplier tube as coming from either the sample or reference flow cell. The setting of the relay, either for normal or reversed flow cell designation, was controlled with an electronic timer. For the nasal spray analysis, the timer switched the flow cell designation every 60 seconds. This switching can be identified by the base line shift in Figure 2-4 which occurs as a result of small differences in alignment of the two flow cells.

This base line shift would be mistaken as a portion of a peak by the integrator. To avoid this problem the integrator is disabled (integration function 9, HP 3390A) just prior to the shift and re-enabled afterwards (function -9). In addition all peaks are designated

(A)



(B)

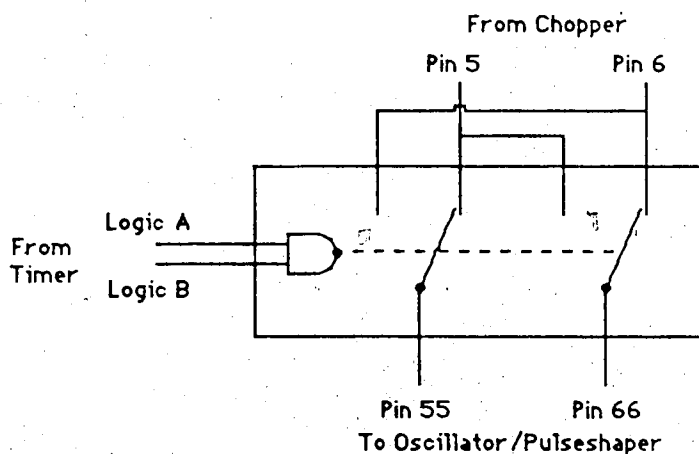


**Figure 2-5** Modification to detector electronics to allow switching of the sample/reference flow cell designation. A. Schematic diagram of chopper modulation dual-beam spectrometer. Dotted lines indicate optical paths and solid lines indicate the electrical circuit. The waveforms associated with the circuits are drawn beside the lines. B. Expansion of the double-pole double-throw relay inserted into the control lines from the chopper. Relay is shown in the normal configuration, i.e. leaves the flow cell designation at its original value.

'solvent' peaks (function 3) so that the integration is not terminated prematurely on the tail of the skewed peaks.

#### 2.2.4 Calibration Curves

In order to demonstrate their linearity calibration curves for phenylephrine and pheniramine were measured using the apparatus shown in Figure 2-1. Standards contained the two compounds of interest in varying concentrations and were matrix matched with the nasal spray samples. The matrix consisted of 0.15 M NaCl, 0.002% thimerosal, and 1:5000 benzalkonium chloride. The concentration of the components of interest in the standard solutions ranged from  $4.9 \times 10^{-3}$  M to  $2.82 \times 10^{-2}$  M for phenylephrine and from  $1.11 \times 10^{-3}$  M to  $6.44 \times 10^{-3}$  M for pheniramine. Peak areas and heights were measured for phenylephrine in the aqueous phase and for pheniramine in the organic phase for 10 replicate injections.

Instrument parameters for the calibration study were: nitrogen pressure, 62 psig; total chloroform flow,  $F_O$ , 2.4 mL/min; total aqueous flow,  $F_a$ , 2.5 mL/min; chloroform flow through membrane,  $F_{m,O}$ , 1.6 mL/min; aqueous flow through membrane,  $F_{m,a}$ , 1.4 mL/min; wavelength, 258.3 nm; absorbance range, 1.0; detector cycle, 60 s in the normal flow cell designation followed by 60 s in reverse designation, started at injection; extraction coil length, 200 cm; delay coil length, 700 cm; volume injected 10  $\mu$ L; sampling frequency, 30 inj/h; peristaltic pump speed, 300.

#### 2.2.5 Nasal Spray Assay

Nasal spray samples were injected into the instrument with no prior treatment. Important instrument parameters for the assay that differed from those used in the calibration were follows:  $F_O$ , 2.8 mL/min;  $F_a$ , 2.8 mL/min;  $F_{m,O}$ , 2.1 mL/min;  $F_{m,a}$ , 1.4 mL/min. A warm-up time of about 30 minutes is used after solvent flow is established.

When assaying nasal spray samples a calibration curve was not usually run. Instead, two standards were run, with concentrations of pheniramine and phenylephrine that "bracketed" the label claim values (i.e. 20% above and 20% below). The concentrations of pheniramine maleate and phenylephrine HCl in these standards were corrected using the assay values supplied by the manufacturer. Also all standards contained the same concentrations of benzalkonium chloride and thimerosal as are present in the nasal spray, and were made isotonic using NaCl. Peak areas and peak heights were measured for six injections of each standard solution and sample.

### 2.3 Results and Discussion

The modifications to the electronics of a dual beam photometric detector will first be discussed. Then, the instrument shown in Figure 2-1 will be discussed as it was used to characterize the extraction behavior of phenylephrine hydrochloride and pheniramine maleate in terms of pH and other instrumental parameters and to determine these two compounds in a commercial nasal spray.

#### 2.3.1 Detector Modification

Several approaches have been used to make dual measurements with one detector in *single phase* FIA [99,100]. All of the methods have in common the incorporation of a time delay between the two measurements by the detector and differ only in the manner in which the two sample streams are presented to the detector. In one method [99] the sample is passed successively through the sample and reference flow cells of the photometer, producing positive and negative peaks. However, the Schoeffel SF770 used herein, like many modern HPLC photometric detectors, utilizes an automatic gain control to maintain the effective power of the light source at a constant level over the entire spectral range [101]. In such an instrument the dc signal from the reference channel is compared with a fixed voltage and any change in this signal activates the automatic gain

control which alters the photomultiplier tube (PMT) sensitivity in the proper direction to restore the reference signal to its original level. Thus, if an absorbing species passes through the reference flow cell, the absorption will be met by an increase in the PMT gain resulting in a truncated negative peak. This is illustrated in Figure 2-6. These peaks were obtained by making injections of caffeine into the sample and the reference flow cells using the single phase FIA system (Sec. 2.2.2.2). Important instrument parameters are: aqueous carrier, distilled water; flow rate, 2.0 mL/min; sample, 30, 60, 90, 120 and 150 ppm caffeine dissolved in distilled water; injection volume, 10  $\mu$ L; wavelength, 264 nm and absorbance range, 2.0 AU. It can be seen that for the sample cell peak height increases in proportion to caffeine concentration, while in the reference cell absorbance increases, in a negative sense, for the 30 and 60 ppm injections, but has become nearly independent of concentration by about 90 ppm.

In order to obtain signals from both of the flow cells which would be analytically useful, the electronics of the detector had to be modified to allow electronic switching of the sample/reference designation of the flow cells. In a chopped dual-beam spectrophotometer, such as is shown in Figure 2-5, the incident light passing through the sample and reference channels is mechanically modulated by a chopper and focused on a single photomultiplier tube. The resulting output from the PMT is a pulsating electrical signal. Conversion of this signal into absorbance or transmittance information requires the identification of each pulse as coming from either the sample or reference flow cell. Demodulation of these pulses is accomplished using two clocking signals from the chopper drive. Interchanging these clocking signals reverses the portions of the chopper cycle identified with the sample and reference flow cell, resulting in a reversal of their designation, without otherwise affecting the detector performance. This interchange is accomplished by inserting a timer controlled double-pole double-throw relay across the two chopper control lines. Each throw of this switch requires less than 1.5 s, so that it is essentially instantaneous.



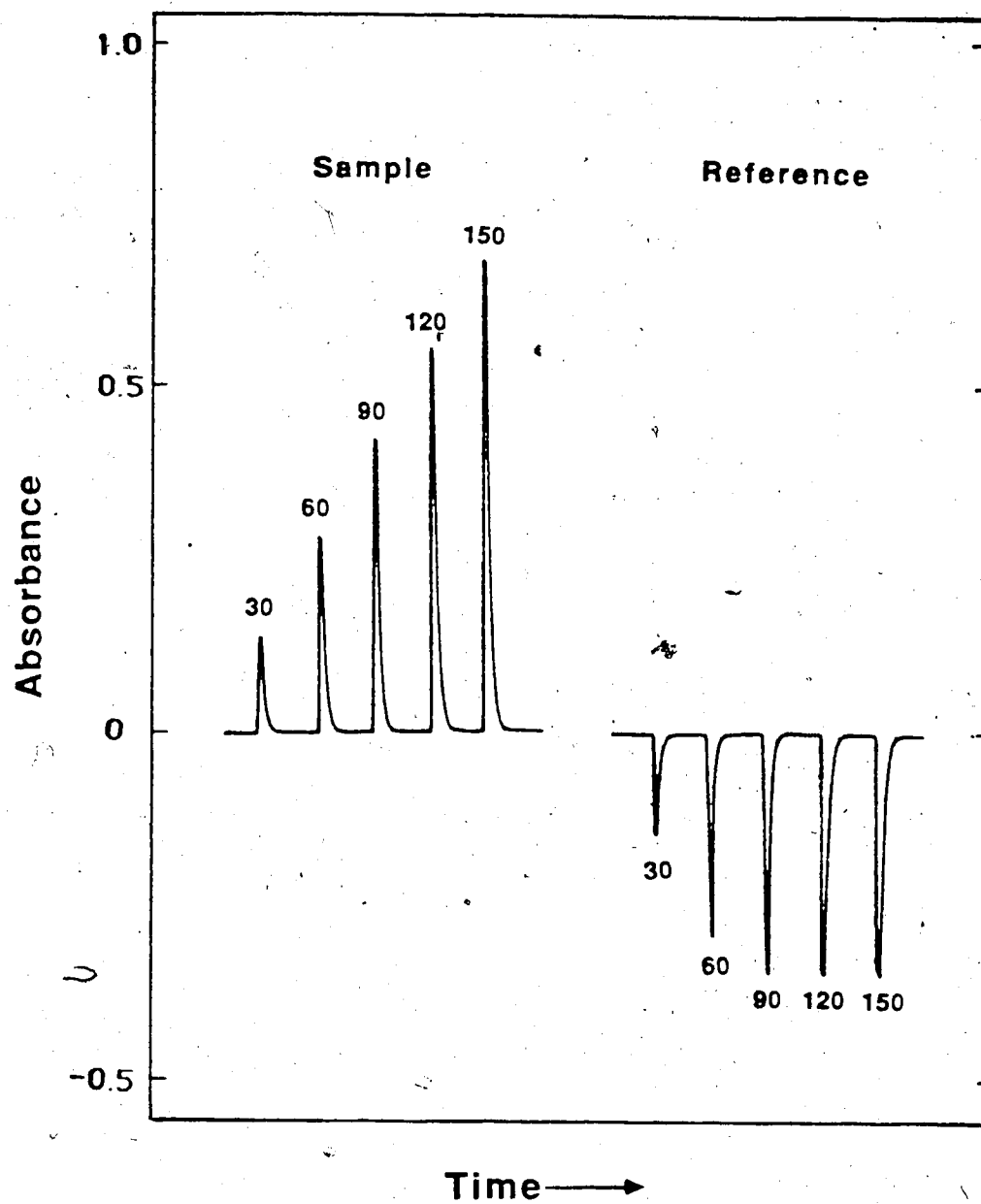


**Figure 2-6** Detector response to caffeine injections into the sample and reference flow cells in a single phase FIA instrument. Numbers on the peaks indicate the caffeine concentrations, in parts per million, injected into the instrument.

As an aside, it may be noted that if a spectrophotometer without automatic gain control were used, analytically useful signals would be obtained from both flow cells. However, conventional integrators cannot monitor negative peaks. Thus it would be necessary to include a timer controlled inverter, such as is shown in Figure 2-7, in the detector output line to produce positive peaks from both flow cells.

With the double-pole double-throw relay addition, the only additional requirement imposed by the SF770 detector in order that it may replace two separate detectors is the need to produce a time differential between the organic and aqueous signals. This time delay between the signals was produced by arranging the phase separators in series with a long length of tubing (Delay coil, D) between them (Figure 2-1).

### 2.3.2 Extraction coil length

The areas of peaks obtained in the chloroform phase upon injection of  $2.2 \times 10^{-3} \text{ M}$  aqueous pheniramine maleate into the instrument shown in Figure 2-1 was studied as a function of the extraction coil length. The reagent was pH 9.0 boric acid buffer. As can be seen in the next section, at this pH the free-base species of pheniramine should be quantitatively extracted at equilibrium.

Instrument parameters for the study were as follows: wavelength, 257 nm; sampling frequency, one injection per minute;  $\text{N}_2$  pressure, 40 psig;  $F_O \sim 2.0 \text{ mL/min}$ ;  $F_a \sim 1.8 \text{ mL/min}$  and  $F_{O,m} \sim 1.0 \text{ mL/min}$ . Since flow rates decreased somewhat with increasing extraction coil length, peak areas were corrected to  $F_O = 2.00 \text{ mL/min}$  using the relationship [20,46]:

$$A_O = \frac{K n}{F_O} \quad (2.1)$$

where  $A_O$  is the peak area in the organic phase,  $K$  is a constant,  $n$  is the number of moles injected and  $F_O$  is the total organic flow rate.

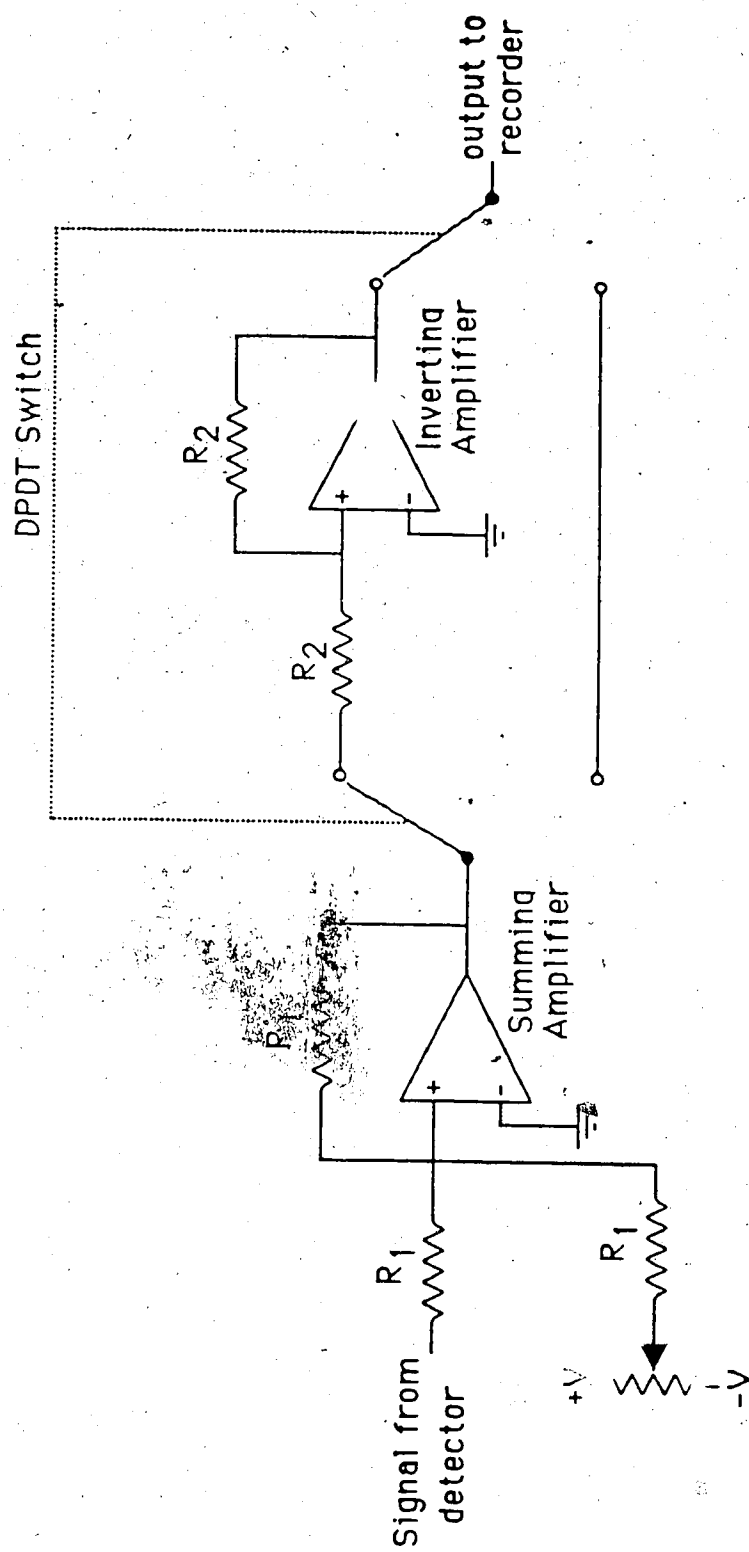
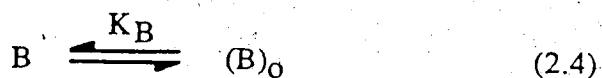
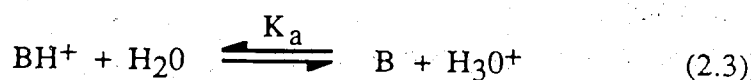
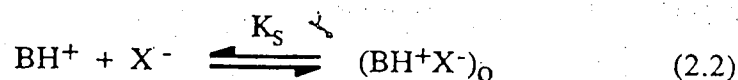


**Figure 2-7** Inverter circuit for dual photodiode spectrometer. Comprised of a summing amplifier, to produce an electronic null, and an inverting amplifier which can be switched into the circuit by a timer controlled DPDT relay.

The plot of corrected peak area in the organic phase versus extraction coil length is shown in Figure 2-8 for lengths between 5 and 330 cm of 0.8 mm i.d. Teflon tubing. Equilibrium is achieved by approximately 120 cm. An extraction coil length of 200 cm was used for subsequent studies and for the nasal spray assay.

### 2.3.3 Extraction pH

Since pheniramine is a weak base, the fraction of this compound extracted into chloroform depends on the pH of the aqueous phase as well as on the distribution coefficients of its two conjugate species,  $BH^+$  and  $B$ . The relevant equilibria are:



Species without a subscript are in the aqueous phase, while those with the subscript "o" are in the organic phase. The equilibrium constant for the extraction of pheniramine as the chloride ion pair into chloroform has been measured as  $10^{-0.1}$  [102]. Thus, given the relative low electrolyte concentration of the buffers used in this work, only the neutral free-base species,  $B$ , is significantly extracted, with a distribution coefficient previously reported as  $10^{3.8}$  [102]. The  $pK_a$  of  $BH^+$  has been reported as 9.3 [102].

A study of the dependence of pheniramine peak area in chloroform on the pH of the aqueous phase was performed with the solvent extraction / flow injection analysis system shown in Figure 2-1 using the multi-reagent pressure cylinder. Reagents used were citric acid/ $Na_2HPO_4$  buffers of pH values 3.86 to 7.56, and boric acid buffers of 8.54 and 10.1. Instrumental parameters for the study were  $F_O \sim 1.9$  mL/min,  $F_a \sim 1.7$  mL/min,

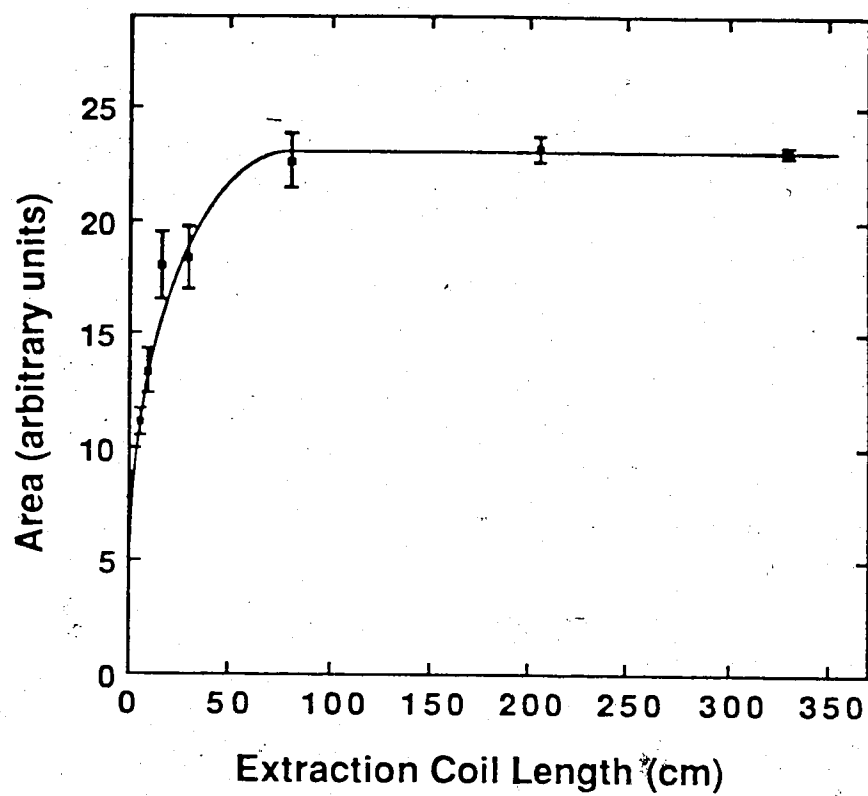


Figure 2-8 Peak area in the organic phase versus the extraction coil length for pheniramine. The error bars are the standard deviation in peak area for each point.

$F_{m,0} \sim 1.1$  mL/min, and extraction coil length = 200 cm. Replicate injections of a  $5.8 \times 10^{-3}$  M aqueous pheniramine maleate solution produced peaks in the organic phase, the integrated areas of which are plotted versus the aqueous reagent pH in curve A of Figure 2-9. It is evident from this plot that a reagent pH of 8 or greater results in the quantitative extraction of pheniramine into chloroform.

The sigmoidal dependence of the peak area in the organic phase,  $A_O$ , on pH has been shown [20,46] to follow the expression:

$$A_O = \frac{f b n \epsilon_{B,0} K_D K_a}{F_a a_H + F_a K_a + F_O K_D K_a} \quad (2.5)$$

where  $f$  is a response factor which relates the absorbance from the detector to a count rate on the integrator,  $b$  is the pathlength of the spectrometer flow cell,  $n$  is the number of moles injected,  $\epsilon_{B,0}$  is the molar absorptivity of the neutral form of the sample species in the organic phase,  $K_D$  is the distribution coefficient,  $K_a$  is the acidity constant,  $a_H$  is the hydrogen ion activity in the aqueous phase and  $F_O$  and  $F_a$  are the total flow rates in the organic and aqueous phases respectively. If  $K_D$  is large, as it is for pheniramine, equation 2.5 predicts that  $A_O$  will be zero at very low pH, will reach a plateau value of  $f b n \epsilon_{B,0} / F_O$  at high pH, and will have a value of  $f b n \epsilon_{B,0} / (F_O + F_a)$  at  $pH = pK_a - \log K_D$  on the rising portion of the sigmoidal curve.

A study of the effect of reagent pH on the extraction of phenylephrine hydrochloride by chloroform was performed in a manner similar to that used for the pheniramine study. This compound was found to remain quantitatively unextracted by chloroform at all reagent pH values, as is shown by curve B in Figure 2-9. This corresponds with previous studies which found that both distribution and ion pair extraction ( $X^- = Cl^-$ ) constant were less than  $10^{-2}$  [102].

On the basis of these studies a reagent pH of greater than 8 could be used in the nasal spray assay. However, between pH 8 and 12 the phenylephrine uv spectrum undergoes a

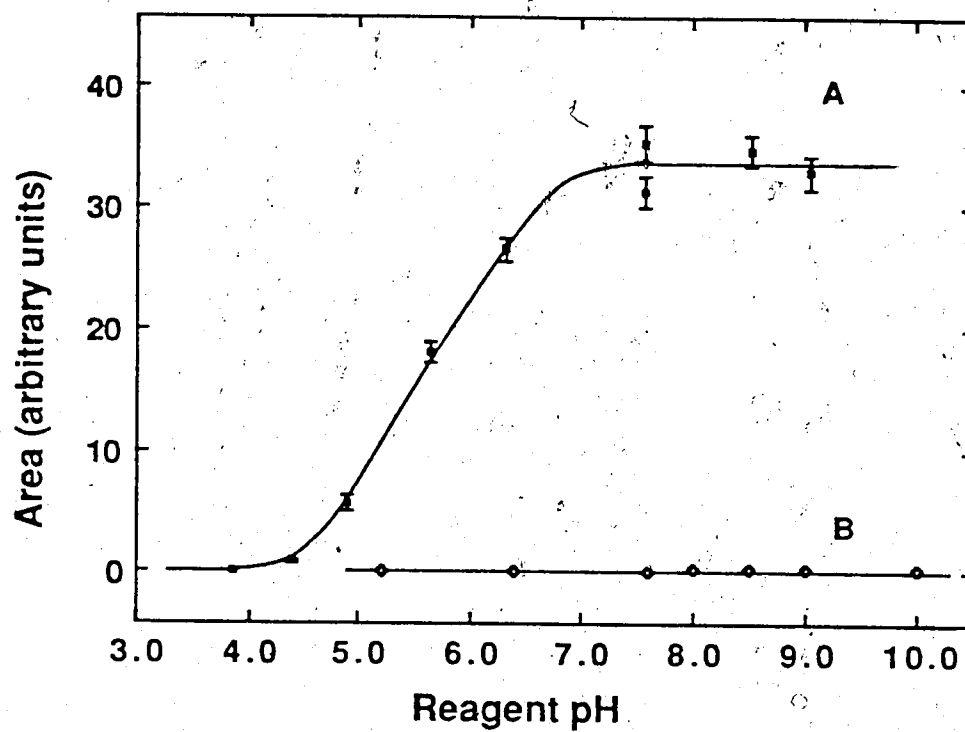


**Figure 2-9** Peak area in the organic phase versus aqueous phase pH for pheniramine (A) and phenylephrine (B). The error bars for A represent the standard deviation of the peak areas. For B the error bars are smaller than the plot symbol.

phenol-phenolate shift ( $pK_a$  of acidic phenolic group is 10.2 [102]. To avoid complications as a result of this spectral shift, the absorbances in subsequent studies were measured at the isosbestic point for phenylephrine (258.3 nm). However due to the 5 nm bandwidth of the photometer, it was subsequently found that a strongly alkaline reagent ( $\sim 0.1$  M NaOH) also had to be used to avoid spectral shifts.

#### 2.3.4 Interferences

Maleate, from the pheniramine salt, thimerosal, which is present in the nasal spray as a preservative, and benzalkonium, which is a disinfectant, were found to interfere with the analysis of phenylephrine and pheniramine. Maleate and thimerosal in the nasal spray formulation absorb at 258.3 nm. At concentrations found in the nasal spray this results in a spectral interference in the phenylephrine analysis of about 14%. Normally such a spectral interference would be eliminated by selecting the analysis wavelength such that the interferent had only a negligible absorbance. In this manner tartrazine interference in the analysis of 8-chlorotheophylline in Dramamine tablets was reduced to only 0.2% [42]. In the present case, however, there is only one detector and one wavelength which is dictated by the spectra of the two components to be analyzed. It would be difficult to have to select a single wavelength that would accommodate the interferents as well. The other interferent, benzalkonium chloride, is a cationic surfactant which, when injected into the instrument, caused the normally excluded aqueous phase to break through the porous Teflon membrane in the organic phase separator. Therefore this compound must be removed from the injected sample plug before it enters the two-phase region of the instrument.

Miniature ion exchange columns have been used to remove interferences in single phase FIA. For example, ion exchange has been used for the removal of anions which interfere in the analysis of calcium by atomic absorption spectroscopy [103] and to remove metal cations which interfere in the chemiluminescence detection of hydrazine by oxidation



with hypochlorite [104]. A separation protocol using ion exchange columns for the removal of the interferents in the nasal spray can be developed based on the acid dissociation characteristics of the compounds, which are shown in Table 2-1. At a neutral pH, as in the nasal spray formulation, maleate and thimerosal are in an anionic form, and so can be removed from the other three components using an anion exchange column (Figure 2-1). Of the three remaining components, only benzalkonium is cationic in the strongly alkaline reagent solution used for the extraction. Therefore use of a cation exchange column (Figure 2-1) will remove this last interferent, leaving phenylephrine anion and pheniramine neutral species to enter the segmentor.

To provide the pH conditions required by each column to remove the interfering species, two aqueous streams were used. The sample was injected into a distilled water stream from the multi-reagent cylinder, in which it flowed through column  $C_a$ . At tee-fitting  $T_1$  this flow stream merged with 0.2 M NaOH from the reagent cylinder. The resultant strong alkaline solution flowed through column  $C_c$ .

#### 2.3.4.1 Cation Column

The column design was patterned after that reported in the literature for the determination of free metals [98]. However since the ion exchange column in this work was not backflushed, it was possible to omit the inlet frit from the column construction. This deletion decreased the column dead volume, reduced the pressure drop across the column and made resin replacement much more convenient. Two cation exchange materials were tested - Amberlyst 15 macroporous polystyrene-divinylbenzene strong acid cation resin and carboxymethyl cellulose, a weak acid cation exchanger. The second exchanger was tested because it was anticipated that the neutral pheniramine species might adsorb onto the polystyrene-divinylbenzene Amberlyst 15 exchanger.

The cation exchange columns were studied using the single phase FIA system described in Section 2.2.2.2. Important instrument settings were: resin bed length, 5 mm

**Table 2-1** Acid Dissociation Behavior of Components of Nasal Spray

compound	pKa	ionic form in:	
		distilled water	0.1 M NaOH
phenylephrine cation (diprotic)	9.0, 10.2 <sup>a</sup>	cationic	anionic
pheniramine cation	9.3 <sup>a</sup>	cationic	neutral
maleic acid (diprotic)	1.8, 6.1	anionic	-
thimerosal	3.7 <sup>b</sup>	anionic	-
benzalkonium	-	cationic	cationic

a. Determined in reference 102.

b. Estimated using the Hammett equation:

$$pK_a = pK_a^o - \rho \sum \sigma$$

where  $pK_a^o$  and  $\rho$  equal 4.20 and 1.00 respectively for the benzoic acid parent compound and  $\sigma$  for the ethylmercuric thioether is estimated by that of the ortho substituent -SH,  $\sim 0.5$  [108].

in the 1.5 mm i.d. column - corresponds to 5.6 mg of Amberlyst 15 (Mesh >325) and 3.1 mg of the carboxymethyl cellulose; injection volume, 10  $\mu$ L; sampling frequency, one injection per minute; wavelength, 257 nm; reagent, pH 12.0 buffer (NaOH/KCl;  $\mu=0.06$ ); nitrogen pressure, 40 psig; flow rate, 1.2 mL/min; connecting tubing, 51 cm of 0.8 mm i.d. Teflon. The sample solutions were  $5.4 \times 10^{-3}$  M pheniramine maleate and 1:5000 benzalkonium chloride in distilled water.

Benzalkonium was quantitatively retained by the Amberlyst 15 resin, but only 30% was retained by the carboxymethyl cellulose resin. In addition, there was no evidence of adsorption of pheniramine on the Amberlyst resin, since peaks obtained with and without the column were equal. Therefore, polystyrene-divinylbenzene resins were used in the rest of the work discussed herein.

For 5 mm long resin beds of the 100-140 Mesh and >325 Mesh Amberlyst 15 cation exchanger, 92 injections of formulation levels of benzalkonium chloride could be made without the column being overloaded. Due to its lower pressure drop, the 100-140 Mesh resin was used in all future work. In the nasal spray analysis a larger column, with a 10 mm long resin bed, was used to ensure a column lifetime of at least 2 weeks. Varying the flow rate between 1 and 3 mL/min did not affect the column performance significantly.

#### 2.3.4.2 Anion column

The design of the miniature anion exchange column,  $C_a$ , was based on the results of the studies above. A 10 mm resin bed of 100-140 Mesh Amberlyst macroporous strongly basic, quaternary amine anion exchange resin was used in these studies. The emphasis in this work was to ensure that the maleate would be removed from the injection plug of nasal spray. Thimerosal is also removed by this column. However, since it is responsible for only a small fraction of the spectral interference, efforts were concentrated on the removal of the primary spectral interferent, maleate. The nasal spray formulation was isotonic [105] (ionic strength equivalent to that of nasal passages, 0.9 g/100 mL

[106] and of neutral pH (experimentally determined). Variation of the injection solution between pH 2.6 and 6.9 did not alter the quantitative removal of  $3.4 \times 10^{-3}$  M maleic acid. Therefore the maleate is removed quantitatively whether it is present as an anion or di-anion. Increasing the NaCl concentration of a  $5.6 \times 10^{-3}$  M pheniramine maleate solution from 0 to 0.9 g/100 mL reduced the number of injections which could be made with quantitative maleate removal. However, for the nasal spray formulation >30 injections could still be run with no evidence of the column capacity being exceeded. This was sufficient for a full analysis set of standards and samples to be run before regeneration of the column was required.

Anion exchange column regeneration was tested using the single phase FIA apparatus. A typical chart tracing for maleate regeneration is shown in Figure 2-10. The resin was equilibrated with the maleate solution until complete breakthrough of the anion was achieved, ~6 minutes. Distilled water was next used to rinse the column and then the maleate was eluted with HCl. The hydrochloric acid supplied the competing ion,  $\text{Cl}^-$ , and also protonated both maleate and thimerosal to their neutral acid forms (see Table 2-1) which were unretained. Maleate was completely removed from the column within two minutes for all acid concentrations tested. Thimerosal (not shown) required longer loading periods due to its lower concentration in the loading solution and was eluted more slowly. Therefore a 5 minute flush with 0.1 M HCl was used to regenerate the column in the nasal spray apparatus, followed by a 2 minute rinse with distilled water. As mentioned above, this regeneration was performed after about 30 injections.

Important instrumental parameters for the regeneration experiments were: nitrogen pressure, 40 psig; flow rate from multi-reagent cylinder, 1.4 mL/min; maleic acid loading solution,  $7.7 \times 10^{-3}$  M maleic acid, isotonic (0.9 g NaCl/100 mL) and adjusted to pH 7.0 using NaOH; thimerosal loading solution,  $5.1 \times 10^{-5}$  M thimerosal, isotonic and adjusted to pH 6.5; regeneration solution, 0.1 to 0.5 M HCl; and wavelength, 260 nm.

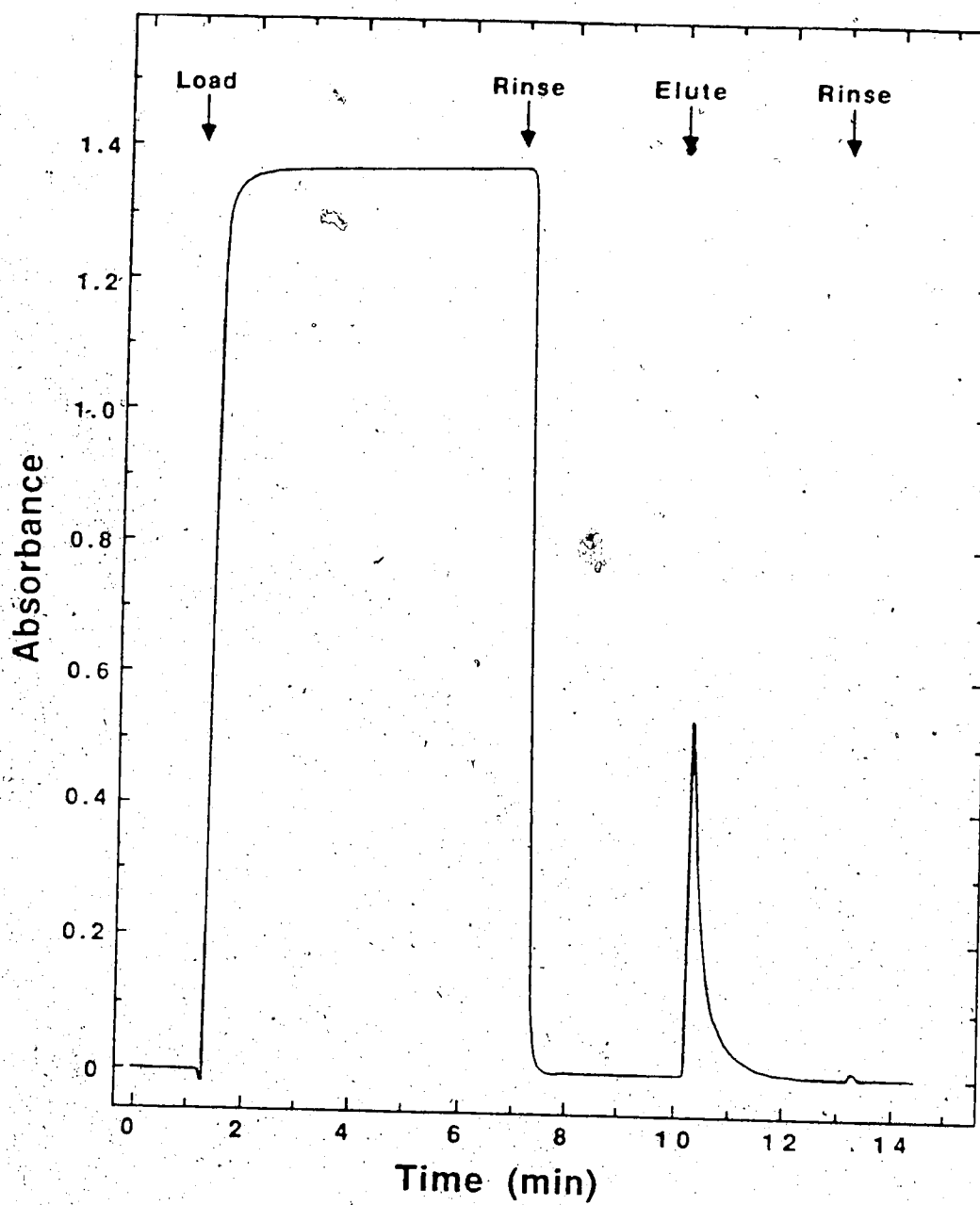


**Figure 2-10** Typical chart tracing for regeneration testing of Amberlyst 26 anion exchange column. Loading solution,  $7.7 \times 10^{-3}$  M maleic acid (isotonic and pH 7.0). Rinse, distilled water. Regeneration solution, 0.1 M HCL.

The merits of using peak height [19] and area [20] for quantification in solvent extraction/FIA have been discussed elsewhere. Both of these measures should be directly proportional to the sample concentration. Figure 2-11 shows the calibration curves for phenylephrine hydrochloride for area (curve A) and height (B). For both peak area and height, the curves are linear, with relative standard deviations of 2.0 and 0.7%, respectively, for the slopes. The y-intercepts and their 95% confidence limits, in arbitrary integrator units, were  $2017 \pm 8190$  for peak area and  $106 \pm 410$  for peak height. Pheniramine maleate also yielded linear calibration curves over the concentrations studied, as is shown in Figure 2-12. The relative standard deviations of the slopes of the calibration curves were 1.1% for peak area (Curve A) and 1.9% for peak height (Curve B). Both plots had y-intercepts equal to zero within their 95% confidence limits;  $246 \pm 4088$  for area and  $-301 \pm 1253$  for height.

### 2.3.6 Nasal Spray Assay

Results of the assay of three lots of commercial nasal spray, using the procedure described in the Experimental section, are shown in Table 2-2. All of the assay values are well within the tolerance limits of the label claims [107] for phenylephrine hydrochloride and pheniramine maleate. The agreement between the assay values obtained using peak area and peak height was very good, being within 1% in all cases. The precision of the analysis method, based on the standard deviations shown in Table 2-2 for the six replicate injections is better than 2% for phenylephrine HCl and pheniramine maleate using either peak area or height for quantification.

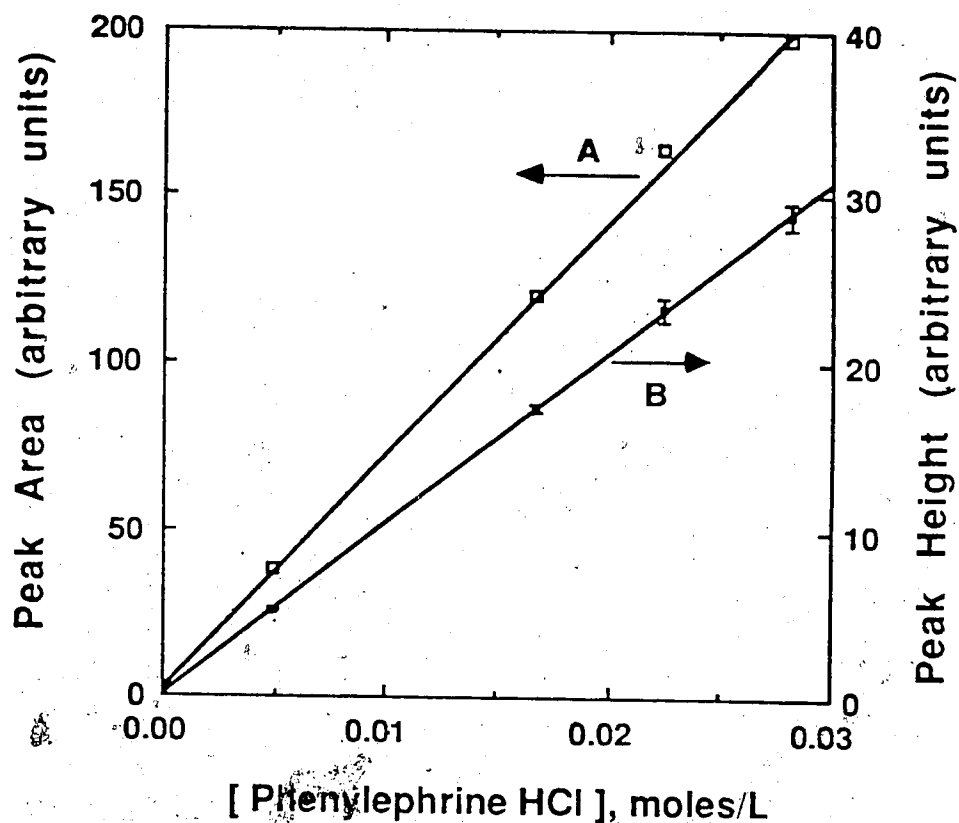


**Figure 2-11** Calibration curves for phenylephrine hydrochloride in the aqueous phase. Curve A is based on peak area, for which the standard deviations for each point range from 1.0 to 1.6 %. Curve B is the calibration plot based on peak height, for which the error bars are the standard deviations (0.8 to 2.9 %, relative).

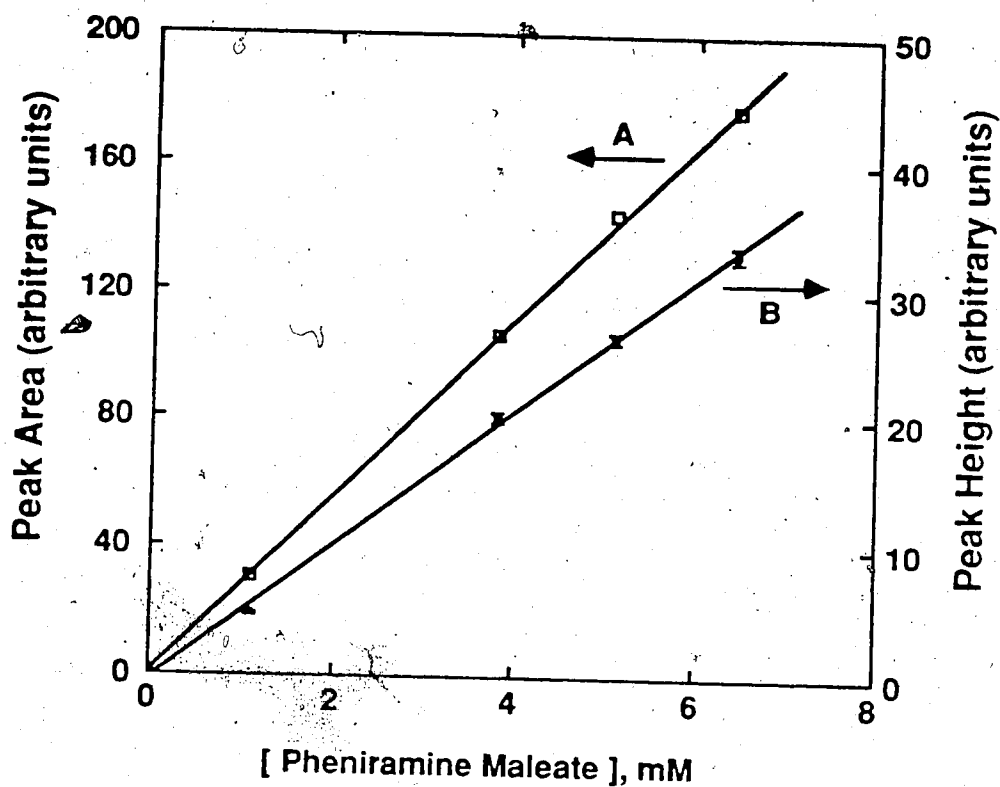


**Figure 2-12** Calibration curves for pheniramine in the organic phase. Curve A is based on peak area, for which the standard deviations for each point range from 0.5 to 1.5 % relative. Curve B is based on peak height data and the error bars indicate standard deviations ranging from 1.7 to 2.2 %, relative.



**Table 2-2** Determination of Active Ingredients in a Commercial Nasal Spray based on the use of Peak Area and Peak Height.

Sample	Phenylephrine HCl <sup>a,c</sup> (w/w%)		Pheniramine Maleate <sup>b,c</sup> (w/w%)	
	Area	Height	Area	Height
Lot A	0.477 ± 0.007	0.472 ± 0.002	0.198 ± 0.001	0.197 ± 0.001
Lot B	0.483 ± 0.005	0.481 ± 0.008	0.198 ± 0.002	0.199 ± 0.004
Lot C	0.481 ± 0.007	0.474 ± 0.002	0.201 ± 0.001	0.200 ± 0.001

- a. Label claim for phenylephrine HCl is 0.50% (w/w).
- b. Label claim for pheniramine maleate is 0.20% (w/w).
- c. ± are the standard deviations based on six replicates.

## 2.4 Conclusions

In this chapter a SE-FIA instrument for monitoring both phases of the segmented flow with only a single photometer was developed. Two membrane phase separators, arranged in series with a delay coil separating them, were used to direct the single phases from the segmented flow to the detector. Use of the single detector greatly reduces the cost of this instrument over previous instruments which required two photometers to monitor the two phases [42,42]. In addition, the detector modifications for switching the sample/reference designation of the flow cells of the detector is quite straight-forward, making it an attractive approach for other analytical techniques, such as valence chromatography, where both positive and negative peaks are obtained.

The instrument was applied to the analysis of the active ingredients of a commercial nasal spray, phenylephrine hydrochloride and pheniramine maleate. Precision and accuracy were 1-2% using either peak height or area for quantification. Sampling frequency was 30 injections/h. Miniature on-line ion exchange columns were found to be an attractive means for the elimination of ionic interferences in SE-FIA.

## Chapter 3

### Instrumental Band Broadening in a Solvent Extraction/FIA Instrument

#### 3.1 Introduction

One of the most important characteristics of an FIA method is its sampling frequency. This sampling frequency is dictated by the width of the elution peaks, which results from the band broadening properties of each instrumental component of the apparatus. Thus, in order to maximize the sampling frequency of an FIA method, it is necessary to minimize the individual instrumental contributions to the overall peak width [109].

In this chapter the band broadening characteristics of the SE-FIA instrument described in Chapter 2 is studied in order to identify which components most require further refinement if the analysis speed is to be improved. The components which must be considered are the injector, the connecting tubing, miniature ion exchange column, the extraction coil, the delay coil, the phase separators and the detector.

#### 3.2 Background and Data Analysis

The band broadening contributions of the various components of a flow injection instrument can be considered to operate independently [109]. That is, each band broadening process is unaffected by all other such processes.<sup>†</sup> Under these conditions the variance contributions of the individual instrument components can be added linearly. For instance, in a single phase FIA instrument the overall instrumental band broadening, expressed in variance, is [109]:

$$\sigma_{\text{FIA}}^2 = \sigma_{\text{injection}}^2 + \sigma_{\text{flow}}^2 + \sigma_{\text{detector}}^2 \quad (3.1)$$

---

<sup>†</sup> An example of band broadening processes which are not independent are the non-uniform flow pattern terms,  $H_{\text{eddy}}$  and  $H_M$ , of the rate equation for chromatography columns.

where  $\sigma_{FIA}^2$  is the variance associated with the full flow-injection system and  $\sigma_{injection}^2$ ,  $\sigma_{flow}^2$  and  $\sigma_{detector}^2$  are the variances associated with the injector, the flow and the detector.

A peak represents the distribution of concentration with time and is, therefore, a probability density curve. A probability density curve can be characterized by a series of statistical moments [110-113]. The ordinary moments are defined by:

$$m_k = \frac{\int_0^{\infty} c(t) t^k dt}{\int_0^{\infty} c(t) dt} \quad (3.2)$$

where  $m_k$  is the  $k^{th}$  ordinary statistical moment and  $c(t)$  is the concentration at time  $t$ .

Generally, only the zeroth and first ordinary statistical moments are used to characterize a probability density curve (i.e. a peak).

The **zeroth moment**,  $m_0$ , gives the area under the curve. However, it is self-normalized and so equals one. The **first statistical moment**,  $m_1$ , defines the center of gravity, or the mean, of the distribution. Greater information about the peak shape is obtained from higher statistical moments if these moments are measured about the center of gravity,  $m_1$ , of the peak. Such moments are referred to as central statistical moments and are mathematically defined as:

$$\bar{m}_k = \frac{\int_0^{\infty} c(t) (t - m_1)^k dt}{\int_0^{\infty} c(t) dt} \quad (3.3)$$

In general only the second, third and fourth central statistical moments are used to describe the shape of a peak.

The **second central statistical moment**,  $\bar{m}_2$ , is the variance,  $\sigma^2$ , of the distribution about the mean. Unlike more traditional methods of measuring peak variance

such as width-at-half-height and the tangent method, the second central statistical moment makes no prior assumptions about the peak shape. Thus, this procedure is a more accurate estimate of the variance when the peaks are asymmetric, such as they typically are in FIA. By way of illustration, Table 3-1 shows a comparison of peak variances determined by various calculation methods for peaks simulated using an exponentially modified Gaussian distribution with a  $\tau/\sigma = 0$  and 2 [114]. For the symmetric Gaussian peak ( $\tau/\sigma = 0$ ), all of these procedures accurately measure the peak variance. For the tailed peak ( $\tau/\sigma = 2$ ), the methods in which measurements are made lower on the peak, where the asymmetry is more pronounced, are more accurate estimators of the variance. However, moment analysis provides the correct peak variance since this procedure uses all of the peak for the determination.

However, while statistical moment analysis can give the most accurate estimate of peak variance, the precision of the method will be strongly dependent on factors such as noise [112,115,116], baseline drift or error [112,117], premature termination of data collection [116,118,119] and too few data points [116]. This sensitivity results from the fact that moment calculation incorporates a difference raised to a power. This power relation makes the higher statistical moments progressively more sensitive to noise such that, generally, moments greater than the fourth are not used, and those above the second must be used with great care.

The **third central statistical moment**,  $\overline{m}_3$ , provides information on the horizontal asymmetry (i.e. with respect to time) and the **fourth central statistical moment**,  $\overline{m}_4$ , is a measure of the vertical asymmetry of the probability distribution curve.

The skewness and excess are two moment-related quantities which are useful measures of the asymmetry of a peak, since they directly reflect deviations from a Gaussian profile. The skewness,  $S$ , is defined from the third central moment as:

**Table 3-1** Comparison of Variances calculated for Synthetic Peaks using Various Measurement Techniques<sup>a</sup>

calculation method <sup>b</sup>	Estimated Variance	
	symmetrical peak <sup>c</sup>	asymmetrical peak <sup>d</sup>
Inflection (two sigma)	1.0	0.44
Width at half height	1.0	0.46
Tangent	1.0	0.47
Height / area ratio	1.0	0.56
Four sigma	1.0	0.64
Five sigma	1.0	0.79
Asymmetry based	1.0	0.98
Second statistical moment	1.0	1.0

a. Based on results of Bidlingmeyer, B. A.; Warren, F. V., Jr. Anal. Chem. 1984, 56, 1583A-1596A.

b. For description of these calculation methods see reference 114.

c. Symmetrical peak is simulated using a Gaussian distribution (i.e. exponentially modified Gaussian with  $\tau/\sigma = 0$ ).

d. Asymmetrical peak is simulated using an exponentially modified Gaussian with  $\tau/\sigma = 2.0$ .

$$S = \frac{\overline{m}_3}{\sigma^3} \quad (3.4)$$

For a Gaussian probability distribution, S will equal zero. A positive value of the skewness indicates a tailing peak, and the magnitude of the skewness reflects the degree of tailing. For instance, the skewness of an exponential distribution (Poisson distribution with zero degrees of freedom) is 2 [113].

The excess, E, is a measure of the flatting of a peak and is defined from the fourth central statistical moment as:

$$E = \frac{\overline{m}_4}{\sigma^4} - 3 \quad (3.5)$$

The excess is an expression of the vertical asymmetry of a probability distribution, relative to that of a Gaussian distribution with the same variance. For a Gaussian distribution E equals 0. If the excess is positive, the curve is more "peaked" than a Gaussian peak of the same variance. For instance, for an exponential peak the excess is 6 [113].

The statistical moments defined by equations 3.2 and 3.3 are calculated using digitized signal, where  $c(t)$  is the concentration (i.e. detector signal) at time  $t$ ,  $dt$  is approximated using the time interval between successive points ( $\Delta t = 0.05$  s) and the integrals are evaluated numerically using Simpson's rule<sup>†</sup> [120] with integration limits set manually. The baseline is determined using linear regression of the data points outside the integration limits, in order to avoid errors due to drift [112,117]. The peaks are defined by more than 100 points to ensure maximal precision in the moments calculated [116].

---

<sup>†</sup> The 1/3 Simpson's rule integration is performed using the word INTEGRATE.DATA incorporated within the ASYST Scientific System (Macmillan Software Co., New York).

## 3.3.1 Chemicals and Solvents

Pheniramine maleate was used as received from Sigma Chemical Co. of St. Louis, Missouri and phenylephrine hydrochloride was used as received from Endo Laboratories of Garden City, NY.

Double distilled water, Chloroform and Methanol were as described in Chapter 2.

Other chemicals, including sodium hydroxide and hydrochloric acid, were analytical reagent grade.

The sample and carrier solutions used in the band broadening experiments are listed with the appropriate apparatus described in the next section.

## 3.3.2 Apparatus

The contributions of the individual instrument components of the nasal spray analysis instrument (Figure 2-1) to the overall observed variance of the peaks were measured using configurations of the instrument designed to isolate the individual band broadening contributions. The flow rates employed in these studies were the same as those used in the nasal spray assay described in Chapter 2. Experimental arrangements for measuring the variances, shown in Figure 3-1, were as follows:

$\sigma_{ID}^2$  (variance due to injector, detector and associated tubing): *Aqueous*.

The apparatus shown in Figure 3-1a was constructed from the nasal spray assay instrument (Figure 2-1) by disconnecting valve  $V_4$  from  $C_a$  and also disconnecting the detector from phase separator  $M_O$ . The tube from  $V_4$  was then connected directly to the detector and aqueous solutions of  $2.5 \times 10^{-3}$  M phenylephrine HCl and  $5.6 \times 10^{-4}$  M pheniramine maleate were injected into the aqueous flow stream. The peak variance observed was defined as  $\sigma_{ID}^2$  (aq).



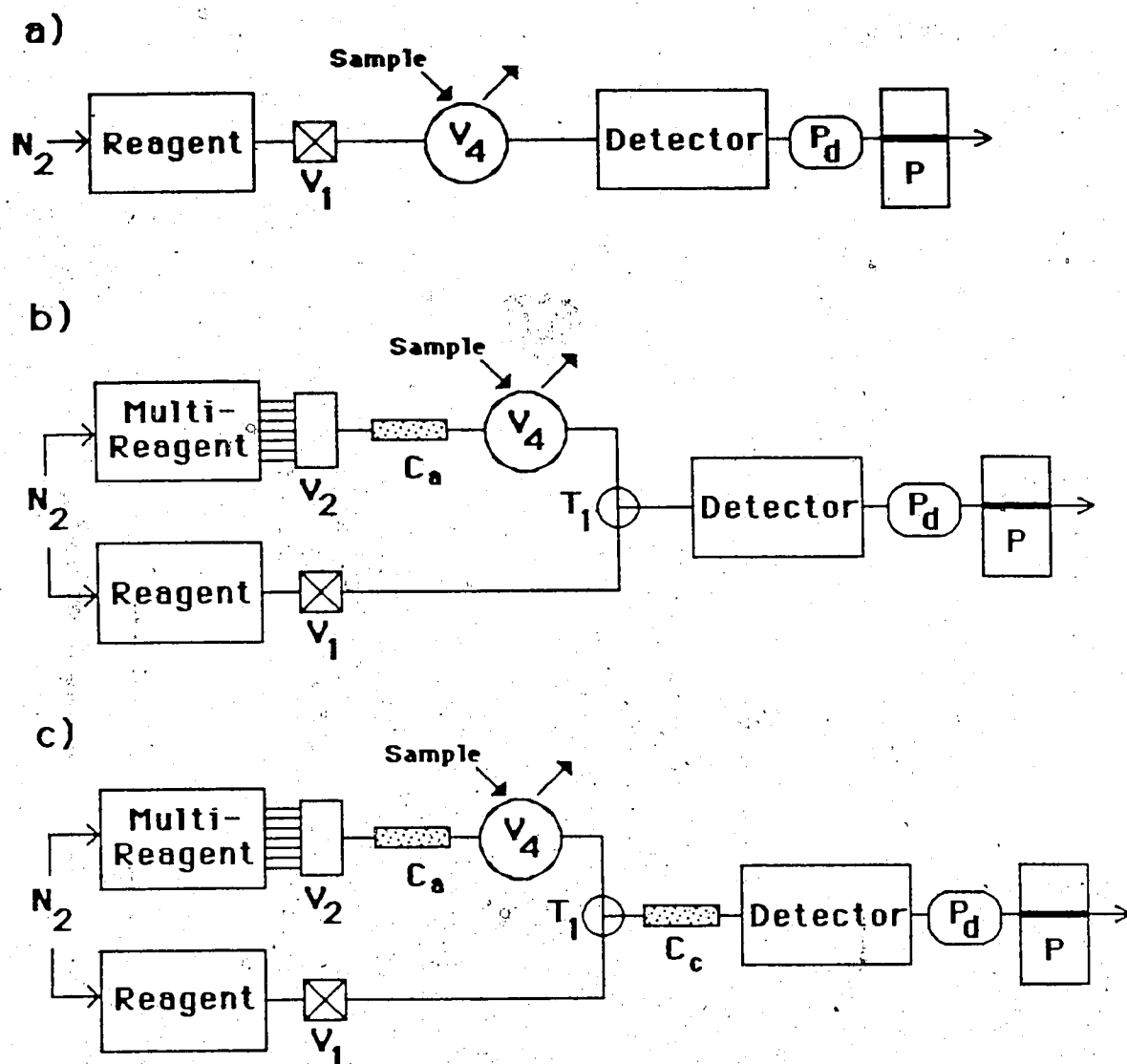


Figure 3-1 Instrumental arrangements for measuring the band broadening due to: a) injector, detector and connecting tubing ( $\sigma_{ID}^2$ ); b) tee-fitting ( $\sigma_{tee}^2$ ); c) cation exchange column ( $\sigma_{Cc}^2$ ). The reagent and multi-reagent cylinders contain aqueous carrier solutions under  $N_2$  pressure.  $V_1$  is a two-way valve;  $V_2$  is a six-port rotary valve;  $V_4$  is a slider injection valve;  $T_1$  is a tee fitting;  $P_d$  is a pulse damper;  $P$  is a peristaltic pump and  $C_a$  and  $C_c$  are miniature anion and cation exchange columns, respectively. See Sections 2.2.2.1 and 3.3.2 for details.

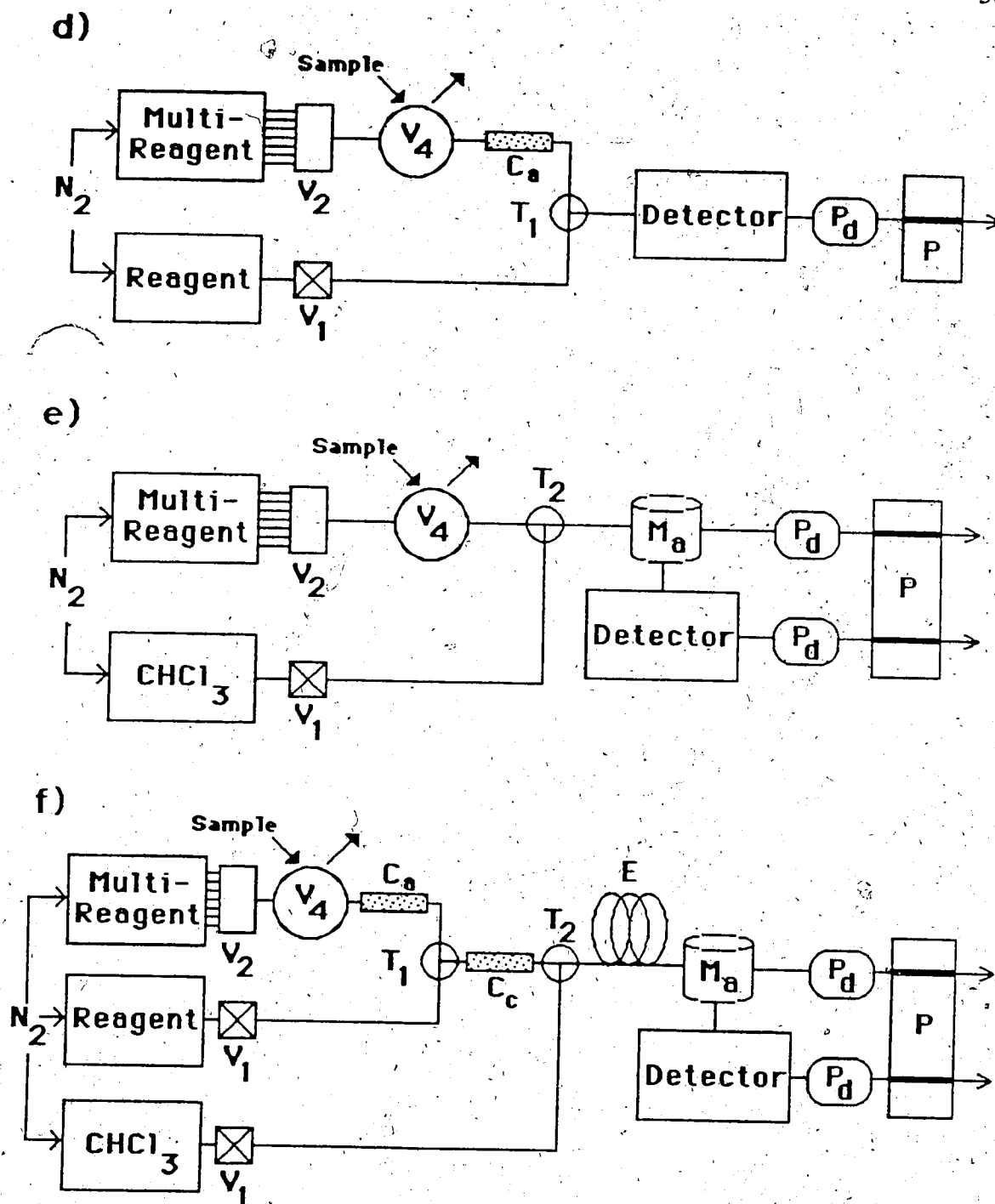


Figure 3-1b Instrumental arrangements for measuring band broadening due to: d) anion exchange column ( $\sigma_{Ca}^2$ ); e) aqueous phase separator ( $\sigma_{ps}^2(aq)$ ) and f) delay coil ( $\sigma_d^2$ ).  $M_a$  is the aqueous phase separator and  $E$  is the extraction coil.

**Organic:** The instrument configuration used was identical to that used for the determination of  $\sigma_{ID}^2$  (aq) (Figure 3-1a), except that flow came from the chloroform cylinder and  $5.6 \times 10^{-4}$  M pheniramine maleate in chloroform was injected into the organic flow stream. The peak variance observed was defined as  $\sigma_{ID}^2$  (org).

$\sigma_{ID}^2 + \sigma_{tee}^2$  The apparatus shown in Figure 3-1b was constructed from the nasal spray apparatus (Figure 2-1) using the following procedure: The tube from  $C_c$  was disconnected from  $T_1$  and the tube from the detector was disconnected from  $M_O$ .  $T_1$  and the detector tubing were connected together.  $C_a$  was moved from downstream of the injector to upstream, in order to remove its band broadening contribution but maintain its back pressure. Aqueous flow from the reagent and the multi-reagent cylinders are equal and merge at tee-fitting  $T_1$ .

The variance attributable to the tee (i.e. the difference between the variance measured for the apparatus shown in Figure 3-1a and that in Figure 3-1b was  $0.0 \pm 0.04$  s<sup>2</sup>. Thus the band broadening contribution of the tee-fitting was negligible.

$\sigma_{Cc}^2$  (variance due to cation exchange column): The required apparatus, shown in Figure 3-1c, was constructed from that in Figure 3-1b by placing the cation column  $C_c$  between tee-fitting  $T_1$  and the detector. Ten microliter plugs of  $2.5 \times 10^{-3}$  M phenylephrine HCl and  $5.6 \times 10^{-4}$  M pheniramine maleate in 0.1 M NaOH were injected into a 0.1 M NaOH carrier stream from the multi-reagent cylinder, which then merged with an identical aqueous stream from the reagent cylinder.  $\sigma_{Cc}^2$  was calculated as the difference between the observed variance and  $\sigma_{ID}^2$ .

$\sigma_{Ca}^2$  (variance due to anion exchange column): The apparatus, shown in Figure 3-1d, was obtained when  $T_1$  was disconnected from  $C_c$  and the tube from the detector was disconnected from  $M_O$ .  $T_1$  and the detector tubing were connected and  $\sigma_{Ca}^2$  was determined for  $2.5 \times 10^{-3}$  M phenylephrine HCl and  $5.6 \times 10^{-4}$  M pheniramine maleate in distilled water as the observed variance minus  $\sigma_{ID}^2$ .

**$\sigma_{ps}^2$  (variance due to the phase separator and segmentor  $T_2$ ): Aqueous.**

The tube from  $V_4$  was disconnected from  $C_a$  and was connected to  $T_2$  in place of  $C_c$ . The tube from  $T_2$  was disconnected from  $V_5$  and the tube from  $V_6$  was disconnected from  $M_a$ . The tube from  $T_2$  was connected to  $M_a$ . This apparatus is shown in Figure 3-1e. The  $2.5 \times 10^{-3} \text{ M}$  phenylephrine HCl sample in  $0.1 \text{ M}$  NaOH was injected into  $0.1 \text{ M}$  NaOH from the multi-reagent cylinder, which then merged with the chloroform flow at  $T_2$  and passed through 5 cm of 0.8 mm i.d. tubing to the aqueous phase separator. The aqueous flow rate was 2.8 mL/min and the organic flow was 0.7 mL/min, which corresponds to the composition of the two phase flow which exits  $M_o$ .  $\sigma_{ps}^2$  is the difference between the observed peak variance and  $\sigma_{ID}^2$ .

**Organic.** The same tubing arrangement as that of  $\sigma_{ps}^2$  (aq) was used.  $M_o$  replaced  $M_a$ , and the chloroform and multi-reagent cylinders traded places. A chloroform solution of  $1.1 \times 10^{-3} \text{ M}$  pheniramine maleate was injected into the chloroform stream, which merged with  $0.1 \text{ M}$  NaOH from the multi-reagent cylinder at the segmentor,  $T_2$ .  $\sigma_{ps}^2$  (org) was calculated as the difference between the observed peak variance minus the  $\sigma_{ID}^2$  (org).

**$\sigma_e^2$  (variance due to the extraction coil):** The extraction coil E (200 cm of 0.8 mm i.d. Teflon tubing) was inserted between  $T_2$  and the membrane phase separator in the arrangements described above for determining  $\sigma_{ps}^2$ .  $\sigma_e^2$  was calculated as the observed peak variance minus the total peak variance observed in the  $\sigma_{ps}^2$  studies.

**$\sigma_{total}^2$  (measured) (total peak variance):** the variance observed upon injecting samples into the instrument in the configuration shown in Figure 2-1.

**$\sigma_d^2$  (variance due to delay):** (Figure 3-1f) The tube from  $V_6$  was disconnected from  $M_a$  and E was disconnected from  $M_o$ . E was connected to  $M_a$ . Experimental conditions were otherwise as described for the nasal spray assay in Section 2.2.4 and the phenylephrine HCl sample was  $2.5 \times 10^{-3} \text{ M}$  in distilled water.  $\sigma_d^2$  is the

difference between the observed variance and the  $\sigma_{\text{total}}^2$  (measured) for phenylephrine HCl.

### 3.3.3 Data analysis

The moment analysis calculations were performed on an IBM-XT microcomputer using the program MOMENTS.ASY (Appendix A) written in ASYST (Macmillan Software Co.). Data were acquired digitally from the photometric detector using a Lab Master ADC interface board (TM-40-PGL, Tecmar, Cleveland, OH), controlled by the program DATACQ.ASY (Appendix B).

The accuracy of the zeroth through fourth statistical moments calculated by the program were verified using Gaussian, Exponential, and Poisson (1 and 2 degrees of freedom) statistical distributions as simulated peaks. The results of this comparison are given in Table 3-2. The accuracy of the peak second moment was further validated by comparison with the Sternberg graphical method [110]. This comparison is shown in Table 3-3 [121], and indicates that the variances produced by the program MOMENTS.ASY are a good estimate of the peak variance.

### 3.3.4 Procedure

As was discussed in Section 3.2, moment analysis is sensitive to experimental artifacts such as noise and baseline drift. Thus, a number of precautions were taken to minimize these effects over and above those which were necessary in order to analyze the nasal spray. These extra experimental precautions were: (i) A pulse damper (Model LP-21 LO-Pulse, Scientific Systems, Inc., State College, PA) was placed in-line between the instrument and the peristaltic pump to eliminate the flow pulsation which results from the pump action. (ii) The two aqueous carrier streams were of the same composition. This reduces the baseline shifts resulting from fluctuations in the refractive index of the carrier upon mixing with the reagent. (iii) The matrix of the sample solution

**Table 3-2 Validation of Moment Analysis Program using Known Statistical Distributions as Simulated Peaks.**

Statistical Function	Area	Center of Gravity	Variance	Skewness	Excess
Gaussian <sup>a</sup>	theor.	1.0	0.0	1.0	0.0
	calc.	1.000	0.000	0.999	0.000
Poisson <sup>b</sup> (n=1)	theor.	1.0	2.0	2.0	1.414
	calc.	1.000	2.000	1.9996	1.412
Poisson <sup>b</sup> (n=2)	theor.	1.0	3.0	3.0	1.155
	calc.	1.000	3.000	2.997	1.148
Exponential <sup>c</sup>	theor.	1.0	1.0	1.0	2.0
	calc.	1.000	1.000	1.000	2.00

a. The probability distribution,  $p(x)$  for a Gaussian distribution is given by [113]:

$$p(x) = \frac{1}{\sqrt{2\pi}\sigma} \exp - \left( \frac{x}{2\sigma} \right)^2$$

where  $x$  is the variable and  $\sigma$  is the standard deviation of the distribution.

b. The Poisson distribution is given by [113]:

$$p(x) = e^{-x} \left( \frac{x^n}{n!} \right)$$

where  $n$  is the degrees of freedom of the distribution.

c. The exponential is a Poisson distribution with zero degrees of freedom ( $n=0$ ).

**Table 3-3** Comparison of Variances for Peaks calculated using the Sternberg Graphical Method and by Moment Analysis<sup>a</sup>

Flow rate (mL/min) <sup>a</sup>	Estimated Variance (mL <sup>2</sup> )	
	Sternberg <sup>b</sup>	Moment Analysis
2.1	0.019	0.019
1.55	0.013	0.014
1.0	0.012	0.011
0.52	0.0097	0.010
0.43	0.0082	0.0080
0.055	0.0048	0.0049
0.0008	0.0051	0.0047

a. The peaks are chromatographic peaks taken from reference 121. Moments are calculated for  $1.1 \times 10^{-4}$  M methyl paraben eluting from a Hamilton PRP-1 column (15 cm x 4.1 mm i.d.) packed with 10  $\mu$ m particles, with a mobile phase of 90% methanol in water. The flow rate was varied in these experiments and is given in the first column of the table. The peaks were asymmetric, with an average skewness of 1.

b. For description of this calculation method see reference 110.

matched that of the carrier for similar reasons as in (ii). (iv) The output of the photometer was increased to 100 mV full scale by undersetting the absorbance range (eg. an absorbance range of 0.02 was typically used even though peak absorbances were typically ~0.1 AU). This output had much greater noise immunity than the normal 10 mVFS output produced by the photometer. A gain of 100 was then used at the ADC to make the signal 10 VFS which was required to fully utilize the range of the ADC.

An additional adjustment which had to be made is that the sample concentration had to be reduced to a tenth of the normal levels in the nasal spray formulation. Otherwise the maximum peak absorbances would exceed the linear absorbance range of the photometer, since the band broadening experienced by the sample in the simpler FIA manifolds used in these experiments is much less than in the full nasal spray instrument.

Experimental conditions were otherwise analogous to those used in the nasal spray assay procedure and were: sample injection volume, 10  $\mu$ L; sample concentration, listed with the various instrumental arrangements in Section 3.3.2; number of replicates, 4; total aqueous flow,  $F_a$ , 2.8 mL/min; total organic flow,  $F_o$ , 2.8 mL/min; flow through membrane of aqueous phase separator, 1.4 mL/min; flow through membrane of the organic phase separator, 2.1 mL/min; detection wavelength, 258.3 nm; full scale absorbance (see point iv above), 0.02 AU; data acquisition rate, 20 pt/s; number of points, 300-800 (typical value, 400) and gain setting, 100.

### 3.4. Results and Discussion.

The statistical moments obtained using these experimental conditions and the various arrangements of the experimental apparatus described in Section 3.3.2 are given in Tables 3-4 and 3-5 for pheniramine and phenylephrine, respectively. The variance is the measure of the band broadening, and will be the subject of the rest of this discussion. The skewness and excess were calculated and reported to provide a complete description of the peak.



**Table 3-4** Statistical Moments for Pheniramine Peaks Observed in the Band  
Broadening Studies of the Nasal Spray SE-FIA Instrument

Apparatus	Variance terms	Variance <sup>a</sup> (s <sup>2</sup> )	Skewness	Excess
Fig. 3-1b	$\sigma_{ID}^2$ (aq)	1.8 (0.2)	1.8 (0.2)	3.5 (1.0)
Fig. 3-1a	$\sigma_{ID}^2$ (org)	1.8 (0.1)	2.0 (0.1)	4.4 (0.7)
Fig. 3-1c	$\sigma_{ID}^2 + \sigma_{Cc}^2$	3.3 (0.3)	2.0 (0.1)	5.0 (0.5)
Fig. 3-1d	$\sigma_{ID}^2 + \sigma_{Ca}^2$	2.8 (0.3)	2.7 (0.3)	6.2 (4.2)
Fig. 3-1e	$\sigma_{ID}^2 + \sigma_{ps}^2$	3.9 (0.2)	1.7 (0.1)	3.5 (0.6)
	$\sigma_{ID}^2 + \sigma_{ps}^2 + \sigma_e^2$	5.0 (0.3)	1.7 (0.3)	3.3 (2.2)
Fig. 2-1	$\sigma_{total}^2$	7.6 (0.7) <sup>b</sup>	1.8 (0.2) <sup>b</sup>	4.7 (0.6) <sup>b</sup>

a. Mean and precision (expressed as the standard deviation) of the variance is based on 4 replicate injections.

b. Mean and precision for 7 replicate injections, rather than 4.

**Table 3-5 Statistical Moments for Phenylephrine HCl Peaks Observed in the Band Broadening Studies of the Nasal Spray SE-FIA Instrument**

Apparatus	Variance terms	Variance <sup>a</sup> (s <sup>2</sup> )	Skewness	Excess
Fig. 3-1a	$\sigma_{ID}^2$	1.5 (0.1)	1.5 (0.1)	2.6 (0.5)
		1.2 (0.1)	2.9 (0.6)	5.2 (4.0)
Fig. 3-1b	$\sigma_{ID}^2 + \sigma_{Cc}^2$	2.6 (0.2)	1.7 (0.3)	3.6 (1.8)
Fig. 3-1d	$\sigma_{ID}^2 + \sigma_{Ca}^2$	2.3 (0.3)	2.2 (0.3)	6.2 (1.4)
Fig. 3-1e	$\sigma_{ID}^2 + \sigma_{ps}^2$	5.1 (0.4)	1.0 (0.3)	1.7 (0.8)
Fig 2-1	$\sigma_{total}^2$	8.8 (0.5) <sup>b</sup>	1.1 (0.1) <sup>b</sup>	1.9 (0.7) <sup>b</sup>
Fig. 3-1e	$\sigma_{ID}^2 + \sigma_{ps}^2$	8.2 (0.2) <sup>c</sup>	1.4 (0.2)	2.6 (0.6)
	$\sigma_{ID}^2 + \sigma_{ps}^2 + \sigma_e^2$	8.3 (0.2) <sup>c</sup>	1.5 (0.2)	2.5 (0.5)
Fig. 3-1f	$\sigma_{total}^2 - \sigma_d^2$	10.9 (0.5) <sup>c</sup>	1.9 (0.3)	4.7 (0.5)
Fig 2-1	$\sigma_{total}^2$	13.0 (0.2) <sup>c</sup>	2.5 (0.1)	3.5 (0.6)

- a. Mean and precision (expressed as the standard deviation) of the variance is based on 4 replicate injections.
- b. Mean and standard deviation for 6 replicate injections rather than 4.
- c. These measurements, to determine  $\sigma_e^2$  and  $\sigma_d^2$ , were made before the injector/detector system had been optimized, so that  $\sigma_{ID}^2$  was larger than in the rest of the table. Thus these variances are larger than the rest in this table, but still the differences between each pair of values is due solely to the instrument component of interest.

### 3.4.1 Pheniramine Band Broadening

In the nasal spray analysis instrument pheniramine is injected as an aqueous phase sample and is subsequently extracted into the organic phase. A portion of this organic phase is separated from the two phase flow by a phase separator and directed to the detector. The total variance of the resultant pheniramine peak can be broken down into contributions from the various instrumental components of the system:

$$\sigma_{\text{total}}^2 = \sigma_{\text{ID}}^2 + \sigma_{\text{ps}}^2(\text{org}) + \sigma_{\text{e}}^2(\text{org}) + \sigma_{\text{Ca}}^2 + \sigma_{\text{Cc}}^2 \quad (3.7)$$

The definitions and values of these contributing variances for pheniramine are shown in Table 3-6. These values are obtained from those in Table 3-4 by the appropriate subtraction. For instance, the anion exchange variance,  $\sigma_{\text{Ca}}^2$ , is obtained by subtracting the variance observed for pheniramine shown in Figure 3-1a ( $\sigma_{\text{ID}}^2$ ) from that observed from the apparatus in Figure 3-1d ( $\sigma_{\text{ID}}^2 + \sigma_{\text{Ca}}^2$ ). The uncertainties of the individual band broadening terms are the standard deviations, which were calculated as the square root of the sum of the squares of the standard deviations of the measurements shown in Table 3-4.

The summation of the individual variances for the instrument components is equal to the  $\sigma_{\text{total}}^2$  measured for pheniramine, indicating that all significant sources of band broadening have been identified. In this instrument the injector/detector and phase separator variances are the most significant. This is consistent with results reported for liquid-liquid segmented postcolumn reaction detectors for HPLC detection [78,79].

The band broadening contributions of the injector and detector are combined in a single term,  $\sigma_{\text{ID}}^2$ , since it is impossible to make measurements without having both of these components in the instrument. In the complete instrument pheniramine is injected into the aqueous phase but passes through the detector as a chloroform solution.

However it is only possible to measure the injector/detector variance in homogeneous aqueous or organic streams, yielding  $\sigma_{\text{ID}}^2(\text{aq})$  and  $\sigma_{\text{ID}}^2(\text{org})$ . Since these two variables

**Table 3-6** Contributions to Band Broadening in the Nasal Spray SE-FIA Instrument

components	Variance <sup>a</sup> (s <sup>2</sup> )	
	Phenylephrine	Pheniramine
$\sigma_{ID}^2$ injector, detector and connecting tubing		
(aq)	1.8 (0.2)	1.3 (0.2)
(org)	1.8 (0.1)	
$\sigma_{ps}^2$ phase separator, segmentor		
(aq)		3.8 (0.5)
(org)	2.1 (0.3)	
$\sigma_e^2$ extraction coil		
(aq)		0.1 (0.3)
(org)	1.2 (0.3)	
$\sigma_{Ca}^2$ anion column	1.0 (0.3)	0.8 (0.3)
$\sigma_{Cc}^2$ cation column	1.5 (0.4)	1.1 (0.2)
$\sigma_d^2$ delay coil and $M_O$		2.1 (0.5)
summation	7.6 (0.7) <sup>b,c</sup>	9.2 (0.9) <sup>b</sup>
$\sigma_{total}^2$		
measured	7.6 (0.7) <sup>d</sup>	8.8 (0.5) <sup>e</sup>

a. Mean and precision, expressed as standard deviation, of the variance for 4 replicate injections.

b. Precision is the square root of the sum of the squares of the individual standard deviations.

c. An average of  $\sigma_{ID}^2(aq)$  and  $\sigma_{ID}^2(org)$  was used in calculating summation.

d. Based on six replicate injections.

e. Based on seven replicate injections.

have the same value,  $1.8 \text{ s}^2$ , this may be taken as  $\sigma_{ID}^2$  for pheniramine in the complete instrument.

The contribution to the overall peak variance from the extraction coil,  $\sigma_e^2$ , has particular significance in relation to the manifold design of the nasal spray system. In a liquid-liquid segmented flow stream one liquid forms a stationary film on the walls of the tube [21,22]. Movement of a solute dissolved in the film-forming liquid is retarded by this film so that some solute is transferred to subsequent segments, resulting in a broadening of the peak [21,22,26,27,122]. However, if the solute is in the non-film forming liquid minimal peak dispersion is observed [21-23]. The tubing being used in this work is preferentially wetted by chloroform making this the film forming phase. As can be seen in Table 3-6, pheniramine, which spends most of its time in the organic phase, undergoes significant broadening in the extraction coil; whereas phenylephrine, which remains in the aqueous phase, undergoes no measurable broadening. These considerations dictated placing the organic phase separator  $M_O$  between the extraction coil and the delay coil and the aqueous phase separator  $M_a$  after the delay coil, rather than vice versa. In this arrangement the pheniramine passes through a minimum length of tubing before being detected.

The variances corresponding to the phase separator and ion exchange columns will be discussed in Sections 3.4.3 and 3.4.5 respectively.

### 3.4.2 Phenylephrine Band Broadening

In the nasal spray assay, phenylephrine is injected as an aqueous phase sample and it remains unextracted as it passes through the instrument. For the phenylephrine peak, the total variance observed is then composed of a number of contributions:

$$\sigma_{\text{total}}^2 = \sigma_{ID}^2(\text{aq}) + \sigma_{ps}^2(\text{aq}) + \sigma_e^2(\text{aq}) + \sigma_{Ca}^2 + \sigma_{Cc}^2 + \sigma_d^2 \quad (3.8)$$

The definitions and values of these variances are shown in Table 3-6, using the experimental results presented in Table 3-5. For phenylephrine the sample passes through the injector and detector in the aqueous phase, so that  $\sigma_{ID}^2$  (aq) accurately describes its injector/detector variance. Otherwise equation 3.8 is the same as equation 3.7 for the pheniramine peak, with the addition of the term  $\sigma_d^2$ , the variance due to the aqueous phase sample passing through the organic phase separator,  $M_O$ , and the delay coil, D. Since phenylephrine experiences no detectable broadening in the extraction coil (200 cm of 0.8 mm i.d. Teflon tubing), one would suspect that the additional 2.1 s<sup>2</sup> of variance arises primarily in the organic phase separator rather than in the delay coil (700 cm of 0.8 mm i.d. Teflon tubing).

As with the pheniramine the summation of the individual variance terms agrees, within the 95% confidence limits with  $\sigma_{total}^2$  measured for the phenylephrine peak, indicating once again that all major sources of band broadening in the instrument have been identified. For the phenylephrine the major source of variance, apart from that associated with the delay, was the phase separator.

### 3.4.3 Phase Separator

The phase separators were observed to contribute significantly to the overall peak variances. This is not a surprising result since the relatively large dead volume of the phase separators (50  $\mu$ L) would be expected to cause significant band broadening. What is somewhat surprising however is the large difference in  $\sigma_{ps}^2$  for phenylephrine and pheniramine; 3.8 and 2.1 s<sup>2</sup> respectively.

In previous studies of the band broadening associated with phase separators, it was observed that the peak broadening varies inversely with the proportion of a phase removed from the two-phase flow [39,41] as is shown in Figure 3-2. In the nasal spray

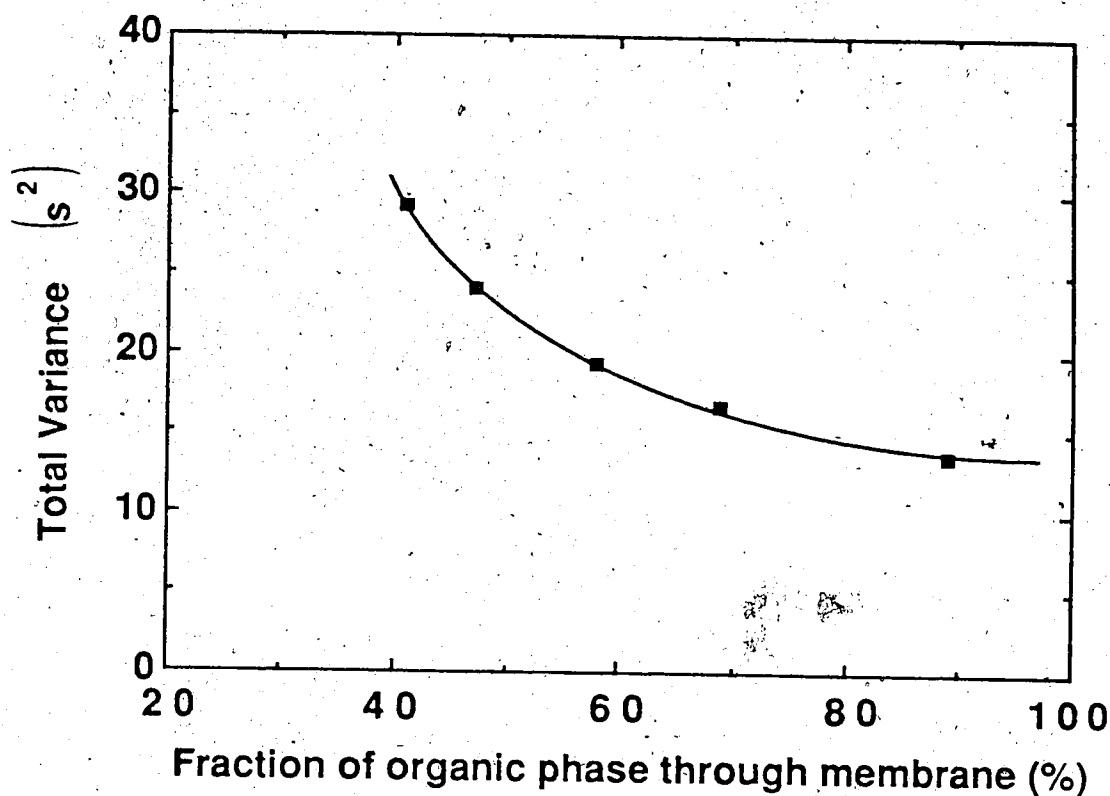


**Figure 3-2** Effect of percentage of organic phase passing through the membrane on the total peak variance, based on data presented in reference 41 for the extraction of  $3.6 \times 10^{-5} \text{ M}$  caffeine extracting from water to chloroform. Peak widths at 5% maximum were converted into variances by assuming a Gaussian peak shape for which the width would correspond to  $4.9 \sigma$ . Other important experimental conditions were:  $F_a$ , 0.83 mL/min;  $F_o$ , 1.07 mL/min; wavelength, 275 nm; and membrane phase separator, 35 x 1.2 x 0.5 mm grooves and 1.0  $\mu\text{m}$  pore size PTFE membrane with polyethylene backing.

by the start-up procedure employed. Unfortunately since the band broadening in reference 41 (Figure 3-2) was only quoted for the total SE-FIA system, it is not possible to determine how much of a change could be expected in the phase separator variance from this change in the fraction of the total flow which passed through the membrane.

Further studies [44] into the band broadening in membrane phase separators have concluded that when the separation efficiency of the phase separator is close to 100% (i.e. when almost all of one phase passes through the membrane), the band broadening occurs in the unsegmented part of the separator. However, when the separation efficiency is less than quantitative, as it was in the nasal spray instrument, the total volume of the phase separator will determine its broadening character. The shape of the cavities in the separator have only a minor affect on the band broadening.

#### 3.4.4 Injector/Detector Variance

The band broadening contributions of the injector and detector are combined in a single term,  $\sigma_{ID}^2$ , since it is impossible to make measurements without having both of these components in the instrument. However, some appreciation for the individual band broadening contributions which combine to yield  $\sigma_{ID}^2$  can be obtained from a theoretical treatment. The injector/detector variance is the summation of a number of instrumental band broadening terms:

$$\sigma_{ID}^2 = \sigma_{inj}^2 + \sigma_{det. cell}^2 + \sigma_{det. elec.}^2 + \sigma_{tubing}^2 \quad (3.9)$$

where the terms on the right hand side refer to the variance produced by the injector, the detector flow cell, the detector electronics and the connecting tubing, respectively. As a worst case (i.e. largest) approximation the injector and detector flow cell can be treated as a *mixing chamber* [110,123]. In this hypothetical device there is such rapid convection within the chamber, that any element of fluid entering the device is instantly mixed



throughout the chamber volume. The variance, in time units, produced by such a device is given by:

$$\sigma^2 = (V/F)^2 \quad (3.10)$$

where  $V$  is the dead volume of the device and  $F$  is the flow rate. Using this approximation for the injector (10  $\mu\text{L}$  dead volume) and detector cell (20  $\mu\text{L}$  dead volume for the flow cell and connectors) yields theoretical variances of 0.05 and 0.18  $\text{s}^2$ . This is very much smaller than  $\sigma_{\text{ID}}^2$  measured in the nasal spray apparatus (Table 3-6).

Detectors, recorders and amplifiers take a finite time to respond to an instantaneous change in their input. The response function of these electronic devices follows an exponential behavior and thus can be characterized by a time constant,  $\tau$ , which is time required for the signal to reach  $\frac{e-1}{e}$  of its final value. The variance associated with these slow electronics is given by [110]:

$$\sigma_{\text{elec}}^2 = \tau^2 \quad (3.11)$$

The time constant of the photometer used in these studies (Schoeffel SF770) is 0.5 s, and so according to equation 3.11 the associated variance would be 0.25  $\text{s}^2$ .

Laminar flow through long, straight connecting tubing is characterized by the Golay equation for a non-sorptive tube [110]:

$$\sigma_{\text{tube}}^2 = \frac{\pi r_t^4 L}{24 D_m F} \quad (3.12)$$

where  $r_t$  is the tube radius,  $L$  is the tube length,  $D_m$  is the molecular diffusion coefficient and  $F$  is the volumetric flow rate. The connecting tubing used in this work, however, is short and curved. Nevertheless, since the short tubing would tend to increase the variance contribution above that predicted by the Golay equation [124,125] and curvature on the tubing would tend to decrease the variance due to the tubing [124,126], the Golay

equation will serve as a useful first approximation of the variance attributable to the connecting tubing. Assuming a diffusion coefficient of  $5 \times 10^{-6} \text{ cm}^2/\text{s}$ , the 30 cm of 0.3 mm i.d. connecting tubing would be expected to produce about  $0.9 \text{ s}^2$  of band broadening.

These calculations indicate that the primary source of band broadening contributing to the injector/detector variance,  $\sigma_{ID}^2$ , is actually that produced by the connecting tubing. A similar result was observed for a segmented postcolumn reaction detector for HPLC [79]. The variance due to the connecting tubing and detector flow cell was  $250\text{-}300 \mu\text{L}^2$ , whereas that for the segmented flow system, including the phase separator was only  $150 \pm 20 \mu\text{L}^2$ . Thus, any effort made to improve the injector/detector band broadening in SE-FIA should be directed first towards the connecting tubing, rather than the miniaturization of either the injector or detector components.

### 3.4.5 Ion Exchange Columns

Two miniature ion exchange columns ( $C_a$ ,  $C_c$ ) were incorporated in the system to remove interferences, and tee-fitting  $T_1$  was added to provide the proper pH at each column for them to function. Each of the columns contributed to the overall peak variance as shown in Table 3-6. The tee-fitting was observed to produce negligible band broadening. The variances for pheniramine and phenylephrine in the cation exchange column differ significantly. Under the strong alkaline conditions present at this column, the phenylephrine is in the anion form and is excluded from the resin pores. Meanwhile pheniramine is in the neutral base form and so can diffuse into the resin bead, resulting in a larger variance contribution. For the anion exchange column both phenylephrine and pheniramine exists as the cationic protonated base, and so both are excluded from the resin pores. Thus for this column the observed variances for the two compounds were statistically the same. The band broadening contribution of the anion column was significantly larger than that of the cation column ( $\sigma_{Ca}^2$  for phenylephrine and

pheniramine vs  $\sigma_{Cc}^2$  for phenylephrine) and can only be attributed to slight differences in the construct of the columns.

However, overall the ion exchange columns contributed only a small proportion of the band broadening, showing them to be an attractive method of dealing with interferences in FIA systems.

### 3.5 Conclusions

Studies of band broadening by various components of a flow injection analysis instrument can reveal the factors which are limiting the sampling frequency of the assay procedure. For the solvent extraction/flow injection instrument developed for the analysis of phenylephrine and pheniramine, the active ingredients in a commercial nasal spray, the band broadening from the injector/detector system and the phase separators most limited the analysis rate. Thus these components are those which most need improvement.

Theoretical calculations and the literature have indicated that the connecting tubing is the major source of band broadening within the injector/detector system and so this component must be addressed first in order to reduce this band broadening term. For the phase separator, it is necessary to reduce the overall volume of the cavities in order to reduce the band broadening. In Chapter 5, an on-tube detector system will be discussed which greatly reduces the band broadening in SE-FIA by actually avoiding the phase separation step.

Finally, the miniature ion exchange columns have been observed to be an effective means of removing interfering species from the sample plug, with only a small additional contribution to the overall band broadening.

## Chapter 4

### Kinetics of Extraction in Solvent Extraction - Flow Injection Analysis

#### 4.1 Introduction

Research on the theory of solvent extraction-flow injection analysis (SE-FIA) has addressed the origin of phase segmentation [31], the dependence of peak area on flow rate [20], the factors influencing peak height [19], the efficiency of the separation process [23], the operation of the porous-membrane phase separators [127], and the band broadening which results from both film formation in the extraction coil [21,22] and from the dead volume of the phase separator [44]. Until recently, a gap in the theory of SE-FIA has been the lack of understanding of the extraction process itself, by which solute is transferred from the aqueous segments into the organic segments.

This process was recently investigated by Nord *et al* [29] for segments of 3 to 40 mm in length. It was found that extraction rate depends on two major factors - the ratio of interfacial area to volume, and mass transfer of solute to and from the interface. This work was apparently conducted using coiled extraction tubes. However, the convective/diffusive processes that control mass transfer were interpreted in terms of a simple toroidal circulation pattern within the segments, which in fact characterizes only segmented flow through straight tubes. Thus, while the major theoretical principles of solvent extraction in segmented flow have been established in the work of Nord *et al* [29], the significant contribution of secondary flow to the convection in coiled tubes, which has been well documented for air-water segmented flow [24,26,27], has apparently been overlooked. In addition, they studied only long segments (many times the tube diameter) and therefore did not observe the effects of the altered hydrodynamic conditions which occur in short segments. In this chapter, the role of secondary flow in this extraction process will be discussed, as well as extensive studies conducted using straight tube. Together these

studies provide a more detail and accurate physico-chemical model for the extraction process in SE-FIA.

## 4.2 Theory

### 4.2.1 Flow hydrodynamics

When two immiscible solvents flow concurrently through narrow tubing under laminar conditions, alternating segments of the two phases are formed. This flow is referred to as *segmented flow* [25] or *slug flow* [24]. The flow profile within segmented flow is influenced by a number of factors, including the tube wall, the segment ends, characteristics of the solvents and the degree and shape of the tube coil, and has "probably the most complex flow pattern" [128]. Despite this, segmented flow has been widely studied due to its importance in the biomechanics of blood flow in cardiovascular capillaries [129-131]. Red blood cells traveling through narrow capillaries act as barriers between segments of plasma, which are subject to the same influences as the segments within the SE-FIA apparatus.

#### 4.2.1.1 Segmented Flow

The equations governing the flow within a segment are the Navier Stokes equations and the equation of continuity [132]. The Navier Stokes equations are the differential form of Newton's second law of motion ( $F=ma$ ). In cylindrical coordinates, for which  $r$  is the radial coordinate,  $z$  the axial and  $\theta$  the azimuthal, they have the form:

$r$  direction (radial)

$$\rho \left( \frac{\partial v_r}{\partial t} + v_r \frac{\partial v_r}{\partial r} + \frac{v_\theta}{r} \frac{\partial v_r}{\partial \theta} - \frac{v_\theta^2}{r} + v_z \frac{\partial v_r}{\partial z} \right) = -\frac{\partial P}{\partial r} + \rho g_r + \eta \left[ \frac{\partial}{\partial r} \left( \frac{1}{r} \frac{\partial(r v_r)}{\partial r} \right) + \frac{1}{r^2} \frac{\partial^2 v_r}{\partial \theta^2} - \frac{2}{r^2} \frac{\partial v_\theta}{\partial \theta} + \frac{\partial^2 v_r}{\partial z^2} \right] \quad (4.1a)$$

$\theta$  direction (azimuthal)

$$\rho \left( \frac{\partial v_\theta}{\partial t} + v_r \frac{\partial v_\theta}{\partial r} + \frac{v_\theta}{r} \frac{\partial v_\theta}{\partial \theta} + \frac{v_r v_\theta}{r} + v_z \frac{\partial v_\theta}{\partial z} \right) = -\frac{1}{r} \frac{\partial P}{\partial \theta} + \rho g_\theta + \eta \left[ \frac{\partial}{\partial r} \left( \frac{1}{r} \frac{\partial(r v_\theta)}{\partial r} \right) + \frac{1}{r^2} \frac{\partial^2 v_\theta}{\partial \theta^2} + \frac{2}{r^2} \frac{\partial v_r}{\partial \theta} + \frac{\partial^2 v_\theta}{\partial z^2} \right] \quad (4.1b)$$

$z$  direction (axial)

$$\rho \left( \frac{\partial v_z}{\partial t} + v_r \frac{\partial v_z}{\partial r} + \frac{v_\theta}{r} \frac{\partial v_z}{\partial \theta} + v_z \frac{\partial v_z}{\partial z} \right) = -\frac{\partial P}{\partial z} + \rho g_z + \eta \left[ \frac{1}{r} \frac{\partial}{\partial r} \left( r \frac{\partial v_z}{\partial r} \right) + \frac{1}{r^2} \frac{\partial^2 v_z}{\partial \theta^2} + \frac{\partial^2 v_z}{\partial z^2} \right] \quad (4.1c)$$

where  $\rho$  is the fluid density,  $v$  is the velocity in the subscript direction,  $t$  is time,  $P$  is the total pressure,  $g$  is the gravity component in the subscript direction and  $\eta$  is the viscosity. The above equation assumes incompressibility, laminar flow and a Newtonian fluid (i.e.  $\eta$  is constant).

The continuity equation is the law of conservation of mass expressed in differential form. Expressed in cylindrical coordinates for an incompressible fluid it has the form:

$$\frac{1}{r} \frac{\partial(r v_r)}{\partial r} + \frac{1}{r} \frac{\partial v_\theta}{\partial \theta} + \frac{\partial v_z}{\partial z} = 0 \quad (4.2)$$

A number of simplifications can be made to the Navier Stokes and continuity equations for the flow within a segment. Gravity can be neglected since the physical scale of the flow is small. Also, bolus flow is axisymmetrical and steady, so that the velocity component in the  $\theta$  direction is zero and the overall flow is time independent. Thus the Navier Stokes equations are simplified to:

$$v_r \frac{\partial v_r}{\partial r} + v_z \frac{\partial v_r}{\partial z} = - \frac{\partial P}{\partial r} + \eta \left[ \frac{\partial}{\partial r} \left( \frac{1}{r} \frac{\partial (rv_r)}{\partial r} \right) + \frac{\partial^2 v_r}{\partial z^2} \right] \quad (4.3a)$$

$$0 = - \frac{1}{r} \frac{\partial P}{\partial \theta} \quad (4.3b)$$

$$v_r \frac{\partial v_z}{\partial r} + v_z \frac{\partial v_z}{\partial z} = - \frac{\partial P}{\partial z} + \eta \left( \frac{1}{r} \frac{\partial}{\partial r} \left( r \frac{\partial v_z}{\partial r} \right) + \frac{\partial^2 v_z}{\partial z^2} \right) \quad (4.3c)$$

and the continuity equation is simplified to:

$$\frac{1}{r} \frac{\partial (rv_r)}{\partial r} + \frac{\partial v_z}{\partial z} = 0 \quad (4.4)$$

For the flow of plasma in segments trapped between red blood cells through narrow capillaries, the Reynolds number is of the order of  $10^{-3}$  to  $10^{-2}$ . Under these conditions, the inertial forces due to convection of the plasma (i.e. left-hand side of equations 4.3) are much smaller than the stress due to viscosity, and so the left-hand side of equations 4.3 reduces to zero. The continuity equation is unaffected. While this assumption would not be strictly valid in the segmented flow in SE-FLA, which in this work operated at Reynolds numbers ranging from 50 to 150, it has been stated that for the related system of flow in square cavities, "the zero Reynolds number solution describes the basic features of the flow quite well for Reynolds numbers as high as 150" [129]. Therefore, the results obtained using the "creeping flow" assumption, in which the inertial terms are neglected, can be used to illustrate the basic features of the convection within segmented flow.

The red blood cells were modelled as moving rectangular solid cylinders of a radius equal to that of the capillary, and the fluid studied is that in the region between two moving boundaries (red blood cells). Results obtained with alternate models in which the moving boundaries were curved indicate that the rectangular model is a reasonable approximation for segments with curved ends [130], and so only the rectangular model results will be discussed herein. No-slip boundary conditions were assumed to apply along the walls of the tubing and at the faces of the moving boundary, i.e. the fluid immediately adjacent to these features has no velocity relative to that of the boundary and so the fluid is stationary at the walls of the tubing and moving at the mean velocity of flow at the face of the moving boundary.

Introduction of the stream function  $\Psi$  allows the combining of the Navier Stokes and continuity equations, which are then solved numerically [130,131]. The significance of the stream function  $\Psi$  is best understood in terms of its partial derivatives:

$$\frac{1}{r} \frac{\partial \Psi}{\partial r} = v_z \quad - \frac{1}{r} \frac{\partial \Psi}{\partial z} = v_r \quad (4.5)$$

where  $v_z$  is the axial flow velocity and  $v_r$  is the radial flow velocity. Thus, the change in the stream function in the radial direction is proportional to the velocity of the fluid moving down the tube, and the change in the stream function down the axis of the tube indicates the velocity at which fluid is moving out to the walls of the tubing. A plot of a path of constant  $\Psi$  represents a streamline. Figure 4-1 is a representation of the streamlines within a segment calculated by Bugliarello and Hsiao for four *segment aspect ratios* [130]. The aspect ratio is the segment length divided by the inner diameter of the tube ( $L_s/d_i$ ). The numbers on the streamlines are the relative values of the stream function  $\Psi$ . These segments are viewed from a reference frame moving at the average linear velocity of the flow.

From these plots it is possible to draw a number of conclusions about the flow within a segment [130]: i) The streamlines form a closed circuit, indicating that there is a



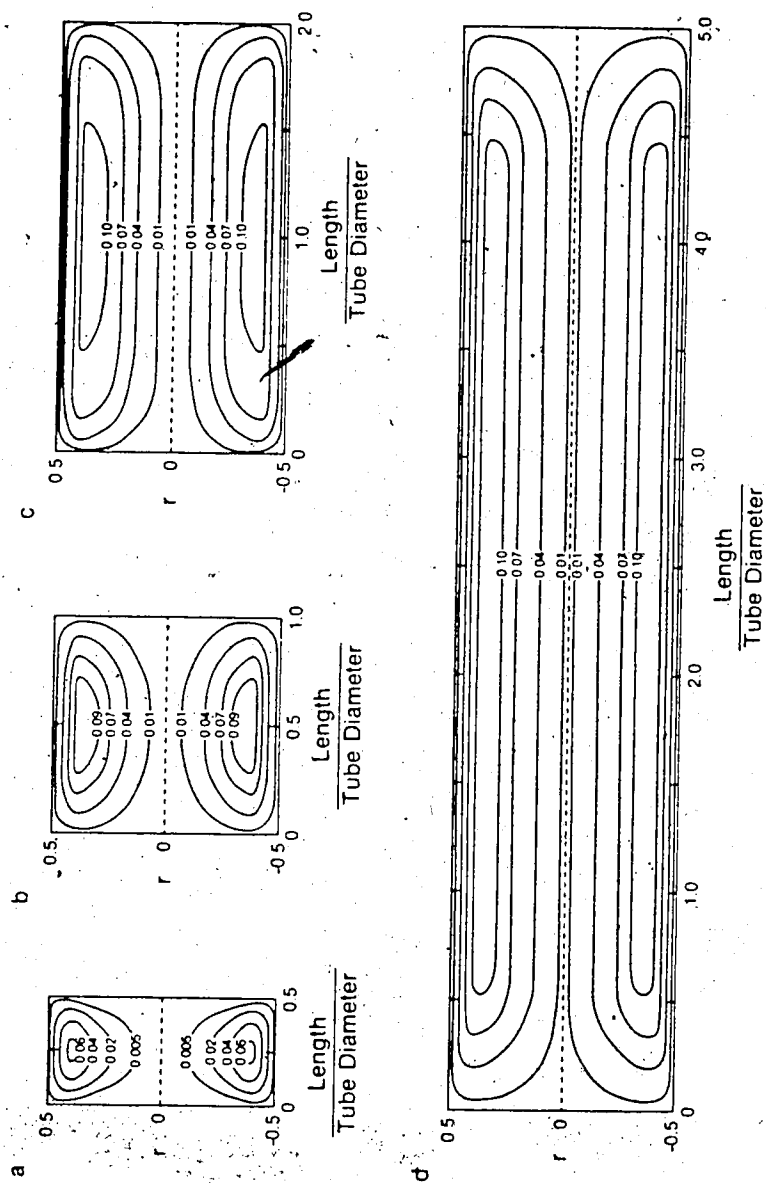


**Figure 4-1** Plots of the streamlines within segments of various lengths from the Navier Stokes hydrodynamic solution of the flow in the plasmatic gaps between red blood cells flowing through narrow capillaries for four different segment aspect ratios: (a) 0.5 ; (b) 1.0; (c) 2.0 and (d) 5.0 tube diameters long segments. Based on results of G. Bugliarello and G. C. Hsiao, *Biorheology* 1970, 7, 5-36.

circulating flow pattern within the segment, in agreement with experimental observations [21,25,26]. If the bulk flow is from left to right, circulation within the top circuit will be counterclockwise and that within the bottom circuit will be clockwise. This overall circulation pattern therefore forms a doughnut like shape and so will be referred to as "toroidal" flow in the rest of this discussion.; ii) As the relative distance between the ends of the segment decreases (Figure 4-1 d to a), the streamline patterns initially are unaffected. Along the mid-range of the longer segments (Figure 4-1 c and d), the streamlines are parallel to the walls, and show a radial component (i.e.  $d\Psi/dr$ ) only near the ends of the segment. However, as the segment length approaches the diameter of the tube the streamlines become less parallel with the walls of the tubing as a result of the ends interacting hydrodynamically [131] and generating radial mixing within the segment.

For longer segments the ends are isolated from one another, the radial velocity components throughout the transition are less significant [130], and the mid-segment axial flow adopts an approximately parabolic profile with the fastest flow at the center of the tube. This behavior can be seen in Figure 4-2 where the mid-segment velocity profiles predicted by the Navier Stokes equation [130] for segments of different lengths is compared with the Poiseuille velocity profile (dotted line). In segments on the order of the tube diameter in length, the ends interact hydrodynamically to generate more radial mixing within the segment resulting in more uniform axial flow within these segments.

#### 4.2.1.2 Secondary Flow

The flow velocity profile is parabolic (Poiseuille) in single phase laminar flow through straight tubing, with a linear velocity of zero at the walls and twice the mean linear velocity at the tube center. Thus, when this flow occurs through coiled tubing, the resultant centrifugal forces are greatest for the flow at the tube center. This fast moving fluid is thrown radially outward from the coil axis, and is replaced by recirculating fluid which flows along the walls [126,133], as is shown in Figure 4-3. A solution of the Navier

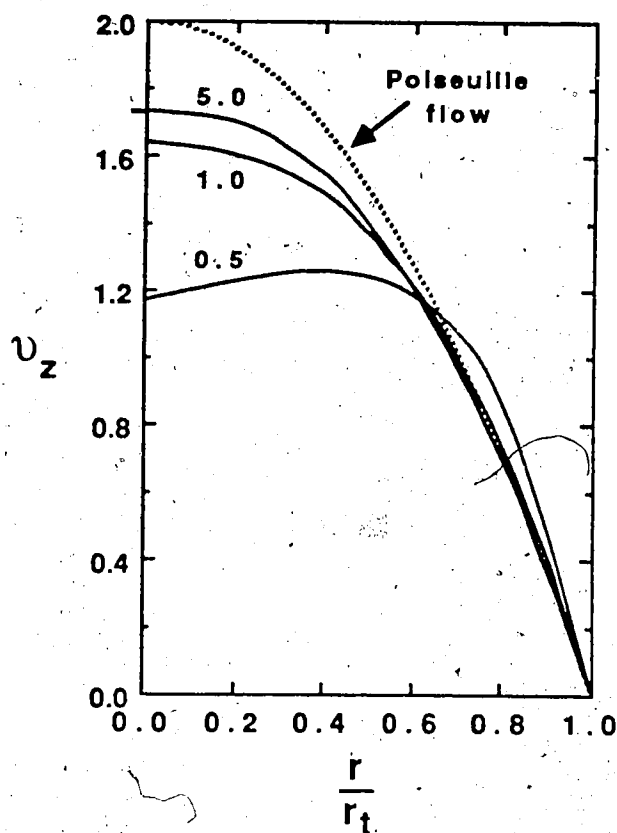


**Figure 4-2** Mid-segment axial velocity profiles for the flow within the plasmatic fluid between red blood cells in narrow capillaries for various segment aspect ratios. Dashed line indicates the velocity profile observed in Poiseuille flow. Solid lines are the profiles predicted by the Navier Stokes equation for the segment aspect ratios indicated on each curve. (Based on the results of G. Bugliarello and G. C. Hsiao *Biorheology* 1970, 7, 5-36.).

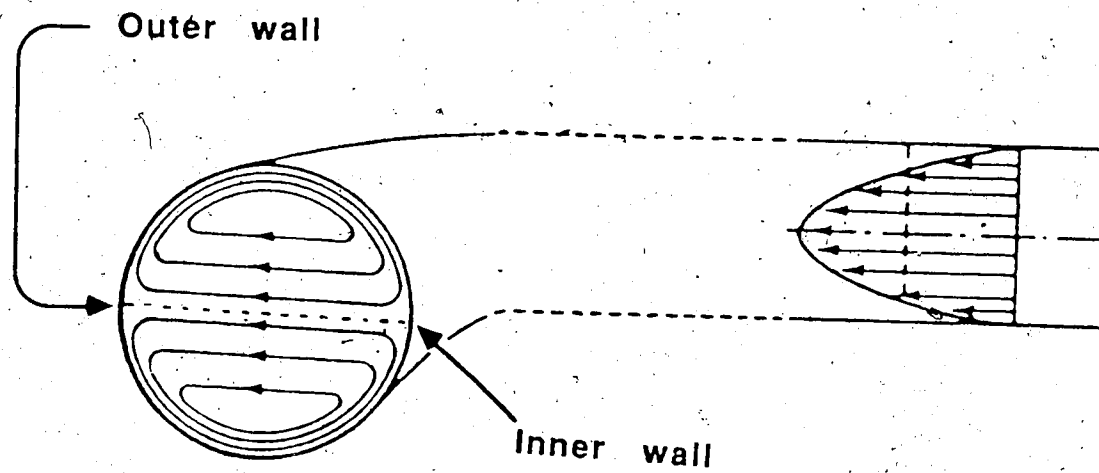


**Figure 4-3** Secondary flow patterns and velocity profiles for single phase flow through coiled tubing under flow velocities typical of the work done herein ( $De^2Sc \sim 10^5$ - $10^6$ ). Based on figure from R. Tijssen, *Anal. Chim. Acta* 1980, 114, 71-89.

Stokes equations for the primary (axial) and secondary (radial and tangential) flow patterns present within laminar flow through curved tubing has recently been presented [109,134,135].

Mass transfer in the presence of this secondary flow has been correlated with the dimensionless velocity parameter  $De^2Sc$  [126,133]:

$$De^2Sc = \left( Re \left( \frac{d_t}{d_c} \right)^{1/2} \right)^2 Sc = \frac{d_t^3 v^2}{\nu D_m d_c} \quad (4.6)$$

in which  $De$ ,  $Sc$  and  $Re$  are the dimensionless Dean, Schmidt and Reynolds numbers,  $d_t$  is the inner diameter of the tubing,  $v$  is the mean linear velocity of the fluid,  $\nu$  is the kinematic viscosity,  $D_m$  is the molecular diffusion coefficient and  $d_c$  is the coil diameter measured at the tube axis.

In segmented flow, the flow, in regions not near the segment ends, approaches a Poiseuille flow profile in longer segments. Thus, "secondary flow" develops within segmented flow in coiled tubes and augments the convection resulting from the toroidal circulation, such that the rates of solute mass transfer controlled processes within the segment are increased. For instance, in a study of band broadening occurring in air-water segmented flow, the mixing rate within the aqueous segments was markedly increased by coiling the tube [27]. Moreover, in studies of radial mass transfer to the walls of a coiled, wall-coated enzyme reactor, the secondary flow effects were found to be even greater for the flow of air-segmented aqueous solution than they are for unsegmented aqueous flow [24].

#### 4.2.2 Wetting Film Formation

In segmented flow, the solvent with the greater affinity for the wall material forms a thin "wetting film" on the walls of the tubing [21-23]. This film formation has significance for the extraction process since analyte can extract through the sides of the aqueous

segment into this film [29]. The thickness of the wetting film,  $d_f$ , of water in a glass capillary about an oil bubble has been found to be best predicted by [136,137] :

$$d_f = 0.67 d_t \left( \frac{v \eta_c}{\gamma} \right)^{2/3} \quad \text{for } 0.0002 < \frac{v \eta_c}{\gamma} < 0.002 \quad (4.7)$$

where  $d_t$  is the tube diameter,  $v$  is the linear velocity of the two phase flow,  $\eta_c$  is the viscosity of the continuous liquid and  $\gamma$  is the liquid interfacial tension. No appreciable change in the film thickness was observed when the viscosity of the bubble fluid was varied between 0.51 and 4.35 times that of the water [136]. The term  $v \eta_c / \gamma$  is known as the capillary number,  $Ca$ , and, for the work discussed in this chapter, ranges from 0.001 to 0.003. In chloroform/water segmented flow under conditions similar to those used in this work ( $v=11$  cm/s,  $d_t=0.7$  mm i.d. Teflon tubing), the observed chloroform wetting film thickness was 7  $\mu\text{m}$ . Using a viscosity of 0.58 cP and an interfacial tension of 32.8 dyn/cm [138], equation 4.7 predicts a film thickness of 7.3  $\mu\text{m}$ .<sup>\*</sup>

This film will not affect the circulation within the chloroform segments. Solutions to the Navier Stokes equation [139] have illustrated that the film thickness must be at least 5% of the tube diameter to have a significant affect on the toroidal circulation. Also the film experiences some convective mixing with trailing organic segments [26,27], and so the organic phase can be considered to be uniform, as is implicitly assumed in the following discussion of the extraction model. Thus, the significance of the wetting to the extraction process in SE-FIA is solely that it ensures that the organic phase completely surrounds each aqueous segment, and so extraction can occur via both the ends and sides of the segment.

---

<sup>\*</sup> In reference 22, the film thickness was actually compared with the wetting film equation of Snyder and Alder [26]. Their equation has an additional constant,  $\pi$ , in the right-hand side of equation 4.7, and so over-predicted the experimental film thickness by 3 times.

This film does have great significance with respect to the band broadening within the segmented flow, as will be discussed in Chapter 5.

#### 4.2.3 Extraction model

During segmented flow through Teflon tubing, a solute extracts from an aqueous segment through the ends of the segment into the adjacent organic segments and also through the sides of the aqueous segment into the wetting film of organic phase along the walls of the tube [29]. If no chemical reaction is involved in the solvent extraction process, or if the chemical reactions are very fast, the extraction will be governed by the mass transfer to and from the aqueous/organic interface. For conditions under which the diffusion coefficient is a constant (i.e. low solute concentration), mass transfer mediated processes follow an exponential behavior [140-143], and so can be mathematically treated in a similar manner to a first order chemical reaction even though no true chemical reaction is involved. The rate of extraction for a solute X is expressed as:

$$\frac{d[X]_o}{dt} = k_{\text{obs}} ([X]_{\text{eq},o} - [X]_{t,o}) \quad (4.8)$$

If concentrations are measured spectrophotometrically the integrated form of the extraction rate expression is:

$$\text{Ln} \left[ \frac{A_{\text{eq},o}}{A_{\text{eq},o} - A_{t,o}} \right] = k_{\text{obs}} t \quad (4.9)$$

where  $A_{\text{eq},o}$  and  $A_{t,o}$  are either the steady state absorbance or the peak area, due to the analyte in the organic phase at equilibrium and at time  $t$ , respectively, and  $k_{\text{obs}}$  is the observed extraction rate constant. This observed rate constant will be a function both of the mass transfer within the segments and of the interfacial area. Thus, it is more appropriate to express the extraction process in terms of a mass transfer coefficient,  $\bar{\beta}$  [142,143]. The mass balance for the extraction process would then appear as:

$$V \frac{d[X]_o}{dt} = a \cdot \bar{\beta} \cdot ([X]_{eq,o} - [X]_{i,o}) \quad (4.10)$$

where  $V$  and  $a$  are the volume and interfacial area associated with a single aqueous segment. Integration of 4.10 yields an analogous equation to 4.9 where:

$$k_{obs} = \bar{\beta} \cdot (a/V) \quad (4.11)$$

$\bar{\beta}$  has the units of a velocity term, and its reciprocal is often viewed as the "resistance to mass transfer" [141-143].

This overall mass transfer coefficient is related to individual mass transfer coefficients by the expression:

$$\bar{\beta} = \left[ \frac{1}{\beta_{aq}} + \frac{1}{\beta_o K_D} + \frac{1}{\beta_i} \right]^{-1} \quad (4.12)$$

where  $\beta_{aq}$  and  $\beta_o$  refer to mass transfer to the interface through the aqueous phase and away from the interface through the organic phase, respectively,  $K_D$  is the equilibrium distribution coefficient of the solute and  $\beta_i$  refers to transfer across the interface itself [141,144]. In the absence of surface active solutes  $1/\beta_i$  is negligible [141,144,145]. Furthermore, if  $K_D$  is large, as it usually is in SE-FIA, then  $(\beta_o K_D)$  is much larger than  $\beta_{aq}$ , and the organic phase acts like a "sink" for solute. Thus the extraction rate is governed by mass transfer within the aqueous phase only:

$$\bar{\beta} \approx \beta_{aq} \quad (4.13)$$

Since solute exits the aqueous phase via both the ends and the side of the aqueous segment,  $\beta_{aq}$  can be considered as the interfacially weighted sum of two aqueous phase mass transfer coefficients, one for axial mass transfer to the ends and one for radial mass transfer to the sides of the aqueous segment:

$$\beta_{aq} = \frac{a_{ends}}{a_{seg}} (\beta_{aq,axial}) + \frac{a_{side}}{a_{seg}} (\beta_{aq,radial}) \quad (4.14)$$



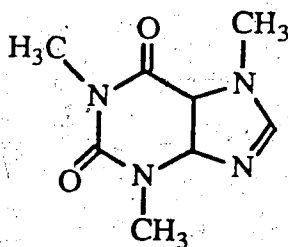
The radial component of the extraction is analogous to the radial mass transfer that has previously been studied in a wall coated open tubular enzyme reactor with air segmented flow [24].

Solute, once extracted into the organic phase, experiences band broadening. This is due to transport "backward" of organic solvent into following organic segments via the wetting film [21,22]. Similar phenomena have been reported in air segmented flow [26,27,122]. In spite of this band broadening, extraction rates, which are measured in the present work by monitoring the absorbance of the organic phase, correctly reflect the rate of extraction of solute out of the aqueous phase as long as the distribution coefficient of solute between the organic and aqueous phases is large. This is true whether the measured signal is a steady state absorbance, as used in experiments described below which employ constant feed, or whether it is a peak area, as used in experiments which employ sample injection.

### 4.3 Experimental

#### 4.3.1 Chemicals, Solvents and Reagents

Caffeine was analytical reagent grade and was used as received from the Aldrich Chemical Company (Milwaukee, Wisconsin). Its structure is:



Double Distilled Water, Chloroform and Methanol were as described in Chapter 2.

Other chemicals including citric acid (Caledon Laboratories, Ltd) and sodium hydroxide (BDH) were analytical reagent grade.

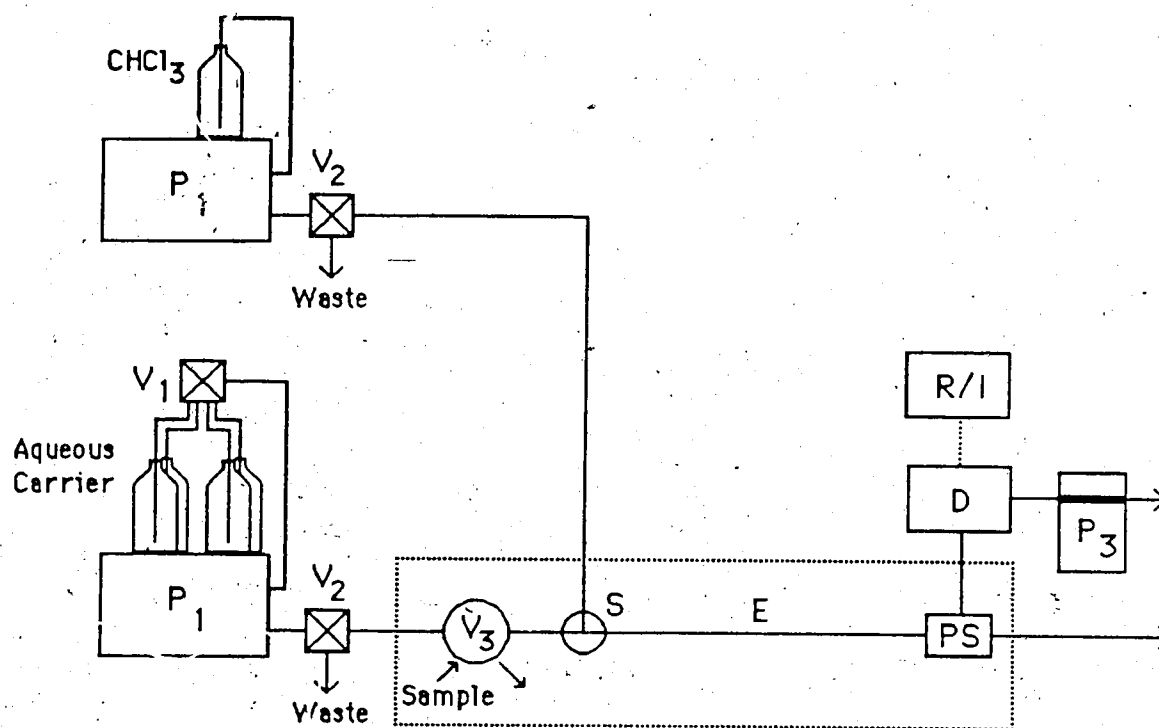
The pH 4.0 buffer, with an ionic strength of 0.1 and buffer capacity of 0.0085, consisted of 0.077 M citric acid adjusted to pH 4.0 with 2.0 M NaOH. The buffer was equilibrated with washed chloroform shortly before use.

Caffeine sample solutions were prepared in freshly made citrate buffer.

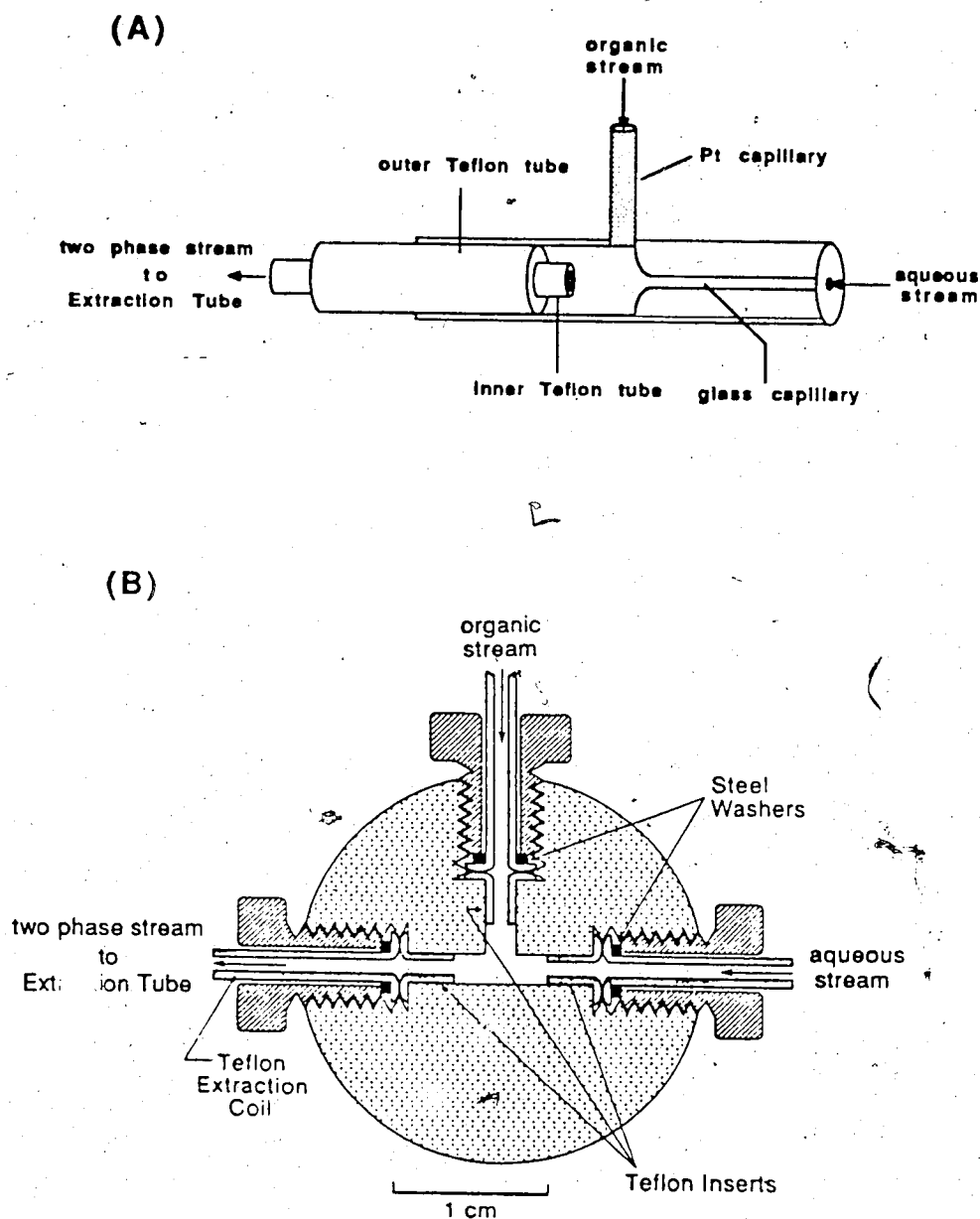
#### 4.3.2 Apparatus

Figure 4-4 provides a schematic diagram of the SE-FIA instrument used in these studies. Solvents are pumped using two liquid chromatographic pumps,  $P_1$  and  $P_2$  (Model B-100-S, Eldex Laboratories, Inc., San Carlos, CA), equipped with pulse dampers (Model LP-21 LO-Pulse, Scientific Systems, Inc., State College, PA). Restrictor columns (15 cm x 1 mm i.d. x 1/4 inch o.d. packed with 40  $\mu$ m glass beads), not shown in the diagram, ensure sufficient backpressure for proper action of the pumps and pulse dampers. Valve  $V_1$  (part no. R6031 V6, Laboratory Data Control (LDC), Riviera Beach, FL) is a six-port rotary valve which allows selection of any one of a number of solutions as the aqueous carrier stream. Valves  $V_2$  (part no. CAV3031, LDC) are three-port valves which direct flow to either the extraction system or to waste. Valve  $V_3$  (part no. CSA-10, LDC) is a 10  $\mu$ L slider injection valve which is actuated by an air solenoid valve (part no. SOL-3-24-VDC, LDC) controlled by an electronic timer [20].

The two solvent streams meet at the segmentor, S. Both Technicon A-8 [16,18,23,24] and tee design [31] segmentors, shown in Figure 4-5, had to be used to produce the range of segment lengths studied. The Technicon A-8 connectors consists of a glass tube with three openings. The aqueous phase enters through a glass capillary and the organic stream enters through the platinum capillary, which is perpendicular to the former. A Teflon tube (2 cm x 2.2 mm o.d. x 1.6 mm i.d.) is inserted into the outlet of the T-connector. A second 1/16 inch o.d. Teflon tube is inserted into the first one. The length of the segments



**Figure 4-4** Schematic diagram of SE-FIA instrument used for kinetic studies.  $P_1$  and  $P_2$  are single piston reciprocating pumps;  $V_1$  is a six-port rotary valve;  $V_2$  are three-port valves;  $V_3$  is a slider injection valve;  $S$  is the segmentor;  $E$  is the extraction tube;  $PS$  is the organic phase separator;  $D$  is the photometric detector;  $R/I$  is either a recorder or integrator and  $P_3$  is a peristaltic pump. Dotted line indicates portion of instrument thermostatted to  $25 \pm 1^\circ\text{C}$ . See Section 4.3.2 for further details.



**Figure 4-5** Segmentors used in the kinetic experiments: (A) Technicon X-8 adjustable segmentor and (B) "Tee" design segmentor. Based on figure from F. F. Cantwell and J. A. Sweileh, *Anal. Chem.* 1985, 57, 329-331.

produced by this segmentor was a function of the flow rates of both solvents, the volume of the chamber (which was varied by the position of the inner insert) and the area of the wetting surface available to the organic phase (which was generally varied by moving the inner insert tube but could also be adjusted using the outer Teflon tube).

The tee design segmentor and the factors which affect its segmentation have been discussed in the literature [31]. In the tee segmentor, shown in Figure 4-5B, the three arms of the Kel-F tee are 1/16" in diameter. The organic phase enters perpendicular to the inlet aqueous stream and the outlet of the two phase flow. Short inserts of flared 1/16 inch o.d. Teflon tubing were inserted into the three branches of the tee. These inserts help to stabilize the regularity of segmentation. In addition, varying the length and internal diameter of the inserts allowed segments of various lengths to be produced. The segment length was also varied by using tee segmentors with arm-diameters other than the 1/16" shown in Figure 4-5. In these segmentors no inserts were used.

The resulting segmented flow passes through the extraction tube, E, (Figure 4-4) in which the extraction between the aqueous and organic phase occurs. Various lengths of 0.3, 0.5, 0.8 and 1.0 mm i.d. Teflon tubing were used as the extraction tube. These tubes were held straight in all studies, except those specifically examining the effect of coiling. Coiled tubing was helically wound around a cylindrical template and held in place with elastic bands.

After exiting the extraction tube, the segmented flow stream enters the porous membrane phase separator, PS, where a portion of the organic phase is separated. The phase separator is based on a design described by Apffel *et al* [33] and is shown in cross section in Figure 4-6. One piece of 4-mil, 10-20  $\mu\text{m}$  pore size Teflon membrane (Zitex, No. E249-122, Chemplast Inc., Wayne, NJ) is sandwiched between two 1.2 mm thick Teflon templates, which are in turn between two Kel-F body pieces. The main body pieces are pressed together with four screws and two stainless steel end plates. Three threaded holes accept standard polypropylene end-pieces (part no. TEF 107, LDC) and flared Teflon

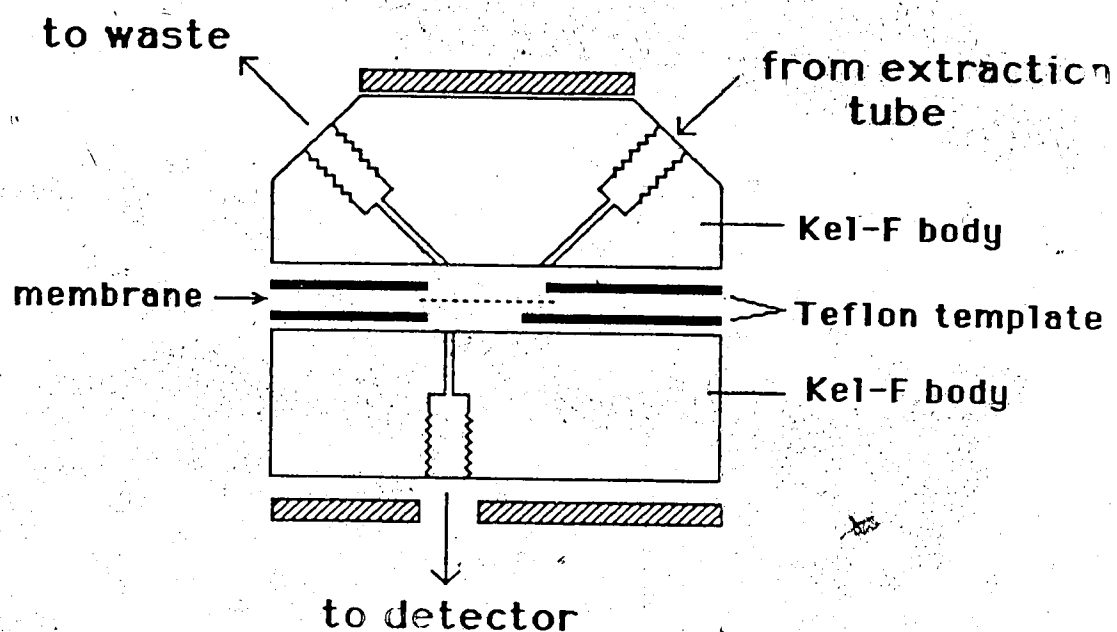


**Figure 4-6** Frei type membrane phase separator used in the work discussed in this chapter. Based on design described by J. A. Apffel, U. A. Th. Brinkman and R. W. Frei, *Chromatographia* 1984, 18, 5-10.

tubing. The chambers on each side of the membrane are cut into the Teflon templates, making it possible to readily alter the size and geometry of these chambers. In this work the downstream unsegmented chamber was a groove (8 mm x 0.8 mm x 1.2 mm) of a nominal volume of 8  $\mu\text{L}$  and the upstream segmented groove (12 mm x 0.8 mm x 1.2 mm) was 11  $\mu\text{L}$  for all studies except those involving the longer segments in 1 mm i.d. tubing, for which the upstream groove was 18  $\mu\text{L}$ .

The organic phase passing through the membrane of the phase separator is directed to the 8  $\mu\text{L}$  flow cell of the uv-vis spectrometer, D (SF770 Spectroflow, Schoeffel Instrument Corp). The detector signal is fed to a strip chart recorder (Fisher 5000), R, in the continuous sample feed experiment and to an integrator (Model 3300A, Hewlett-Packard), I, in the sample injection experiments. The membrane flow is regulated by a downstream peristaltic pump, P<sub>3</sub> (Minipuls, Gilson, Instruments, Ville-de-Belle, France), which is connected to the detector by 30 cm of 1.5 mm i.d. Teflon tubing to dampen pulsations from the pump.

The extraction system is thermostatted at  $25 \pm 1^\circ\text{C}$  in a water bath shown as dashed lines in Figure 4-4. An adjustable rail system allows clamping of the segmentor and phase separator to ensure that the extraction tube is straight.

#### 4.3.3 Measurement of extraction rates

Experiments were performed using either injection of sample or continuous feed of sample, as described below. Time ( $t$  in equation 4.9) is varied by varying the length of the extraction tube at a constant flow rate. Measurements were made prior to the attainment of equilibrium using extraction tubes between 5 and 85 cm in length, while equilibrium measurements were made using an extraction tube of 310 cm wound in a 4 cm coil diameter. If this equilibrium tube were straight, it would correspond to  $4\frac{1}{2}$  half-lives for the slowest extraction observed. However, since secondary flow enhances the extraction

rate (see Sec. 4.4.9), this coiled tubing corresponds to greater than ten half-lives (i.e. equilibrium) for all extractions studied.

The various lengths of tubing were run in random order to avoid systematic errors in the rates from any slight instrument drift. Once a measurement had been completed for a given extraction tube, the aqueous and organic flow was stopped using valves  $V_2$ , and the segment length was measured using the formula:

$$L_{aq} = \frac{X F_a}{N (F_a + F_o)} \quad (4.15)$$

where  $L_{aq}$  is the length of the aqueous segments,  $X$  is the total distance measured,  $N$  is the number of aqueous-organic segment pairs measured, and  $F_a$  and  $F_o$  are the total aqueous and organic flow rates, respectively.

For the sample injection experiment the instrument was used as shown in Figure 4-4. Peak areas were measured with a digital integrator. In setting the integrator measurement parameters, all peaks were declared to be "solvent" peaks to ensure integration of the entire tailed peak. The injected sample was  $5 \times 10^{-4}$  M caffeine in citrate buffer and the detector wavelength was 278 nm. All other parameters were varied as described in Section 4.4. Either straight or coiled tubes were used, as specified.

In the steady state experiment a baseline was first established by pumping chloroform with pump  $P_1$  and an aqueous blank solution with pump  $P_2$ . Aqueous sample solution was then substituted for blank by switching  $V_1$  and was fed continuously into the system. The difference between steady state sample absorbance and blank absorbance was measured. Important experimental conditions in the steady state experiments were: extraction tubing, 0.8 mm i.d. Teflon, the orientation of which was not fixed; total chloroform flow rate,  $F_o$ , 3.0 mL/min; flow rate of chloroform through the porous membrane of the phase separator,  $F_{o,m}$ , 1.9 mL/min; total aqueous flow rate,  $F_a$ , 3.0 mL/min citrate buffer containing sample; sample concentrations,  $1.0 \times 10^{-3}$  M,  $9.9 \times 10^{-5}$  M and  $1.0 \times 10^{-5}$  M caffeine;



blank solution, citrate buffer, segmentor, "tee" type; segment length, ~1 mm; detector wavelength, 295 nm for  $10^{-3}$  M caffeine and 278 nm for the other caffeine concentrations and the absorbance range, 1 AU.

#### 4.4 Results and Discussion

Extraction within a SE-FIA instrument is a mass transfer controlled process. Therefore factors which affect the convection within a segment will influence the kinetics of the extraction. The influence of phase ratio, segment length, flow rate and tube diameter on the extraction rate observed in straight tubes was investigated and are reported herein. The effect of secondary flow on the extraction rate was studied by varying the coiling of the extraction tube. To ensure that the extraction rates studied were controlled only by the toroidal and secondary flows associated with segmented flow through the extraction tubing, it was necessary to control or eliminate extraction occurring within the other components of the instrument and as a result of random mixing in the segments.

##### 4.4.1 Instrumental considerations

Random mixing within segments in the extraction tube was minimized by taking the following precautions:

- i) The solvents were pre-equilibrated; otherwise their mutual dissolution when they meet at the segmentor would lead to interfacial turbulence [30,144].
- ii) The extraction system was thermostatted to avoid thermal gradients which would cause additional convection within the segments, and to avoid changes in the equilibrium constants and diffusion coefficients.
- iii) The aqueous phase contained a buffer to maintain constant pH and ionic strength.
- iv) Surface active compounds were excluded from this study. There are two reasons for avoiding surface active compounds. First, their presence has been observed to reduce

the natural circulation occurring within falling and rising drops [30,144]. As in SE-FIA, the circulation within a moving droplet results from momentum transfer across the interface. This fluid flow drives material adsorbed at the interface towards the rear of the drop, resulting in a greater surface concentration and consequently a higher surface pressure. This surface pressure damps down the circulation inside the drop by resisting further local compression of the monolayer and thus reducing the movement of the interface and hence the transfer of momentum across it [30]. This type of behavior has been observed in the extraction of ethyl violet in SE-FIA [53] where aqueous segments are stratified, with the front of the segment clear and the back violet.

A second manner in which surface active material affects extraction is that, when it is adsorbed onto the interface, the surfactant acts as a physical "barrier" to diffusion, thus generating an interfacial resistance to mass transfer [145].

v) Pulsations in the flow were minimized because they would result in irregularities in the segmentation and affect convection [146].

vi) The extraction tubing was held straight to avoid any secondary flow which results from coiling. The theory of secondary flow is discussed in Section 4.2.1.2 and the need for this precaution is demonstrated in Section 4.4.8.

## 4.2 Extra-tube extraction

In order to study the extraction occurring with the extraction tube it is necessary to minimize and control the extraction occurring in the segmentor and phase separator. In the segmentor, a growing "drop" of one phase is dislodged to produce a segment when the hydrodynamic force exerted on the drop as a result of flow of the other solvent is equal to the interfacial force holding the drop in place [31]. The hydrodynamic force is governed by the flow rates of the two solvents and the physical dimensions of the drop and the segmentor. The interfacial force is dependent on the liquid-liquid interfacial tension, the solid-liquid-liquid contact angle and the segmentor geometry and dimensions. Thus, for a

given segmentor with constant flow, the segments formed are of constant length which means that the elapsed time and drop size at dislodgement must be constant. Thus the amount of extraction occurring within the segmentor is a constant for a given set of conditions.

The amount of extraction accompanying coalescence in the porous membrane phase separator will depend upon the interfacial area and contact time between the two phases. Coalescence occurs in the chamber on the upstream side of the membrane where the two phases are in contact. Thus, reducing the size of this chamber and minimizing the mixing within it should reduce the extraction accompanying the phase separation process.

In order to assess the tendency for a phase separator to produce extraction an instrument was used with the smallest possible extraction tube (i.e. 5 cm) in order to minimize the extraction taking place before the sample zone reaches the phase separator. Figure 4-7 shows the percentage of caffeine extracted versus the proportion of the organic phase passing through the porous Teflon membrane. Curve A represents the Fossey phase separator shown in Figure 2-3 which was used in the previous studies discussed in Chapter 2, and curve B represents the Frei phase separator shown in Figure 4-6. Table 4-1 compares the designs of these two phase separators. The % extraction shown in the figure is the total due to the extraction in the segmentor, in the 5 cm extraction tube and in the phase separator. Since the extraction in the segmentor and extraction tube are the same regardless of which phase separator is used, the difference between curves A and B, as well as the changes in the percentage extraction with changing  $F_{O,m}/F_O$  reflect what is happening in the phase separator.

The extraction occurring in the Frei phase separator (curve b) was much lower than that occurring in the Fossey design (curve a). This is due to the smaller volume of the former and, in addition to its grooved geometry which helps stabilize the segmented flow, thus reducing the amount of coalescence.

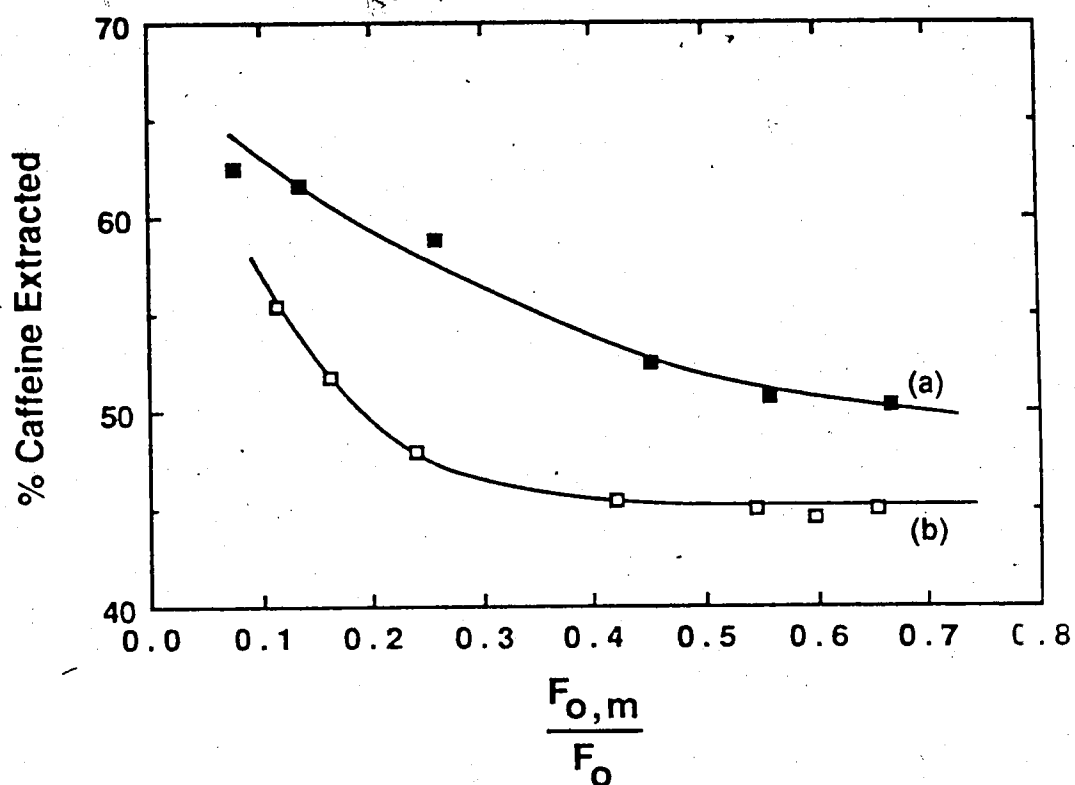


**Figure 4-7** Extraction occurring in the phase separator measured as the percentage of caffeine extracted into the organic phase versus the proportion of the organic phase flowing through the porous Teflon membrane for (a) the Fossey phase separator and (b) the Frei phase separator. Experimental conditions were:  $F_O$ , 3.1 mL/min;  $F_a$ , 3.2 mL/min; sample, 20 PPM caffeine in distilled water introduced continuously as the aqueous carrier stream; extraction tube, 5.0 cm of 0.8 mm i.d. Teflon; wavelength, 258 nm and absorbance range, 1.0 AU. Proportion of the organic phase passing through the membrane of the phase separator was controlled using the peristaltic pump speed.

**Table 4-1** Specifications of the Phase Separators

Parameter	Phase Separator Type	
	Fossey <sup>a</sup>	Frei <sup>b</sup>
segmented chamber volume	50 $\mu\text{L}$	11 $\mu\text{L}$
unsegmented chamber volume	25 $\mu\text{L}$	8 $\mu\text{L}$
chamber geometries	cylindrical disk	groove
membrane (organic)	2 x 10-20 $\mu\text{m}$	1 x 10-20 $\mu\text{m}$

a. Design shown in Figure 2-3 and described in Section 2.2.2.1.

b. Design shown in Figure 4-6 and described in Section 4.3.2.

For both phase separators increasing the flow through the membrane decreased the amount of extraction occurring in the phase separator. This is because an increase in flow decreases the residence time of the organic phase within the segmented chamber, and thus decreases the contact time between the two phases.

The Frei phase separator was used in all further work and the proportion of the organic phase passing through the membrane was maintained constant at greater than 40% in all further studies. Using these conditions, the fraction of extraction occurring in the extra-tube ranged between 20 and 60%, depending inversely on the segment length.

#### 4.4.3 Extraction rate

Data for a typical extraction rate experiment are presented in Figure 4-8. This experiment involved continuous sample feed. Results from sample injection experiments are identical, except that peak area is used instead of steady state absorbance. Plot A of Figure 4-8 shows the steady state absorbance in the organic phase at various extraction tube lengths for the extraction of caffeine. The ordinate intercept reveals that 33% of the caffeine has extracted in the extra-tube portion of the instrument. As well, under these segmented flow conditions the caffeine is 90% extracted after flowing through 25 cm of extraction tubing. Application of equation 4.9 to these data yields the line shown in Plot B. The extraction tube length is converted into time units by dividing the length by the linear velocity of flow, 19.9 cm/s. The slope of this line is the observed extraction rate constant,  $k_{\text{obs}}$ ,  $1.29 \pm 0.07 \text{ s}^{-1}$ , and the intercept reflects the extraction which has occurred in the segmentor and phase separator.

If the extraction of caffeine is a mass transfer controlled process,  $k_{\text{obs}}$  should be independent of the sample concentration at low concentrations. The values of  $k_{\text{obs}}$  measured at three concentrations of caffeine using continuous sample feed are shown in Table 4-2. They are statistically equivalent at the 95% confidence level.

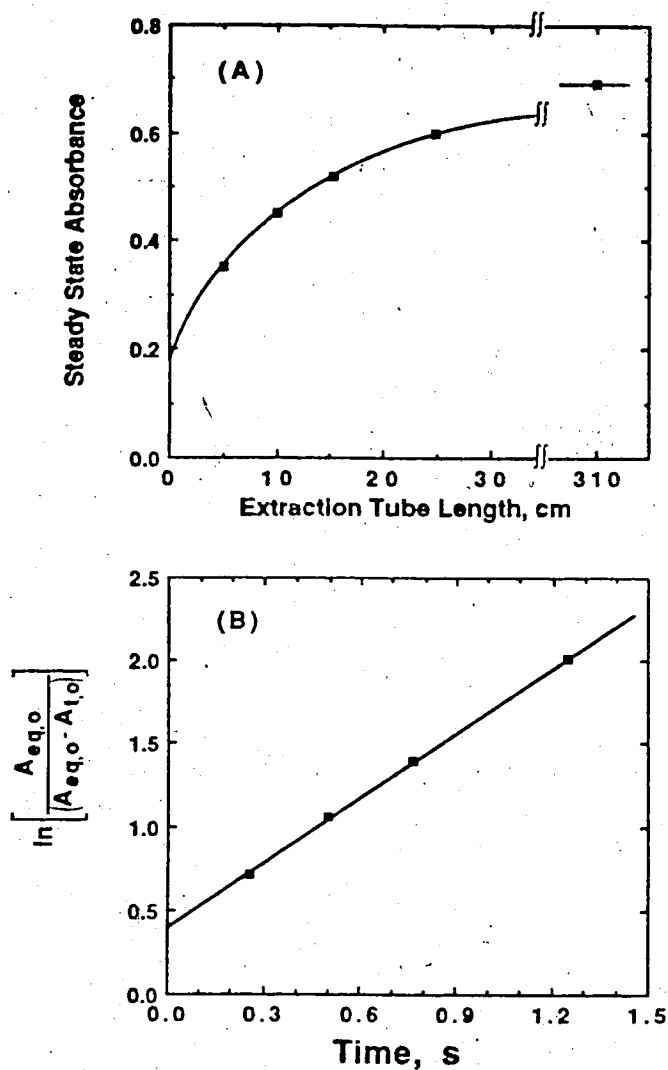


**Figure 4-8** Extraction of caffeine into chloroform. (A) Measured absorbance in organic phase for a constant feed of  $9.9 \times 10^{-5} \text{ M}$  caffeine at extraction tube lengths from 0 to 25 cm, and for 310 cm in the inset. (B) Kinetic plot according to equation 4-8. Experimental conditions were: total aqueous flow rate,  $F_a$ , 3.0 mL/min of pH 4.0 citrate buffer containing  $9.9 \times 10^{-5} \text{ M}$  caffeine; total organic flow rate,  $F_o$ , 3.0 mL/min; portion of organic flow passing through membrane,  $F_{o,m}/F_o$ , 0.63; tubing, 0.8 mm i.d. Teflon, orientation not fixed - 5-25 cm for kinetic measurements and 310 cm for equilibrium; wavelength, 278 nm and absorbance range, 1.0 AU.

**Table 4-2** Rate constants for the extraction of caffeine using continuous sample feed <sup>a</sup>

Concentration (M)	$k_{\text{obs}}$ ( $\text{s}^{-1}$ ) <sup>c</sup>
$1.0 \times 10^{-5}$	$1.42 \pm 0.11^{\text{b}}$
$9.9 \times 10^{-5}$	$1.29 \pm 0.07^{\text{b}}$
$1.0 \times 10^{-3}$	$1.36 \pm 0.15^{\text{b}}$

- a. Experimental conditions were: total aqueous flow rate,  $F_{\text{a}}$ , 3.0 mL/min of pH 4.0 citrate buffer containing caffeine of the concentration given in the table; total organic flow rate,  $F_{\text{o}}$ , 3.0 mL/min; portion of organic flow passing through membrane,  $F_{\text{o,m}}/F_{\text{o}}$ , 0.63; tubing, 0.8 mm i.d. Teflon, orientation not fixed - 5-25 cm for kinetic measurements and 310 cm for equilibrium; wavelength, 295 nm for  $10^{-3}$  M caffeine and 278 nm for the lower concentrations; absorbance range, 1.0 AU.
- b. Uncertainty is given as the standard deviation of the slope of the first order kinetic plot.
- c. Value of  $k_{\text{obs}}$  measured in a sample injection experiment was  $1.26 \pm 0.11 \text{ s}^{-1}$ . See Section 4.4.3 for details.



Injection of a sample, as opposed to continuous sample feed, results in a sample band comprised of a peaked concentration profile. However, since the extraction is mass transfer controlled, and therefore independent of concentration, it should be possible to monitor the extraction rate by using sample injection just as well as by using continuous sample feed. Under the same experimental conditions that pertain to Table 4-2, an extraction rate constant of  $1.26 \pm 0.11 \text{ s}^{-1}$  was observed for injections of  $2 \mu\text{L}$  of  $5 \times 10^{-4} \text{ M}$  caffeine. This is statistically equal to the rate constants in Table 4-2, indicating that sample injection is a valid procedure for measuring  $k_{\text{obs}}$ . All subsequent studies employed sample injections, as this is the manner in which flow injection analysis is generally performed [18].

#### 4.4.4 Phase ratio

Extraction rate constants observed at phase ratios of 2:1, 1:3 and 1:4 at a constant total flow rate of  $4.0 \text{ mL/min}$  ( $v=13.3 \text{ cm/s}$ ) are given in Table 4-3. The experimental conditions are listed with the table. Also shown in Table 4-3 are rate constants observed using aqueous segments of the same three lengths and using the same total flow rate, but at a phase ratio of 1:1. For reasons discussed in Section 4.4.6,  $k_{\text{obs}}$  is larger for smaller aqueous segment lengths. However, the important observation here is that the two values of  $k_{\text{obs}}$  obtained for a given aqueous segment length are equal to one another and independent of the organic segment length. This means that the distribution coefficient of caffeine between chloroform and water ( $10^{1.3}$  measured in this work and in ref. 147) is sufficiently high to make the mass transfer in the organic phase fast compared to that in the aqueous phase [141]. Thus  $\bar{\beta}$  is equal to  $\beta_{\text{aq}}$  as expressed in equation 4.13 in Section 4.2.3. Thus convection within only the aqueous segment need be considered in studying the extraction rate in SE-FIA.

**Table 4-3** Effect of phase ratio on extraction rate constant <sup>a</sup>

$L_{aq}$ (mm)	Phase Ratio <sup>b</sup>	$k_{obs}$ (s <sup>-1</sup> )
0.9	2:1	$0.63 \pm 0.03$
0.9	1:1	$0.65 \pm 0.05^c$
2.8	1:3	$0.25 \pm 0.01$
2.8	1:1	$0.22 \pm 0.03$
3.3	1:4	$0.23 \pm 0.01$
3.3	1:1	$0.20 \pm 0.02^c$

a. Experimental conditions for the sample injection experiments were: total two phase flow,  $F_T$ , 4.0 mL/min ( $v=13.3$  cm/s);  $F_{O,m}/F_O$ , 0.56-0.60; sample injected, 10  $\mu$ L of  $5 \times 10^{-4}$  M caffeine in pH 4.0 citrate buffer; tubing, 0.8 mm i.d. Teflon, straight; wavelength, 278 nm and absorbance range, 0.4 AU.

b. Phase ratio =  $F_O/F_a$

c. Interpolated from the curve for 4.0 mL/min shown in panel A of Figure 4-9.

Uncertainties are based on the relative standard deviation of the points making up the curve.

#### 4.4.5 Segmentor Type

In Table 4-4 is shown extraction rate constants observed for segments of similar length formed with both the "tee" and Technicon A-8 segmentors (see Figure 4-5). The extraction rate varies with the aqueous segment length, as will be discussed in Section 4.4.6, but the rates observed in Table 4-4 are independent of the type of segmentor, since the observed rate constants for each segmentor are within the 95% confidence interval of the other. This verifies that the extraction rate constants measured herein are attributable to the extraction occurring within the segmented flow.

#### 4.4.6 Segment length

In panel A of Figure 4-9 is shown the dependence of the extraction rate constant on aqueous segment length in a straight tube, for three flow rates. At a given flow rate,  $k_{obs}$  approaches a constant value for segment lengths greater than about 4 mm, but increases with decreasing segment length for shorter segments. The increase in  $k_{obs}$  with decreasing segment length at a constant flow rate could reflect an increase in either the interfacial area or  $\beta$ . The former factor can be accounted for by converting  $k_{obs}$  to  $\beta$  using equation 4.11. The interfacial area-to-volume ratio for the aqueous segments is given by:

$$\frac{a}{V} = \frac{2(L_{aq} + r_t)}{r_t \left( L_{aq} - \frac{1}{3}r_t \right)} \quad (4.16)$$

where  $L_{aq}$  is the aqueous segment length calculated using equation 4.15 and  $r_t$  is the tubing radius. This expression assumes hemispherical ends for the aqueous segments and a negligibly thin wetting film of chloroform. The resulting three plots of mass transfer coefficient versus segment length, shown in panel B of Figure 4-9, constitute a family of curves very similar in appearance to those in panel A. Thus, for straight tubes, the increase

**Table 4-4** Extraction rate constants observed in Segmented Flow formed by the "Tee" and Technicon A-8 Segmentors at two Aqueous Segment Lengths<sup>a</sup>

$L_{aq}$ (mm) <sup>b</sup>	$k_{obs}$ (s <sup>-1</sup> )	
	"Tee" type <sup>c</sup>	Technicon A-8 <sup>c</sup>
$1.1 \pm 0.1$	$0.59 \pm 0.03$	$0.55 \pm 0.05$
$7 \pm 1$	$0.16 \pm 0.01$	$0.17 \pm 0.01$

- a. Experimental conditions were:  $F_a$ , 2.0 mL/min;  $F_o$ , 2.0 mL/min;  $F_{o,m}/F_o$ , 0.50-0.62; sample injected, 10  $\mu$ L of  $5 \times 10^{-4}$  M caffeine in pH 4.0 citric acid buffer; tubing, 0.8 mm i.d. Teflon, straight; wavelength, 278 nm and absorbance range, 0.4 AU.
- b. Uncertainties reflect the variation among segment lengths formed by each segmentor.
- c. See Figure 4-5 for the design of these segmentors.

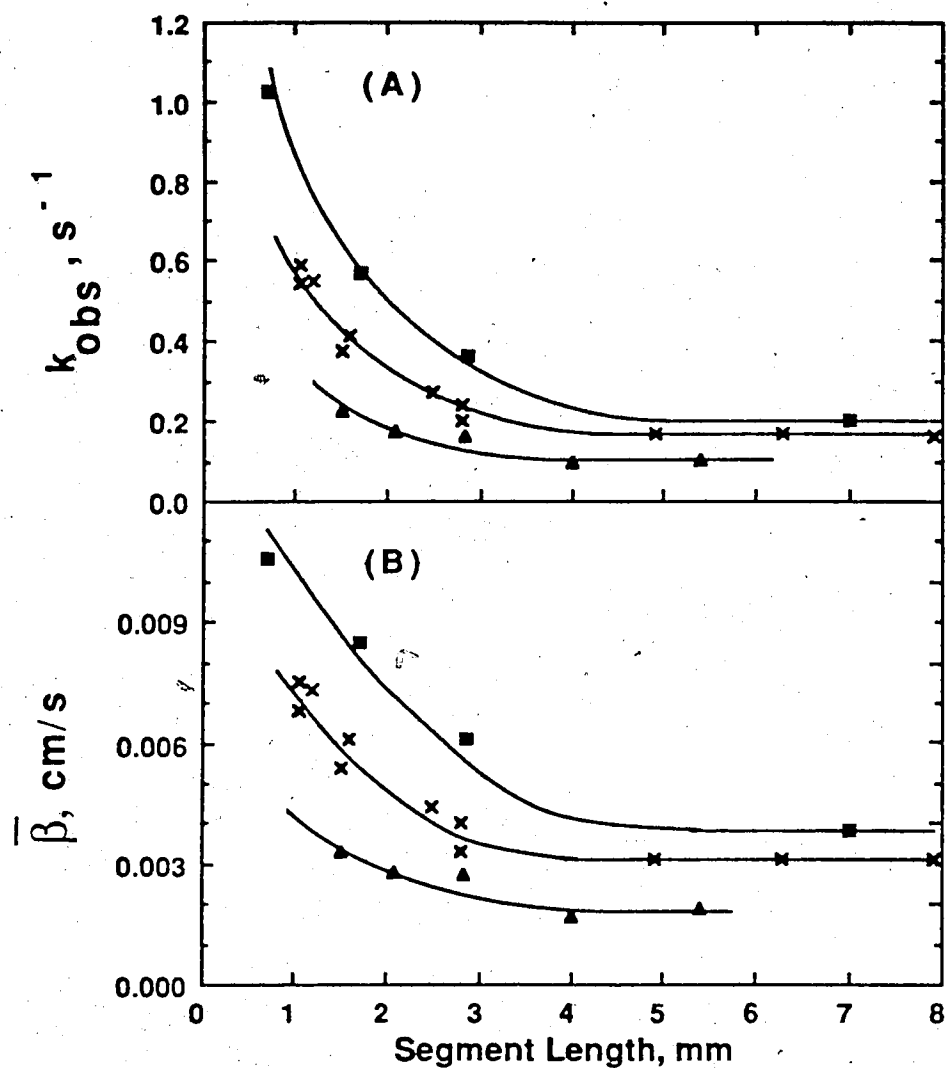


**Figure 4-9** Effect of segment length on (A) Observed extraction rate constants ( $k_{obs}$ ) and (B) Mass transfer coefficients ( $\bar{\beta}$ ) for segments between 0.7 and 8 mm in length at three total flow rates,  $F_T$ : (a) 2.0 mL/min ( $v=6.6$  cm/s) ( $\blacktriangle$ ); (b) 4.0 mL/min ( $v=13.3$  cm/s) ( $\times$ ); (c) 6.0 mL/min ( $v=19.9$  cm/s) ( $\blacksquare$ ). Experimental conditions are: phase ratio, 1:1;  $F_{O,m}/F_O$ , 0.58-0.66; tube orientation, straight; sample,  $5 \times 10^{-4}$  M caffeine in pH 4.0 citrate buffer; injection volume, 10  $\mu$ L; wavelength, 278 nm and absorbance range, 0.4 AU.

in interfacial area accompanying a decrease in segment length can explain only a minor portion of the increase in extraction rate the major portion being due to increased  $\beta_{aq}$ .

It is important to note that  $\beta_{aq}$  is constant above a segment length of 4 mm. This indicates that no saturation of the wetting film of organic phase by the solute is occurring. Therefore the assumption that the organic phase acts as an infinite sink (equation 4.12) is valid even for this localized stagnant portion of the phase.

For  $\beta_{aq}$  to increase there must be some enhancement in the convection within the segment. Solutions of the Navier Stokes equation for the toroidal circulation [129-131] discussed in Section 4.2.1.1 indicate that for long segments the mid-segment axial velocity profile approaches the parabolic Poiseuille profile, in which the flow streamlines are parallel to the tubing wall - i.e. the radial velocity component is minor. However, when the segment length is reduced sufficiently that the ends of the segment are on the order of a tube diameter apart, the ends interact hydrodynamically to dramatically increase the radial velocity component of the circulation. This enhances the convective mixing in the segment and thus increases the mass transfer coefficient.

Very similar behavior to that shown in Figure 4-9 was observed in a study of radial mass transfer of solute to the wall during air-segmented flow of aqueous solution through straight tubes (Figure 2 of ref. 24). (In that study results were expressed in terms of the dimensionless quantities Nusselt number, segment aspect ratio and Reynolds number rather than by their respective dimensional counterparts - mass transfer coefficient, segment length and flow rates, which are used herein.) This suggests that in liquid-liquid segmented flow the extraction results either from solely the radial mass transfer ( $\beta = \beta_{aq,radial}$ ) or from both the axial and radial routes (equation 4.14) with the axial and radial mass transfer coefficients having a similar dependence on the segment length. This question is addressed in Chapter 5.

Intercomparison of the three curves in Figure 4-9 shows that, at a given segment length, the extraction rate constant increases with flow rate. In an analogous study in air segmented flow through straight tubing,  $\beta_{\text{radial}}$  was related to the linear velocity  $v$  by a power relationship  $v^\alpha$  where  $\alpha$  was observed to be 0.50 for short segments and 0.34 for long segments. From the observed extraction rate constants in Figure 4-9,  $\ln(k_{\text{obs}})$  was plotted versus  $\ln(\text{flow rate})$  for segment lengths of 1.5 and 6.0 mm and the resultant plots, shown as curves A and B in Figure 4-10, are straight lines with slopes of  $0.89 \pm 0.08$  and  $0.68 \pm 0.08$ , respectively. The uncertainties in these slopes reflects both the regression error and the interpolation error of the original values from Figure 4-9. Also shown plotted in this double logarithmic fashion as curve C in Figure 4-10, are data obtained by Nord *et al* for the extraction of caffeine from long (8 mm) segments flowing through 0.7 mm i.d. coiled tubing (data from Figure 6B of ref. 29). A linear plot of slope  $0.58 \pm 0.02$  is obtained. Thus, mass transfer in both air segmented and liquid segmented flow is related to linear velocity via a power relationship, the power of which decreases with increasing segment length and is greater for corresponding segment lengths in liquid segmented flow than in air segmented flow.

The larger value of  $\alpha$  in liquid segmented systems may be understood in the following way. Increasing the linear velocity increases both the circulation within the segments and the thickness of the wetting film on the tube wall [21,22,26,122]. In air segmented flow the radial mass transfer occurs in the film forming phase, and studies of axial dispersion [26,27,122] have shown that there is slow mass transfer within the quasistatic liquid film at the tube wall. Thus, in air segmented flow an increased linear velocity generates two opposing effects. The enhanced convective mass transfer due to increased circulation would be offset by the decreased diffusional mass transfer within the thicker wetting film. In the liquid segmented flow employed in SE-FIA, on the other hand, the increased thickness of the film of organic phase will have no effect on the mass transfer rate, since

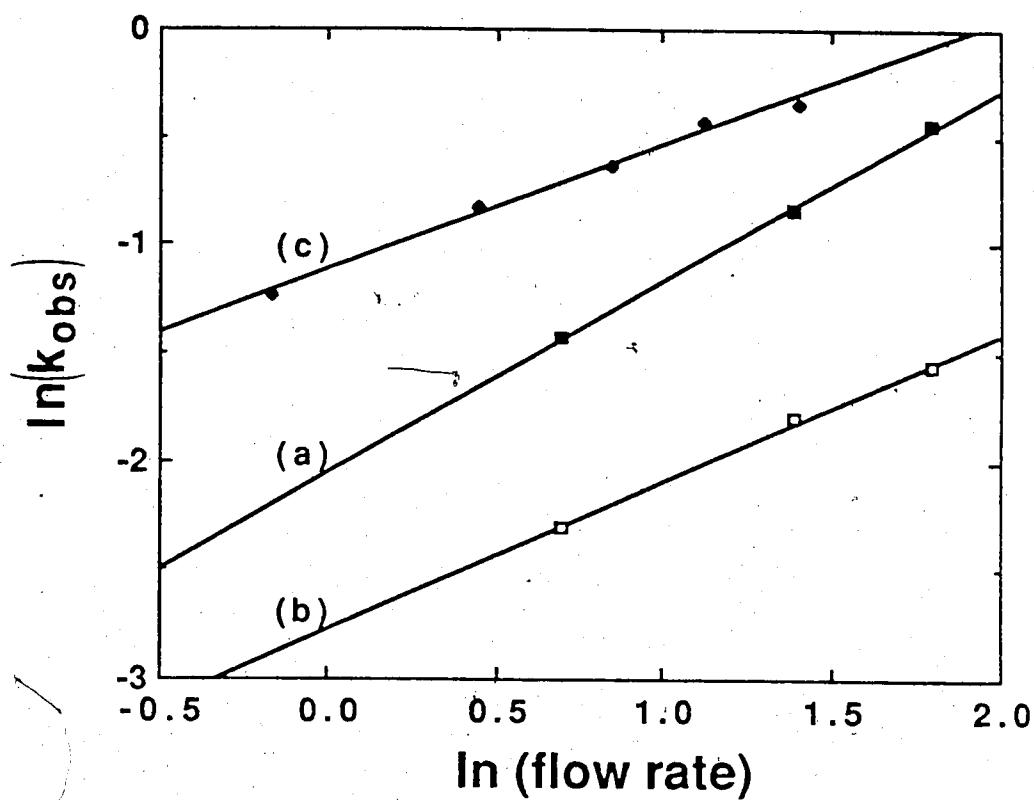


**Figure 4-10** Double logarithmic plots of  $k_{\text{obs}}$  as a function of flow rate for: (A) 1.5 mm and (B) 6.0 mm segments studied in this work, and (C) 8 mm segments studied in L. Nord, K. Bäckström, L-G. Danielsson, F. Ingman and B. Karlberg, *Anal. Chim. Acta* **1987**, *194*, 221-233.



the rate determining mass transfer process occurs in the non-film forming aqueous phase. Thus for corresponding segment lengths,  $\alpha$  will be greater in liquid segmented flow.

#### 4.4.8 Tube diameter

The effect of varying tube diameter on the observed extraction rate is strongly dependent on the segment length, as can be seen by intercomparing the curves in panel A of Figure 4-11. For long segments,  $> 4$  mm, the extraction rate increases as the tubing diameter is decreased. However, a crossover is observed, so that for shorter segments the extraction is fastest in the wider tubing.

Conversion of the observed extraction rates into the corresponding mass transfer coefficients eliminates this crossover and greatly simplifies the observed trends, now shown in panel B of Figure 4-11. This indicates that to a large extent the behavior of  $k_{obs}$  results from the increase in  $a/v$  as the segment length is decreased. However, while  $\bar{\beta}$  does appear to become independent of the tubing diameter for extremely long segments,  $\sim 8$  mm, it still increases with increasing tubing diameter for shorter segments.

The hydrodynamics within a segment are determined by boundary conditions defined by the walls and the ends of a segment. In reflection of this, solutions of the Navier Stokes equations use the dimensionless *segment aspect ratio*, which is the segment length divided by the tubing diameter, rather than the segment length. Horvath *et al* [24] observed two regions of behavior in plots of radial mass transfer in air segmented flow *versus* the segment aspect ratio. For large segment aspect ratios down to  $\sim 3-5$ , the mass transfer was approximately constant, but when the aspect ratio was reduced below about 3-5 the radial mass transfer increased rapidly. Figure 4-12 is a replotting of the mass transfer coefficients of Figure 4-11B versus the segment aspect ratio. In this plot the data collected at the four tube diameters follow the general trends observed by Horvath *et al* [24]. This behavior is consistent with the hydrodynamic studies discussed in Sec. 4.2.1.1 in which it

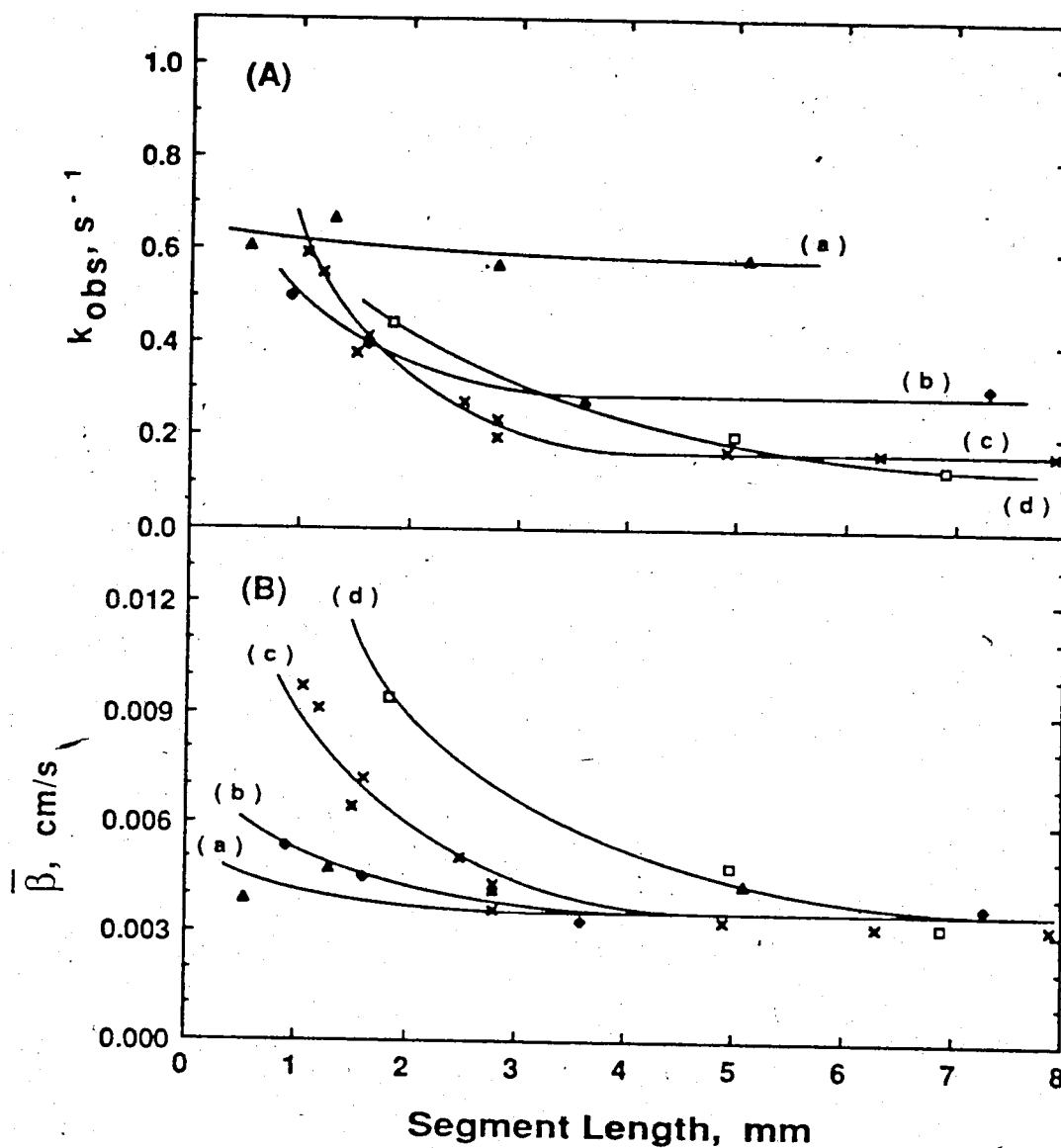


**Figure 4-11** Observed extraction rate constants (A) and the mass transfer coefficients (B) in four different diameter extraction tubes; (a) 0.3 mm i.d. (▲); (b) 0.5 mm i.d. (●); (c) 0.8 mm i.d. (✕); (d) 1.0 mm i.d. (□). Experimental conditions are: linear velocity,  $v$ , 13.3 cm/s; phase ratio, 1:1;  $F_{O,m}/F_O$ , 0.35-0.65; tube orientation, straight; sample,  $5 \times 10^{-4}$  M caffeine in pH 4.0 citrate buffer; injection volume, 10  $\mu$ L; wavelength, 278 nm and absorbance range, 0.4 AU.

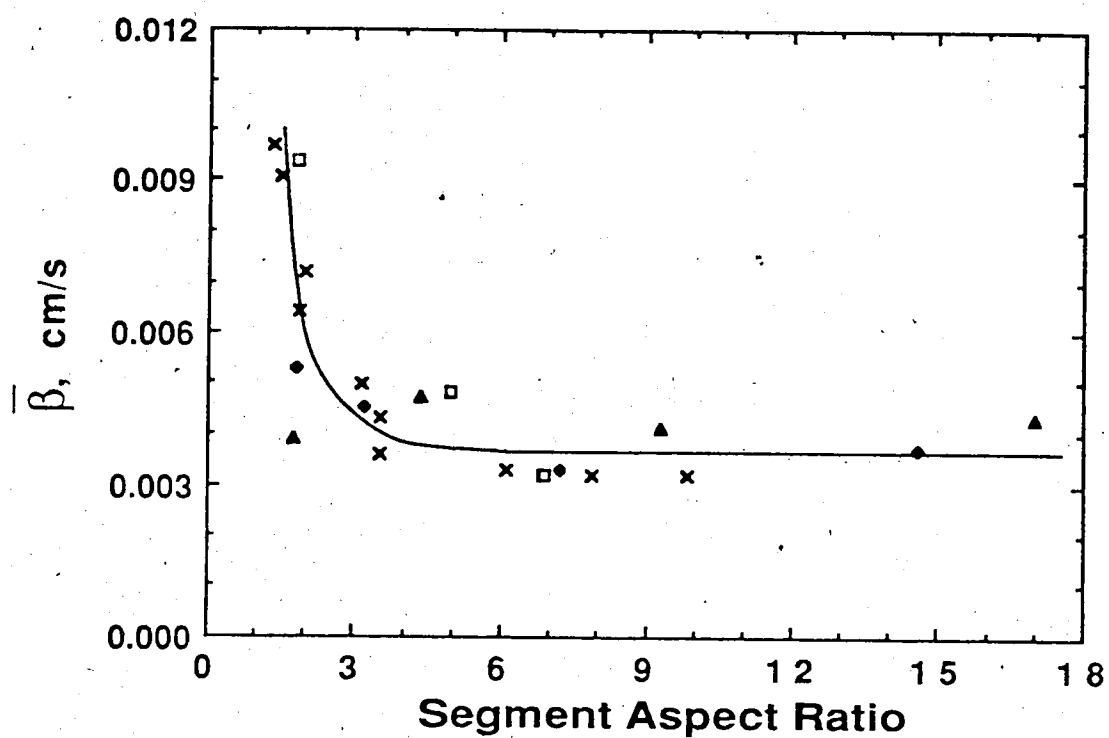


**Figure 4-12** Mass transfer coefficients at different segment aspect ratios in four different diameter extraction tubes: 0.3 mm i.d. (▲); 0.5 mm i.d. (◆); 0.8 mm i.d. (✕); 1.0 mm i.d. (◻). Experimental conditions as described in Figure 4-11. Segment aspect ratio is the segment length relative to the inner diameter of the tubing.

was found that when the segment length approaches the tube diameter, the segment ends interact hydrodynamically to enhance convection [130,131] and mass transfer.

#### 4.4.9 Coiling

For a homogeneous single phase fluid flowing through a coiled tube, the secondary flow is well developed when  $De^2Sc > 10^4$  [126]. For caffeine, under the segmented flow conditions used in this study,  $De^2Sc$  ranged between  $10^5$  to  $10^6$ , so coiling of the extraction tube is expected to strongly effect the extraction rate. In Figure 4-13 are shown the rate constants observed for caffeine extraction in coiled tubing. The reciprocal of the coil diameter is used as the abscissa since the secondary flow is related to this term [126,133], as is shown in equation 4.6. Three segment lengths were used, corresponding to the steeply rising region, to the "knee" region and to the flat region in Figure 4-12. The results shown in Figure 4-13 are phenomenologically similar to the results of a study of the effect of coiling on radial mass transfer in air segmented flow [24].

In Figure 4-13 two classes of behavior are evident. For the longer segments (curves b and c in Figure 4-13)  $k_{Obs}$  rises rapidly as coil diameter is decreased to reach a final limiting value, whereas for the short segments (curve a) there is a slight decrease in  $k_{Obs}$  between  $1/d_c$  of zero (uncoiled) and 0.2 ( $d_c = 5$  cm), followed by a rapid rise to a final limiting value. The values of  $k_{Obs}$  and  $\bar{\beta}$  obtained with a straight extraction tube and the corresponding value of  $k_{Obs}$  and  $\bar{\beta}$  obtained at the limiting plateau for the tightly coiled tube are presented in Table 4-5 for each of the three segment lengths.

The differences in behavior for the long and short segments in Figure 4-13 can be understood in terms of the two regions of the curve in Figure 4-12. In long segments, whose aspect ratio is greater than 3 (curve b and c in Figure 4-13), the mid-segment axial velocity distribution in a straight tube approaches the parabolic profile characteristic of Poiseuille flow, with the highest velocity along the center of the tube. When the tube is coiled the centrifugal force acts upon this flow in the same way that it does in single phase

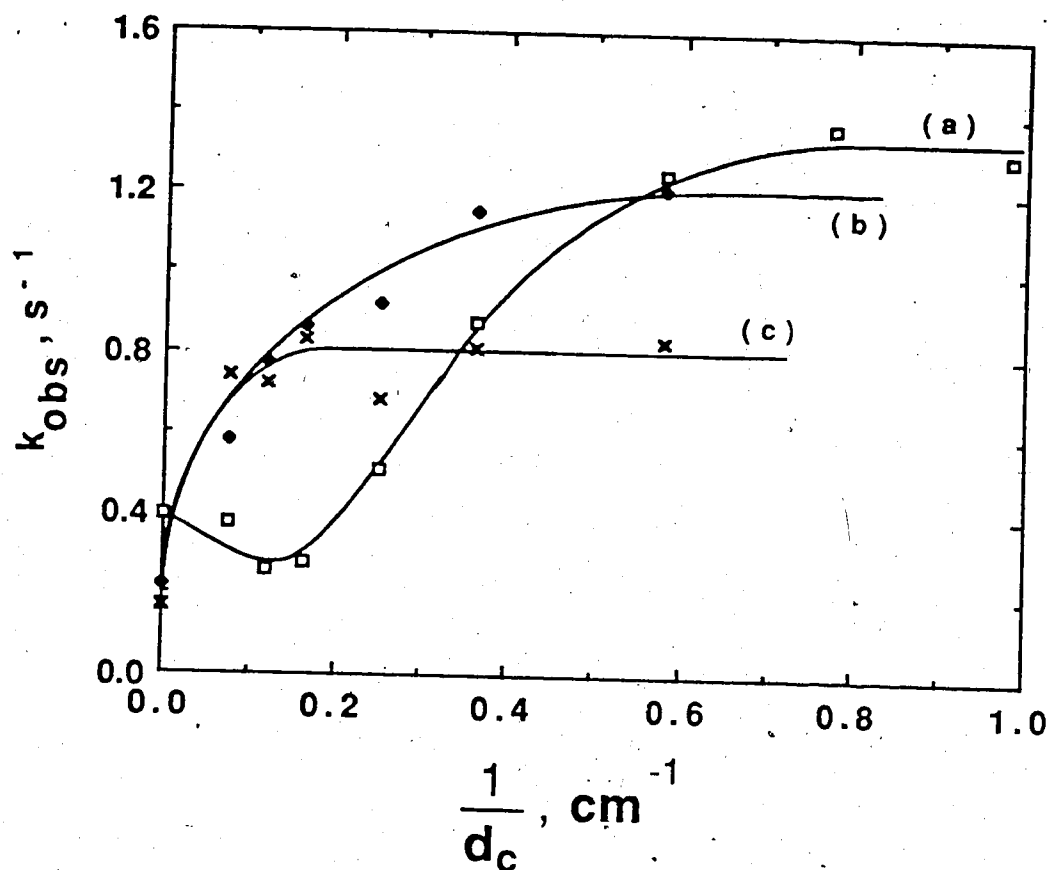


**Figure 4-13** Observed extraction rate constant for various degrees of coiling at three different segment lengths: (a) 1.6 mm (□); (b) 2.8 mm (●); (c) 7.9 mm (×). Experimental parameters:  $F_a$ , 2.0 mL/min;  $F_o$ , 2.0 mL/min;  $F_{o,m}/F_o$ , 0.50-0.58; tubing diameter, 0.8 mm i.d.; linear velocity, 13.3 cm/s; sample,  $5 \times 10^{-4}$  M caffeine in pH 4.0 citrate buffer; injection volume, 10  $\mu$ L; wavelength, 278 nm and absorbance range, 0.4 AU.

**Table 4-5** Dependence of extraction rate constant and mass transfer coefficient on Segment Length in Straight and Tightly Coiled Extraction Tubes<sup>a</sup>

$L_{aq}$ (mm)	<u>Straight</u> <sup>b</sup>		<u>Tightly Coiled</u> <sup>c</sup>	
	$k_{obs}$ (s <sup>-1</sup> )	$\bar{\beta}$ (cm/s)	$k_{obs}$ (s <sup>-1</sup> )	$\bar{\beta}$ (cm/s)
1.6	$0.39 \pm 0.04$	$0.0058 \pm 0.0005$	$1.34 \pm 0.08$	$0.020 \pm 0.001$
2.8	$0.22 \pm 0.03$	$0.0037 \pm 0.0005$	$1.21 \pm 0.05$	$0.020 \pm 0.001$
7.9	$0.16 \pm 0.01$	$0.0031 \pm 0.0002$	$0.83 \pm 0.04^d$	$0.015 \pm 0.001^d$

- a. Experimental conditions were:  $F_a$ , 2.0 mL/min;  $F_o$ , 2.0 mL/min;  $F_{o,m}/F_o$ , 0.50-0.58; tubing diameter, 0.8 mm i.d.; linear velocity, 13.3 cm/s; sample,  $5 \times 10^{-4}$  M caffeine in pH 4.0 citrate buffer, injection volume, 10  $\mu$ L; wavelength, 278 nm and absorbance range, 0.4 AU.
- b. Data at  $1/d_c = 0$  in Figure 4-13.
- c. Refers to the plateau observed for each segment length; i.e.  $1/d_c > 0.15$  for 7.9 mm segments,  $1/d_c > 0.6$  for 2.8 mm segments and  $1/d_c > 0.8$  for 1.6 mm segments. The mean value of the points on this plateau are reported.
- d. The data point at  $1/d_c = 0.25$  was excluded in calculating the mean for the plateau on the basis of the Q-test [148];  $Q_{obs} = 0.81$ ,  $Q_{90\%,n=4} = 0.76$ .

flow, generating a secondary flow which enhances the mass transfer from the segment. However, while the intensity of the secondary flow continues to increase as the coil is made tighter (i.e.  $De^2Sc \propto 1/d_c$  from equation 4.6), the extraction rate constant increases more gradually, so that the plots of  $k_{obs}$  vs.  $1/d_c$  in Figure 4-13 tend to flatten out at large  $1/d_c$  values. In the studies of the effect of flow rate on the extraction rate in straight tubes (see Section 4.4.7),  $k_{obs}$  was related to  $v^\alpha$  where  $\alpha < 1$ . It might then also be expected that  $k_{obs}$  would be related to  $(1/d_c)^\alpha$ . The  $\alpha$  would have to be lower than in the flow rate case, however, in order to produce the flattening behavior observed in the curves in Figure 4-13.

For short 1.6 mm segments in straight tubing ( $1/d_c = 0$ ), there is considerable radial convection within the segment due to the hydrodynamic interaction of the segment ends, resulting in a more uniform axial flow profile (Figure 4-2). Coiling of the tubing will then generate much less intense secondary flow within these segments since the centrifugal forces will be weaker. It can then be speculated that a much greater  $De^2Sc$  than  $10^4$  would be required to achieve a well developed secondary flow within the short segments. This would then account for the delay in the curve a in Figure 4-13 in which the coiling had no effect on  $k_{obs}$  for the short segment. A similar general behavior has been observed for the radial mass transfer in air segmented flow [24].

It would further be expected then that, once the secondary flows were well developed in the short segments, the secondary flow effects would still not be as significant for the short segments as the long. In Table 4-5 are shown the rate constants and mass transfer coefficients for extraction within straight and tightly coiled tubing. In straight tubing both  $k_{obs}$  and  $\beta$  increase rapidly with decreasing segment length when the segment length is below about three times the tube diameter (Section 4.4.8). In contrast, in coiled tubing  $k_{obs}$  increases only 11% when the segment length is reduced from 2.8 to 1.6 mm ( $L_{aq}/d_t$ : 3.5 to 2.0), and the mass transfer coefficients for these two segment lengths are the same. For the 7.9 mm segment in the coiled tube,  $\beta$  is significantly lower than for the shorter

segments. These observations for a coiled tube are similar to results reported for radial mass transfer in air segmented flow, where the Nusselt number was approximately constant up to a segment aspect ratio of about 4 and then decreased gradually with increasing segment length [24].

In the studies by Nord *et al* [29] on the rate of extraction in segmented flow, the segments were between 3 and 40 mm in length. For these long segments almost any curvature in the tubing would be sufficient to induce a strong secondary flow. Thus, in spite of the fact that the extent of coiling was not specified for their coiled extraction tube it is clear that the data Nord *et al* should be interpreted in terms of the effects of both the toroidal and secondary flows. In this light, the influence of segment length on the extraction of bromocresol green which they observed (Figure 4 of ref. 29) is analogous to the results shown in Table 4-5 for the tightly coiled tubing.

#### 4.5 Conclusions

The experiments reported in this chapter, in which both straight and coiled extraction tubes are used, have shown that the rate of extraction of solute from the aqueous into the organic phase in SE-FIA can be quantitatively understood in terms of the established principles of hydrodynamics. The results obtained herein allow a refinement of the guidelines of Nord *et al.* [29] for experimentally increasing the rate of extraction in SE-FIA:

- (i) The extraction rate is increased by increasing the interfacial area to volume ratio which can be best accomplished by decreasing the tubing diameter,
- (ii) Decreasing the segment length increases the extraction rate.
- (iii) Increasing the linear velocity increases the extraction rate with respect to time, but in a less than linear fashion.
- (iv) Tightening the coiling of the tubing increases the extraction rate with respect to time, in a much less than linear way and to a greater extent for short segments than long, although for short segments it may initially decrease the extraction rate.
- (v) Decreasing the linear velocity or tightening the coiling will increase the extraction rate based on the tube length. However, decreasing



the linear velocity is not recommended since experimental studies [33,48] have shown that the band broadening produced in the extraction coil is overshadowed by that produced in the phase separator, injector and detector. Since these components contribute a constant volume variance, their effect would be magnified when the flow rate is lowered [33].

## Chapter 5

### Mechanism of Solvent Extraction and Band Broadening within Segmented Two Phase Flow

#### 5.1 Introduction

Studies of liquid-liquid segmented flow streams have established that extraction occurs across the interface at both the ends (axial extraction) and the sides (radial extraction) of the aqueous segments [29,38,149]. Experimental techniques which measure the total concentration of solute extracted as a function of time [29,149] permit a determination of the overall extraction rate constant,  $k_{\text{obs}}$ , which is the sum of the products of the axial ( $\beta_{\text{axial}}$ ) and radial ( $\beta_{\text{radial}}$ ) mass transfer coefficients times the respective ratios of interfacial area and segment volume:

$$k_{\text{obs}} = \frac{a_{\text{ends}}}{V_{\text{seg}}} \beta_{\text{axial}} + \frac{a_{\text{side}}}{V_{\text{seg}}} \beta_{\text{radial}} \quad (5.1)$$

Here  $a_{\text{ends}}$  is the combined interfacial area of the segment ends,  $a_{\text{side}}$  is the interfacial area of the side of the cylindrical aqueous segment and  $V_{\text{seg}}$  is the volume of an aqueous segment. In this chapter only the practical analytical situation in which, at equilibrium, the solute is quantitatively extracted into the organic phase will be considered.

While previous studies have permitted measurement of  $k_{\text{obs}}$ , they have not addressed the relative magnitudes of the axial and radial extraction rates. In the present chapter this question is probed using a solvent extraction - flow injection analysis (SE-FIA) system employing on-tube photometric detection and single segment injection. On-tube detectors have been used in studies of band broadening in air-water [26,27,122] and liquid-liquid [22] segmented flow, as well as in a routine fluorescence SE-FIA instrument [38]. In an on-tube photometric detector the absorbance due to solute in individual segments is measured as the segments pass through the section of extraction tube in the detector.

It is observed that solute in an aqueous segment extracts into the organic segment just ahead of it, as well as into the organic segment behind it. Once in the organic phase, the solute is dispersed backward (band broadened) into trailing organic segments via the stagnant wetting film along the walls of the tubing [21-23]. The solute which is observed in the organic segment ahead (downstream) of the aqueous injection segment must have extracted through the front end of the aqueous segment, *i.e.* only the axial mass transfer process. Thus, if the loss due to band broadening is accounted for, the amount of solute which has extracted into this downstream segment will reflect the rate of the axial mass transfer process relative to the overall extraction rate.

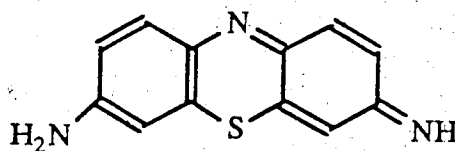
## 5.2 Experimental

### 5.2.1 Chemicals and Solvents

Double Distilled Water and Chloroform were as described in Chapter 2.

Reagent grade acetone was used as received from BDH.

Thionine, which was used as an unextracted marker, was supplied by Eastman Kodak and has the structure:



Reagent buffers used in the iodine clock reaction\*kinetic studies were prepared by combining the appropriate volumes of 2 M NaOH and 2 M citric acid to provide solutions of pH 2.1 to 4.0 [97].

Iodine was analytical reagent grade and was used as received from BDH. The spectrum of iodine in chloroform has absorption maxima at 284 ( $\epsilon=50 \text{ L mol}^{-1} \text{ cm}^{-1}$ ) and 512 nm (890), and in water it absorbs at 274 (17,200) and 460 (746) nm [150].

Other chemicals, such as  $\text{NaHSO}_3$  (J. T. Baker),  $\text{KIO}_3$  (Fisher) and KI (Fisher) were analytical reagent grade and were used as received.

### 5.2.2 Iodine Clock Reaction

Studies of the kinetics of the iodine clock reaction in homogeneous aqueous solution were conducted in a stirred 1.00 cm cuvette, thermostatted to  $25.2^\circ\text{C}$  in a Hewlett Packard 8451A diode array spectrophotometer. The iodine absorbance was measured at 420 nm at an acquisition rate of one point every 2 seconds for  $\text{pH} < 2.5$  and one point every 5 seconds for higher pH solutions. Buffer solutions (1800  $\mu\text{L}$ ), 0.023 M  $\text{KIO}_3$  (100  $\mu\text{L}$ ) and 0.048 M  $\text{NaHSO}_3$  (100  $\mu\text{L}$ ) were introduced into the cuvette using an automatic pipette (Micropipette 821, Socorex, Renens, Switzerland). Data acquisition was started immediately after the the bisulfite was mixed with the rest of the reaction solution.

### 5.2.3 Apparatus

A schematic diagram of the SE-FIA instrument used in these studies is shown in Figure 5-1. Solvents are pumped using two liquid chromatographic pumps,  $P_1$  and  $P_2$  (Model B-100-S, Eldex Laboratories, Inc., San Carlos, CA), equipped with pulse dampers (Model LP-21 LO-Pulse, Scientific Systems, Inc., State College, PA). Restrictor columns (15 cm x 1mm i.d. x 1/4 inch o.d. packed with 40  $\mu\text{m}$  glass beads), not shown in diagram, ensure sufficient backpressure for proper action of the pumps and pulse dampers. All connecting tubing downstream of the restrictor columns is 0.8 mm i.d. Teflon tubing. Valves  $V_1$  are three-port valves (part no. CAV3031, Laboratory Data Control (LDC), Riviera Beach, FL) which direct flow to either the extraction system or to waste.

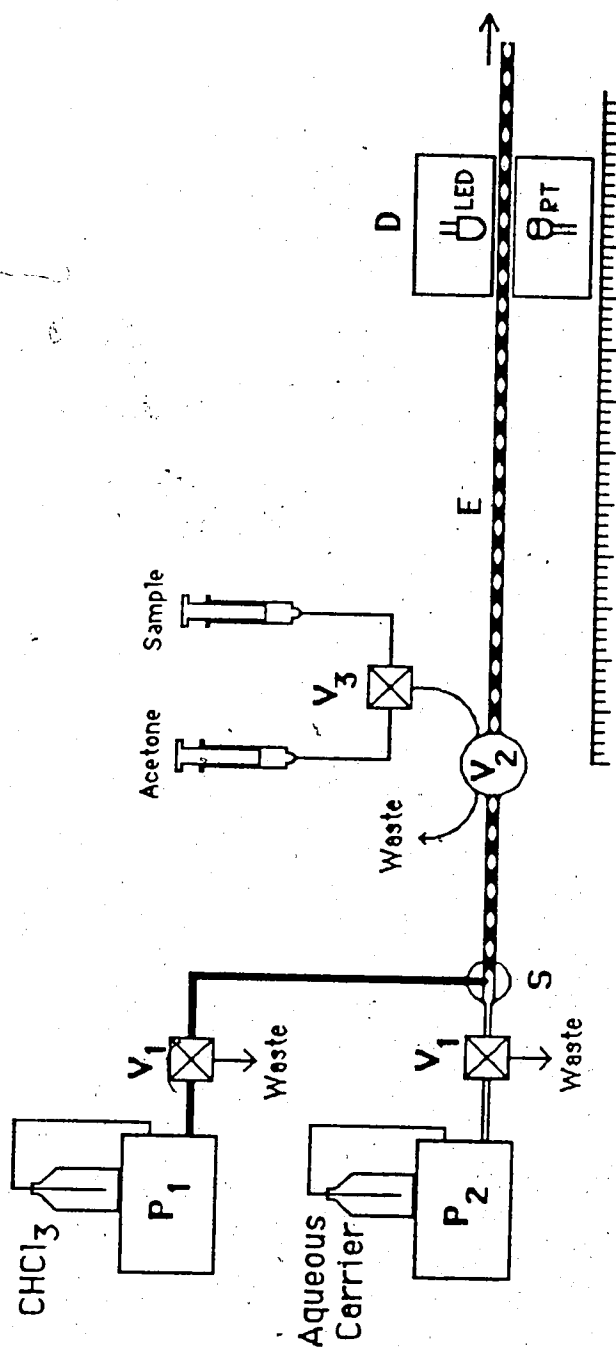


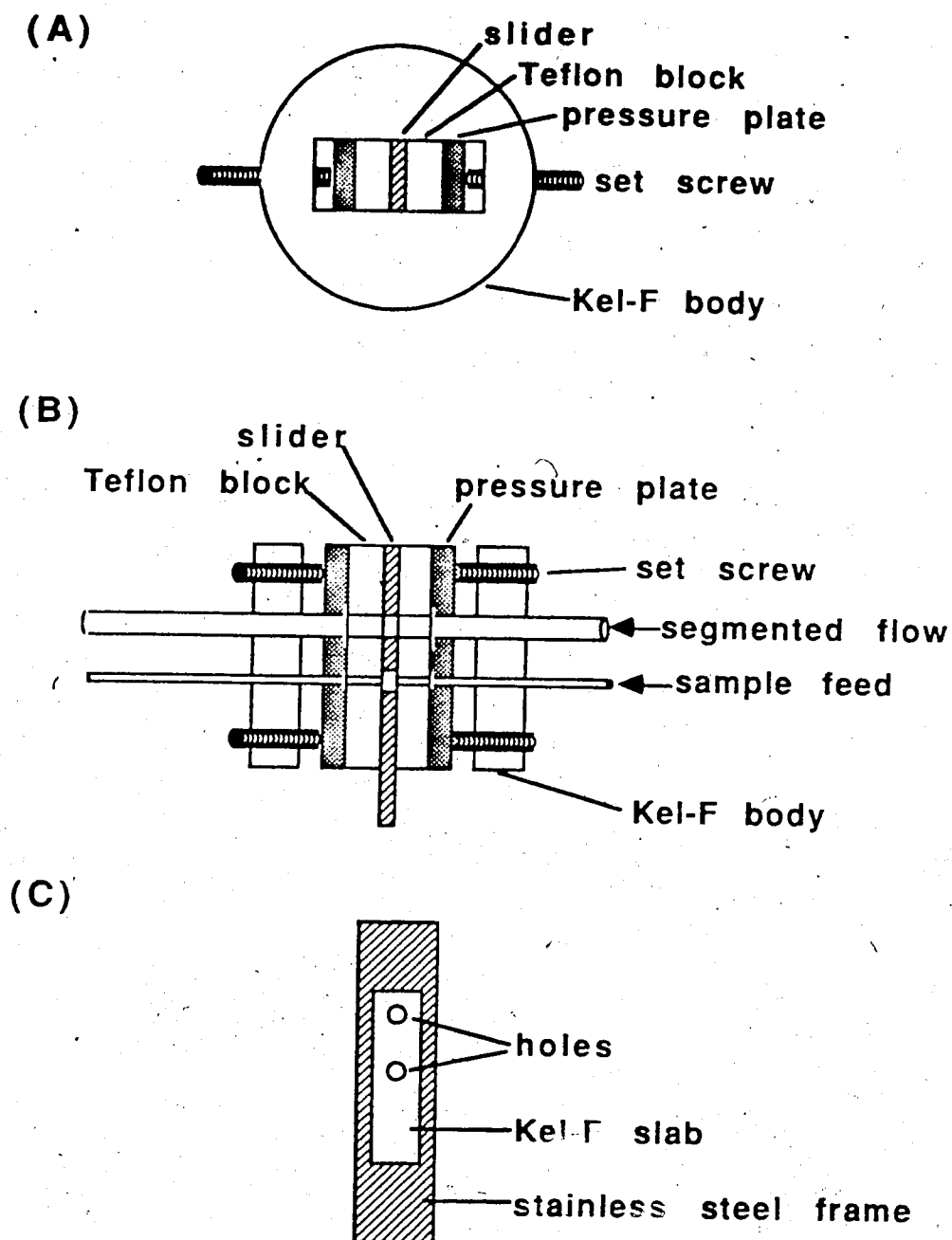
**Figure 5-1** Schematic diagram of the SE-FIA instrument used in Chapter 5.  $P_1$  and  $P_2$  are chromatographic pumps;  $V_1$  and  $V_3$  are three-port valves;  $V_2$  is a slider injection valve modified to inject into a single segment within the two phase flow;  $S$  is the segmentor,  $E$  is the extraction tube and  $D$  is an on-tube photometer constructed of a light emitting diode (LED) and a phototransistor (PT). The position of the detector along the extraction tube can be varied and is measured relative to  $V_2$ . See Section 5.2.3 for details.

The chloroform phase meets the aqueous flow at the tee-segmentor, S (part no. CJ-3031, LDC), the channels of which have been bored out to 3.0 mm in diameter. The length of the segments was varied by tilting the tee fitting, since gravity, as well as the hydrodynamics and interfacial tension [31], plays a role in the formation of these large segments.

The segmented flow passes through 60 cm of 3.0 mm i.d. FEP Teflon tubing in order to stabilize the flow streamlines within the segments, and then enters the segment injector,  $V_2$ . This valve is based on a slider injection valve (part no. CSVA, LDC) and has been modified to inject into a single moving segment. Figure 5-2 shows a top (A) and cross sectional side (B) view of this injection valve. The valve contains a slider (C) having two 3.0 mm diameter holes cut through a 7 x 25 x 1.8 mm Kel-F slab molded into a 1.5 mm thick stainless steel frame. The steel frame of the slider provides sufficient structural support for it to be moved rapidly between the Load and Inject positions. The slider moves between two Teflon blocks (shown in A and B). Stainless steel pressure plates press the flared ends of the connecting tube, the Teflon blocks and the slider together, making a seal between these parts. Four set screws adjust the force of this seal.

When the slider is in the Load position, as is shown in Figure 5-2B, the segmented flow stream passes through the upper hole of the slider. At the same time, sample can be syringed through the lower hole, which is the sample chamber. When the slider is pushed into the Inject position (upward in Figure 5-2B), the contents of the sample chamber are inserted into the segmented flow stream. The volume of the sample injected is approximately 14  $\mu\text{L}$ . The injector was manually switched to the Load position, but a pneumatic actuator (part no. PA-875, LDC) connected to an air solenoid valve (part no. SOL-3-24VDC, LDC) was used to switch the slider to the Inject position to ensure sufficient speed to inject into the middle of a single segment.

At the start of each Load cycle the sample feed tube and the lower hole of injector  $V_2$  were rinsed with acetone, which could be selected using the three port valve  $V_3$  shown in



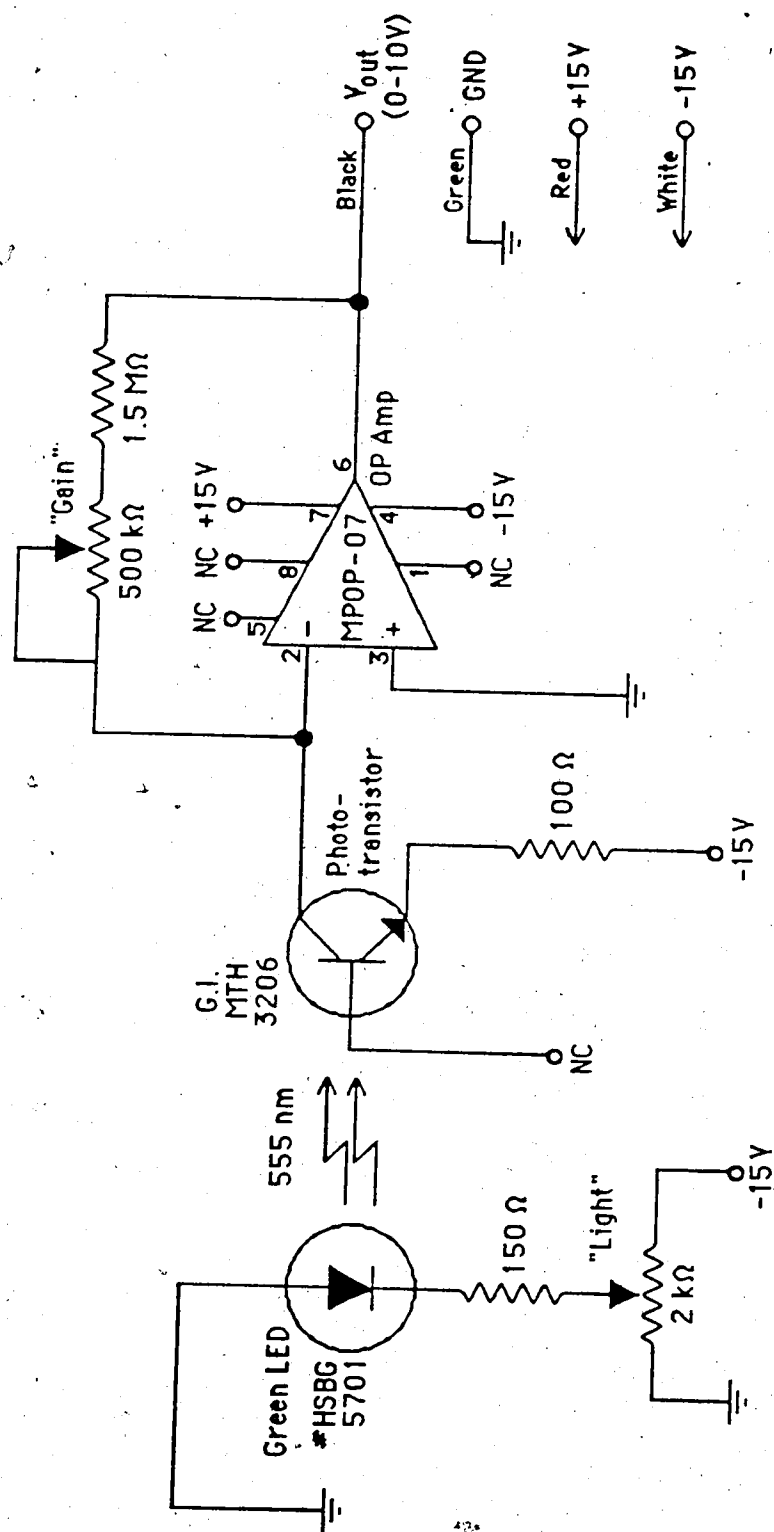
**Figure 5-2** Single segment injection valve shown in (A) top view and (B) cross sectional side view. The injector is in the Load position in (B). A front view of the slider is shown separately in (C).

Figure 5-1. If this rinse was not used the relative standard deviation of replicate injections of nonextracting thionine into a single aqueous segment was large (4.0%) as a result of chloroform adhering to the walls of the slider hole. With the acetone flush the injection relative standard deviation improved to 1.1%.

After exiting injector  $V_2$  the segmented flow enters the 3.0 mm i.d. FEP Teflon extraction tube, E, which is held straight in all experiments. At a variable position along this tube, transmittances of the segmented flow stream are measured using an on-tube photometric detector, D. The effective extraction tube length is varied by repositioning the detector along the 3.0 mm i.d. tubing. The detector was based on a design described in the literature [151,152] and is shown schematically in Figure 5-3. A green GaP LED (part no. HSBG 5701, Stanley Electric Co., Tokyo), with an emission maximum of 555 nm and a bandwidth of 30 nm, and a phototransistor (part no. MTH 3206, General Instrument, Palo Alto, CA) are mounted opposite one another in a black Delrin block. The extraction tube passes through a snug cylindrical channel drilled through this block between the LED and phototransistor (PT). The faces of the LED and PT were located 2 mm away from the walls of this extraction tube channel and opened into it via a 1.0 mm light channel. The signal from the phototransistor is amplified (part no. MPOP07, Precision Monolithics Inc, Santa Clara, CA) and feed into an analog-to-digital converter (Lab Master, TM-40-PGL, Tecmar, Cleveland, OH) in an IBM-XT microcomputer. Data acquisition is controlled by the program DATAcq.ASY (Appendix B).

Absorbances of the aqueous and organic segments were calculated from the transmittance signals, using the signal measured for the organic segments before the peak as the incident light intensity ( $I_0$ ). A typical segment absorbance profile measured with this detector is shown in Figure 5-4. The ends of the segments deflect the light causing the sharp absorbance spikes in the signal. The aqueous and organic segment absorbances are the plateaus between these spikes, with the aqueous segments having a higher background absorbance. The absorbances of the organic segments within this complex signal were





**Figure 5-3** Electronic circuit for the on-tube photometric detector. (Based on drawing 239 of the Chemistry Department Electronics Shop). NC means not connected. "Light" and "Gain" are the markings on the detector housing identifying the two variable resistor set screws, which are the light intensity and gain controls respectively. See Section 5.2.3 for details.

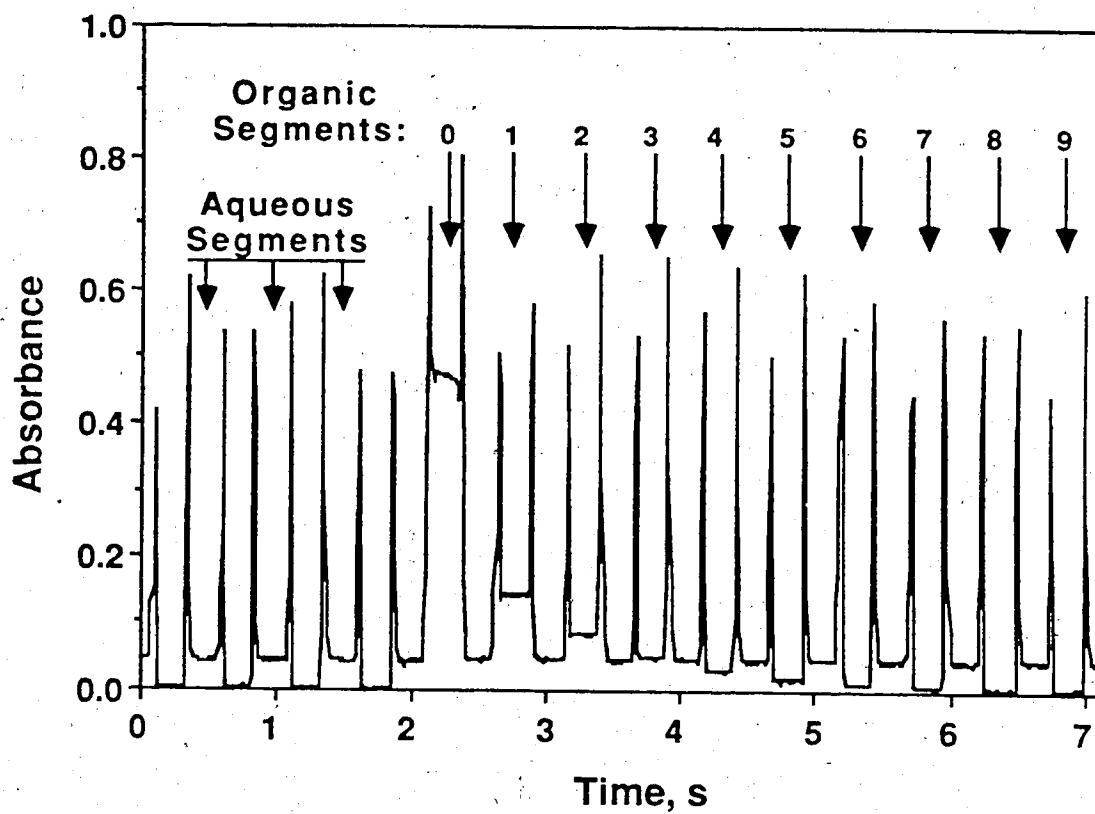


Figure 5-4 Absorbance *versus* time profile obtained after injecting iodine with injector  $V_2$  into a single chloroform segment, with the on-tube photometric detector positioned some distance downstream of the injector.

obtained semi-automatically using the program SEGMENT.ASY (Appendix C) written in ASYST (Macmillan Software Co.). This program first located the absorption spikes due to the segment ends, and then calculated the mean for each plateau, which was defined as starting 4 data points after the spike. Plateaus extended from 14 points for the 5.4 mm segments to 32 points for the 14.3 mm segments. The program then identified the first organic segment, which was on the baseline, and defined the organic segment absorbances as being that of every second plateau after the initial organic segment. The aqueous segment absorbances were not used in this work.

#### 5.2.4 Extraction Studies

For these experiments, the aqueous carrier solution contained iodate, and the injection solution contained bisulfite and iodide. The concentrations of these solutions were adjusted so that upon injection the reagent concentrations within the injection segment were 0.02 M  $\text{KIO}_3$ , 0.03 M  $\text{NaHSO}_3$  and 0.03 M  $\text{KI}$ . The pH of the injection solution was adjusted to 6.0 by adding  $\text{NaOH}$  and sparged with water saturated  $\text{N}_2$  to prevent air oxidation of iodide. All solutions were prepared just prior to use.

Injector  $V_2$  was first flushed with acetone and then rinsed and loaded with the bisulfite/iodide solution. The pneumatic actuator was manually triggered based on visual observation of the segments flowing into injector  $V_2$ . A number of criteria were used to evaluate if the injection had been made cleanly into a single aqueous segment (designated as segment number 0). These were: i) no changes in segment length and no droplets of chloroform within the injection segment, ii)  $\text{I}_3^-$  formation was observed after the correct time delay (8-9 s) and iii) no  $\text{I}_3^-$  was formed in any other aqueous segment. For the 9.6 and 14.3 mm long segments, the injection efficiency was almost absolute, but for the 5.4 mm segment only about a quarter of the attempted injections went cleanly into a single segment to yield useable data. The minimum segment length which could be studied using this technique was limited by the difficulty of injecting into a single segment.

The point at which the yellow color of the  $I_3^-$  was first observed in the injection segment was recorded as the reaction point (time=0) and was typically about 30 cm from  $V_2$ . Data collection was initiated when the injection segment was 5 cm from the detector and continued for 20 s at a rate of 100 pt/s. The length of the extraction tube is taken as the distance between the reaction point and the on-tube detector, and ranged from 10 to 200 cm. The detector was positioned between these extremes at approximately 10 cm intervals.

The segment absorbances measured in these experiments were treated in two ways. In the first, the absorbances of all of the organic segments obtained with the detector at each particular location for the injection into a single segment were summed together. The variation of these summed absorbance with detector position (i.e. time) was used to determine the overall extraction rate,  $k_{obs}$ , using equation 5.9 in Section 5.3.4.2. In the second procedure, only the absorbance of segment -1 (i.e. the segment immediately ahead (downstream) of the aqueous injection segment) at each detector position was used. These data were fit to equation 5.16 using the nonlinear least squares program KINET [153], with the absorbance of iodine in segment -1 at time zero,  $A_{-1,t=0}$ , the band broadening rate constant,  $k_2$ , and the rate for extraction into segment -1,  $k_1$ , as variables. The overall extraction rate,  $k_{obs}$ , and the concentration of iodine in the aqueous segment at time zero,  $[I_2]_{aq,t=0}$ , were used as constants, since these were obtained from the total absorbance of all the organic segments using equation 5.9. In equation 5.16, all concentrations were converted to their corresponding organic phase absorbance. For  $[I_2]_{aq,t=0}$  this corresponds to the total organic phase absorbance at equilibrium,  $A_{org,t=\infty}$ , minus the organic phase absorbance at time zero,  $A_{org,t=0}$ . All data points were equally weighted and the convergence criterion was a maximum relative change of 0.01 in any of the variables between successive iterations.

The aqueous carrier reagent was the same as in the extraction studies described in Section 5.2.4. The injection solution was iodine in chloroform, at the concentration required to match the maximum absorbance observed in the corresponding extraction study. This ranged from 0.012 to 0.043 M, depending on the segment length. Injection was made into a single chloroform segment, designated as segment number 0. As in the extraction studies, injector  $V_2$  was flushed with acetone before being loaded with the injection solution. Triggering of the pneumatic actuator was based on observation of the segments entering the injector. Since no reaction occurred in this study, the only criteria of proper injection which could be used were no changes in segment length and no droplets of chloroform within aqueous segments adjacent to the chloroform injection segment. The distance between  $V_2$  and the detector was recorded as the extraction tube length, and ranged between 10 and 200 cm at 10 cm intervals. The data acquisition conditions were as in the extraction studies. Variances were calculated as the second central moment,  $\overline{m}_2$ . Since the signals observed in this work were discrete distributions, summations were used in the calculation of the moments, rather than the Simpson's rule integration which was used for the continuous distributions studied in Chapter 3.

### 5.2.6 Measurement of Segment Shape

Segments flowing through the extraction tube at 3.5 cm/s were photographed using a 35 mm Cosina SLR camera fitted with a 50 mm lens and a 9 cm extension tube: f-stop, 2.1 and shutter speed 1/500 s. The tubing was illuminated at an oblique angle using two 100W incandescent lamps. The film used was black and white with an ASA of 400 (HP5). The shape of the segment end was measured directly from the photographs, such as that shown in Figure 5-5. The segment ends were semi-ellipsoids with the major axis being the radius of tube (0.15 cm), and the minor axis,  $b$ , being measured as  $0.097 \pm 0.006$  cm,

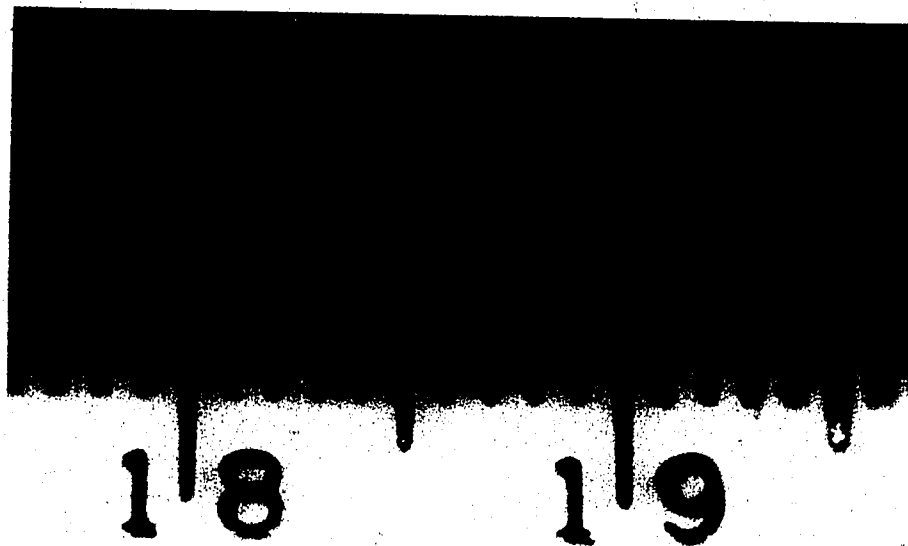


Figure 5-5 Photograph of 5.4 mm long aqueous segment flowing through the 3.0 mm i.d. Teflon tubing at a linear velocity of 3.5 cm/s. Organic phase is chloroform. See Section 5.2.6 for details.

independent of the segment length. The expressions for segment interfacial area and volume based on this semiellipsoid end shape are:

$$a_{\text{seg}} = 2(a_{\text{end}}) + a_{\text{side}} = 2 \left( \pi r_t^2 + \frac{\pi b^2}{2\epsilon} \ln \frac{1+\epsilon}{1-\epsilon} \right) + ((L_{\text{aq}} - b) 2\pi r_t) \quad (5.2)$$

$$V_{\text{seg}} = 2(V_{\text{end}}) + V_{\text{cylinder}} = 2 \left( \frac{2}{3} \pi r_t^2 b \right) + ((L_{\text{aq}} - b) \pi r_t^2) \quad (5.3)$$

where  $\epsilon$  is the eccentricity of the ellipsoid, and is given by:

$$\epsilon = \frac{\sqrt{r_t^2 - b^2}}{r_t} \quad (5.4)$$

These expressions are used in all interfacial area and volume calculations in this chapter.

### 5.3 Results and Discussion

From Chapter 4, it is evident that the behavior of segments both longer and shorter than about 2-3 times the tubing diameter must be studied in order to characterize the processes occurring within the segmented flow fully. In this work the extraction of solute from a single aqueous segment and its subsequent band broadening among trailing organic segments was studied. In order to be able to inject into single segments which were less than twice the tube diameter in length, it was necessary from a practical point of view to employ an extraction tube with an internal diameter of 3.0 mm, which is wider than is typically used in SE-FIA [18]. However, previous studies of extraction (Chapter 4) and band broadening [22] in SE-FIA have indicated that results obtained in wider tubing [24,26,27], such as used in Technicon Auto-Analyzers, is applicable to the narrower tubing, since it is the segment length relative to the tube diameter (segment aspect ratio) which is the important parameter of flow in a segmented stream (see Section 4.4.8).

Therefore the results obtained herein in wider tubing are relevant to the extraction and band broadening processes occurring within the extraction tube in SE-FIA.

### 5.3.1 On-Tube Detection.

The light from the LED passes perpendicularly through the center of the 3.0 mm i.d. PTFE Teflon extraction tube and is detected by the phototransistor, which produces a current proportional to the amount of light incident upon it. Since the dark current of this photometer was negligible ( $\sim 5$  mV for a 10V full transmittance signal), absorbances were calculated directly from the transmittance, using the pure chloroform segments prior to the peak as the incident light,  $I_0$ . As an example, the absorbance *versus* time profile obtained after injection of iodine into a single chloroform segment is shown in Figure 5-4, and is similar to the output of the transverse photometers used in a study of band broadening in air segmented flow [26,27,122]. As a segment end passes through the light beam, it deflects the beam, causing a sharp absorbance spike. The width of this spike reflects the physical dimensions of the segment end and the detector slit, and not the response time of the detector components, which for both the LED and phototransistor are on the order of nanoseconds. The absorbance of the bulk portion of the segments appear as plateaus in Figure 5-4, with the aqueous segments having a background absorbance about 0.05 AU higher than the organic segments.

Using the apparatus as shown in Figure 5-1, a Beers Law plot was conducted for chloroform solutions of iodine between 0.006 to 0.040 M. Sample solutions were injected via valve  $V_2$  into a single 9.9 mm long organic segment within the segmented flow and the absorbance of the injection segment (segment number 0) was monitored with the on-tube detector, positioned 10 cm from injector  $V_2$ . Iodine, injected into chloroform segment 0, is carried back into following upstream segments (segment numbers  $> 0$ ), for reasons to be discussed in Section 5.3.2. At a distance of 10 cm about 82% of the injected iodine remained in the injection segment. Five replicates were made of each standard. Important



instrumental parameters were: chloroform flow rate, 7.5 mL/min; aqueous reagent flow rate, 7.5 mL/min of 0.025 M  $\text{KIO}_3$ ; injection volume of  $V_2$ , 14  $\mu\text{L}$ ; data acquisition rate, 100 pts/s and the number of points collected, 800.

The plot of absorbance of injection-segment 0 *versus* iodine concentration injected is shown in Figure 5-6. It is rectilinear with a relative standard deviation for the slope of 1.5% and an intercept equal to zero within the 95% confidence limit. The precision of the absorbance of segment 0 for replicate injections was 5.4%.

### 5.3.2 Band Broadening

Band broadening occurs within the organic phase in liquid-liquid segmented flow, through Teflon tubing as a result of the formation of an organic wetting film along the walls of the tubing [21-23]. In this study, iodine in chloroform was injected into a single organic segment, segment number 0. As segment 0 travels down the tube, fluid from it will be left behind as a stagnant film on the tube wall adjacent to the trailing aqueous segment. This stationary film is then overtaken by the next organic segment (number 1) and mixed within it. Thus iodine is transferred from segment 0 to the upstream segment 1. This process is repeated for transfer from segment 1 into segment 2, and so on along the train of organic segments. The segment profiles which result from this band broadening process are shown in Figure 5-7 to 5-9 at various points along the extraction tube for three segment lengths. In these graphs the organic phase absorbances are indicated by the solid bars and the interface and aqueous phase absorbances are omitted. The absorbances have been normalized so that the total absorbance of all of the organic segments equals 1. The position of the detector along the extraction tube is given at the top of each graph. The profiles in Figure 5-7 to 5-9 display a Poisson-type distribution not unlike that observed for air segmented flow [26,27]. That is, the profile is exponential at short extraction tube lengths but gradually becomes more Gaussian as the segments flow further down the tube. This is most clearly illustrated by the band broadening of the 5.4 mm segment (Figure 5-9).

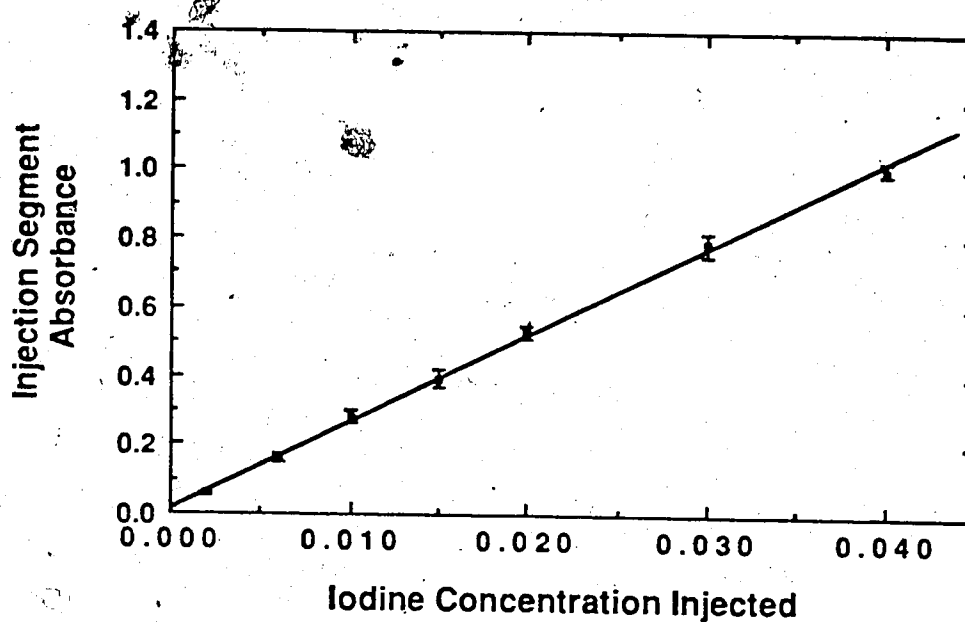


**Figure 5-6** Linearity of iodine absorbance at 10 cm in chloroform-injection segment measured by the On-tube Photometric Detector for Single Segment Injection. Important instrumental parameters were: chloroform flow rate, 7.5 mL/min; aqueous reagent flow rate, 7.5 mL/min of 0.025 M  $\text{KIO}_3$ ; segment length, 9.9 mm; injection volume of  $\text{V}_2$ , 14  $\mu\text{L}$  of  $\text{I}_2$  in  $\text{CHCl}_3$ ; number of replicates, 5; data acquisition rate, 100 pts/s and the number of points collected, 800.

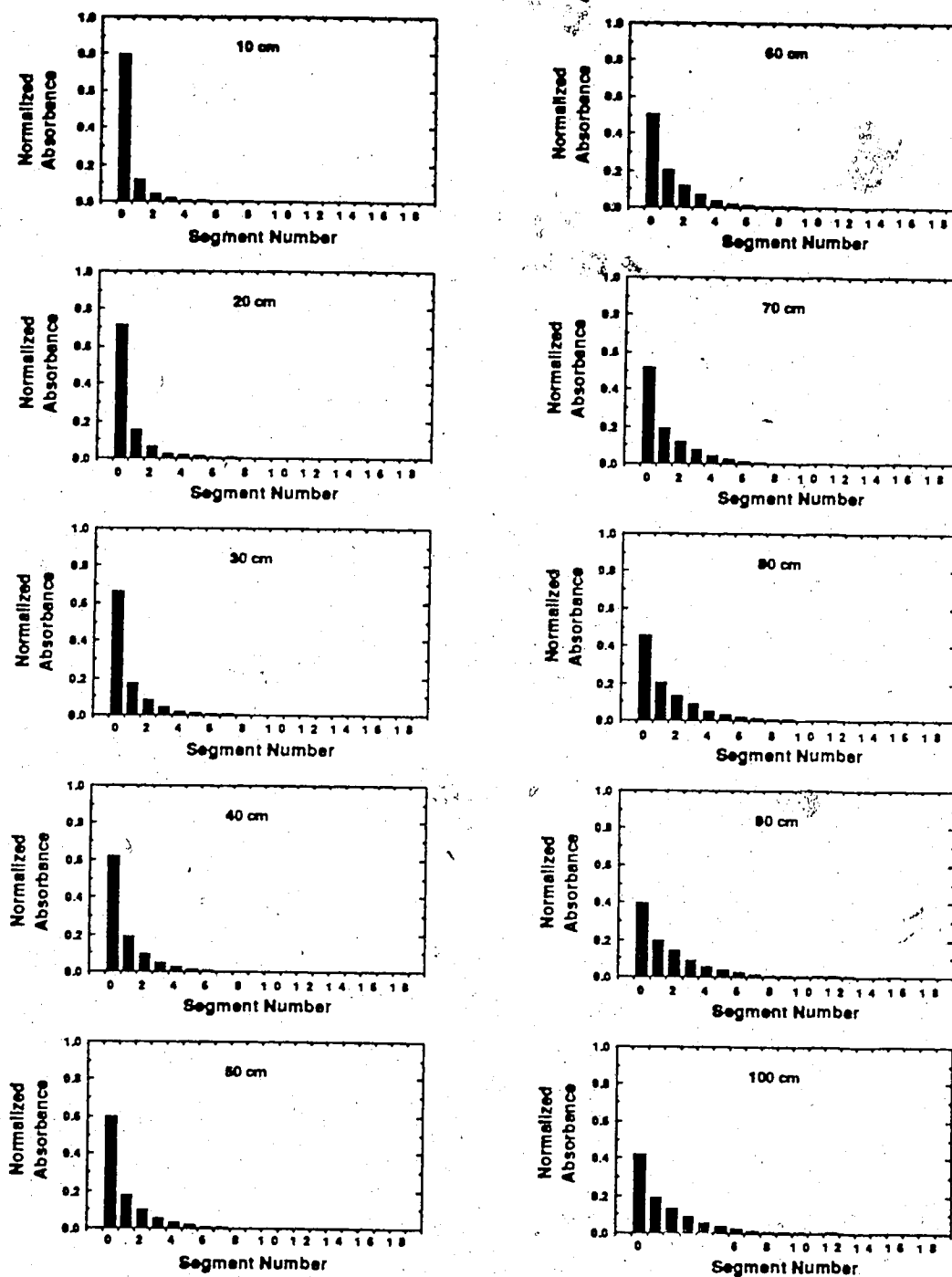


**Figure 5-7a** Organic segment profiles due to band broadening of iodine from a single 14.3 mm organic segment. Segment number is the position relative to injection segment 0, with positive segments being upstream, i.e. following. At the top of each graph is the distance separating injector  $V_2$  and on-tube detector, D.

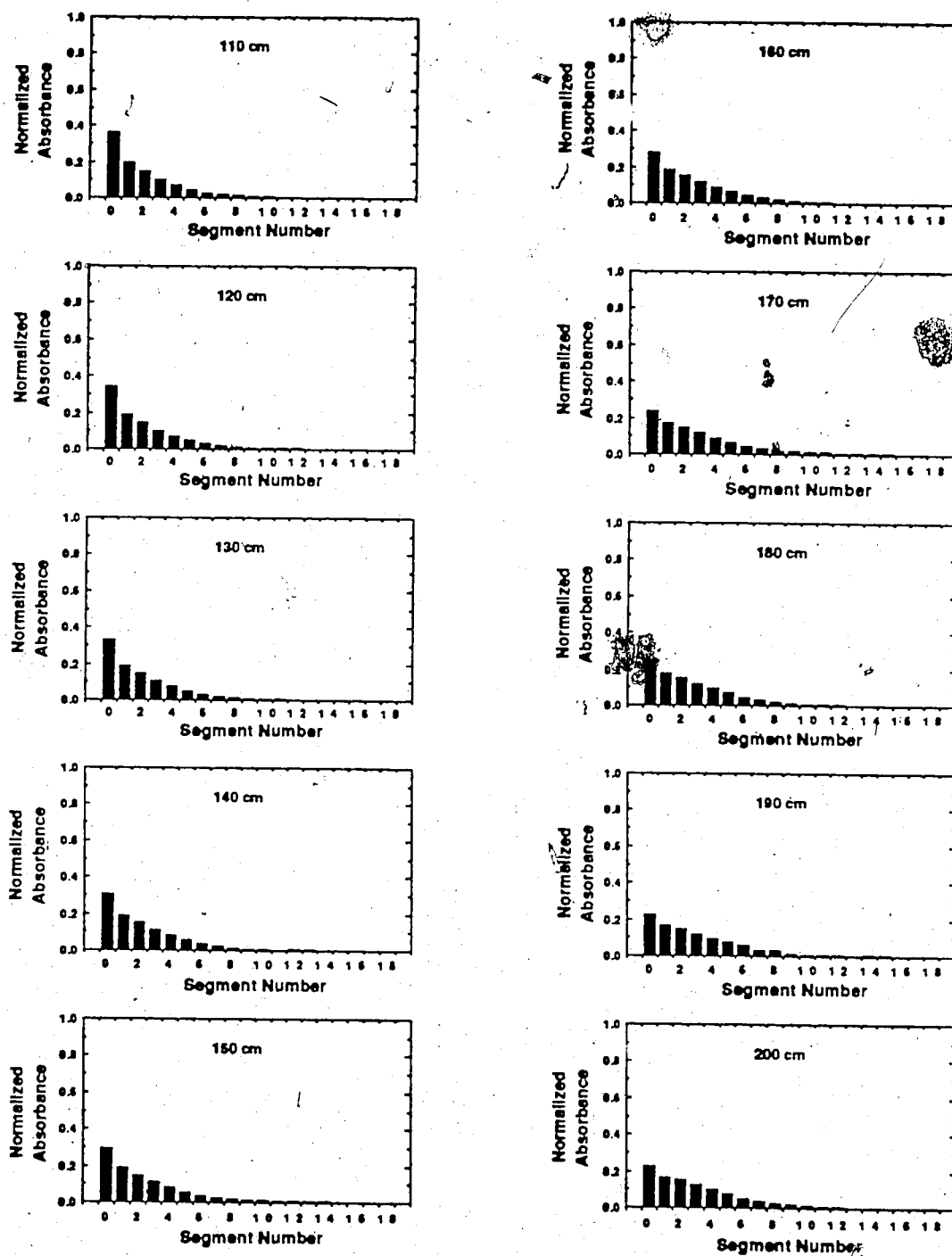
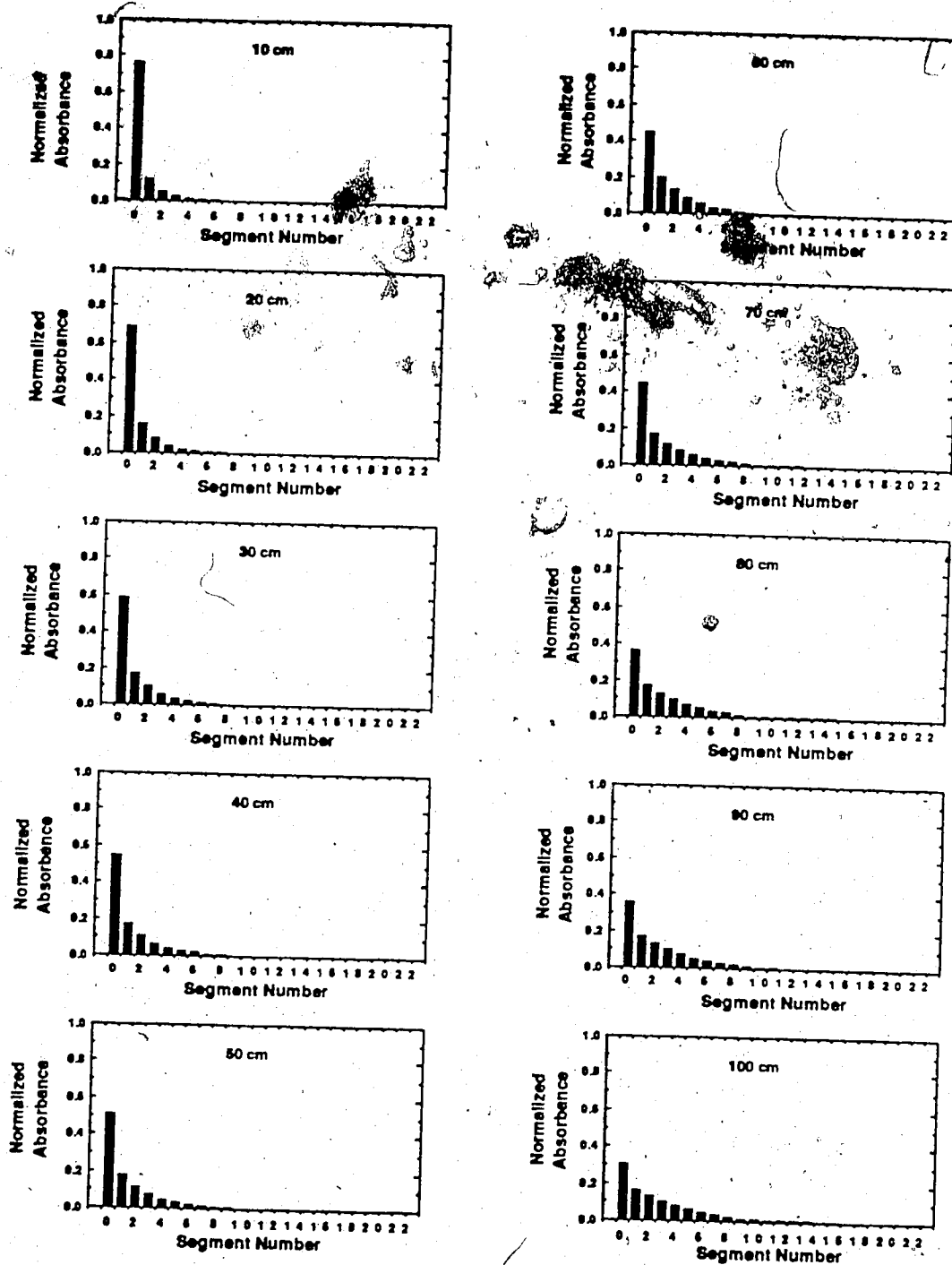


Figure 5-7b Continued from Figure 5-7a. Band broadening of iodine from a single 14.3 nm segment.



**Figure 5-8a** Organic segment profiles due to band broadening of iodine from a single 9.6 mm organic segment. Segment number is the position relative to injection segment 0, with positive segments being upstream, i.e. following. At the top of each graph is the distance separating injector  $V_2$  and on-tube detector, D.

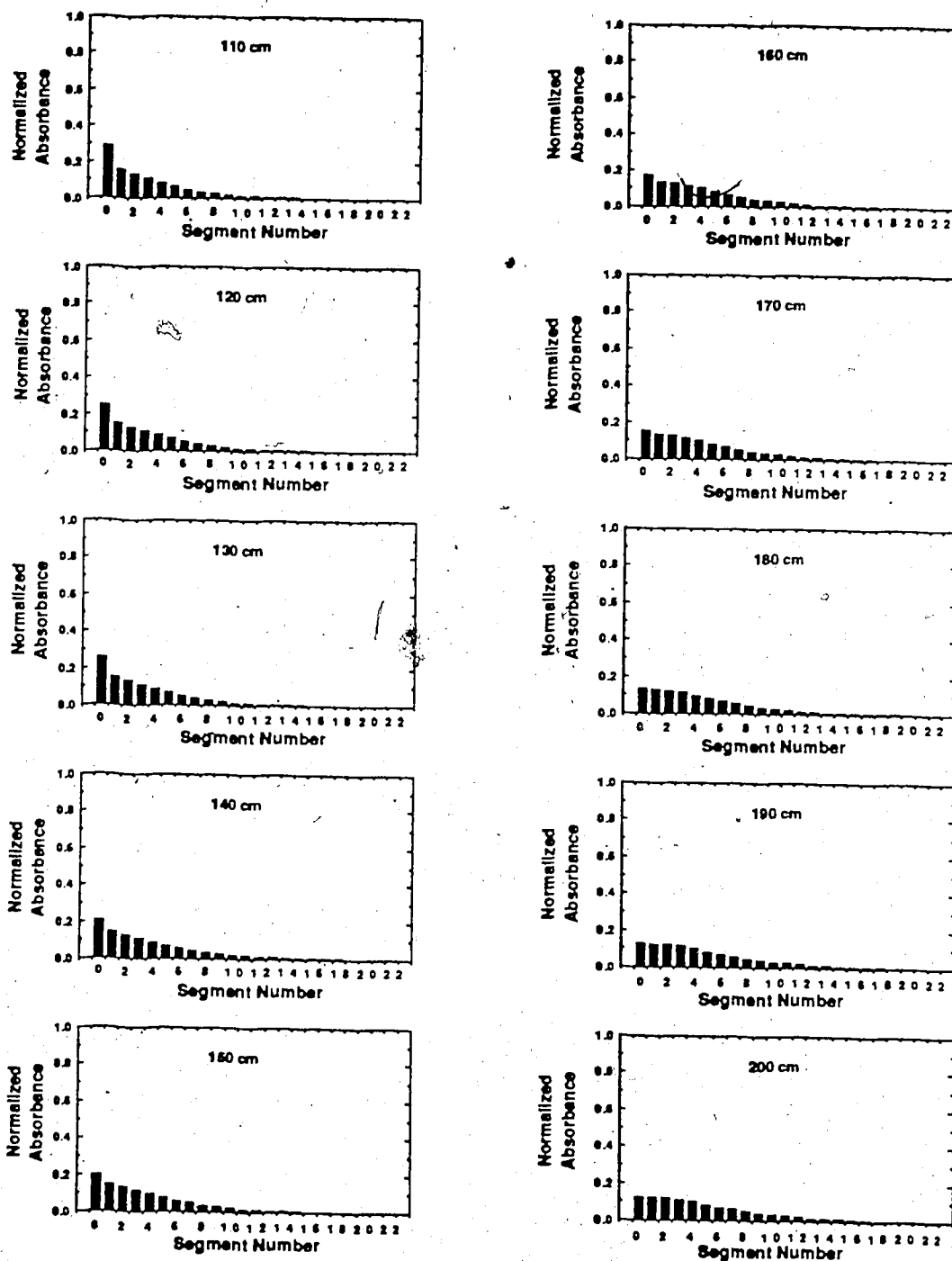


Figure 5-8b Continued from Figure 5-8a. Band broadening of iodine from a single 9.6 mm segment.

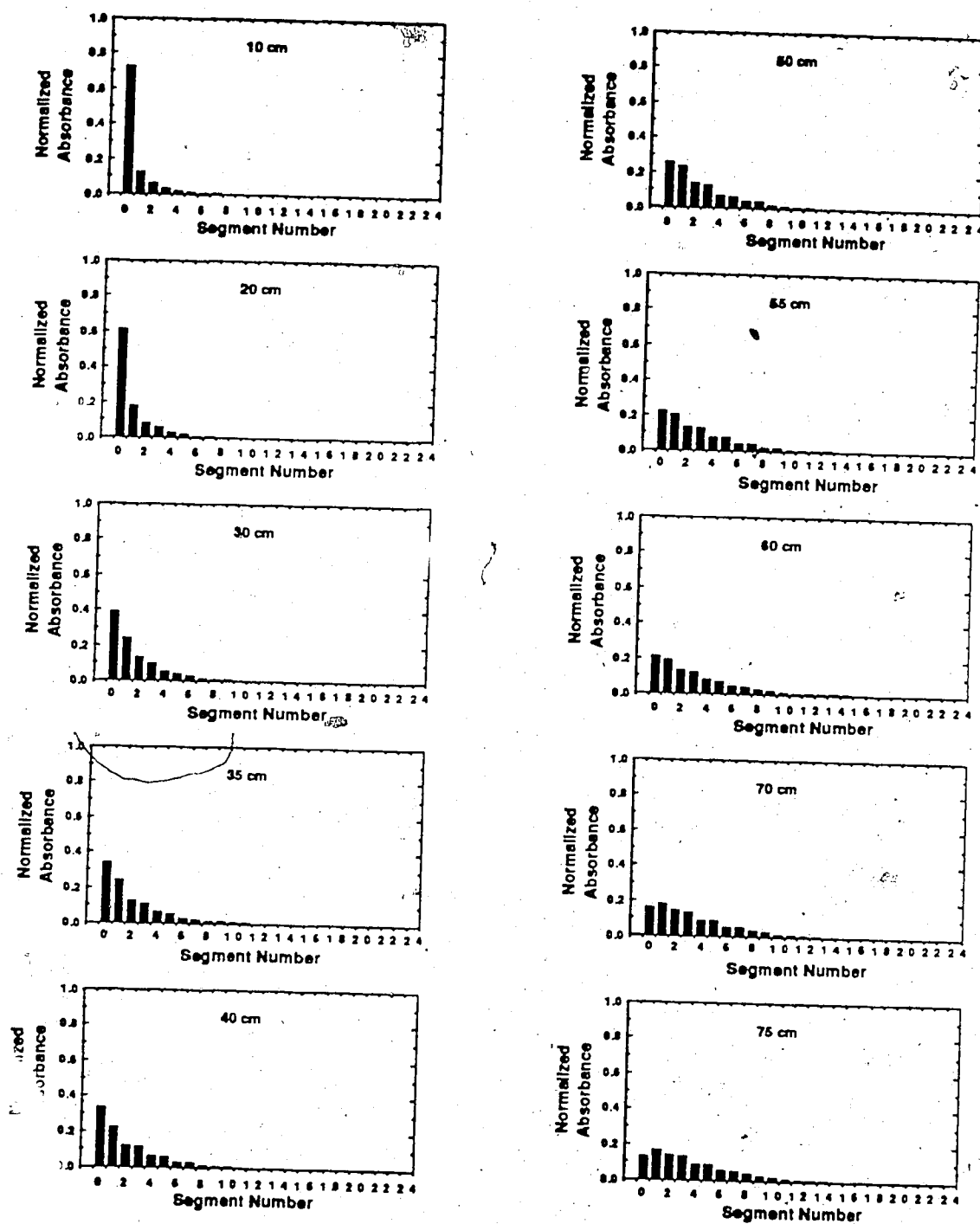


Figure 5-9a Organic segment profiles due to band broadening of iodine from a single 5.4 mm organic segment. Segment number is the position relative to injection segment 0, with positive segments being upstream, i.e. following. At the top of each graph is the distance separating injector  $V_2$  and on-tube detector, D.

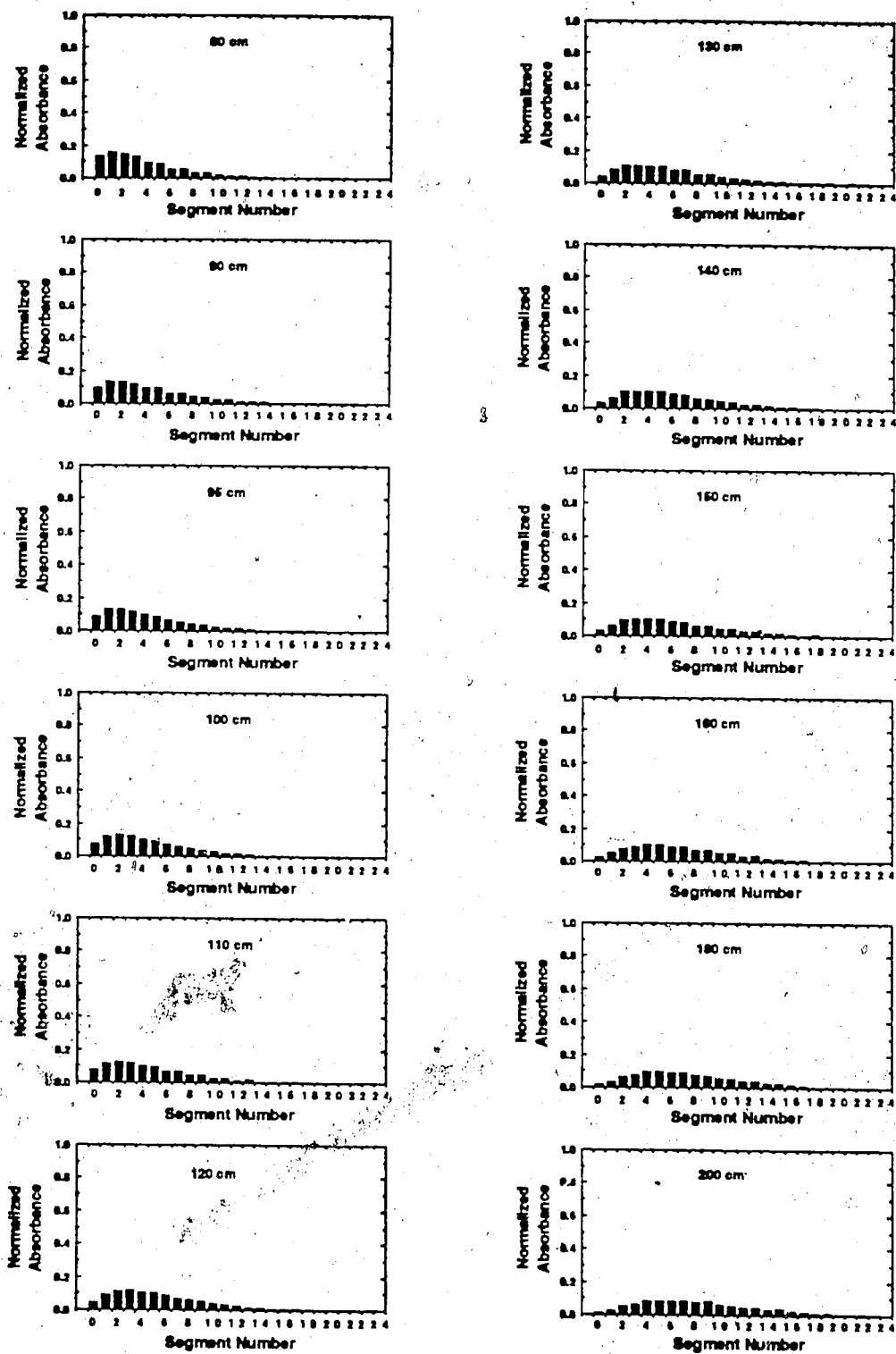


Figure 5-9b Continued from Figure 5-9a. Band broadening of iodine from a single 5.4 mm segment.



Two limiting models have been developed to describe the band broadening in air segmented flow [26,27]. In the Ideal model [26], it is assumed that the organic segments act as mixing chambers, such that all of the liquid in the wetting film adjacent to the aqueous segment mixes completely and instantly with the next organic segment that comes along. The variance predicted by the Ideal model is:

$$\sigma^2 = \frac{V_f}{V_{seg}} = \frac{4 d_f L}{L_s d_t} \quad (5.5)$$

where  $V_f$  is the total volume of film deposited from any segment during its passage through a given length of tube  $L$ ;  $V_{seg}$  and  $L_s$  are the volume and length of a single organic segment;  $d_f$  is the thickness of the wetting film and  $d_t$  is the inner diameter of the tube. In Figure 5-10, the Ideal model is compared with the experimentally determined variances for the band broadening profiles shown in Figures 5-7 to 5-9. The points are the experimentally determined variances for tube lengths between 10 and 200 cm and the solid line marked I indicates the variance predicted by the Ideal model for  $d_f = 14.6 \mu\text{m}$ . This film thickness was calculated using equation 4.6 for:  $\eta_c = 0.0058 \text{ P}$ ;  $\gamma = 32.8 \text{ dyn/cm}$  [154] and  $v = 3.5 \text{ cm/s}$ . It is clearly evident that the Ideal model underestimates the band broadening in the chloroform/water segmented flow, as has been observed to be the case in air segmented systems as well [26].

To account for the additional band broadening, over-and-above that predicted by the Ideal model, a second model was developed which assumes instant and full mixing within the bulk organic segment, but no mixing between this bulk fluid and the wetting film. Thus, in this Nonideal model [27], solute transfers from the film into the bulk organic segment only via diffusion. The variance predicted by this model is the variance due to the diffusion from the stagnant film ( $\sigma_f^2$ ) along with that predicted by the Ideal model ( $\sigma_i^2$ ):

$$\sigma^2 = \sigma_i^2 + \sigma_f^2 = \frac{V_f}{V_s} + \frac{L V_f^2 d_t^2 v}{36 D_m L_s^2 v^2} \quad (5.6)$$

where  $v$  is the linear velocity,  $D_m$  is the diffusion coefficient of the solute in the organic solvent and  $V$  is the internal volume of the tube of length  $L$ .

Variances predicted by the Nonideal model are also compared with the experimental variances in Figure 5-10. The solid line marked N indicates the variance predicted by the Nonideal model based on a diffusion coefficient of  $2.1 \times 10^{-5} \text{ cm}^2/\text{s}$  for  $\text{I}_2$  in chloroform at  $20^\circ\text{C}$  [154]. For all three segment lengths studied the observed band broadening lies between the behavior predicted by the Ideal and the Nonideal models, as has been observed for air segmented flow [26,27]. This indicates that convection does play a significant role in the mixing between the wetting film and the bulk of the organic segment ( $\sigma_{\text{obs}}^2 < \sigma_{\text{nonideal}}^2$ ), as has been noted previously [22], but this convection is not strong enough to mix the film completely with the bulk fluid ( $\sigma_{\text{obs}}^2 > \sigma_{\text{ideal}}^2$ ). For the two longer segments, 9.6 and 14.3 mm, the band broadening appears to be more nonideal ( $\sigma_{\text{obs}}^2 = 0.45 \sigma_{\text{nonideal}}^2$ ) than for the 5.4 mm segment ( $\sigma_{\text{obs}}^2 = 0.18 \sigma_{\text{nonideal}}^2$ ). This difference in band broadening behavior can be understood in terms of the increased radial convection with segments of small aspect ratio (Section 4.4.6). In segments whose length is many times the diameter of the tubing, the flow at mid-point of the segment is largely parabolic and has no radial component. However, when the segment length is on the order of the tube diameter, the ends of the segment interact hydrodynamically to generate a much stronger radial flow [130], which enhances mixing between the bulk organic phase and the stagnant film, just as it enhances the mass transport within the aqueous segments. Thus with the short segments there is less band broadening because of the greater convective mixing between the film and the bulk liquid in the segment.

For the mixing chamber process assumed in the Ideal model, the concentration of solute  $C_n$  in the  $n^{\text{th}}$  segment following the injection segment is:

$$\frac{C_n}{C} = \frac{(\sigma^2)^n}{n!} e^{-\sigma^2} \quad (5.7)$$

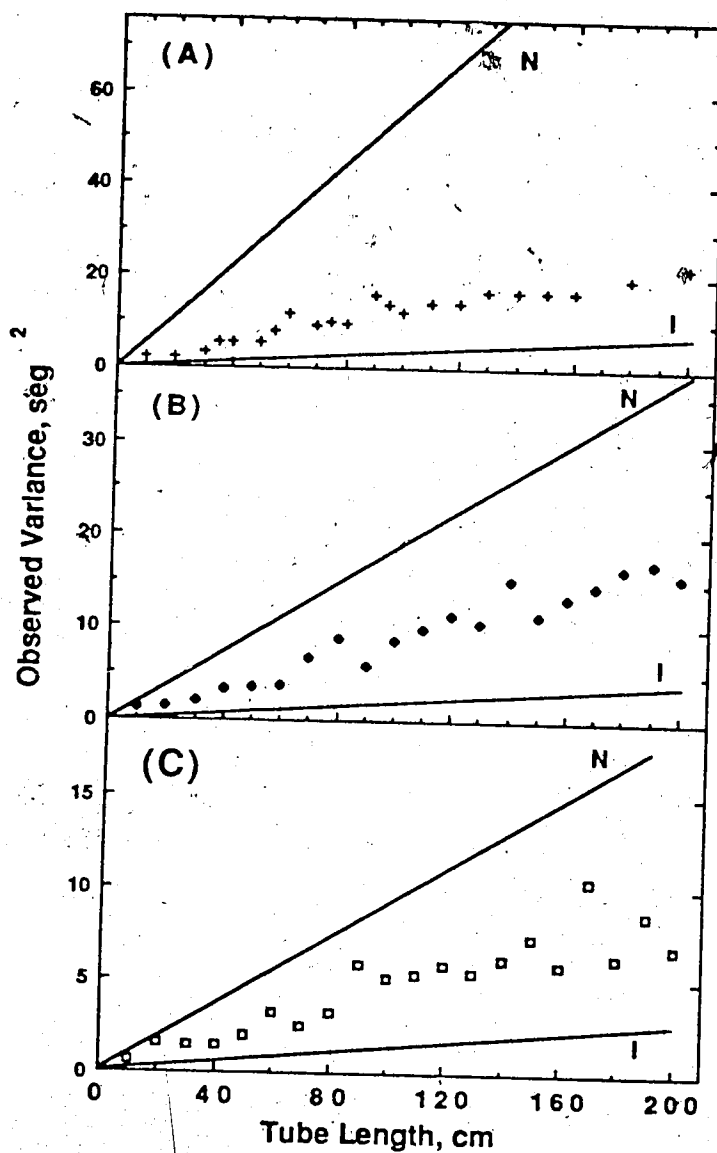


**Figure 5-10** Observed variance resulting from band broadening in segmented flow for extraction tube lengths of 10 to 200 cm for three segment lengths: (A) 5.4 mm (+); (B) 9.6 mm (•) and (C) 14.3 mm (□). The solid lines are the variances predicted by the Nonideal (equation 5.6) (N) and by the Ideal (equation 5.5) (I) models for band broadening.

The right hand side of this equation is the discrete Poisson distribution, where  $n$  is the number of degrees of freedom. This equation predicts an exponential decrease (Poisson with  $n=0$ ) in the concentration of solute in the injection segment (segment number 0), where the rate of disappearance follows mixing chamber behavior. The Nonideal model would predict a slower rate of loss from the injection segment, but the general exponential behavior would still be expected since the bulk of the segment is assumed to be well mixed.

The experimentally observed dependence of iodine absorbance of segment 0 on tube length is shown in Figure 5-11. It is an exponential decay. The observed rate constants for these experimental results and the rate constants predicted using the Ideal model for the three segment lengths are given in Table 5-1. As expected, the observed loss of iodine was slower than predicted by the Ideal model; for 5.4 mm  $k_{bb}$  was 65% of that predicted and for the longer segments it was 49%. This is another way of showing that the band broadening is greater than predicted by the Ideal model ( $\sigma^2 = (1/k_{bb})^2$ ), as was observed in Figure 5-10.

A second important feature of Figure 5-11 is that the nonlinear (exponential) least squares regression curves do not have an intercept of 1.0 on the normalized absorbance axis. This indicates that there must be a rapid loss of iodine from segment 0 over the first 10 cm. It is believed that this is an artifact of the injection. As was stated in Section 5.2.3 some chloroform adheres to the hole of the slider. This would cause some of the sample to trail the injection segment. Also, the sliding of the injection valve gives an extra convective "kick" to the chloroform solution in the injection segment which requires a short time to settle down. Visual studies indicate that the injection plug is not fully homogenized within a segment until it has passes through 15 cm of tubing.

An alternative means of increasing the radial convection within a segment is to coil the tubing (Section 4.2.1.3). Indeed, in air segmented flow coiling greatly reduced the band broadening [27]. Also, in a study of band broadening in pentanol-water segmented flow,

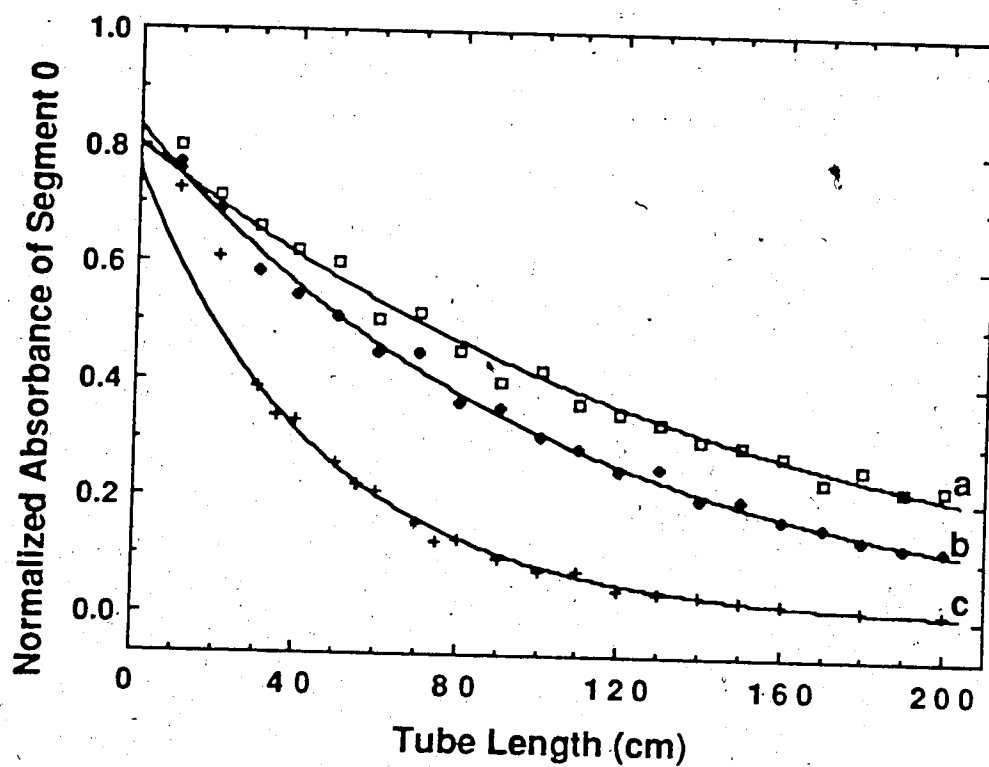


**Figure 5-11** Normalized absorbances of iodine in the injection segment 0 as it travels through the extraction coil for three different segment lengths: (a) 14.3 mm (□), (b) 9.6 mm (●) and (c) 5.4 mm (+). Absorbances of segment 0 are normalized by dividing them by the absorbance summed over all the organic segments.

**Table 5-1** Rate Constants Observed and Predicted by the Ideal Model for Iodine leaving the Injection Segment

Segment Length (mm)	Experimentally Observed Rate Constant (s <sup>-1</sup> ) <sup>a</sup>	Ideal Model's Predicted Rate Constant (s <sup>-1</sup> ) <sup>b</sup>
5.4	0.077 ± 0.002	0.118 ± 0.006
9.6	0.034 ± 0.001	0.069 ± 0.003
14.3	0.023 ± 0.001	0.047 ± 0.002

- a. From linear least squares slope of the plot of ln (absorbance of the injection segment) vs time for extraction tubes from 10 to 200 cm in length. Plots were linear with regression coefficients better than 0.99. Uncertainties are the standard deviation of the nonlinear regression coefficient.
- b. The band broadening rate,  $k_{bb}$ , predicted by the Ideal Model is given by:

$$k_{bb} (\text{pred.}) = \frac{V_f v}{V_{\text{seg}}}$$

where  $V_f$  and  $V_{\text{seg}}$  are the film and segment volumes as defined in Section 5.3.3 and  $v$  is the linear velocity of the segmented flow. Uncertainty is that associated with the theoretical film thickness, which was quoted as 5% [137].

Nord and Karlberg [22] noted that in uncoiled tubing the injection segment was washed out slowly, resulting in a distribution with a spuriously high absorbance in the injection segment, but when the tubing was coiled this injection segment maximum disappeared as a result of the improved convection within the segment.\* Unfortunately, the tangent method was used to calculate the variance of the dual-maximum peak. This method neglected to include the contribution of the high injection segment absorbance in the variance, which would have greatly influenced the peak variance.

Thus, the general conclusion can be drawn that the band broadening in segmented flow will be reduced by any experimental parameter which increases the radial flow within the segment. However the precise role of secondary flow in reducing the band broadening has yet to be fully illustrated.

### 5.3.3 Iodine Clock Reaction

Any study of the extraction process within segmented flow will be complicated by the extra, momentary convection induced by the injection process, as was discussed in the preceding section. To avoid this problem in the studies of the extraction of  $I_2$ , the bisulfite/iodate (Landolt) clock reaction [155] was used in this work to form iodine *in situ* within the segmented flow. The delay between the mixing of the reagents upon injection and the formation of iodine allows the segment sufficient time for the reagents to become fully mixed within the segment and for the toroidal circulation streamlines to be re-established before the extraction process commences. After this delay, the iodine must be formed rapidly, so that the kinetics of iodine extracted are a function of only the mass transfer processes, and not of the chemical processes involved in the clock reaction.

---

\* The film thickness for the pentanol/water segmented flow was 8 times thicker than for corresponding chloroform/water flow.

A proposed reaction sequence for the iodine clock reaction is given in Figure 5-12 [155]. The first two-electron reduction step to iodite is speculative, as other iodine oxides may be involved in a more complex reaction sequence. The disproportion of iodosous to hypiodous acid is the slow step. The delayed appearance of  $I_3^-$  in the clock reaction results from the hypiodous acid produced by this slow step being rapidly consumed by the bisulfite. Once the bisulfite has been exhausted, the hypiodous acid reacts with iodide to form iodine (actually present as  $I_3^-$ ).

The results of a study of the dependence of the iodine clock reaction on pH are given in Table 5-2. The reaction was monitored by following the absorbance at 420 nm after mixing of the reagents. An example of a typical tracing observed in this study is given in Figure 5-13. The delay is the time between mixing of reagents are mixed ( $t=0$ ) and first appearance of the iodine absorbance. The rate constant for the formation of iodine ( $k_{I_2}$ ), after the delay was recorded as the initial reaction rate constant.

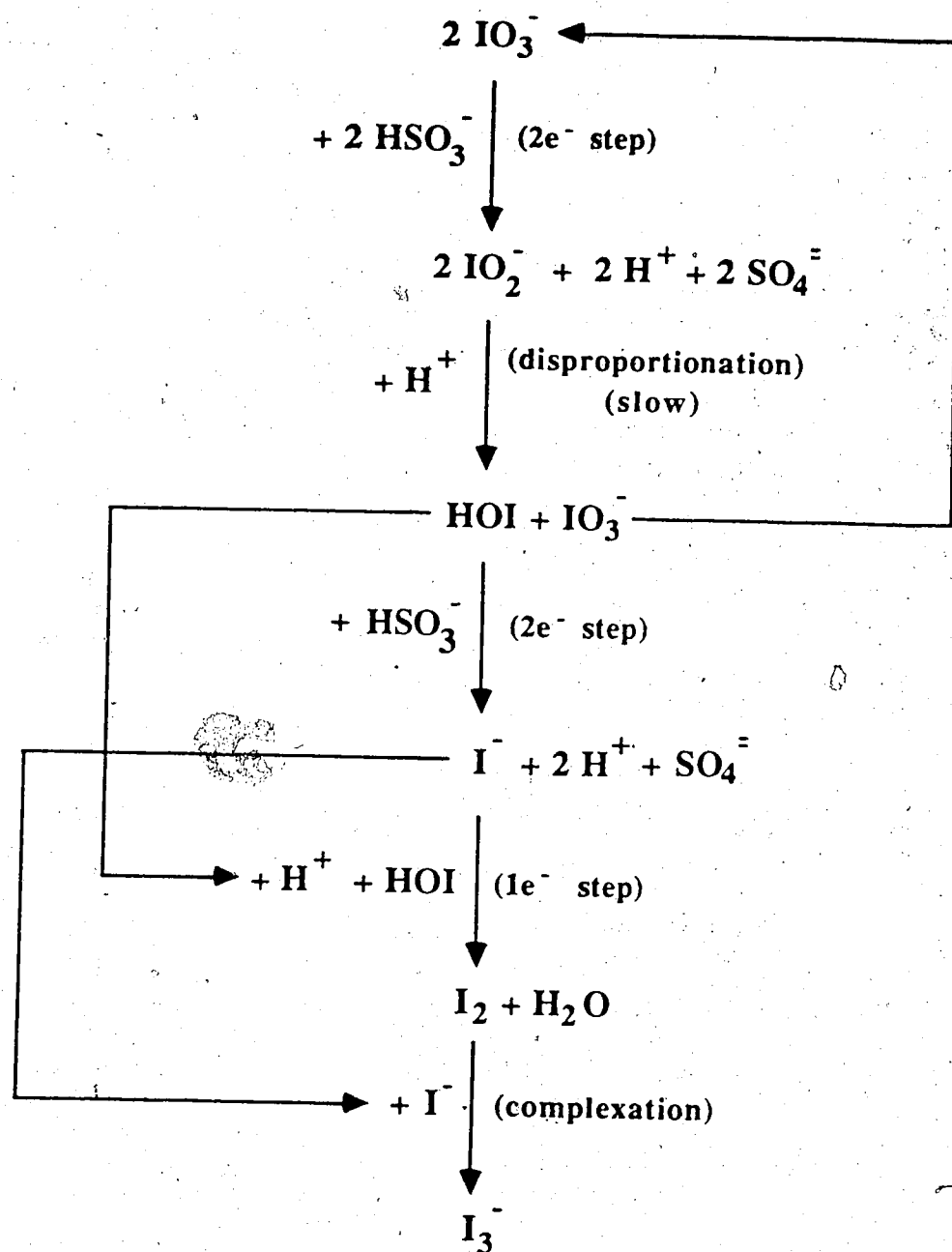
{ The reaction of bisulfite with iodate has previously been shown to follow the rate law [156]:

$$-\frac{d[IO_3^-]}{dt} = 5.3 \times 10^5 [H^+][IO_3^-][HSO_3^-] + 6.7 \times 10^2 [IO_3^-][SO_3^{2-}]^2 \quad (5.8)$$

(Units for the rate constants were not stated.) For acidic conditions, then, the first term of this expression should predominate. For  $[H^+]$  between  $10^{-4}$  and  $6.5 \times 10^{-3} \text{ M}$  the observed delay was found to depend inversely on the hydrogen ion concentration (Figure 5-14), in agreement with equation 5.8. Given reactant concentrations of  $2.4 \times 10^{-3} \text{ M}$  for  $NaHSO_3$  and  $1.2 \times 10^{-3} \text{ M}$  for  $KIO_3$ , the rate constant for this reaction would be  $(7.9 \pm 0.4) \times 10^5 \text{ s}^{-1}$ .

In the same experiment, it was observed that the initial rate of iodine formation, after the delay, had a larger (absolute) dependence than 1.0 on the hydrogen ion concentration. As is shown in the logarithmic plot in Figure 5-15, this dependence was 1.5. This was of





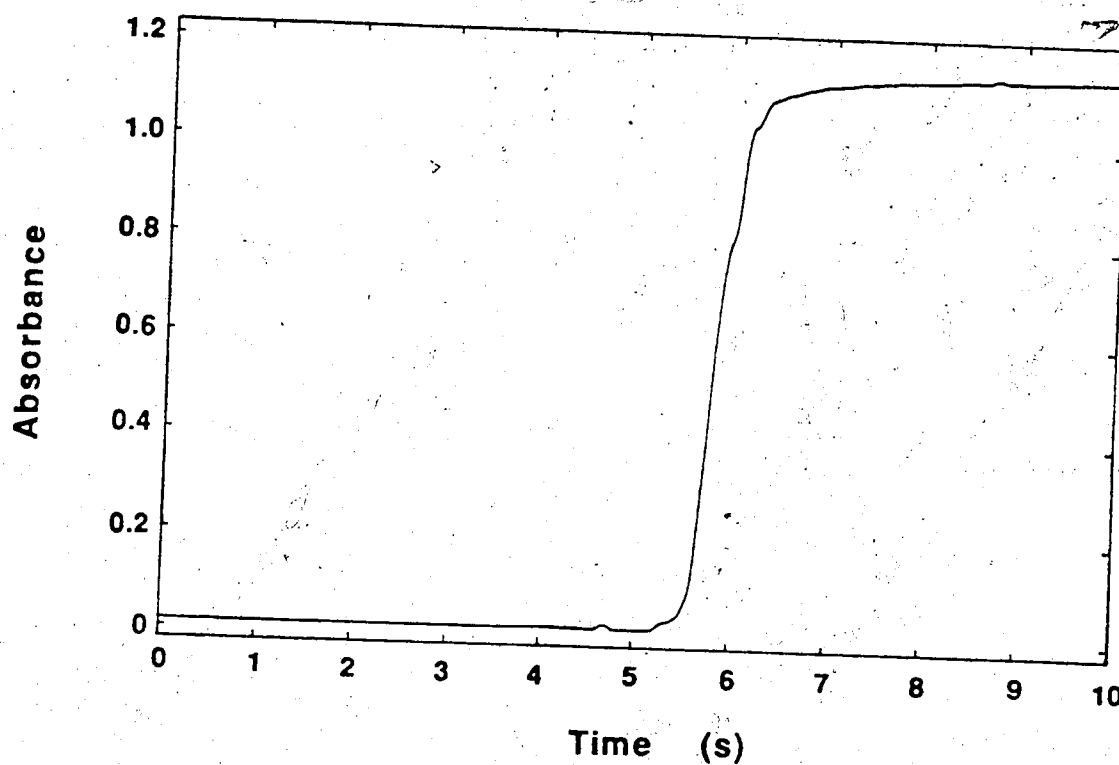
**Figure 5-12** Reaction sequence of the bisulfite/iodate clock reaction. Initial coefficients are doubled for stoichiometric reasons. Based on scheme proposed by J. L. Lambert and G.T. Fina, *J. Chem. Educ.* 1984, 61, 1037-1038.

Table 5-2    Dependence of the Iodine Clock Reaction on pH <sup>a</sup>

pH	[H <sup>+</sup> ], <u>M</u>	Observed Delay (s)	k <sub>I<sub>2</sub></sub> (s <sup>-1</sup> )
2.19	0.0065	65	0.10
2.60	0.0025	193	0.013
3.05	0.00089	400	0.0024
3.58	0.00026	805	0.00053
4.00	0.00010	1710	0.00015
4.0 <sup>b</sup>	~10 <sup>-4</sup> <sup>b</sup>	680 <sup>b</sup>	0.016 <sup>b</sup>

a. Experimental conditions: [NaHSO<sub>3</sub>], 2.4 x 10<sup>-3</sup> M; [KIO<sub>3</sub>], 1.2 x 10<sup>-3</sup> M; temp., 25.2°C; λ(nm), 420; buffers, citric acid/ NaOH.

b. Reaction solution does not contain buffer. Initial pH is that indicated in the table and is determined by the bisulfite reagent. The final pH of the solution was 2.7.



**Figure 5-13** Iodine formation via the Iodine Clock reaction under the conditions used in the extraction studies. Experimental conditions:  $[\text{NaHSO}_3]$ , 0.030 M;  $[\text{KIO}_3]$ , 0.020 M;  $[\text{KI}]$ , 0.030 M; initial pH adjusted using 1.0 M NaOH; temperature, 25.2°C; wavelength, 556 nm and pathlength, 1.00 cm.

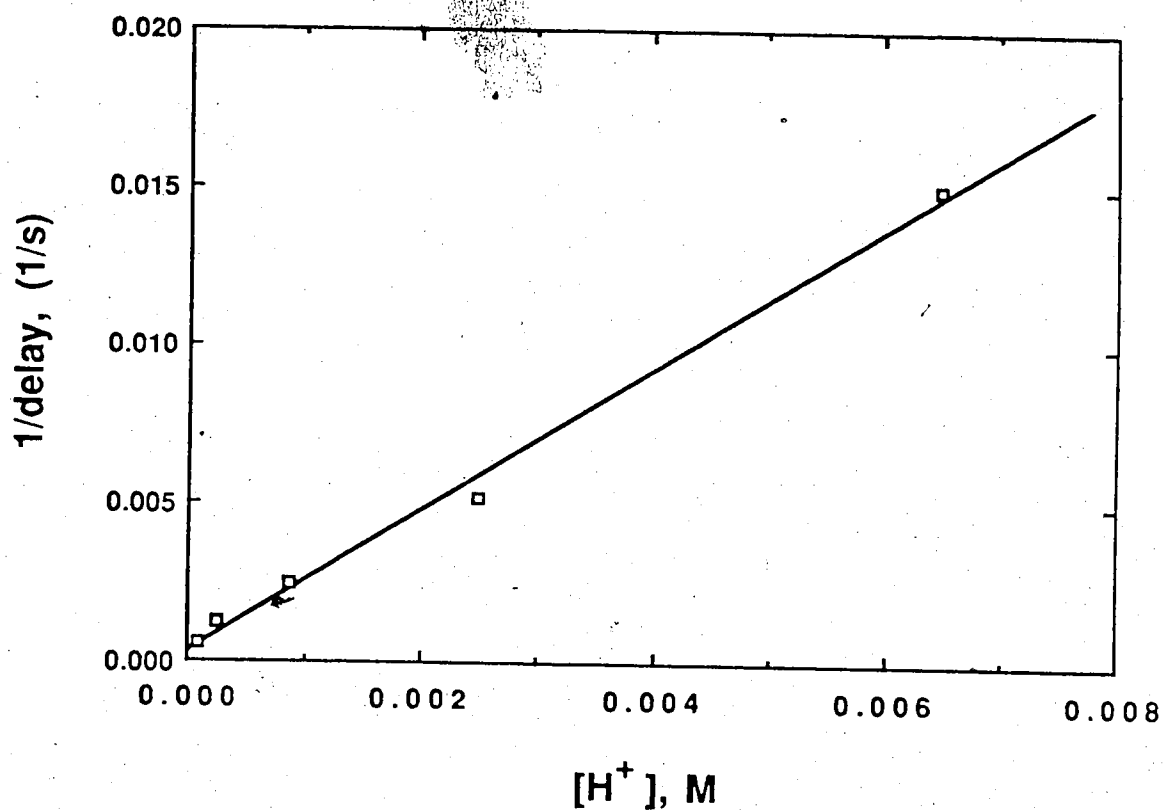


**Figure 5-14** Acid catalysis of the delay period of the bisulfite/iodate clock reaction.

Experimental conditions:  $[\text{NaHSO}_3]$ ,  $2.4 \times 10^{-3} \text{ M}$ ;  $[\text{KIO}_3]$ ,  $1.2 \times 10^{-3} \text{ M}$ ; temp.,  $25.2^\circ\text{C}$ ;  $\lambda(\text{nm})$ , 420 and pH buffers, citric acid/ NaOH solutions from 2.1 to 4.0. The slope and intercept are  $2.3 \pm 0.1$  and  $(3.1 \pm 3.2) \times 10^{-4}$ ;  $r = 0.997$ .

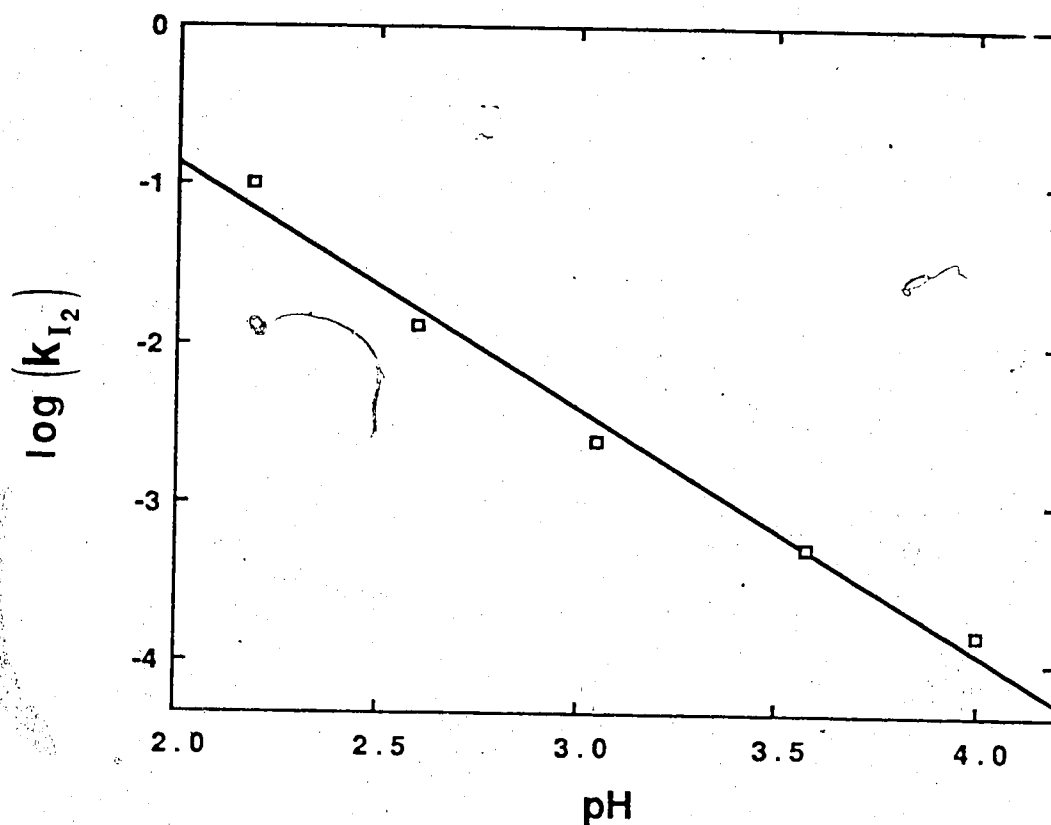


**Figure 5-15** Dependence of iodine formation rate of the bisulfite/iodate clock reaction on the pH. Experimental conditions:  $[\text{NaHSO}_3]$ ,  $2.4 \times 10^{-3} \text{ M}$ ;  $[\text{KIO}_3]$ ,  $1.2 \times 10^{-3} \text{ M}$ ; temperature,  $25.2^\circ\text{C}$ ;  $\lambda(\text{nm})$ , 420 and pH buffers, citric acid/NaOH solutions from 2.1 to 4.0. The slope is  $-1.53 \pm 0.10$ ;  $r = 0.993$ .

importance since, for the concentrations of  $\text{KIO}_3$  and  $\text{NaHSO}_3$  that had to be used to form a measurable amount of iodine, the delay was too short to ensure thorough mixing within the segment before iodine formation. This reactant solution was buffered by the bisulfite to a pH of 4.7. Given that the post-delay reaction shows a stronger dependence on  $[\text{H}^+]$  than does the delay time, it would not be possible to prolong the reaction by increasing the buffer pH of the solution without also slowing down the rate of the post-delay reaction. However, if unbuffered high pH reactant solutions are used, it is possible to obtain a reasonable delay and fast iodine formation since  $\text{H}^+$ , formed as a by-product of the bisulfite oxidation, will lower the pH of the solution during the delay period such that acidic conditions are present for the iodine formation. For the reactant concentrations quoted in the last paragraph, the pH was observed to decrease from an initial value of 4.5 to a final value of 2.7 at the end of the delay period. The effect of this pH shift can be seen in Table 5-2, where the unbuffered solution shows a delay corresponding to a buffered solution of a pH of 3.3 but has an iodine formation rate which is more typical of pH 2.6.

Thus, using the reaction conditions listed in the experimental section, where the bisulfite solution is adjusted to pH 6, the iodine forming reaction proceeds from initiation to 97% completion within 1.5 s, after a time delay of 8-9 s, as is shown in Figure 5-13. The delay of about 8.5 s, corresponded to a distance from injector  $V_2$  of about 30 cm, which is more than sufficient to ensure homogenization of the reaction mixture throughout the segment before the reaction occurs. Also since the fastest extraction studied herein has a half-life of 5.3 s, the iodine formed under these reaction conditions can be considered instantaneous.

## 5.3.4.1 Extraction Profiles

In Figure 5-16 to 5-18 are presented the absorbance vs segment number profiles for the organic segments, resulting from the extraction of iodine that was produced in aqueous injection segment (segment 0) by the iodine clock reaction. The distance indicated at the top of each bar graph is the distance between the point at which the iodine is formed and the detector. From these profiles it can be seen that iodine has extracted from the aqueous injection segment into the leading (i.e. downstream) organic segment, -1. Since the band broadening process in segmented flow results only in upstream movement of analyte, this iodine could only have entered segment -1 by extracting through the front end of the aqueous injection segment. Also the absorbance of segment +1 is of much greater magnitude than that of segment -1 because iodine entering it has been extracted from the aqueous injection segment through both its side and back end. Thus extraction occurs at both the ends and sides of the aqueous segments in SE-FIA. However, in order to quantify the relative magnitudes of these two modes of extraction, it is necessary to account for the band broadening which accompanies the extraction process in segmented flow. This will be discussed in Section 5.3.5.

## 5.3.4.2 Overall extraction rates

As the iodine extracts into the organic phase the total absorbance of the organic phase increases. This total absorbance is the sum of the absorbances of all organic segments. The overall extraction rate constant ( $k_{obs}$ ) can be determined by using the integrated form of the extraction rate expression [140,149]:

$$\ln \left[ \frac{A_{eq,o}}{A_{eq,o} - A_{t,o}} \right] = k_{obs} t \quad (5.9)$$

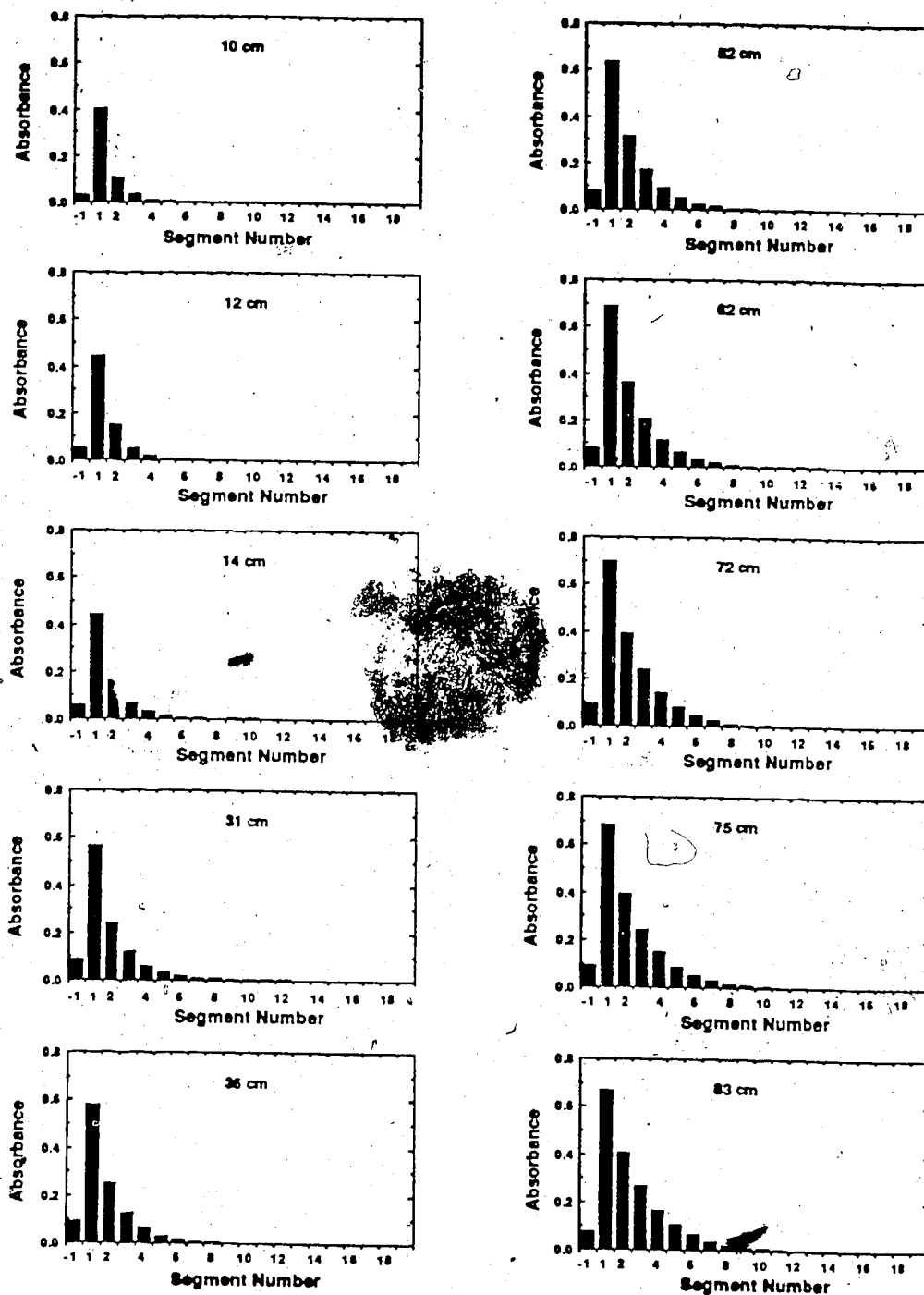


Figure 5-16a Organic segment profiles for iodine extracted from a single 14.3 mm aqueous segment. Segment number is the position relative to injection segment 0, with positive segments being upstream (following) the injection segment and negative being downstream (leading). At the top of each graph is the length of extraction tube between the point of  $I_2$  formation and on-tube detector, D.



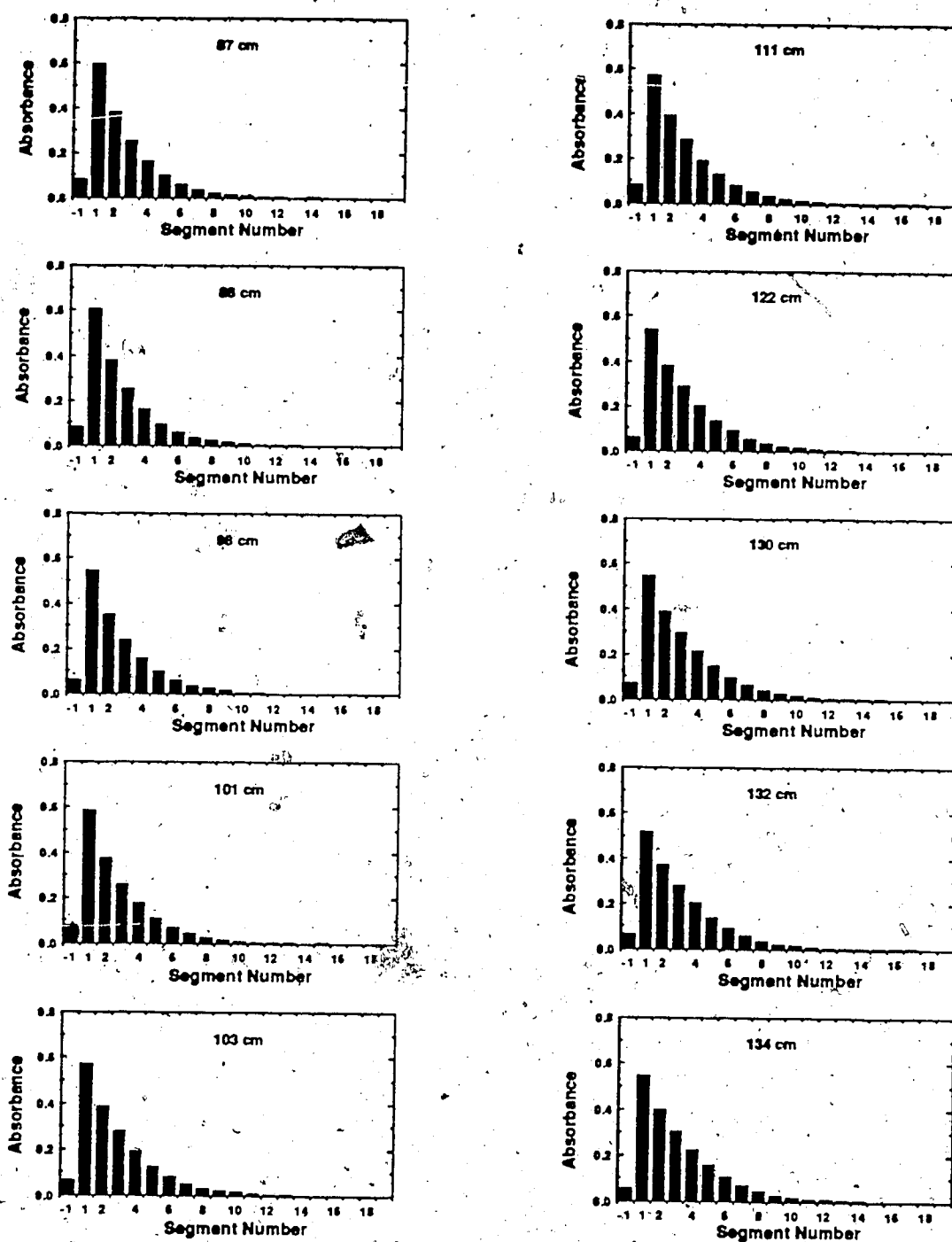


Figure 5-16b Continued from Figure 5-16a. Iodine extraction from a single 14.3 mm segment.

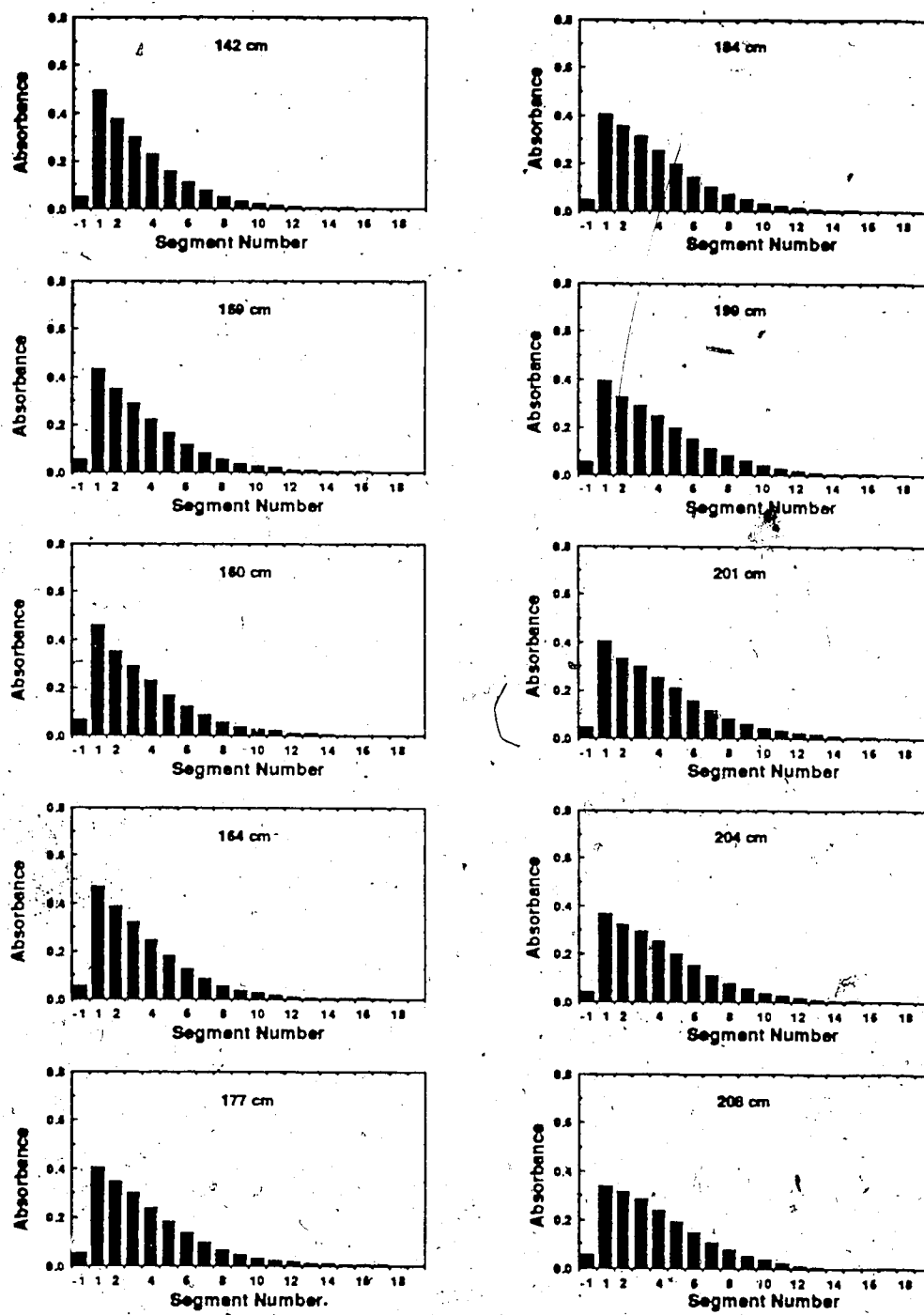
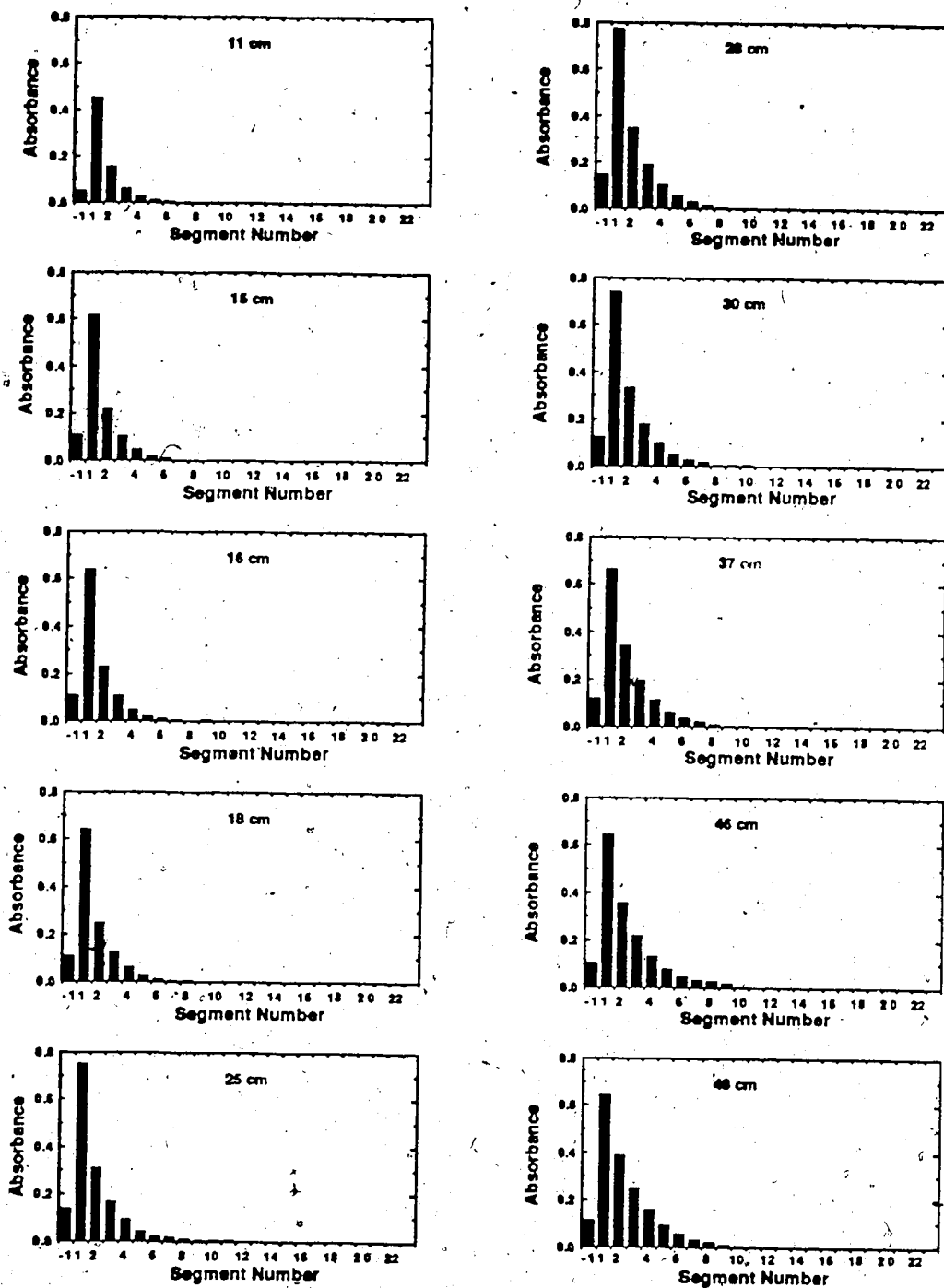


Figure 5-16c Continued from Figure 5-16b. Iodine extraction from a single 14.3 mm segment.



**Figure 5-17a** Organic segment profiles for iodine extracted from a single 9.6 mm aqueous segment. Segment number is the position relative to injection segment 0, with positive segments being upstream (following) the injection segment and negative being downstream (leading). At the top of each graph is the length of extraction tube between the point of  $I_2$  formation and on-tube detector, D.

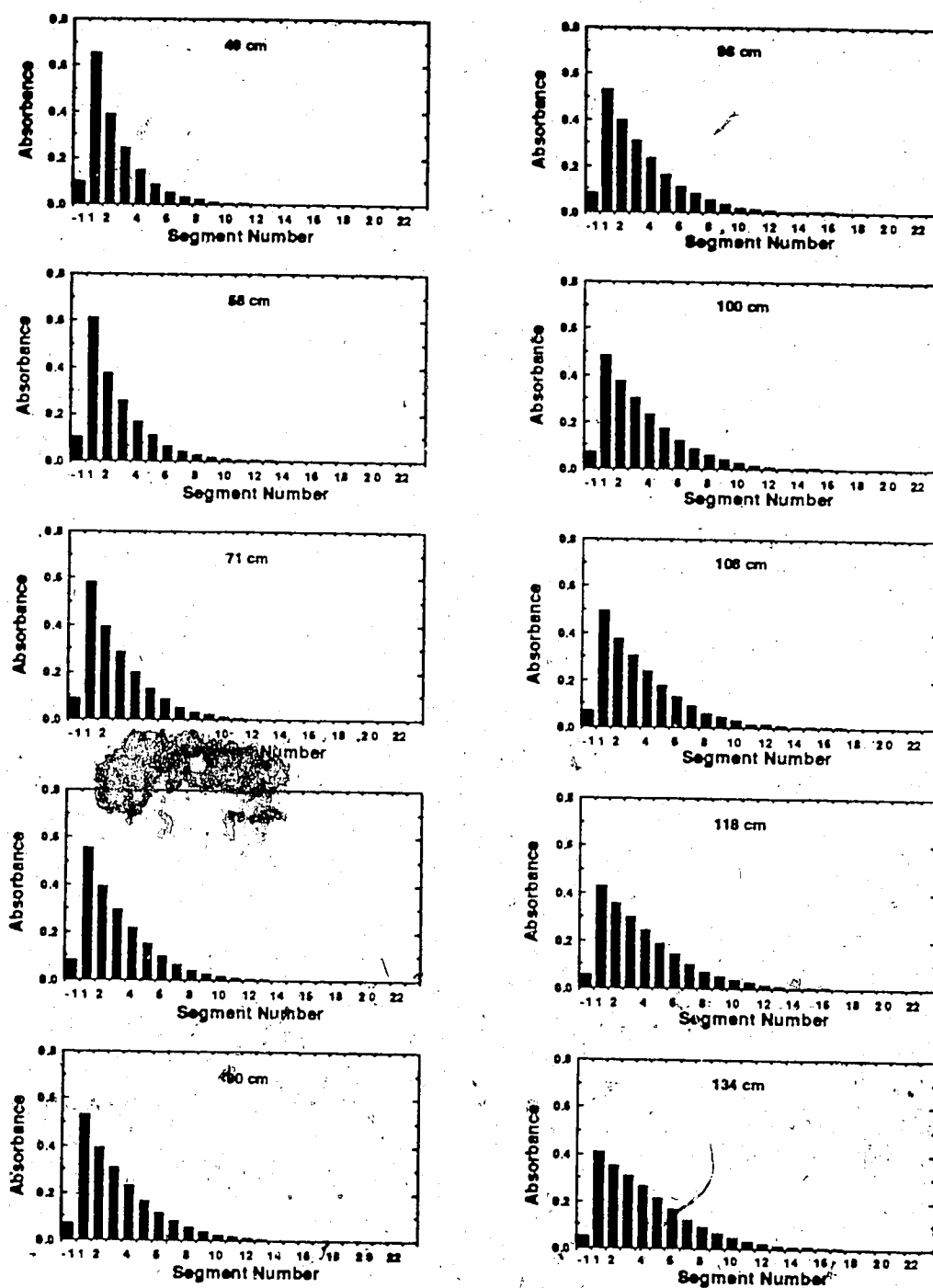


Figure 5-17b Continued from Figure 5-17a. Iodine extraction from a single 9.6 mm segment.

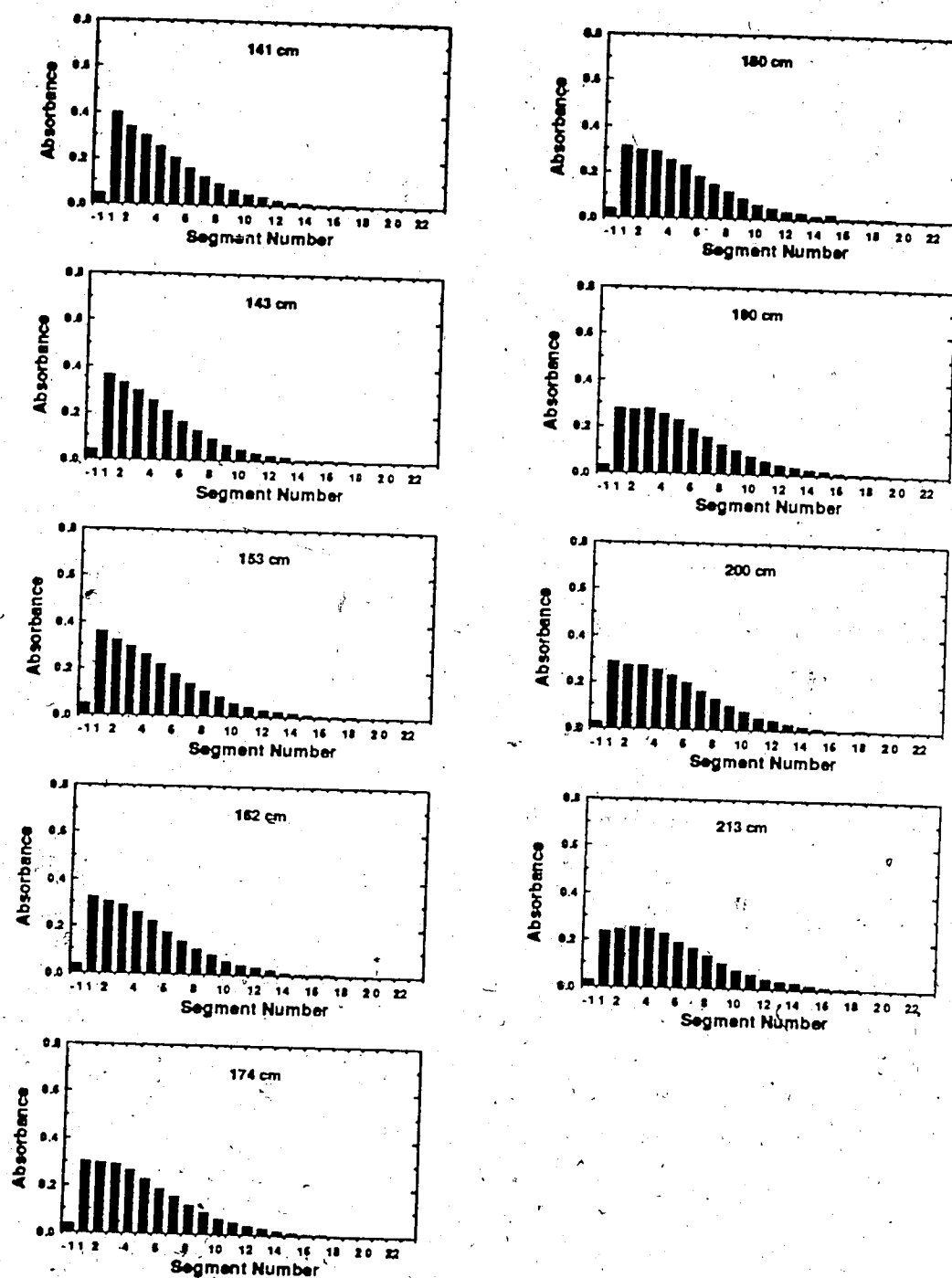


Figure 5-17c Continued from Figure 5-17b. Iodine extraction from a single 9.6 mm segment.

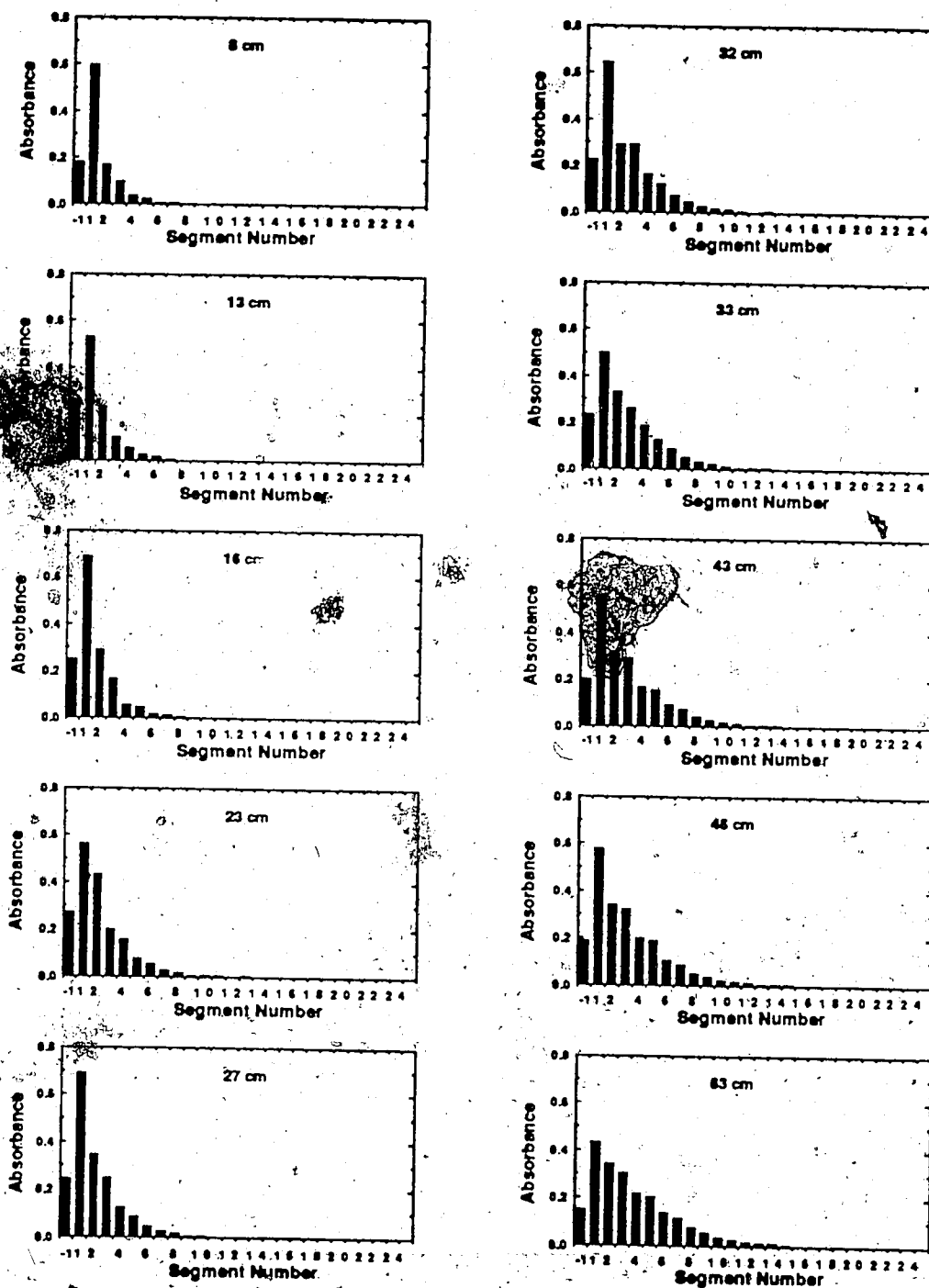
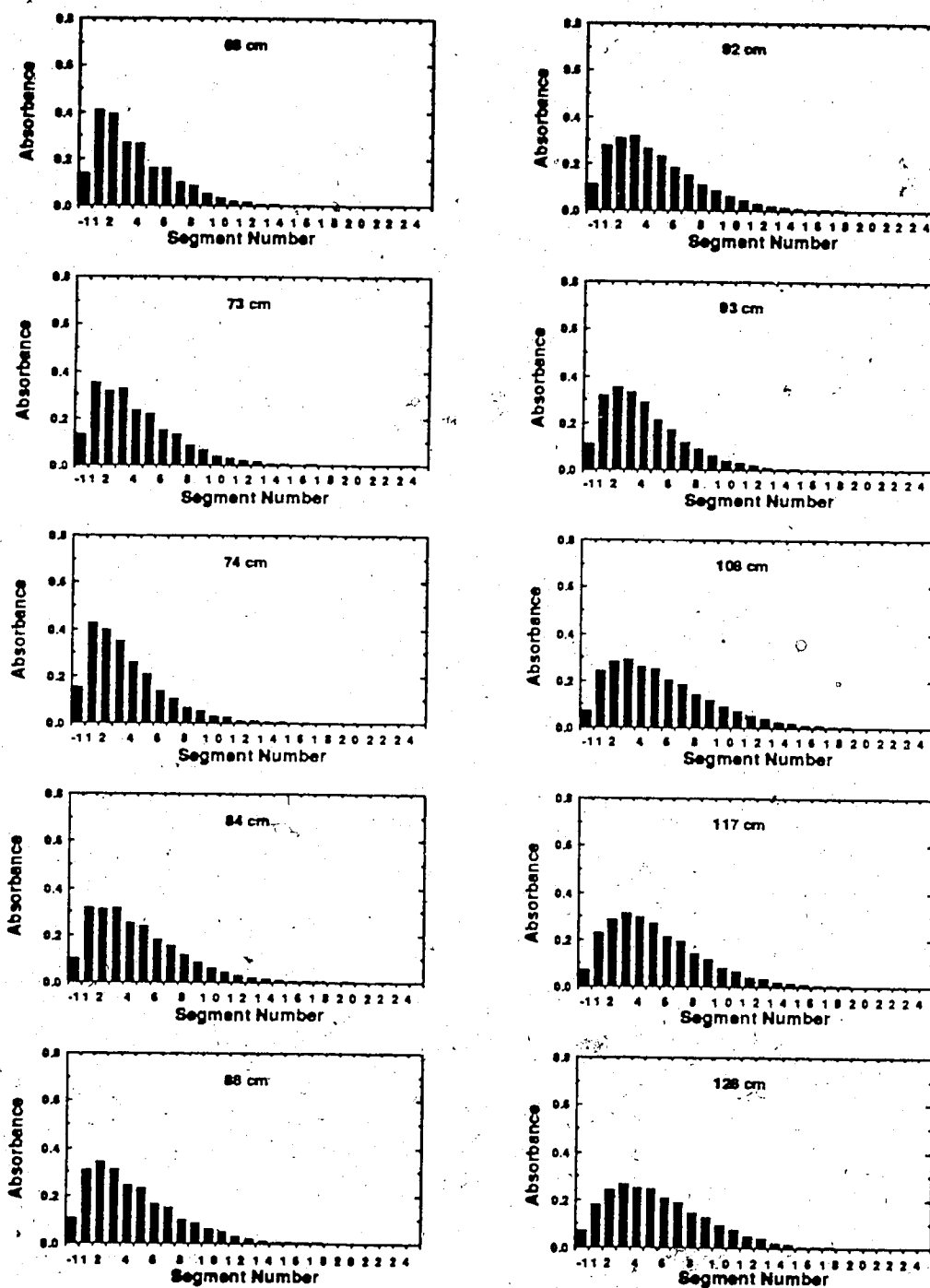


Figure 5-18a Organic segment profiles for iodine extracted from a single 5.4 mm aqueous segment. Segment number is the position relative to injection segment 0, with positive segments being upstream (following) the injection segment and negative being downstream (leading). At the top of each graph is the length of extraction tube between the point of  $I_2$  formation and on-tube detector, D.



**Figure 5-18b** Continued from Figure 5-18a. Iodine extraction from a single 5.4 mm segment.

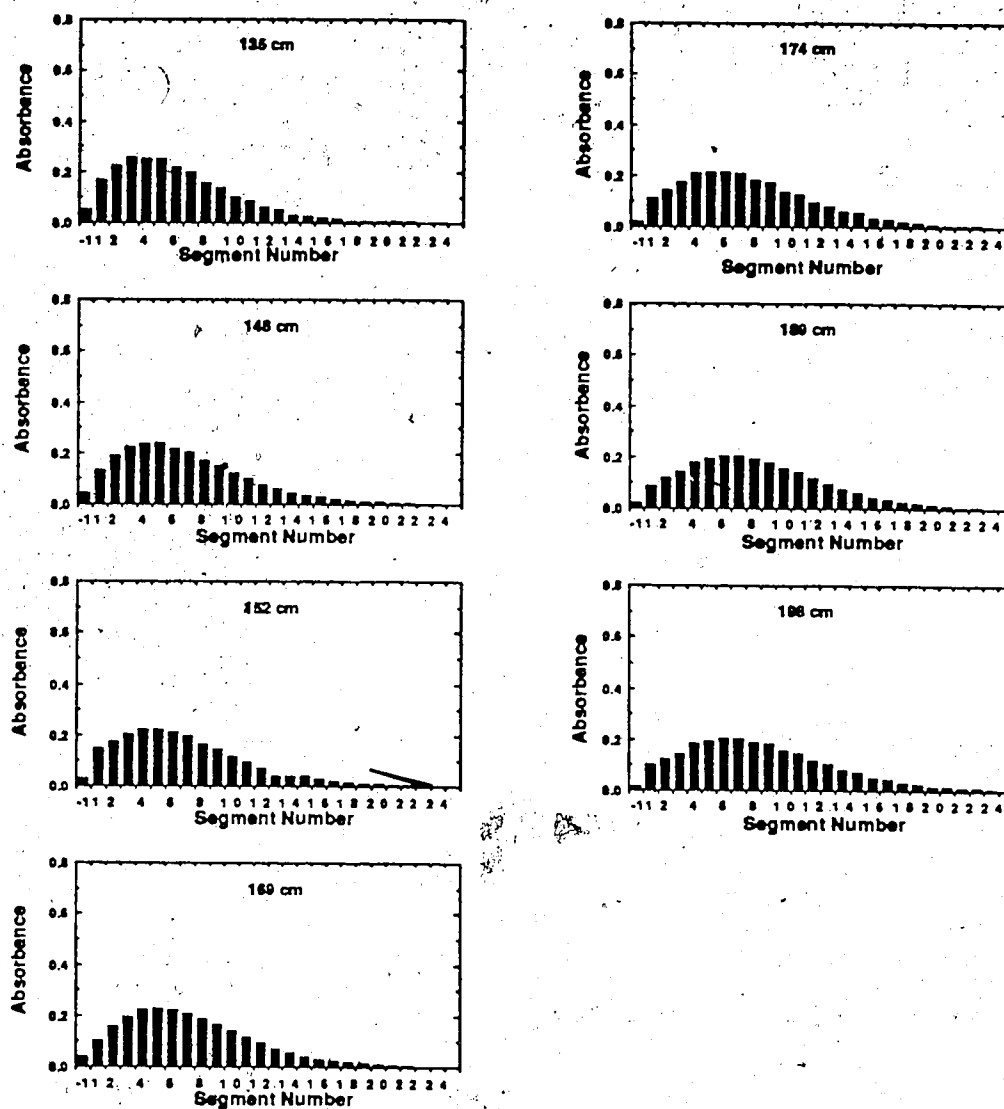


Figure 5-18c Continued from Figure 5-18b. Iodine extraction from a single 5.4 mm segment.



where  $A_{eq,0}$  and  $A_{t,0}$  are the total iodine absorbance at equilibrium and at time  $t$ , respectively. The slopes ( $k_{obs}$ ) and intercepts of the kinetic plots for the three segment lengths studied are presented in Table 5-3. The increase in  $k_{obs}$  with decreasing segment length is analogous to that observed previously for the extraction of caffeine in segmented flow through straight tubing (Section 4.4.6) and is explained in the same way.

Positive intercepts were observed in the kinetic plots. These result from a rapid nonsteady state component of the extraction. Typically, in cases such as diffusion across a membrane [157] or extraction of a reaction product which is formed only in the bulk aqueous phase [140], the establishment of steady state diffusion conditions results in a time lag [158]. However, in the present experiment iodine is formed simultaneously both in the bulk aqueous phase and in the Nernst film. Thus rather than a time lag, a brief period of accelerated extraction occurs, as a result of the nonsteady state diffusion (Appendix D). This would appear in the kinetic plots as a rapid initial slope followed by the ~~more~~ gradual one reported in Table 5-3. However, no such feature was observed for the first order plots at short extraction times and so the steady state extraction conditions must have been established prior to the first measurements. Under these conditions, the true mass transfer behavior (nonsteady state diffusion followed by steady state) can be accurately approximated by an assumption of steady state extraction with a positive intercept [158].

### 5.3.5 Successive Reaction Approximation

In the above discussions it has been shown that extraction and band broadening are exponential processes. Thus, the behavior of the absorbance in segment -1 in the iodine extraction studies (Figure 5-16 to 5-18) is formally analogous to that of the concentration of an intermediate species formed between successive first order chemical reactions:

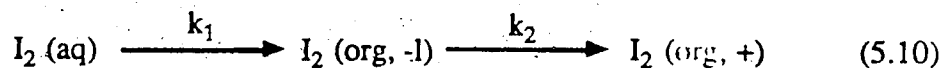


**Table 5-3** Observed Rate Constants for Extraction of Iodine formed within the Segmented Flow

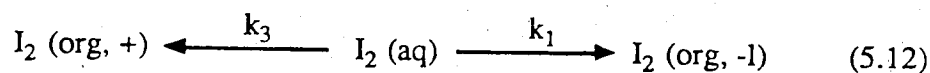
$L_{aq}$ (mm)	$k_{obs}$ ( $s^{-1}$ ) <sup>a</sup>	Intercept <sup>b</sup>	$A_{org,t=0}$ <sup>c</sup>
5.4	$0.13 \pm 0.03$	$0.42 \pm 0.32$	$0.80 \pm 0.49$
9.6	$0.092 \pm 0.014$	$0.41 \pm 0.27$	$0.73 \pm 0.39$
14.3	$0.082 \pm 0.014$	$0.18 \pm 0.31$	$0.32 \pm 0.42$

- a. Calculated using equation 5.9, with  $A_{t,0}$  being the total absorbance of all the organic segments at time  $t$  and  $A_{eq,0}$  estimated by the average total absorbance observed after 5 half lives. Uncertainty is the 95% confidence interval of the slope of this plot.
- b. Intercept of the plot of  $\ln(A_{eq,0}/(A_{eq,0}-A_{t,0}))$  vs time, which reflects the initial nonsteady state extraction of iodine. Uncertainty is the 95% confidence interval of the intercept of this plot. See Section 5.3.4.2 for details.
- c. Total absorbance of the iodine in the organic phase at time equal to zero which would correspond to the intercepts observed in the kinetic plots.

where the bracketed terms (aq), (org,-1) and (org,+) refer to the iodine concentration in the aqueous segment, organic segment -1 and all the organic segments trailing the injection segment (segment numbers > 0) respectively. The extraction rate constant,  $k_1$ , corresponds to the extraction through the front end of the aqueous segment, since this is the only means by which iodine can enter this segment, and the rate constant  $k_2$  is associated with the rate at which iodine leaves segment -1 due to band broadening. The differential equation describing the change in concentration of iodine in segment -1 with time for this extraction scheme is:

$$\frac{d[I_2]_{-1}}{dt} = k_1[I_2]_{aq} - k_2[I_2]_{-1} \quad (5.11)$$

However iodine also extracts from the aqueous segment via the rest of the interface (Section 5.3.4.1). This simultaneous extraction of iodine from both the front end and the rest of the interface of the aqueous segment is analogous to parallel first order reactions:

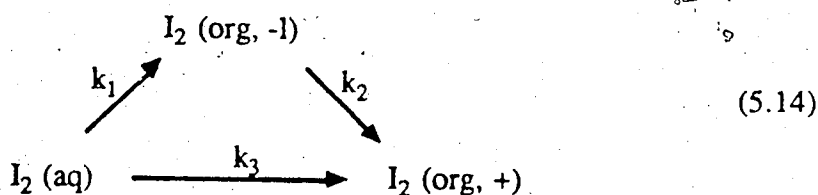


and so the concentration of iodine in the injection segment at time  $t$  is [159]:

$$[I_2]_{aq} = [I_2]_{aq,t=0} e^{-(k_1 + k_3)t} \quad (5.13)$$

where  $(k_1 + k_3)$  is equal to the observed extraction rate constant,  $k_{obs}$ , discussed in Section 5.3.4.2.

Thus the overall scheme governing the concentration of iodine in segment -1 is:



where, as above,  $k_1$  and  $k_3$  are the extraction rate constants for the front end and for the rest of the segment interface respectively, and  $k_2$  is the band broadening rate at which iodine leaves an organic segment. Combining equation 5.11 and 5.13, and solving the resulting differential equation gives [159]:

$$[I_2]_{-1} = [I_2]_{-1,t=0} e^{-k_2 t} + \frac{k_1 [I_2]_{aq,t=0}}{k_2 - k_{obs}} \left[ e^{-k_{obs} t} - e^{-k_2 t} \right] \quad (5.15)$$

The term  $[I_2]_{-1,t=0}$  corresponds to the iodine which extracts into organic phase via the rapid transient nonsteady state process, which was discussed above with regard to the positive intercept of the kinetic plots. Using the steady state extraction approximation of an exponential (steady state), some iodine will be in the organic phase at  $t=0$ . Iodine present in segment at time zero,  $[I_2]_{-1,t=0}$ , will subsequently leave segment -1 via the band broadening process ( $e^{-k_2 t}$ ). The second term on the right hand side of equation 5.15 corresponds to the successive reactions approximation for the simultaneous extraction ( $e^{-k_{obs} t}$ ) and band broadening ( $e^{-k_2 t}$ ) occurring in segment -1. The amount of iodine present in the aqueous injection segment at time zero,  $[I_2]_{aq,t=0}$ , is equal to the total iodine minus that corresponding to the intercept from the kinetic plots (Table 5-3).

The absorbances in the organic phase were used in place of the concentration terms in equation 5.15 in all calculations.

$$A_{-1,t} = A_{-1,t=0} e^{-k_2 t} + \frac{k_1 A_{aq,t=0}}{k_2 - k_{obs}} \left[ e^{-k_{obs} t} - e^{-k_2 t} \right] \quad (5.16)$$

Since the molar absorptivity of iodine is not the same in both the aqueous and organic phase,  $A_{aq,t=0}$  is taken as the organic phase absorbance which would correspond to the iodine present in the aqueous injection segment at time zero. Absorbances of segment -1 from the segment profiles shown in Figures 5-16 to 5-18 were fit to equation 5.16 using the nonlinear least squares program KINET [153]. The terms  $A_{aq,t=0}$  and  $k_{obs}$  were

treated as constants, since they are determined using the total absorbance in these same experiments. The terms  $A_{-1,t=0}$ ,  $k_1$  and  $k_2$  were the variables to be fit by the least squares program. The results for the three segment lengths studied are shown in Figure 5-19. The points are experimentally observed absorbances of segment -1 and the lines are the best fit curves based on equation 5.16. In general the fit between the "Successive Reactions Model" and the experimental data shown in Figure 5-19 is quite good for all three segment lengths. However, at short extraction tube lengths the theoretical curve does not fully follow the extremes of the experimental behavior. This may be a result of the band broadening not being a purely exponential process. In Figure 5-11 it was observed that there is an initial very rapid loss of material from the segment. This is believed to be due to momentarily enhanced convection caused by the injection, but it can not be ruled out that at least a portion of this might be due to a rapid band broadening process. However, this possible additional band broadening character is too speculative to be incorporated within the model.

The regression values of  $A_{-1,t=0}$ ,  $k_1$  and  $k_2$  are given in Table 5-4 for all three segment lengths. The uncertainties are the square root of the sum of the squares of the regression standard deviation and the standard deviation resulting from the uncertainty in the constants,  $A_{aq,t=0}$  and  $k_{obs}$ . The most significant result in Table 5-4 for SE-FIA is that the ratio of  $k_1/k_{obs}$ , which corresponds to the ratio of the rate of extraction out the front end of an aqueous segment to the total rate of extraction from the segment, is identical to the interfacial ratio,  $a_{end}/a_{seg}$ . This means that the mass transfer coefficient through the front end of the segment must be equal to the overall mass transfer coefficient, and so  $\beta_{axial}$  must equal  $\beta_{radial}$  (see equation 4.14). This equality is observed for segments whose mixing is typical of long segments, short segments and in transition between the two behaviors (Figure 4-12). Thus, the enhance radial which is introduced into the segment as a result of the hydrodynamic interaction of the segment ends is reflected in an increase in the extraction rate through all parts of the segment equally.

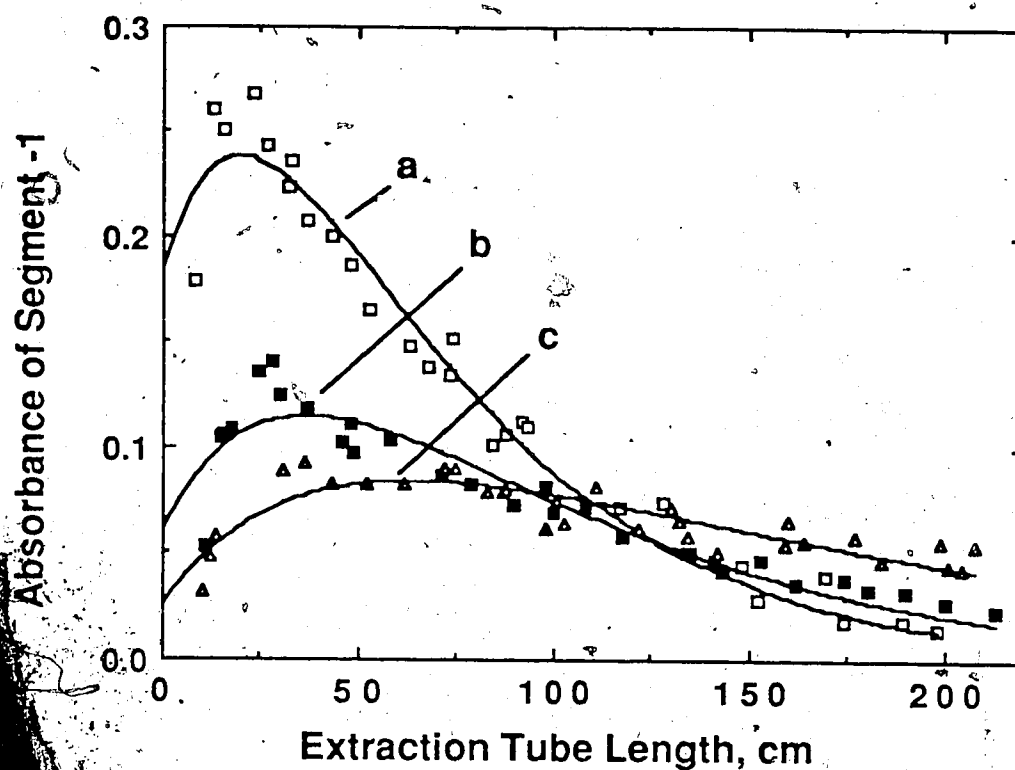


**Figure 5-19** Absorbance of segment -1 observed after iodine formation within a single aqueous segment within: (a) 5.4 mm ( $\square$ ) segmented flow; (b) 9.6 mm ( $\blacksquare$ ) segmented flow and (c) 14.3 mm ( $\blacktriangle$ ) segmented flow. The lines are the nonlinear least squares best-fit curve for equation 5.16. The regression coefficients are given in Table 5-4. See Section 5.3.6 for further details.

**Table 5-4** Estimates of the Extraction Rate through the Front End of a Segment and of the Band Broadening based on Nonlinear Least Squares Fitting of Segment -1 Absorbance Data to the Successive Reaction Approximation

$L_{aq}$ (mm)	$k_1^a$ ( $s^{-1}$ )	$\frac{k_1}{k_{obs}}$	$\frac{a_{end}}{a_{seg}}$	$k_2^a$ ( $s^{-1}$ )	$k_{bb}^c$ ( $s^{-1}$ )	$A_{-1,t=0}^a$	$A_{-1,t=0}^d$ Predicted
5.4	$0.023 \pm 0.005$	$0.18 \pm 0.04$	0.17	$0.071 \pm 0.008$	$0.077 \pm 0.002$	$0.185 \pm 0.023$	$0.14 \pm 0.09$
9.6	$0.011 \pm 0.002$	$0.12 \pm 0.02$	0.11	$0.053 \pm 0.006$	$0.034 \pm 0.001$	$0.062 \pm 0.016$	$0.08 \pm 0.05$
14.3	$0.0057 \pm 0.0009$	$0.07 \pm 0.01$	0.074	$0.025 \pm 0.003$	$0.023 \pm 0.001$	$0.026 \pm 0.008$	$0.02 \pm 0.03$

a. Uncertainty is the square root of the sum of the squares of the standard deviations resulting from the nonlinear regression and the experimental error associated with the constants used in the calculations.

b. The term  $a_{end}$  is the interfacial area of one end of an aqueous segment, measured as described in the experimental section; and  $a_{seg}$  is the total interfacial area of an aqueous segment.

c. From the band broadening study (Section 5.3.2) where chloroformic iodine was injected into a single organic segment and then the absorbance of the segment was monitored as it flowed through the extraction tube (Table 5-1).

d. Assumes that the nonsteady state extraction occurs uniformly through all parts of the interface. Calculated by:

$$A_{-1,t=0}(\text{pred.}) = \frac{a_{end}}{a_{seg}} \times A_{org,t=0}$$

where  $A_{org,t=0}$  is the absorbance of the total organic phase at time zero obtained from the kinetic plot intercepts, Table 5-3.

In addition, the band broadening rates,  $k_2$ , determined from the absorbances of segment -1 using the Successive Reactions Model should be the same as the rates observed in the band broadening studies,  $k_{bb}$ , discussed in Section 5.3.2. This comparison is shown in Table 5-4. For the 5.4 and 14.3 mm segment lengths, the two sets of values are within one standard deviation. For the 9.6 mm segment length the two measures of the band broadening rate agree within three standard deviations of each other.

It has been observed that the steady-state extraction occurs uniformly across all parts of the interface (i.e.  $k_1/k_{obs} = a_{end}/a_{seg}$ ). It would be assumed that the nonsteady state extraction should also occur uniformly over all of the interface, both the ends and sides. The absorbance in segment -1 at time zero,  $A_{-1,t=0}$ , determined from the segment -1 absorbances using the Successive Reactions Model is shown in Table 5-4. Also shown in the last column of this same table is the iodine absorbance which would be predicted for uniform nonsteady state extraction across all of the interface. It can be seen that these two sets of values are in excellent agreement.

#### 5.4 Conclusions

In this chapter it has been demonstrated, using a "Successive Reactions Model", that in segmented flow solute extracts from segments of the dispersed aqueous phase uniformly through all of the interface, both at the ends and the side of the segment, independent of segment length. Thus the enhanced radial mixing resulting from the hydrodynamic interaction of the ends of a short segment, discussed in Chapter 4, will result in a uniform increase in the mass transfer across all of the interface.

Also, the band broadening in the chloroform/water segmented flow is intermediate between that predicted by the Ideal mixing chamber model [26] and the Nonideal model [27]. The generation of greater radial mixing upon shortening the segment length reduced the band broadening to only 18% of that predicted by the Nonideal model, compared to



45% for longer segments. This indicates that any experimental parameter which generates radial convection will reduce the band broadening within segmented flow.

## Chapter 6

### Future Studies

A better understanding of the phenomena affecting the speed of analysis of SE-FIA has been gained from the studies discussed in this thesis. In this chapter, additional studies designed to further this understanding are discussed. Also some potential applications of this understanding and of the experimental techniques developed in this research to new analytical methods are suggested.

#### 6.1 On-Tube Detection

In Chapter 3, it was shown that a sample plug flowing through a SE-FIA instrument undergoes severe band broadening in the phase separator and during unsegmented flow through the connecting tubing. In order to increase the sampling frequency of this technique, these contributions to the overall peak variance must be reduced. The on-tube photometric detector used in Chapter 5 offers a means by which these sources of band broadening could actually be eliminated. The on-tube detector displayed rapid response times and excellent linearity, but the complexity of a typical signal, such as is shown in Figure 6-1A, seems to require the use of an on-line computer, which makes the detector much less attractive for routine use. However, the spikes resulting from the deflection of the light beam by the segment ends are merely a form of structured noise superimposed on a peak. Consequently, low-pass filtering of the on-tube detector signal should reveal the underlying peak, devoid of the otherwise overwhelming noise, making it possible to eliminate the need for an interfaced computer. For an analytical instrument, the on-tube detector signal could be low-pass filtered using a simple RC circuit such as is shown in Figure 6-2. Alternately, if a sharper frequency cutoff is required then higher order low pass filters [160] could be used.

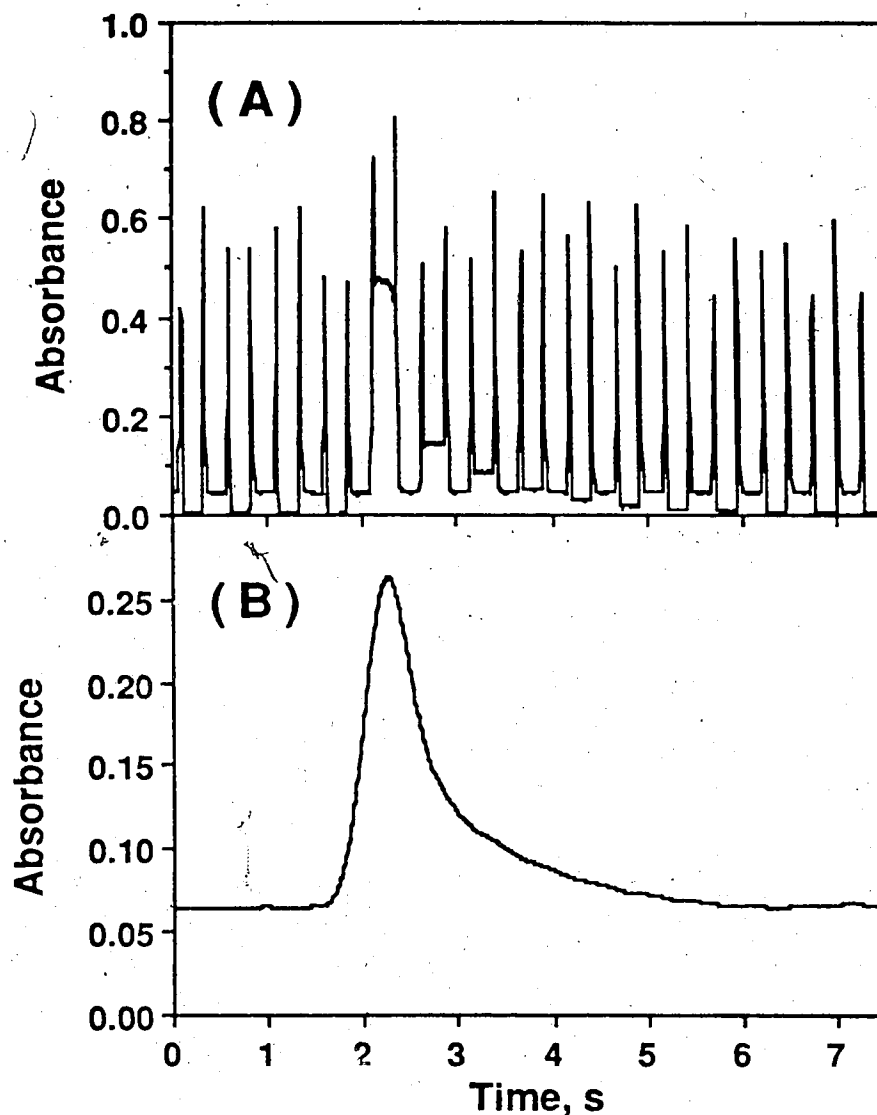


**Figure 6-1** On-tube detector signal of iodine injected into a single organic segment displayed as: (A) the raw absorbance signal. The segment absorbances are the short plateaus between the sharp absorbance spikes caused by the deflection of the light beam by the curved ends of the segment; (B) the smoothed signal obtained using a digital low pass filter with a cut-off frequency of 3 Hz. See Section 6.1 for details.

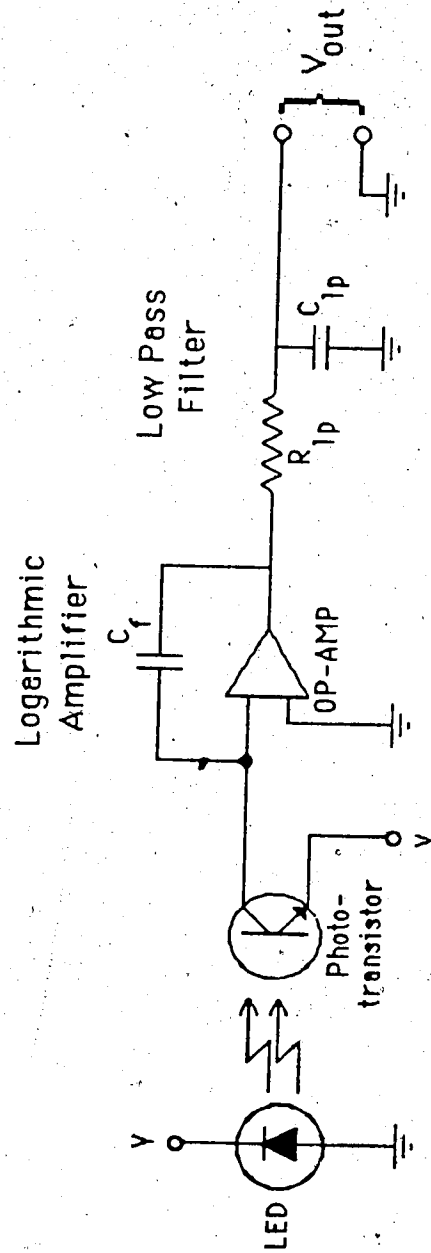


**Figure 6-2** Electronics diagram of an on-tube photometer for routine use in a SE-FIA instrument. The transmittance signal passes through a logarithmic amplifier and then into a simple RC low-pass filter. The subscripts for the capacitors (C) and resistor (R) are "f" for the feedback capacitor in the logarithmic amplifier and "lp" for the low-pass filter components. See Section 6.1 for discussion.

As a feasibility study, and since the detector was already interfaced to a computer in this research, the concept of low-pass filtering the data was tested using a nonrecursive digital filter [161]:

$$y_n = \sum_{k=-\infty}^{\infty} w_k x_{n-k} \quad (6.1)$$

where  $y_n$  is the filtered signal,  $w_k$  are the convolution weights obtained from the inverse Fourier transform of the Blackman window, and  $x_{n-k}$  are the raw data points. This filter was defined as the word SMOOTH in the ASYST Scientific System (MacMillan Software Co.). Figure 6-1B shows the effect of this digital filter, with a cutoff frequency of 3 Hz, on the raw on-tube detector signal. The peak underlying the segmentation noise is now clearly evident. Some sensitivity has been sacrificed, but the most important feature is that the signal to noise for Figure 6-1 was increased from about 0.7 to ~90, and thus is an analytically useful signal. Also, in an analytical SE-FIA method the sample would be distributed over many more segments than in Figure 6-1, making the frequency difference between the peak and noise much greater than in this test case, and consequently the filtering much easier.

Practical on-tube photometric detection of a segmented flow stream would be of great benefit for two reasons. First, the use of the on-tube detector would reduce the instrumental band broadening, and consequently would lead to an increase in the sampling frequency. Second, on-tube detection would remove the need for phase separation, thus making the instrument simpler and more robust.

## 6.2 Further Studies of Extraction Rate in SE-FIA

The studies of extraction kinetics presented in Chapters 4 and 5 have led to the development of a physico-chemical model by which the extraction occurring within the segmented flow in SE-FIA can be interpreted. One factor, however, which was not

considered in these studies, is the effect of surface active compounds on the extraction rate. Many of the analytical methods based on SE-FIA are either for the determination of surfactants [32,36,53-55] or involve ion-pair reagents which are potentially surface active [38,53,57,85, 87].

Surface active compounds have been observed to reduce mass transfer from falling and rising drops [30,144], and in segmented flow they have been observed to produce anomalous behavior. A monolayer of surfactant at the liquid-liquid interface is swept to the back of the segment resulting in this portion of the segment becoming stagnant, while the front of the segment is stirred by the toroidal flow. This causes the segment stratification which has been observed previously [53], resulting in, speculatively, two extraction processes - a rapid extraction from the front portion of the segment followed by a much slower extraction as material diffuses forward from the stagnant portion of the segment into the well stirred front. Such a dual extraction rate behavior has been observed for the extraction of the gallium-lumogallion complex from water into isoamyl alcohol [38].

The experimental variables which would effect the extraction rate in the presence of a surface active compound are the linear velocity, the segment aspect ratio, the interfacial area, coiling and the fraction of the interface covered by the monolayer of surfactant. The importance of the first four parameters has been demonstrated in this thesis. The final parameter, the fractional coverage of the interface, would be important for it would determine the proportion of the interface by which extraction would occur unimpeded, and what proportion of the segment would be stagnant.

A second area which warrants study is the effect of the experimental variables on the rate of back-extraction, i.e. from the film forming phase to the non-film forming phase. In all of the studies conducted herein, the rate determining mass transfer step occurred within the dispersed aqueous phase throughout which the convection was homogeneous. This would not be the case for the film forming phase in which there would be two distinct

regions: the bulk phase in the segments; and the more or less stagnant fluid along the walls of the tubing. Thus extraction would not be expected to occur at the same rate through the sides and the ends of the segment for this extraction process. The band broadening studies conducted in Chapter 5 demonstrated that these two regions are not fully mixed with each other.

In this thesis and the study suggested in the last paragraph, the extractions are quantitative. It would also be of interest to study the behavior of a solute which is not quantitatively extracted. The rate of extraction of such a compound should be affected by the factors which affect the extraction in the quantitative extraction system. The more interesting behavior, however, would be the band broadening behavior, where the material trailing back in following segments of the film forming phase could distribute back into the faster flowing nonfilm forming phase.

Finally, in Chapter 4 it was shown that coiling of the extraction tube is far and away the most powerful means of increasing the rate of extraction. However, the studies were conducted at only a single linear velocity and so could not fully characterize the transition in the extraction behavior exhibited when the segment is shortened. Knowledge of the position of this transition behavior for varying linear velocities and coil diameters would be crucial for analyst trying to optimize the dead time of their SE-FIA instruments. Until this work has been done, the experimentalist will have to utilize segments of >3 times the tube diameter to confidently assure rapid extraction in coiled tubing.

The variables which would be most important to study are believed to be the linear velocity, the tightness of coiling and the coiling shape. The first two parameters are related to the secondary flow in Section 4.2.1.2 and the last parameter has been shown to be an important factor in studies of radial mass transfer in air segmented flow [24]. If studies are to be conducted at higher linear velocities than utilized in Section 4.4.9, a slower extraction process than distribution of caffeine from water to chloroform would be required

to ensure measurable extraction rates. This could best be achieved by using a solute with a greater molecular weight (~~ie. decrease~~  $D_m$ ) or a smaller distribution coefficient. Slow extractions due to either slow chemical kinetics or interfacial adsorption could not be used for obvious reasons.



## References

1. Ružička, J.; Hansen, E. H. *Flow Injection Analysis* (Chemical Analysis Vol. 62), 2<sup>nd</sup> ed.; Wiley: New York, 1988.
2. Valcárcel, M.; Luque de Castro, M. D. *Flow Injection Analysis: Principles and Applications* (Ellis Horwood Series in Analytical Chemistry); Ellis Horwood: Chichester, 1987.
3. Stewart, K. K. "Flow Injection Analysis - New Tool for Old Assays - New Approach to Analytical Measurements" *Anal. Chem.* **1983**, *55*, 931A-937A.
4. Ružička, J.; Hansen, E. H. "Recent Developments in Flow Injection Analysis. Gradient Techniques and Hydrodynamic Injection" *Anal. Chim. Acta* **1983**, *145*, 1-15.
5. Ružička, J. "Flow Injection Analysis - From Test Tubes to Integrated Microconduits" *Anal. Chem.* **1983**, *55*, 1040A-1053A.
6. Ružička, J.; Hansen, E. H. "The First Decade of Flow Injection Analysis: From Serial Assay to Diagnostic Tool" *Anal. Chim. Acta* **1986**, *179*, 1-58.
7. Appelqvist, R. *et al* (36 authors) "Flow injection analysis (FIA) - a personal view" *Anal. Chim. Acta* **1986**, *180*, 1-67.
8. Luque de Castro, M. D.; Valcárcel Cases, M. "Simultaneous Determinations in Flow Injection Analysis. A Review" *Analyst (London)* **1984**, *109*, 413-419.
9. Ružička, J. "Flow Injection Analysis - A Survey of Its Potential for Spectroscopy" *Fresenius Z. Anal. Chem.* **1986**, *324*, 745-749.
10. Tyson, J. F. "Flow Injection Analysis Techniques for Atomic-absorption Spectrometry. A Review" *Analyst (London)* **1985**, *110*, 419-429.
11. Linares, P.; Luque de Castro, M. D.; Valcárcel, M. "Flow Injection Analysis in Clinical Chemistry" *Rev. Anal. Chem.* **1985**, *8*, 229-257.

12. Riley, C.; Rocks, B.; Sherwood, R. A. "Flow-Injection Analysis in Clinical Chemistry" *Talanta* **1984**, *31*, 879-888.
13. Růžicka, J. "Flow Injection Analysis - A Survey of its Potential for Continuous Monitoring of Industrial Processes" *Anal. Chim. Acta* **1986**, *190*, 155-163.
14. Bauer, H. H.; Christian, G. D.; O'Reilly, J. E. *Instrumental Analysis*; Allyn and Bacon: Boston, 1978. Chapter 24.
15. Valcárcel, M.; Luque de Castro, M. D. "Continuous Separation Techniques in Flow Injection Analysis. A Review" *J. Chromatogr.* **1987**, *393*, 3-23.
16. Karlberg, B.; Thelander, S. "Extraction based on the Flow-Injection Principle: Part I. Description of the Extraction System" *Anal. Chim. Acta* **1978**, *98*, 1-7.
17. Bergamin F<sup>o</sup>., H.; Medeiros, J. X.; Reis, B. F.; Zagatto, E. A. G. "Solvent Extraction in Continuous Flow Injection Analysis" *Anal. Chim. Acta* **1978**, *101*, 9-16.
18. Luque de Castro, M. D. "Flow Injection Analysis: a new tool to automate extraction processes" *J. Autom. Chem.* **1986**, *8*, 56-62.
19. Sweileh, J. A.; Cantwell, F. F. "Use of Peak Height for Quantification in Solvent Extraction/Flow Injection Analysis" *Can. J. Chem.* **1985**, *63*, 2559-2563.
20. Fossey, L.; Cantwell, F. F. "Characterization of Solvent Extraction/Flow Injection Analysis with Constant Pressure Pumping and Determination of Procyclidine Hydrochloride in Tablets" *Anal. Chem.* **1982**, *54*, 1693-1697.
21. Karlberg, B. "Flow Injection Analysis - Or the Art of Controlling Sample Dispersion in a Narrow Tube" *Anal. Chim. Acta* **1986**, *180*, 16-22 (Part F of reference 7).
22. Nord, L.; Karlberg, B. "Extraction based on the Flow-Injection Principle: Part 6. Film Formation and dispersion in liquid-liquid segmented flow extraction systems" *Anal. Chim. Acta* **1984**, *164*, 233-249.
23. Shelly, D. C.; Rossi, T. M.; Warner, I. M. "Multiple Solvent Extraction System with Flow Injection Technology" *Anal. Chem.* **1982**, *54*, 87-91.

24. Horvath, C.; Solomon, B. A.; Engasser, J.-M. "Measurement of Radial Transport in Slug Flow Using Enzyme Tubes" *Ind. Eng. Chem. Fundam.* **1973**, *12*, 431-439.
25. Prothero, J.; Burton, A. C. "The Physics of Blood Flow in Capillaries. I. The Nature of the Motion" *Biophysical J.* **1961**, *1*, 565-579.
26. Snyder, L. R.; Alder, H. J. "Dispersion in Segmented Flow through Glass Tubing in Continuous-Flow Analysis: The Ideal Model" *Anal. Chem.* **1976**, *48*, 1017-1022.
27. Snyder, L. R.; Alder, H. J. "Dispersion in Segmented Flow through Glass Tubing in Continuous-Flow Analysis: The Nonideal Model" *Anal. Chem.* **1976**, *48*, 1022-1027.
28. Snyder, L.; Levine, J.; Stoy, R.; Conetta, A. "Automated Chemical Analysis: Update on Continuous-Flow Approach" *Anal. Chem.* **1976**, *48*, 942A-956A.
29. Nord, L.; Bäckström, K.; Danielsson, L.-G.; Ingman, F.; Karlberg, B. "Extraction Rate in Liquid-Liquid Segmented Flow Injection Analysis" *Anal. Chim. Acta* **1987**, *194*, 221-233.
30. Davies, J. T.; Rideal, E. K. *Interfacial Phenomena*; Academic Press: New York, 1961; Chapter 7.
31. Cantwell, F. F.; Sweileh, J. A. "Hydrodynamic and Interfacial Origin of Phase Segmentation in Solvent Extraction/Flow Injection Analysis" *Anal. Chem.* **1985**, *57*, 329-331.
32. Kawase, J. "Automated Determination of Cationic Surfactants by Flow Injection Analysis Based on Ion-Pair Extraction" *Anal. Chem.* **1980**, *52*, 2124-2127.
33. Apffel, J. A.; Brinkman, U. A. Th.; Frei, R. W. "Design and Application of a Post-Column Extraction System Compatible with Miniaturized Liquid Chromatography" *Chromatographia* **1984**, *18*, 5-10.

34. Karlberg, B.; Johansson, P.-A.; Thelander, S. "Extraction based on the Flow-Injection Principle: Part 2. Determination of Codeine as the Picrate Ion-pair in Acetylsalicylic acid Tablets" *Anal. Chim. Acta* **1979**, *104*, 21-28.
35. Burguera, J. L.; Burguera, M. "Determination of Cadmium in Human Urine by Extraction with Dithizone in a Flow Injection System" *Anal. Chim. Acta* **1983**, *153*, 207-212.
36. Whitaker, M. J. "Spectrophotometric Determination of Nonionic Surfactants by Flow Injection Analysis utilizing Ion-pair Extraction and an Improved Phase Separator" *Anal. Chim. Acta* **1986**, *179*, 459-462.
37. de Ruiter, C.; Wolf, J. H.; Brinkman, U. A. Th.; Frei, R. W. "Design and Evaluation of a Sandwich Phase Separator for On-line Liquid-Liquid Extraction" *Anal. Chim. Acta* **1987**, *192*, 267-275.
38. Imasaka, T.; Harada, T.; Ishibashi, N. "Fluorimetric Determination of Gallium with Lumogallion by Flow Injection Analysis based on Solvent Extraction" *Anal. Chim. Acta* **1981**, *129*, 195-203.
39. Ogata, K.; Taguchi, K.; Imanari, T. "Phase Separator for Flow Injection Analysis" *Anal. Chem.* **1982**, *54*, 2127-2129.
40. Bäckström, K.; Danielsson, L.-G.; Nord, L. "Design and Evaluation of a New Phase Separator for Liquid-Liquid Extraction in Flow Systems" *Anal. Chim. Acta* **1985**, *169*, 43-49.
41. Nord, L.; Karlberg, B. "Extraction based on the Flow-Injection Principle: Part 5. Assessment with a Membrane Phase Separator for Different Organic Solvents" *Anal. Chim. Acta* **1980**, *118*, 285-292.
42. Fossey, L.; Cantwell, F. F. "Simultaneous Monitoring of Both Phases in the Solvent Extraction/Flow Injection Analysis of Dramamine Tablets" *Anal. Chem.* **1983**, *55*, 1882-1885.

43. Fossey, L.; Cantwell, F. F. "Determination of Acidity Constants by Solvent Extraction/Flow Injection Analysis using a Dual-Membrane Phase Separator" *Anal. Chem.* **1985**, *57*, 922-926.
44. Bäckström, K.; Danielsson, L.-G.; Nord, L. "Dispersion in Phase Separators for Flow-Injection Extraction Systems" *Anal. Chim. Acta* **1986**, *187*, 255-269.
45. Nord, Lage: Ph.D. Thesis, *Extraction in Liquid-Liquid Segmented Flow Systems Applied to the Mechanization of Sample Pretreatment*. Royal Inst. Techn., Stockholm, Sweden, 1984.
46. Fossey, Lynette P.: Ph.D. Thesis, *Solvent Extraction / Flow Injection Analysis for the Assay of Drugs and the Determination of Acidity Constants*. Univ. of Alberta, Edmonton, Canada. 1985.
47. Karlberg, B.; Thelander, S. "Extraction based on the Flow-Injection Principle: Part 3. Fluorimetric Determination of Vitamin B<sub>1</sub> (Thiamine) by the Thiochrome Method" *Anal. Chim. Acta* **1980**, *114*, 129-136.
48. Lucy, C. A.; Cantwell, F. F. "Simultaneous Determination of Phenylephrine Hydrochloride and Pheniramine Maleate in Nasal Spray by Solvent Extraction-Flow Injection Analysis using Two Porous-Membrane Phase Separators and One Photometric Detector" *Anal. Chem.* **1986**, *58*, 2727-2731.
49. Sahleström, Y.; Karlberg, B. "Flow-Injection Extraction with a Microvolume Module based on Integrated Conduits" *Anal. Chim. Acta* **1986**, *185*, 259-269.
50. Canham, J. S.; Pacey, G. E. "Automated free fatty acid determination using flow injection analysis solvent extractions" *J. Am. Oil Chem. Soc.* **1987**, *64*, 1004-1007; *Chem. Abstr.* **1987**, 114359g.
51. Ekström, L.-G. "An Automated Method for Determination of Free Fatty Acids" *J. Am. Oil Chem. Soc.* **1981**, *58*, 935-938.

52. Maeda, M.; Tsuji, A. "Fluorescence and Chemiluminescence Determination of Steroid and Bile Acid Sulphates with Lucigenin by Flow Injection Analysis Based on Ion-pair Solvent Extraction" *Analyst (London)* **1985**, *110*, 665-668.
53. Castaneda, Eduardo: M.Sc. Thesis, *Solvent Extraction / Flow Injection Analysis for the Determination of Anionic Surfactants*. Univ. of Alberta, Edmonton, Canada. 1986.
54. Hirari, Y.; Tomokuni, K. "Extraction-Spectrophotometric Determination of Anionic Surfactants with a Flow-Injection System" *Anal. Chim. Acta* **1985**, *167*, 409-412.
55. Kawase, J.; Nakae, A.; Yamanaka, M. "Determination of Anionic Surfactants by Flow Injection Analysis Based on Ion-Pair Extraction" *Anal. Chem.* **1979**, *51*, 1640-1643.
56. Sweileh, Jamal A.: Ph.D. Thesis, *Solvent Extraction / Flow Injection Analysis and Copper Ion Speciation by Ion Exchange*. Univ. of Alberta, Edmonton, Canada. 1986.
57. Atallah, R. H.; Christian, G. D.; Hartenstein, S. D. "Continuous Flow Solvent Extraction System for the Determination of Trace Amounts of Uranium in Nuclear Waste Reprocessing Solutions" *Analyst (London)* **1988**, *113*, 463-469.
58. Klinghoffer, O.; Růžicka, J.; Hansen, E. H. "Flow-Injection Analysis of Traces of Lead and Cadmium by Solvent Extraction with Dithizone" *Talanta* **1980**, *27*, 169-175.
59. Kumamaru, T.; Nitta, Y.; Nakata, F.; Matsuo, H.; Ikeda, M. "Determination of Cadmium by Suction-Flow Liquid-Liquid Extraction combined with Inductively-Coupled Plasma Atomic Emission Spectrometry" *Anal. Chim. Acta* **1985**, *174*, 183-189.
60. Kumamaru, T.; Nitta, Y.; Matsuo, H.; Kimura, E. "Inductively Coupled Plasma Atomic Emission Spectrometric Determination of Copper by Suction-Flow On-Line

- Liquid-Liquid Extraction of Its Macrocyclic Dioxotetramine Chelate" *Bull. Chem. Soc. Jpn.* **1987**, *60*, 1930-1932.
61. Lynch, T. P.; Taylor, A. F.; Wilson, J. N. "Fully Automatic Flow Injection System for the Determination of Uranium at Trace Levels in Ore Leachates" *Analyst (London)* **1983**, *108*, 470-475.
62. Motomizu, S.; Oshima, M. "Spectrophotometric Determination of Phosphorus as Orthophosphate Based on Solvent Extraction of the Ion Associate of Molybdophosphate with Malachite Green using Flow Injection" *Analyst (London)* **1987**, *112*, 295-300.
63. Ogata, K.; Tanabe, S.; Imanari, T. "Flame Atomic Absorption Spectrometry coupled with Solvent Extraction / Flow Injection Analysis" *Chem. Pharm. Bull.* **1983**, *31*, 1419-1421.
64. Sweileh, J. A.; Cantwell, F. F. "Sample Introduction by Solvent Extraction/Flow Injection Analysis to Eliminate Interferences in Atomic Absorption Spectroscopy" *Anal. Chem.* **1985**, *57*, 420-424.
65. Johansson, P.-A.; Karlberg, B.; Thelander, S. "Extraction based on the Flow-Injection Principle: Part 4. Determination of Extraction Constants" *Anal. Chim. Acta* **1980**, *114*, 215-226.
66. Kinkel, J. F. M.; Tomlinson, E. "Phase-Transfer Catalysis in a Segmented Flow Assembly. Study of Transfer and Reaction Rates" *Sep. Sci. Techn.* **1983**, *18*, 857-866.
67. Johnson, C. C.; Hellgeth, J. W.; Taylor, L. T. "Reversed-Phase Liquid Chromatography with Fourier Transform Infrared Spectrometric Detection Using a Flow Cell Interface" *Anal. Chem.* **1985**, *57*, 610-615.
68. Nord, L.; Johansson, S.; Brötell, H. "Flow-Injection Extraction and Gas Chromatographic Determination of Terodiline in Blood Serum" *Anal. Chim. Acta* **1985**, *175*, 281-287.

69. Rossi, T. M.; Shelly, D. C.; Warner, I. M. "Optimization of a Flow Injection Analysis System for Multiple Solvent Extraction" *Anal. Chem.* **1982**, *54*, 2056-2061.
70. Bäckström, K.; Danielsson, L.-G.; Nord, L. "Sample Work-up for Graphite Furnace Atomic-absorption Spectrometry Using Continuous Flow Extraction" *Analyst (London)* **1984**, *109*, 323-325.
71. Bengtsson, M.; Johansson, G. "Preconcentration and Matrix Isolation of Heavy Metals through a Two-stage Solvent Extraction in a Flow System" *Anal. Chim. Acta* **1984**, *158*, 147-156.
72. Frei, R. W.; Jansen, H.; Brinkman, U. A. Th. "Postcolumn Reaction Detectors for HPLC" *Anal. Chem.* **1985**, *57*, 1529A-1539A.
73. Jansen, H.; Brinkman, U. A. Th.; Frei, R. W. "Post-Column Reaction and Extraction Detectors for Narrow-Bore High Performance Liquid Chromatography" *J. Chromatogr. Sci.* **1985**, *23*, 279-284.
74. Lawrence, J. F. "Use of Post-column Ion-pair Extraction with Absorbance Detection for the Liquid Chromatographic Determination of Cyclamate and Other Artificial Sweeteners in Diet Beverages" *Analyst (London)* **1987**, *112*, 879-881.
75. Lawrence, J. F.; Brinkman, U. A. Th.; Frei, R. W. "Extraction Detector for High Performance Liquid Chromatography using Solvent Segmentation of the Column Effluent" *J. Chromatogr.* **1979**, *171*, 73-80.
76. Lawrence, J. F.; Brinkman, U. A. Th.; Frei, R. W. "Continuous Post-Column Ion-Pair Extraction Detection of some Basic Organic Compounds in Normal-Phase Chromatography" *J. Chromatogr.* **1979**, *185*, 473-481.
77. Reddingius, R. J.; De Jong, G. J.; Brinkman, U. A. Th.; Frei, R. W. "Simple Extraction Detector for the Liquid Chromatographic Determination of Secoverine in Biological Samples" *J. Chromatogr.* **1981**, *205*, 77-84.



78. Scholten, A. H. M. T.; Brinkman, U. A. Th.; Frei, R. W. "Solvent Segmentation in Liquid Chromatography - Application to Photochemical Reaction Detectors" *J. Chromatogr.* **1981**, *205*, 229-237.
79. Scholten, A. H. M. T.; Brinkman, U. A. Th.; Frei, R. W. "Comparison of Liquid Segmented with Nonsegmented Flow Systems in Postcolumn Reactors for Liquid Chromatography" *Anal. Chem.* **1982**, *54*, 1932-1938.
80. Smedes, F.; Kraak, J. C.; Werkhoven-Goewie, C. F.; Brinkman, U. A. Th.; Frei, R. W. "High-Performance Liquid Chromatographic Separation and Selective Detection of Anionic Surfactants. Application to Commercial Formulations and Water Samples" *J. Chromatogr.* **1982**, *247*, 123-132.
81. Tsuji, K. "Fluorimetric Determination of Erythromycin and Erythromycin Ethylsuccinate in Serum by a High-Performance Liquid Chromatographic Post-Column, On-Stream Derivatization and Extraction Method" *J. Chromatogr.* **1978**, *158*, 337-348.
82. van Buuren, C.; Lawrence, J. F.; Brinkman, U. A. Th.; Honigberg, I. L.; Frei, R. W. "Reversed Phase-Liquid Chromatography of Basic Drugs and Pesticides with a Fluorogenic Ion-Pair Extraction Detector" *Anal. Chem.* **1980**, *52*, 700-704.
83. Werkhoven-Goewie, C. E.; Brinkman, U. A. Th.; Frei, R. W. "The Use of Solvent Segmentation in Continuous-Flow Systems, and Fluorescence Labelling by Derivatization" *Anal. Chim. Acta* **1980**, *114*, 147-154.
84. Coello, J.; Danielsson, L.-G.; Hernandez-Cassou, S. "Continuous Flow Extraction of Indium with Bis(2-ethylhexyl)phosphoric acid in 4-methylpentane-2-one coupled On-line with Flame Atomic Absorption Spectrometry" *Anal. Chim. Acta* **1987**, *201*, 325-329.
85. Gallego, M.; Valcárcel, M. "Indirect Atomic Absorption Spectrometric Determination of Perchlorate by Liquid-Liquid Extraction in a Flow-Injection System" *Anal. Chim. Acta* **1985**, *169*, 161-169.

86. Gallego, M.; Silva, M.; Valcárcel, M. "Indirect Atomic Absorption Determination of Anionic Surfactants in Wastewaters by Flow Injection Continuous Liquid-Liquid Extraction" *Anal. Chem.* **1986**, *58*, 2265-2269.
87. Gallego, M.; Silva, M.; Valcárcel, M. "Determination of nitrate and nitrite by continuous liquid-liquid extraction with a flow-injection atomic-absorption detection system" *Fresenius Z. Anal. Chem.* **1986**, *323*, 50-53.
88. Nord, L.; Karlberg, B. "An Automated Extraction System for Flame Atomic Absorption Spectrometry" *Anal. Chim. Acta* **1981**, *125*, 199-202.
89. Nord, L.; Karlberg, B. "Sample Preconcentration by Continuous Flow Extraction with a Flow Injection Atomic Absorption Detection System" *Anal. Chim. Acta* **1983**, *145*, 151-158.
90. Silva, M.; Gallego, M.; Valcárcel, M. "Sequential Atomic Absorption Spectrometric Determination of Nitrate and Nitrite in Meats by Liquid-Liquid Extraction in a Flow-Injection System" *Anal. Chim. Acta* **1986**, *179*, 341-349.
91. Fogelqvist, E.; Krysell, M.; Danielsson, L.-G. "On-Line Liquid-Liquid Extraction in a Segmented Flow Directly Coupled to On-Column Injection into a Gas Chromatograph" *Anal. Chem.* **1986**, *58*, 1516-1520.
92. Roeraade, J. "Automated Monitoring of Organic Trace Components in Water. I. Continuous Flow Extraction together with On-line Capillary Gas Chromatography" *J. Chromatogr.* **1985**, *330*, 263-274.
93. Kraak, J. C. "Automated sample handling by extraction techniques" *TrAC* **1983**, *2*, 183-187.
94. Atallah, R. H.; Růžicka, J.; Christian, G. D. "Continuous Solvent Extraction in a Closed Loop System" *Anal. Chem.* **1987**, *59*, 2909-2914.
95. Kina, K.; Shiraishi, T.; Ishibashi, N. "Ultramicro Solvent Extraction and Fluorimetry based on the Flow-Injection Method" *Talanta* **1978**, *25*, 295-297.

96. Sahleström, Y.; Karlberg, B. "An Unsegmented Extraction System for Flow Injection Analysis" *Anal. Chim. Acta* **1986**, *179*, 315-323.
97. Perrin, D. D.; Dempsey, B. *Buffers for pH and Metal Ion Control*, Chapman and Hall, London, 1974, Appendix II.
98. Treit, J.; Nielsen, J.S.; Kratochvil, B.; Cantwell, F.F. "Semiautomated Ion Exchange / Atomic Absorption System for Free Metal Determinations" *Anal. Chem.* **1983**, *55*, 1650-1653.
99. Fernandez, A.; Luque de Castro, M. D.; Valcárcel, M. "Comparison of Flow Injection Analysis Configurations for Differential Kinetic Determination of Cobalt and Nickel" *Anal. Chem.* **1984**, *56*, 1146-1151.
100. Stewart, J.W.B.; Růžicka, J. "Flow Injection Analysis Part V. Simultaneous Determination of Nitrogen and Phosphorus in Acid Digests of Plant Material with a Single Spectrophotometer" *Anal. Chim. Acta* **1976**, *82*, 137-144.
101. Scott, R. P. W. *Liquid Chromatography Detectors*, Jour. of Chromatogr. Library, Vol. 11, Elsevier Scientific Publishing Co., 1977, pg. 109-120.
102. Doyle, T. D.; Levine, J. "Selection of Partition Chromatographic Systems from Distribution Diagrams: Determination of Dextromethorphan in Cough Syrups" *J. Assoc. Off. Anal. Chem.* **1968**, *51*, 191-199.
103. Kamson, O. F.; Townshend, A. "Ion-Exchange Removal of Some Interferences on the Determination of Calcium by Flow Injection Analysis and Atomic Absorption Spectrometry" *Anal. Chem. Acta* **1983**, *155*, 253-257.
104. Faizullah, A. T.; Townshend, A. "Flow Injection Analysis with Chemiluminescence Detection: Determination of Hydrazine" *Anal. Proc.* **1985**, *22*, 15-16.
105. *Physician's Desk Reference*, 38<sup>th</sup> ed.; Medical Economics Co. Inc.: Oradell, NJ, 1984.
106. Jenkins, G. L.; Sperandio, G. J. Latiolais, C. J. *Clinical Pharmacy: A Text for Dispensing Pharmacy*; McGraw-Hill: New York, 1966. Pg. 139.

107. *U.S. Pharmacopeia, National Formulary*, 20<sup>th</sup> revision; Rockville, MD., 1979.
108. Perrin, D. D.; Dempsey, B.; Serjeant, E. P. *pKa Prediction for Organic Acids and Bases*; Chapman and Hall: New York, 1981. Chapter 5 and Appendix A.5.
109. Růžicka, J.; Hansen, E. H. *Flow Injection Analysis* (Chemical Analysis Vol. 62), 2nd ed.; Wiley: New York, 1988. Chapter 3.
110. Sternberg, J. C. In *Advances in Chromatography*; Giddings, J. C.; Keller, R. A., Eds.; Marcel Dekker: New York, 1966; Vol. 2. Chapter 6.
111. Grubner, Otto "Interpretation of Asymmetric Curves in Linear Chromatography" *Anal. Chem.* **1971**, *43*, 1934-1937.
112. Grushka, E.; Myers, M. N.; Schettler, P. D.; Giddings, J. C. "Computer Characterization of Chromatographic Peaks by Plate Height and Higher Central Moments" *Anal. Chem.* **1969**, *41*, 889-892.
113. Said, A. S.; Al-Ali, H.; Hamad, E. "Mathematics for Chromatography Part I: Concentration Distributions and Their Moments" *J. High Res. Chrom. Chrom. Commun.* **1982**, *5*, 306-310. —
114. Bidlingmeyer, B. A.; Warren, F. V., Jr. "Column Efficiency Measurement" *Anal. Chem.* **1984**, *56*, 1583A-1596A.
115. Petitclerc, T.; Guiochon, G. "Determination of Higher Moments of a Non-symmetrical Chromatographic Signal" *J. Chromatogr. Sci.* **1976**, *14*, 531-535.
116. Chesler, S. N.; Cram, S. P. "Effect of Peak Sensing and Random Noise on the Precision and Accuracy of Statistical Moment Analysis from Digital Chromatographic Data" *Anal. Chem.* **1971**, *43*, 1922-1933.
117. Anderson, D. J.; Walters, R. R. "Effect of Baseline Errors on the Calculation of Statistical Moments of Tailed Chromatographic Peaks" *J. Chromatogr. Sci.* **1984**, *22*, 353-359.

118. Kirkland, J. J.; Yau, W. W.; Stoklosa, H. J.; Dilks, C. H. "Sampling and Extra-Column Effects in High-Performance Liquid Chromatography; Influence of Peak Skew on Plate Count Calculations" *J. Chromatogr. Sci.* **1977**, *15*, 303-316.
119. Rony, P. R.; Funk, J. E. "Retention Time and the First Time Moment in Elution Chromatography. III General Conclusions. *J. Chromatogr. Sci.* **1971**, *9*, 215-219.
120. LaFara, R. L. *Computer Methods for Science and Engineering*; Heyden: Philadelphia, PA, 1973. Pg. 221-222.
121. Dubetz, Terry Ann: Ph.D. Thesis, *Study of the Origin of Excessive Bandbroadening on PRP-1*. University of Alberta, 1988.
122. Pedersen, H.; Horvath, C. "Axial Dispersion in a Segmented Gas-Liquid Flow" *Ind. Eng. Chem. Fundam.* **1981**, *20*, 181-186.
123. Hupe, K.-P.; Jonker, R. J.; Rozing, G. "Determination of Band-Spreading Effects in High-Performance Liquid Chromatographic Instruments" *J. Chromatogr.* **1984**, *285*, 253-265.
124. Horvai, G.; Pungor, E. "Theoretical Backgrounds of Flow Analysis" *ERC Crit. Rev. Anal. Chem.* **1987**, *17*, 231-264.
125. Atwood, J. G.; Golay, M. J. E. "Dispersion of Peaks by Short Straight Open Tubes in Liquid Chromatography Systems" *J. Chromatogr.* **1981**, *218*, 97-122.
126. Tijssen, R. "Axial Dispersion and Flow Phenomena in Helically Coiled Tubular Reactors for Flow Analysis and Chromatography" *Anal. Chim. Acta* **1980**, *114*, 71-89.
127. Persaud, G.; Xiu-min, T.; Cantwell, F. F. "Behavior of Solute Adsorbed at the Liquid-Liquid Interface during Solvent Extraction with Porous-Membrane Phase Separators" *Anal. Chem.* **1987**, *59*, 2-7.
128. Kordyban, E. S. "A Flow Model for Two-Phase Slug Flow in Horizontal Tubes" *Trans. ASME, Ser. D* **1961**, *83*, 613-618.

129. Duda, J. L.; Vrentas, J. S. "Steady flow in the region of closed streamlines in a cylindrical cavity" *J. Fluid Mech.* **1971**, *45*, 247-260.
130. Bugliarello, G.; Hsiao, G. C. "A Mathematical Model of the Flow in the Axial Plasmatic Gaps of the Smaller Vessels" *Biorheology* **1970**, *7*, 5-36.
131. Lew, H. S.; Fung, Y. C. "The Motion of the Plasma between the Red Cells in the Bolus Flow" *Biorheology* **1969**, *6*, 109-119.
132. Welty, J. R.; Wicks, C. E.; Wilson, R. E. *Fundamentals of Momentum, Heat, and Mass Transfer*, 3<sup>rd</sup>, ed.; Wiley: New York, 1984. Chapter 9.
133. Truesdell, L. C., Jr.; Alder, R. J. "Numerical Treatment of Fully Developed Laminar Flow in Helically Coiled Tubes" *AIChE J.* **1970**, *16*, 1010-1015.
134. S  berg, H. "Viscous Flow in Curved Tubes - I. Velocity Profiles" *Chem. Eng. Sci.* **1988**, *43*, 855-862.
135. S  berg, H. *Chem. Eng. Sci.* In press.
136. Chen, Jing-Den "Measuring the Film Thickness Surrounding a Bubble inside a Capillary" *J. Colloid Interface Sci.* **1986**, *109*, 341-349.
137. Bretherton, F.P. "The motion of long bubbles in tubes" *J. Fluid Mech.* **1961**, *10*, 166-188.
138. *International Critical Tables of Numerical Data: Physics, Chemistry and Technology*, Vol. IV, 1st ed.; National Research Council; McGraw-Hill: New York, 1929.
139. Zongyi, Y. "The "Bolus Flow" Solution of the Plasma between the Red Blood Cells Flowing through a Capillary" *Scientia Sinica* **1981**, *24*, 1636-1648.
140. Cantwell, F. F.; Freiser, H. "Kinetics of Ion Pair Extraction" *Anal. Chem.* **1988**, *60*, 226-230.
141. Danesi, P. R.; Chiarizia, R. "The Kinetics of Metal Solvent Extraction" *C.R.C. Critical Rev. Anal. Chem.* **1986**, *10*, 1-126.
142. Cussler, E. L. *Diffusion. Mass transfer in fluid systems*; Cambridge University Press: New York, 1984. Chapters 9 and 11.

143. Cussler, E. L. "A Mass Transfer Tutorial" *Chemtech* 1986, 16, 422-425.
144. Lo, T. C.; Baird, M. H. I.; Hanson, C. *Handbook of Solvent Extraction*; Wiley: New York, 1983. Chapters 2.2 and 3.
145. Borwankar, R. P.; Wasan, D. T. "Effect of Surfactants on Interphase Solute Transport. A Theory of Interfacial Resistance" *Ind. Eng. Chem. Fundam.* 1986, 25, 662-668.
146. Saylor, R. D.; Berman, J. "Convective Mass Transfer with Pulsatile Flow in Straight Rigid Tubes" *Chem. Eng. Commun.* 1987, 52, 215-235.
147. Leo, A.; Hansch, C.; Elkins, D. "Partition Coefficients and Their Uses" *Chem. Reviews* 1971, 71, 525-616.
148. Harris, W.E.; Kratochvil, B. *An Introduction to Chemical Analysis*; Saunders: Philadelphia, 1981. Chapter 1.
149. Lucy, C. A.; Cantwell, F. F. "Kinetics of Solvent Extraction - Flow Injection Analysis" Submitted to *Anal. Chem.*
150. Awtrey, A. D.; Connick, R. E. "The Absorption Spectra of  $I_2$ ,  $I_3^-$ ,  $I^-$ ,  $IO_3^-$ ,  $S_4O_6^{2-}$  and  $S_2O_3^{2-}$ . Heat of the Reaction  $I_3^- \leftrightarrow I_2 + I^-$ ." *Jour. Amer. Chem. Soc.* 1951, 73, 1842-1843.
151. McClintock, S. A.; Weber, J. R.; Purdy, W. C. "The Design of a Computer-Controlled Flow-Injection Analyzer: An Undergraduate Experiment" *J. Chem. Educ.* 1985, 62, 65-67.
152. Betteridge, D.; Dagless, E. L.; Fields, B.; Graves, N. F. "A Highly Sensitive Flow-through Phototransducer for Unsegmented Continuous-flow Analysis Demonstrating High-Speed Spectrophotometry at the Parts per  $10^9$  Level and a New Method of Refractometric Determinations" *Analyst (London)* 1978, 103, 897-908.
153. Dye, J. L.; Nicely, V. A. "A General Purpose Curvefitting Program for Class and Research Use" *J. Chem. Educ.* 1971, 48, 443-448.

154. *International Critical Tables of Numerical Data: Physics, Chemistry and Technology*, Vol. V, 1st ed.; National Research Council; McGraw-Hill: New York, 1929.
155. Lambert, J. L.; Fina, G. T. "Iodine Clock Reaction Mechanisms" *J. Chem. Educ.* **1984**, *61*, 1037-1038.
156. Wilson, I. R. In *Comprehensive Chemical Kinetics*; Bamford, C. H.; Tipper, C. F. H., Eds.; Elsevier: Amsterdam, 1972; Vol. 6. Pg. 388-389.
157. Guy, R. H.; Fleming, R. "Transport across a Phospholipid Barrier" *J. Colloid Interface Sci.* **1981**, *83*, 130-137.
158. Crank, J. *The Mathematics of Diffusion*, 2<sup>nd</sup> ed.<sup>a</sup>; Oxford University Press (Clarendon): Oxford, 1975. Pg. 49-53.
159. Szabó, Z. G. In *Comprehensive Chemical Kinetics*; Bamford, C. H.; Tipper, C. F. H., Eds.; Elsevier: Amsterdam, 1969; Vol. 2. Chapter 1.
160. Malmstadt, H. V.; Enke, C. G.; Crouch, S. R. *Electronics and Instrumentation for Scientists*; Benjamin/Cummings: Menlo Park, CA, 1981. Pg. 208-210.
161. Hamming, R. W. *Digital Filters*, 2<sup>nd</sup> ed.; Prentice-Hall: Englewood Cliffs, NJ, 1983.



## Appendix A

### Moment Analysis Program

#### \ PEAK MOMENT ANALYSIS PROGRAM

- \ Program name: MOMENTS.ASY (ASYST Version 2.0)
- \ Directory: ASYST2
- \ Updated by: C. Lucy, 18 September 1987
- \ ( This program is based on XYDPP.DMO shown in the ASYST
- \ Module 1 manual, pg. I-20-16 to I-20-23. )

- \ The program is designed to calculate the moments of data entered manually or
- \ recalled from previously written files. Graphical displays are provided to aid the
- \ operator. Various operations - smoothing, baseline set, derivatives - are available
- \ for use.

---

#### \ Program Structure

- \ The program is designed to be menu driven. The menus are two-tiered. The upper
- \ most menu is Main Menu, from which either the Plot Menu or Summary menu can be
- \ accessed.

#### \ Main Menu

- \ F1) Quit - exits operation from the moments program and from Asyst.
- \ F2) Plot - plots the data on the screen along with its baseline. Accesses the Plot Menu
- \ where data massaging options are available.
- \ F3) Enter data - sets up the input array for manual entry of data.
- \ F4) Read file - scrolls all files with the extension .DAT on the screen, and then reads
- \ the file requested.
- \ F5) Save file - stores the current data file. The filename should include the extension
- \ ".DAT".
- \ F6) Edit data - displays the current data array on the screen and allows editing of the
- \ data. Three columns appear; the retention time, the signal, and the
- \ baseline.
- \ F7) Moments - calculates the first five moments for the current data, i.e. the
- \ unnormalized peak area, the center-of-gravity, and the variance, and
- \ from the third and fourth moments the skew and excess are calculated.
- \ The asymmetry factor (10%) is also calculated.
- \ F8) Summary - accesses the Summary Menu. Purpose is to produce a hard copy of
- \ the moments.

## \ Plot Menu

- \ F1) Exit - will return operation to the Main Menu.
- \ F2) Plot - plots the signal on the screen.
- \ F3) Plot baseline - plots the baseline onto the signal plot.
- \ F4) Change symbols - allows selection of the symbol to be used for the signal and baseline data. Default values are "." for signal and "." for baseline.
- \ F5) Lin. Reg. Baseline - sets baseline by performing linear regression on the data before and after the peak. The before/after limits are set using manually controlled cursors.
- \ F6) Derivative - calculates the derivative of the signal and automatically sets the baseline by drawing a straight line between the first and last data points.
- \ F7) Smooth - applies a low pass filter to the data to remove noise.
- \ F9) (hidden function) - stalls the computer until the baseline limits for F5 have been set.

## \ Summary Menu

- \ F1) Exit - returns operation to the Main menu.
- \ F2) Print summary - prints out the data file specifications and the calculated moments.
- \ F3) Print data - prints out the data file specifications and the data.
- \ F4) Plot summary - prints out a copy of the data plot along with the file identification, specifications, and the calculated moments.

## \ Overlay check

ECHO.OFF

: OLOAD?

CR BELL

." Are the overlays AR-EDIT.SOV, DATAFILE.SOV, MATFIT.SOV and WAVEOPS.SOV"

CR ." in the system (Y/N) ? "

KEY DUP EMIT

DUP 90 > IF 32 - THEN 89 = NOT

IF

CR CR ." Please use the Configuration menu <F2> to load the Array Editor,"

CR ." Data File, Matrix manipulation and Waveform analysis overlays"

CR ." permanently in the system before continuing."

CR ." The last two overlays are located in Analysis overlays." CR CR

57 ERROR

THEN

;

\ Variable declarations

INTEGER SCALAR MAXSETS

SCALAR MAX.IN.SET

SCALAR #SETS

SCALAR COL#

SCALAR LIN.END

\ End of baseline before peak

SCALAR LIN.REG.#

\ No. of data points defining baseline.

SCALAR FIRST#

\ First data point of the peak.

SCALAR LAST#

\ Last data point of the peak.

SCALAR #IN.PEAK

\ No. of data points defining peak.

SCALAR ARRAY.SIZE

2000 MAXSETS :=

\ Either of these lines may be changed

3 MAX.IN.SET :=

\ to allow larger data sets to be used.

DIM[ 2 ] ARRAY HOLDIT

\ Output buffer for #SETS & MAX.IN.SETS

REAL SCALAR DELTA.T

\ Interval between successive data points.

SCALAR PEAK.LIMITS

\ % of max that defines the peak edges

SCALAR PEAK.AREA

\ - zeroth moment

SCALAR PEAK.CENTER

\ Moments variables - first moment

SCALAR PEAK.VAR

\ - second moment

SCALAR PEAK.SKEW

\ - from 3rd moment

SCALAR PEAK.EXCESS

\ - from 4th moment

SCALAR ASYM.FACTOR

\ Asymmetry factor at 10% maximum

SCALAR W(1/2)

\ Width at half height

SCALAR %MAX

0.1 PEAK.LIMITS :=

DIM[ MAXSETS , MAX.IN.SET ] ARRAY PEAK.DATA \ Create the peak.data  
set(s) buffer.

DIM[ MAXSETS ] ARRAY CONC.I

\ Net peak intensities

DIM[ 4 ] ARRAY BASELINE.LIMITS

\ Coordinates of markers.

DIM[ MAXSETS ] ARRAY LIN.REG.X

\ x values of baseline

DIM[ MAXSETS ] ARRAY LIN.REG.Y

\ y values of baseline

DIM[ 2 ] ARRAY PEAK.MAX

\ location & mag of max

25 STRING OP.NAME

\ Operator's name.

25 STRING TITLE

\ Experiment title.

25 STRING EXP#

\ Experiment number.

25 STRING XLBL

\ X-axis label

10 STRING YLBL

\ Y-axis label

1 STRING DATA.SYM.S

\ Data symbol for signal

1 STRING DATA.SYM.B

\ Data symbol for baseline

14 STRING FILENAME

---

**\ Window definitions**

\ Divides screen into small windows which are used to present plots, menus and specs.

0 0	0 79	WINDOW {TOPLINE}	\ Top banner line across screen.
1 0	6 19	WINDOW {SPECS}	\ Top left window for experiment specs.
8 0	17 19	WINDOW {SPEC.MOM}	\ Mid left window for moments.
19 0	19 79	WINDOW {SPLIT1}	\ Middle window for menu banners.
20 0	21 79	WINDOW {SPLIT2}	\ Middle window for menus.
24 0	24 79	WINDOW {BOTLINE}	\ Bottom line of screen for prompt.
1 0	24 79	WINDOW {DEF-1}	\ Excludes top banner line.

---

: DATA.VU \ Defines plotting parameters for graph.

.270 .300	VUPOINT.ORIG	\ Defines the position and
.730 .650	VUPOINT.SIZE	\ size of the plot window.
HORIZONTAL	AXIS.FIT.OFF GRID.OFF	\ Removes the grids from
VERTICAL	AXIS.FIT.OFF GRID.OFF	\ the graph.
.180 .210	AXIS.ORIG	\ Sets the graph position and
.800 .740	AXIS.SIZE	\ size with the window.
.025 .008	TICK.SIZE	
.5 .8	TICK.JUST	

---

**\ Screen Messages**

: BANNER \ Program banner  
 {TOPLINE} SCREEN.CLEAR  
 25 SPACES ." Peak Moment Analysis Program"

: PROMPT \ Prompt on bottom line while menu is displayed.  
 {BOTLINE} SCREEN.CLEAR ." Your choice please "

: WAIT \ Message signifying that the computer is performing calculations.  
 {BOTLINE} SCREEN.CLEAR ." Please wait "

---

## \ Screen Menus

## : MAIN.MENU

{SPLIT2} HOME SCREEN.CLEAR

13 SPACES ." F1) Quit F2) Plot F3) Enter data F4) Read file"

CR 13 SPACES ." F5) Save file F6) Edit data F7) Moments F8) Summary"

{SPLIT1} HOME SCREEN.CLEAR 32 SPACES ." \*\* Main Menu \*\*"

PROMPT

CURSOR.OFF

;

## : PLOT.MENU

{SPLIT1} SCREEN.CLEAR

32 SPACES ." \*\* Plotting menu \*\*"

{SPLIT2} SCREEN.CLEAR

8 SPACES

." F1) Exit F2) Plot F3) Plot baseline F4) Change symbols "

CR 8 SPACES ." F5) Lin. reg. baseline F6) Derivative F7) Smooth "

;

## : SUMMARY.MENU

{SPLIT2} HOME SCREEN.CLEAR

10 SPACES ." F1) Exit F2) Print summary F3) Print data F4) Plot summary"

{SPLIT1} SCREEN.CLEAR

27 SPACES ." \*\* Summary Menu \*\*"

{BOTLINE} SCREEN.CLEAR

;

## \ Data Plotting functions

## : DATA.VU.SET

\ Word to setup data viewport axis area

PEAK.DATA XSECT[ 2 ] SUB[ 1 , #SETS ] \ Sets the origin of the graph

[]MIN/MAX \ Offsets the baseline from the

SWAP \ horizontal axis. The offset is

DUP \ calculated by the expression

ROT \  $[\text{min}] - ([\text{max}] - [\text{min}]) / 5$ 

-

5. /

+ DUP

PEAK.DATA XSECT[ 2 ] SUB[ 1 , #SETS ]

[]MAX

WORLD.COORDS

VERTICAL WORLD.SET

PEAK.DATA XSECT[ 1 ] SUB[ 1 , #SETS ] DUP

[]MIN/MAX HORIZONTAL WORLD.SET

[]MIN SWAP WORLD.COORDS AXIS.POINT

;

```

: SHOW.SPECS          \Displays experimental identification specs on screen.
  {SPECS} SCREEN.CLEAR
  " Date: " DATE CR
  " Operator: "      OP.NAME "TYPE CR
  " Exp. title: " CR  TITLE "TYPE CR
  " Exp. number: "   EXP# "TYPE
;

: SHOW.MOMENTS        \Displays the peak moments on the left side of screen.
  {SPEC.MOM} SCREEN.CLEAR
  " Area=" 4 SPACES  PEAK.AREA . CR
  " Center=" 2 SPACES PEAK.CENTER . CR
  " Variance="      PEAK.VAR . CR
  " Skew=" 4 SPACES  PEAK.SKEW . CR
  " Excess=" 2 SPACES PEAK.EXCESS . CR
  " B/A (10%)="    ASYM.FACTOR . CR
  " W(1/2) "      W(1/2) .
;

: LABEL.PLOT          \Positions the x and y labels for the plot axes.
  NORMAL.COORDS
  .0250 .75 POSITION 270 LABEL.DIR      \Positioning the y label
  YLBL LABEL                          \Writing the y label
  XLBL "LEN 2. /                      \1/2 the number of XLBL sets
  .0175 * .5 SWAP -                  \ the position of the y-label
  .05 POSITION 0 LABEL.DIR
  ABEL                               \Writing the x label
  CURSOR.OFF
;

: PLOT.DATA           \ Command which plots signal data on the screen.
  DATA.VU
  VUPORT.CLEAR          \Setting up the axes of the
  DATA.VU.SET          \ graph based on the range
  XY.AXIS.PLOT          \ of the data.
  DATA.SYM.S SYMBOL
  PEAK.DATA XSECT[ 1 ] SUB[ 1 , #SETS ] \
  PEAK.DATA XSECT[ 2 ] SUB[ 1 , #SETS ] \Plotting the signal data
  XY.DATA.PLOT          \
  LABEL.PLOT
  OUTLINE
  SHOW.SPECS
;

```

---

```

: PLOT.BASELINE                                \Overlays the baseline on the signal plot.
  WAIT
  DATA.VU
  DATA.VU.SET
  DATA.SYM.B SYMBOL
  PEAK.DATA XSECT[ 1 ] SUB[ 1 , #SETS ]          \Plotting the baseline
  PEAK.DATA XSECT[ 3 ] SUB[ 1 , #SETS ]          \ using the axes established
  XY.DATA.PLOT                                    \ for the signal data.
  PROMPT
;

: CHANGE.SYMBOL                                \ Changing the plotting symbol for data plots.
  {SPLIT2} SCREEN.CLEAR ." Change " DATA.SYM.S "TYPE
  ." to (enter character <cr>)"
  "INPUT DATA.SYM.S ":=                          \ Changing the signal
  DATA.SYM.S " " "= IF MYSELF THEN                \ plotting symbol
  PLOT.MENU
  SCREEN.CLEAR ." Change " DATA.SYM.B "TYPE
  ." to (enter character <cr>)"
  "INPUT DATA.SYM.B ":=                          \ Changing the baseline
  DATA.SYM.B " " "= IF MYSELF THEN                \ plotting symbol
  PLOT.MENU
;

: SET.BASELINE                                \ Allows operate to declare the start and end of peak
  0 BASELINE.LIMITS :=
  BASELINE.LIMITS
  READOUT>ARRAY
  ARRAY.READOUT \ Activates the cursor controls for setting the baseline limits
  {SPLIT2} HOME SCREEN.CLEAR
  ." Use cursor controls to position markers at"
  ." the baseline limits (left first)"
  CR ." Review ARRAY.READOUT for listing of key functions."
  {BOTLINE} SCREEN.CLEAR
  ." Press F9 when done" \ Purpose of F9 is to get the computer to wait for the
  \ operator to declare the peak limits.
;

: LIN.REG.BASELINE                            \ Calculates the best fit line through the
  {BOTLINE} SCREEN.CLEAR                        \ baseline declared using SET.BASLINE.
  0 LIN.REG.# :=
  #SETS 1 + 1 DO
    PEAK.DATA [ 1 , 1 ] DUP
    BASELINE.LIMITS [ 1 ] =
    IF
      I LIN.END :=
    THEN
      DUP BASELINE.LIMITS [ 1 ] <=
      BASELINE.LIMITS [ 3 ] >=

```

OR  
IF

```

LIN.REG.# 1 + LIN.REG.# :=
PEAK.DATA [ 1, 1 ] LIN.REG.X [ LIN.REG.# ] :=
PEAK.DATA [ 1, 2 ] LIN.REG.Y [ LIN.REG.# ] :=

```

THEN

LOOP

```

LIN.REG.X SUB[ 1, LIN.REG.# ]

```

```

LIN.REG.Y SUB[ 1, LIN.REG.# ]

```

```

1 LEASTSQ.POLY.FIT

```

```

DUP

```

```

[ 1 ]

```

```

PEAK.DATA XSECT[ 1 ] SUB[ 1, #SETS ] *

```

```

SWAP[ 2 ] +

```

```

PEAK.DATA XSECT[ 3 ] SUB[ 1, #SETS ] :=

```

```

PLOT.MENU

```

\ First order polynomial least squares  
\ i.e. linear least squares.

: DERIVATIVE \ Calculates the derivative of the signal data using the  
\ equation:  $f'(x) = [f(x + dx) - f(x)] / dt$   
(Written by L. Amankwa for his research. Not used in C. Lucy research.)

```

#SETS 1 -

```

```

#SETS :=

```

```

PEAK.DATA XSECT[ 2 ] SUB[ 2, #SETS ]

```

```

PEAK.DATA XSECT[ 2 ] SUB[ 1, #SETS ]

```

\ Calculating change in response  
\ for a dt change in time

```

PEAK.DATA XSECT[ 1 ] [ 2 ]

```

```

PEAK.DATA XSECT[ 1 ] [ 1 ]

```

\ Calculating dt

```

/

```

\ change in response / dt

```

PEAK.DATA XSECT[ 2 ] SUB[ 1, #SETS ] :=

```

```

PEAK.DATA XSECT[ 2 ] SUB[ 1, #SETS ] [ 1 ] DUP

```

```

PEAK.DATA XSECT[ 2 ] SUB[ 1, #SETS ] [ #SETS ]

```

```

SWAP - #SETS 1. - /

```

```

PEAK.DATA XSECT[ 3 ] SUB[ 1, #SETS ] [ RAMP

```

```

PEAK.DATA XSECT[ 3 ] SUB[ 1, #SETS ] 1. -

```

```

* + PEAK.DATA XSECT[ 3 ] SUB[ 1, #SETS ] :=

```

\ Calculating the  
\ baseline - setting  
\ a straight line  
\ between the first &  
\ last points

: PEAK.SMOOTH \ Smoothing of data by convolution with weights from a low  
\ pass BLACKMAN window frequency response (lp filter)  
(Written by L. Amankwa for his research. Not used in C. Lucy research.)

```

PEAK.DATA XSECT[ 2 ] SUB[ 1, #SETS ]

```

```

SMOOTH

```

```

PEAK.DATA XSECT[ 2 ] SUB[ 1, #SETS ] :=

```

---



: PRINT.SUMMARY \ Prints out experimental specs and moments.

{SPLIT2} SCREEN.CLEAR

." <cr> when printer is ready..." BELL

." (Any other key aborts)"

PCKEY ?DROP 13 <

IF

SUMMARY.MENU

ELSE

{DEF-1} SCREEN.CLEAR OUT>PRINTER CR CR CR

4 SPACES ." Date: " .DATE 5 SPACES ." Time: " .TIME

8 SPACES ." Operator: " OP.NAME "TYPE CR CR

4 SPACES ." Experiment name: " TITLE "TYPE CR

4 SPACES ." Experiment number: " EXP# "TYPE CR CR

4 SPACES ." AREA: " PEAK.AREA . CR

4 SPACES ." CENTER " PEAK.CENTER . CR

4 SPACES ." VARIANCE " PEAK.VAR . CR

4 SPACES ." SKEW " PEAK.SKEW . CR

4 SPACES ." EXCESS " PEAK.EXCESS . CR

4 SPACES ." B/A (10%) " ASYM.FACTOR . CR

4 SPACES ." W(1/2) " W(1/2) . \_CR CR

CONSOLE

CR ." Press any key to continue."

PCKEY ?DROP DROP

{DEF-1} SCREEN.CLEAR

SUMMARY.MENU

THEN

: PRINT.DATA \ Prints out a full listing of the data

{SPLIT2} SCREEN.CLEAR

." <cr> when printer is ready..." BELL

." (Any other key aborts)"

PCKEY ?DROP 13 <

IF

SUMMARY.MENU

ELSE

{DEF-1} SCREEN.CLEAR OUT>PRINTER CR CR CR

4 SPACES ." Date: " .DATE 5 SPACES ." Time: " .TIME

8 SPACES ." Operator: " OP.NAME "TYPE CR CR

4 SPACES ." Experiment name: " TITLE "TYPE CR

4 SPACES ." Experiment number: " EXP# "TYPE CR CR

." X-values Signal Baseline"

CR CR

#SETS 1 + 1 DO

PEAK.DATA [1, 3]

PEAK.DATA [1, 2]

PEAK.DATA [1, 1]

.18 ?COL - SPACES . 36 ?COL - SPACES . CR

LOOP

CONSOLE

```

CR ." Press any key to continue."
PCKEY ?DROP DROP
{DEF-1} SCREEN.CLEAR
SUMMARY.MENU
THEN
;

: PLOT.SUMMARY                                \ Prints out a plot of the data with the moments
SCREEN.CLEAR
PLOT.DATA
SHOW.MOMENTS
{SPLIT1} SCREEN.CLEAR
{SPLIT2} SCREEN.CLEAR
." <cr> when printer is ready ..." BELL
." (Any other key aborts) "
PCKEY ?DROP 13 <
IF
    SUMMARY.MENU
ELSE
    {SPLIT2} SCREEN.CLEAR
    SCREEN.PRINT
    CONSOLE
    CR ." Press any key to continue. "
    PCKEY ?DROP DROP
    {DEF-1} SCREEN.CLEAR
    SUMMARY.MENU
THEN
;

```

\ Saving the data in memory.

```

: WRITE.FILE                                \ Default drive for data storage is C (Hard Drive).
FILE.TEMPLATE
5 COMMENTS
INTEGER DIM[ 2 ] SUBFILE                    \ Defines the format of
REAL DIM[ #SETS ] SUBFILE                    \ the data file.
REAL DIM[ #SETS ] SUBFILE
REAL DIM[ #SETS ] SUBFILE
END

HOME
." Opening file " FILENAME "TYPE
13 EMIT FILENAME DEFER> FILE.CREATE
." Writing file " FILENAME "TYPE
13 EMIT FILENAME DEFER> FILE.OPEN

TITLE    1  >COMMENT
OP.NAME  2  >COMMENT
EXP#     3  >COMMENT
XLBL     4  >COMMENT
YLBL     5  >COMMENT

```

\ Outputs the variables to the appropriate positions in the data file.

```
#SETS HOLDIT [ 1 ] :=
MAX.IN.SET HOLDIT [ 2 ] :=
1 SUBFILE HOLDIT ARRAY>FILE
2 SUBFILE PEAK.DATA XSECT[ 1 ] SUB[ 1 , #SETS ] ARRAY>FILE
3 SUBFILE PEAK.DATA XSECT[ 2 ] SUB[ 1 , #SETS ] ARRAY>FILE
4 SUBFILE PEAK.DATA XSECT[ 3 ] SUB[ 1 , #SETS ] ARRAY>FILE
FILE.CLOSE
```

```
ONERR:                                     \Error trap.
    ." Can't open file for writing. "
    ." Type any key to continue." BELL PCKEY ?DROP DROP
    ?FILE.OPEN IF FILE.CLOSE THEN
```

```
;
: GET.FILENAME                             \Requests name for data file.
    ." filename please ? " "INPUT
    FILENAME ":="
    SCREEN.CLEAR
```

```
;
: OUTPUT.DATA.FILE                         \Invokes the words above to save the data.
    #SETS 0 >
    IF
        SCREEN.CLEAR
        {SPLIT2} SCREEN.CLEAR ." Output "
        GET.FILENAME
        WRITE.FILE
        MAIN.MENU
    THEN
```

\-----

\Data input - either from memory (READ.FILE) or from the keyboard (ENTER.DATA)

```
: READ.FILE                               \Must be in format used by DATACQ, MOMENTS & SEGMENT
    {SPLIT2} SCREEN.CLEAR
    ." Reading " FILENAME DEFER> FILE.OPEN
    FILENAME "TYPE 13 EMIT
    1 COMMENT> TITLE ":=
    2 COMMENT> OP.NAME ":=
    3 COMMENT> EXP# ":=
    4 COMMENT> XLBL ":=
    5 COMMENT> YLBL ":=
    1 SUBFILE HOLDIT FILE>ARRAY
    HOLDIT [ 1 ] #SETS :=
    HOLDIT [ 2 ] MAX.IN.SET :=
    2 SUBFILE PEAK.DATA XSECT[ 1 ] SUB[ 1 , #SETS ] FILE>ARRAY
    3 SUBFILE PEAK.DATA XSECT[ 2 ] SUB[ 1 , #SETS ] FILE>ARRAY
    4 SUBFILE PEAK.DATA XSECT[ 3 ] SUB[ 1 , #SETS ] FILE>ARRAY
    FILE.CLOSE
```

ONERR:

\Error trap.

210

." Can't open file for writing. "

." Type any key to continue." BELL PCKEY ?DROP DROP  
?FILE.OPEN IF FILE.CLOSE THEN

;

: INPUT.DATA.FILE

\ Prints out a list of files available & requests choice

{DEF-1} SCREEN.CLEAR

DIR \*.DAT

CR CR ." Input "

GET.FILENAME

READ.FILE

MAIN.MENU

;

: ED.DATA

\ Word allows editing of the data array.

#SETS 0 >

IF

PEAK.DATA SUB[ 1 , #SETS ; COL# , MAX.IN.SET ] ARRAY.EDIT

INTEN.ON BELL

." Use the cursor keys to move cursor."

CR CR

." Press <cr> to exit back to main menu"

ARRAY.EDIT.WORDS

\ Sets up array for editing

INSERT

GRAPHICS.DISPLAY

BANNER

\ Returns to main menu when done

MAIN.MENU

\ editing file.

THEN

;

: ENTER.DATA

\ Word allows manual entry of data.

{DEF-1} SCREEN.CLEAR

." New data set:" CR CR

." Your name (or initials) please? " "INPUT OP.NAME ":= CR CR

." Title of experiment? (name for data set) " "INPUT TITLE ":= CR CR

." Experiment identification number? " "INPUT EXP# ":= CR CR

." X-axis label? (15 chars. or less) " "INPUT XLBL ":= CR

." Y-axis label? (10 chars. or less) " "INPUT YLBL ":= CR CR

BEGIN

." Number of data sets in this experiment ? " #INPUT CR CR

IF #SETS :=

ELSE GRAPHICS.DISPLAY {SPLIT1} HOME ." Press F1" EXIT

THEN

#SETS MAXSETS >

IF ." Maximum #sets allowable is " MAXSETS

-1 0 FIX.FORMAT MAXSETS.

-1 4 SCI.FORMAT FALSE

ELSE TRUE

THEN

UNTIL

```

2 COL# :=
1 MAX.IN.SET :=
PEAK.DATA XSECT[ 1 ] SUB[ 1 , #SETS ] []RAMP
PEAK.DATA XSECT[ 1 ] SUB[ 1 , #SETS ] 1. -
." The first x-value is: " #INPUT CR
SWAP
." The interval between points is: " #INPUT
* + PEAK.DATA XSECT[ 1 ] SUB[ 1 , #SETS ] :=
ED.DATA
1 COL# :=
3 MAX.IN.SET :=
PEAK.DATA XSECT[ 2 ] SUB[ 1 , #SETS ] [ 1 ] DUP
PEAK.DATA XSECT[ 2 ] SUB[ 1 , #SETS ] [ #SETS ]
SWAP - #SETS 1. - /
PEAK.DATA XSECT[ 3 ] SUB[ 1 , #SETS ] []RAMP
PEAK.DATA XSECT[ 3 ] SUB[ 1 , #SETS ] 1. -
* + PEAK.DATA XSECT[ 3 ] SUB[ 1 , #SETS ] :=
;

```

\ Filling in the  
\ retention values  
\ into the data array  
\  
\  
\ Calculating the  
\ baseline - setting  
\ a straight line  
\ between the first &  
\ last points

---

```

: LOCATE.PEAK.MAX \Locates the maximum value in a data set. Stores the
                  \array index and the intensity of this maximum in the
                  \two-element array PEAK.MAX

```

```

\Stack in : array containing peak
\Stack out: empty
0 PEAK.MAX [ 1 ] :=
0 PEAK.MAX [ 2 ] :=
#SETS 1 DO
  DUP
  [ 1 ] PEAK.MAX [ 2 ] >
  IF
    DUP [ 1 ] PEAK.MAX [ 2 ] :=
    I PEAK.MAX [ 1 ] :=
  THEN
LOOP
DROP
;

```

```

: FIND.?.%MAX \Locates the array index of the point along the front
              \and tail of a peak which have an intensity of __% of the
              \maximum. Stores these positions in the variables
              \FIRST# AND LAST#

```

```

\Stack in : array size
\            % of maximum to be found
\            array containing peak
\Stack out: empty
ARRAY.SIZE := \The top number on the stack denotes the array size
1 FIRST# := \Set variables to their default settings
PEAK MAX [ 1 ] LAST# := \ - i.e. the extremes of the array.
100. / \The second number on the stack is the percentage
PEAK.MAX [ 2 ] * \ of the peak height. This % is converted to its
%MAX := \ numerical counterpart and stored in %MAX.

```

```

PEAK.MAX[1] 1 DO
  DUP[1] %MAX <
  IF
    I FIRST# :=
    THEN
  LOOP
  ARRAY.SIZE PEAK.MAX[1] DO
    DUP[1] %MAX >
    I LAST# - 3 < AND
    IF
      I LAST# :=
      THEN
  LOOP
  DROP
  LAST# FIRST# - 1 + #.IN.PEAK :=

```

```

: PEAK.MOMENTS

```

\ Calculation of the moments of the peak.

```

  WAIT
  PEAK.DATA XSECT[ 1 ][ 2 ]
  PEAK.DATA XSECT[ 1 ][ 1 ] -
  DELTA.T :=
  PEAK.DATA XSECT[ 2 ] SUB[ 1 , #SETS ]
  PEAK.DATA XSECT[ 3 ] SUB[ 1 , #SETS ] -
  DUP DUP
  CONC.I SUB[ 1 , #SETS ] :=
  LOCATE.PEAK.MAX
  PEAK.LIMITS
  #SETS
  FIND.?.%MAX

```

\ The zeroth moment = unnormalized peak area

\ Zeroth moment = summation(  $C_i * dt$  )

\ Stack in: empty

\ Stack out: (  $C_i * dt$  )

```

  CONC.I SUB[ FIRST# , LAST# ] DELTA.T *

```

```

  DUP

```

```

  INTEGRATE.DATA [ #.IN.PEAK ]

```

```

  PEAK.AREA :=

```

\ approx integration

\ with 1/3 Simpson's

\ rule and store.

\ The first moment = peak center

\ First moment =  $1/\text{area} * \text{integration}(t * C_i * dt)$

\ Stack in: (  $C_i * dt$  )

\ Stack out: empty

```

  PEAK.DATA XSECT[ 1 ] SUB[ FIRST# , LAST# ] *

```

```

  INTEGRATE.DATA [ #.IN.PEAK ]

```

```

  PEAK.AREA /

```

```

  PEAK.CENTER :=

```

\ t = time or volume

\ along the x axis

\ approx. integration

\ divide by area.

\ and store.

\ The second moment = peak variance  
 \ Second moment =  $1/\text{area} * [ \text{integration}( (t-t_r)^2 * C_i * dt ) ]$

\ Stack in: empty

\ Stack out: (t-t<sub>r</sub>)

PEAK.DATA XSECT[ 1 ] SUB[ FIRST# , LAST# ]

PEAK.CENTER - DUP

DUP \*

CONC.I SUB[ FIRST# , LAST# ] \*

DELTA.T \*

INTEGRATE.DATA [ #.IN.PEAK ]

PEAK.AREA /

ABS

PEAK.VAR :=

\ save t-tr on stack

\ calc (t-t<sub>r</sub>)<sup>2</sup>

\ and mult by C<sub>i</sub>

\ and mult by dt

\ and integrate

\ and normalize.

\ and store.

\ Third moment =  $1/\text{area} * [ \text{integration}( (t-t_r)^3 * C_i * dt ) ]$

\ Peak skew = third moment / variance<sup>3/2</sup>

\ Stack in: (t-t<sub>r</sub>)

\ Stack out: (t-t<sub>r</sub>)

DUP

3 \*\*

CONC.I SUB[ FIRST# , LAST# ] \*

DELTA.T \*

INTEGRATE.DATA [ #.IN.PEAK ]

PEAK.AREA /

PEAK.VAR 1.5 \*\* /

PEAK.SKEW :=

\ save extra t-tr

\ calc (t-t<sub>r</sub>)<sup>3</sup>

\ and mult. by C<sub>i</sub>

\ and mult. by dt

\ and integrate

\ and normalize

\ and convert to the

\ skew and store.

\ Fourth moment =  $1/\text{area} * [ \text{integration}( (t-t_r)^4 * C_i * dt ) ]$

\ Peak excess = fourth moment / variance<sup>2</sup> - 3

\ Stack in: (t-t<sub>r</sub>)

\ Stack out: empty

4 \*\*

CONC.I SUB[ FIRST# , LAST# ] \*

DELTA.T \*

INTEGRATE.DATA [ #.IN.PEAK ]

PEAK.AREA /

PEAK.VAR DUP \* /

3. -

PEAK.EXCESS :=

\ calc (t-t<sub>r</sub>)<sup>4</sup>

\ and mult. by C<sub>i</sub>

\ and mult. by dt

\ and integrate

\ and normalize

\ and convert to the

\ excess

\ and store.

; ASYM.MEAS

CONC.I SUB[ 1 , #SETS ]

10 #SETS

FIND.?.%MAX

LAST# PEAK.MAX [ 1 ] -

PEAK.MAX [ 1 ] FIRST# -

/ ASYMFACTOR :=

\ Asymmetry factor (B/A) at 10% of the peak max.

\ Locates the points at 10% of the peak max

;

```

: WIDTH.AT.HALF.HEIGHT
  CONC.I SUB[ 1 , #SETS ]
  50 #SETS
  FIND.?.%MAX
  LAST# FIRST# -
  DELTA.T *
  W(1/2) :=
;

```

\Calculates the width at half height

```

: MOMENTS
  PEAK.MOMENTS
  ASYM.MEAS
  WIDTH.AT.HALF.HEIGHT
  SHOW.MOMENTS
  PROMPT
;

```

\Primary word for initiating calculation of the moments.

```

: SUMMARY.KEYS
  F1 FUNCTION.KEY.DOES ESCAPE
  F2 FUNCTION.KEY.DOES PRINT.SUMMARY
  F3 FUNCTION.KEY.DOES PRINT.DATA
  F4 FUNCTION.KEY.DOES PLOT.SUMMARY
  F5 FUNCTION.KEY.DOES NOP
  F6 FUNCTION.KEY.DOES NOP
  F7 FUNCTION.KEY.DOES NOP
  F8 FUNCTION.KEY.DOES NOP
  F9 FUNCTION.KEY.DOES NOP
;

```

\Redefines the keys to the summary options.

```

: MAIN.SUMMARY
  SCREEN.CLEAR
  STORE.FUNCTION.KEYS
  SUMMARY.KEYS
  SUMMARY.MENU
  INTERPRET.KEYS
  0. PEAK.AREA :=
  0. PEAK.CENTER :=
  0. PEAK.VAR :=
  0. PEAK.SKEW :=
  0. PEAK.EXCESS :=

```

ONESCAPE: RESTORE.FUNCTION.KEYS MAIN.MENU



: **PLOT.KEYS** \ Redefines the function key to the plotting options

F1 FUNCTION.KEY.DOES ESCAPE  
 F2 FUNCTION.KEY.DOES PLOT.DATA  
 F3 FUNCTION.KEY.DOES PLOT.BASELINE  
 F4 FUNCTION.KEY.DOES CHANGE.SYMBOL  
 F5 FUNCTION.KEY.DOES SET.BASELINE  
 F6 FUNCTION.KEY.DOES DERIVATIVE  
 F7 FUNCTION.KEY.DOES PEAK.SMOOTH  
 F8 FUNCTION.KEY.DOES NOP  
 F9 FUNCTION.KEY.DOES LIN.REG.BASELINE

: **MAIN.PLOT.DATA**

#SETS 0 >

IF

SCREEN.CLEAR

STORE.FUNCTION.KEYS

PLOT.KEYS

PLOT.MENU

PLOT.DATA

PLOT.MENU

INTERPRET.KEYS

THEN

\  
 \  
 \ Sets up the plotting  
 \ screen and plots  
 \ the data.  
 \

ONESCPE: RESTORE.FUNCTION.KEYS MAIN.MENU

: **PEAK.QUIT**

\ Word to quit application of this program.

SCREEN.CLEAR \ Clears prompt

{SPLIT2} SCREEN.CLEAR BELL ." Quit ?"

PCKEY ?DROP 89 = IF BYE THEN

MAIN.MENU

: **MAIN.KEYS**

\ Sets up function keys for MAIN.PROGRAM.

F1 FUNCTION.KEY.DOES PEAK.QUIT

F2 FUNCTION.KEY.DOES MAIN.PLOT.DATA

F3 FUNCTION.KEY.DOES ENTER.DATA

F4 FUNCTION.KEY.DOES INPUT.DATA.FILE

F5 FUNCTION.KEY.DOES OUTPUT.DATA.FILE

F6 FUNCTION.KEY.DOES ED.DATA

F7 FUNCTION.KEY.DOES MOMENTS

F8 FUNCTION.KEY.DOES MAIN.SUMMARY

F9 FUNCTION.KEY.DOES NOP

```
: MAIN.PROGRAM  
  MAIN.KEYS  
  MAIN.MENU  
  INTERPRET.KEYS
```

```
\ Defines the function keys.  
\ Displays the selection menu.
```

```
;
```

```
\-----  
: INIT
```

```
\ Starts the program once it has been loaded
```

```
  CLEAR.FUNCTION.KEYS  
  GRAPHICS.DISPLAY  
  BANNER  
  "." DATA.SYM.S ":=  
  "." DATA SYM.B ":=  
  -1 3 SCLFORMAT  
  MAIN.PROGRAM
```

```
\ Default values for  
\ plotting symbols.
```

```
;
```

## **Appendix B**

### **Data Acquisition Program**

#### **\ DATA ACQUISITION PROGRAM**

**\**  
**\ Program name: DATACQ.ASY (ASYST Version 2.0)**  
**\ Directory: ASYST2**  
**\**

**\ The program is menu driven for ease of use and assumes nothing of the**  
**\ operator. The maximum number of data sets allowed in the present**  
**\ version is 2000. This may be changed by editing the program and changing**  
**\ MAXSETS to whatever value is desired.**

**\ Data acquisition is with a Tecmar LAB MASTER, configured as described**  
**\ in Module 3 of the ASYST manuals with one exception - the data is unipolar.**

**\ Written by C. Lucy, 15 July 1985**

**\ -----**

#### **\ Program Structure**

**\ This program is designed to be menu driven and utilizes a**  
**\ two-tiered structure. The upper most tier is Main Menu from which**  
**\ the Summary Menu can be accessed. Most primary functions are**  
**\ available in the Main Menu**

#### **\ Main Menu**

- \ F1) Quit - exits operation from the acquisition program and from ASYST.**
- \ F2) Data Acquisition - will request information about the data to be acquired and then**  
**\ on manual initiation will collect data in the fore-ground mode.**
- \ F3) Repeat Acq. - will perform acquisition using the last stored acquisition**  
**\ parameters. Only the experiment identification number will be**  
**\ requested.**
- \ F4) Plot - plots the data on the screen. Y-axis goes from 0 to 4096 to indicate how**  
**\ much of the ADC's dynamic range is being utilized.**
- \ F5) Save Data - stores the collected data. The filename should include the extension**  
**\ ".DAT".**
- \ F6) Summary - accesses the Summary Menu for creation of a hard copy of the data.**

## \ Summary Menu

- \ F1) Exit - returns operation to the Main Menu.
- \ F2) Print Summary - prints out the data file specifications and acquisition settings.
- \ F3) Print Data - prints out a table of the data points collected.
- \ F4) Plot Summary - prints out a copy of the data plot along with the file specs and the acquisition parameters.

## \ Overlay check

- \ Some functions used in this program are not available in the base ASYST system,
- \ so it is necessary to install the extra overlays into the system. These required
- \ overlays are already installed in the system ASYST in Directory ASYST2.

```

ECHO.OFF
: OLOAD?
  CR BELL
  ." Are overlays DATAFILE.SOV, ACQUIS.SOV and ACQLM.SOV in the
  system (Y/N) ?"
  KEY DUP EMIT
  DUP 90 > IF 32 - THEN 89 = NOT
  IF
    CR CR ." Please use the Configuration menu <F2> to load the ,"
    CR ." Data files, Data acquisition and Lab Master overlays in the"
    CR ." system before continuing." CR CR
    57 ERROR
  THEN
;
OLOAD?
ECHO.ON

```

## \ Variable declarations

```

INTEGER
  SCALAR MAXSETS
  SCALAR MAX.IN.SET
  SCALAR #SETS
  SCALAR COL#
  SCALAR ACQ.RATE      \Time between successive data points (msec)
  SCALAR ACQ.GAIN      \Programmable gain setting for Lab Master

2048 MAXSETS :=      \Either of these lines may be changed
3 MAX.IN.SET :=      \to allow larger data sets to be used.

DIM[ 2 ] ARRAY HOLDIT  \Output buffer for #SETS & MAX.IN.SETS
DIM[ MAXSETS ] ARRAY ACQ.BUF \Integer buffer for acquisition data
DIM[ 4 ] ARRAY CAP.REQ  \Capacitances required for gains used.

```

REAL

DIM[ MAXSETS , MAX.IN.SET ] ARRAY PEAK.DATA \Peak data buffer

25	STRING OP.NAME	\Operator's name.
25	STRING TITLE	\Experiment title.
25	STRING EXP#	\Experiment number.
25	STRING XLBL	\X-axis label
10	STRING YLBL	\Y-axis label
14	STRING FILENAME	

\-----+

### \Data acquisition structure

\Defining A/D template for input on channel 0 of the acquisition board.

LAB.MASTER		
0 0	A/D.TEMPLATE CHAN.0	\Sets channel 0 as the input channel.
	ACQ.BUF TEMPLATE.BUFFER	\Data will be temp. saved in ACQ.BUF

\-----

### \Window definitions

\Divides screen into small windows in which plots, menus and specs will be presented.

0 0	0 79	WINDOW {TOPLINE}	\Top banner line across screen.
1 0	6 19	WINDOW {SPECS}	\Top left window for experiment specs.
8 0	10 19	WINDOW {SPEC.ACQ}	\Lower left window for acquisition specs.
12 0	12 20	WINDOW {SPEC.SAVE}	\Window to record saving of file
19 0	19 79	WINDOW {SPLIT1}	\Middle window for menu banners.
20 0	21 79	WINDOW {SPLIT2}	\Middle window for menus.
24 0	24 79	WINDOW {BOTLINE}	\Bottom line of screen for prompt.
1 0	24 79	WINDOW {DEF-1}	\Excludes top banner line.

\-----

: DATA.VU \ Defines plotting parameters for graph.

.270 .300	VUPORT.ORIG	\Defines the position and
.730 .650	VUPORT.SIZE	\ size of the plot window.
HORIZONTAL AXIS.FIT.OFF GRID.OFF		\Removes the grids from
VERTICAL AXIS.FIT.OFF GRID.OFF		\ the graph.
.180 .210	AXIS.ORIG	\Sets the graph position &
.800 .740	AXIS.SIZE	\ size within the window.
.025 .008	TICK.SIZE	
.5 .8	TICK.JUST	
VERTICAL LABEL.SCALE.OFF		\Inhibits automatic printing
HORIZONTAL LABEL.SCALE.OFF		\ of the scaling factor

;

\-----

---

## : MAIN.MENU

```
: SUMMARY.MENU          \ Presents & performs the summary options.
  {SPLIT2} HOME SCREEN.CLEAR
  10 SPACES ." F1) Exit  F2) Print summary  F3) Print data  F4) Plot summary"
  {SPLIT1} SCREEN.CLEAR
  32 SPACES ." ** Summary Menu  **"
  {BOTLINE} SCREEN.CLEAR
  ." For more than 50 data points, F2 or F4 are recommended. "
;
```

## : DATA.VU.SET

```

WORLD.COORDS
0.4095. VERTICAL WORLD.SET
PEAK.DATA XSECT[ 1 ] SUB[ 1 , #SETS ]
DUP
[MIN/MAX HORIZONTAL WORLD.SET
[MIN 0. WORLD.COORDS AXIS.POINT

```

```

: SHOW.SPECS          \Displays experimental specifications on screen
  {SPECS} SCREEN.CLEAR
  ." Date: " DATE CR
  ." Operator: "      OP.NAME "TYPE CR
  ." Exp. title: " CR  TITLE "TYPE CR
  ." Exp. number: "   EXP# "TYPE
;

```

```

: SHOW.ACQ            \Shows settings for data acquisition on screen.
  {SPEC.ACQ} SCREEN.CLEAR
  ." Acq Rate=" ACQ.RATE . CR
  ." # Points=" #SETS . CR
  ." Gain= " ACQ.GAIN .
;

```

```

: SHOW.SAVE           \Indicates on screen that the data has been saved.
  {SPEC.SAVE} SCREEN.CLEAR
  FILENAME "TYPE
  ." saved"
;

```

```

: LABEL.PLOT          \Positions the x and y labels on the graph.
  NORMAL.COORDS
  .0250 .75 POSITION 270 LABEL.DIR      \Positioning the y-label
  YLBL LABEL                          \Writing the y-label.
  XLBL "LEN 2. /                      \1/2 the letters of XLBL sets
  .0175 * .5 SWAP -                  \ the position of the x-label
  .05 POSITION 0 LABEL.DIR
  LABEL                              \Writing the x-label
  CURSOR.OFF
;

```

```

: PLOT.DATA           \Routine to draw labelled graph on screen.
  DATA.VU
  VUPORT.CLEAR          \Setting up the
  DATA.VU.SET          \axes of the graph.
  XY.AXIS.PLOT
  PEAK.DATA XSECT[ 1 ] SUB[ 1 , #SETS ] \
  PEAK.DATA XSECT[ 2 ] SUB[ 1 , #SETS ] \Plotting the signal data
  XY.DATA.PLOT
  LABEL.PLOT
  OUTLINE
  SHOW.SPECS
  SHOW.ACQ
  MAIN.MENU
;

```

: MAIN.PLOT.DATA

\ Checks data before plotting

222

#SETS 0 >

IF

SCREEN.CLEAR

\ Clears prompt and

PLOT.DATA

\ plots the data and

INTERPRET.KEYS

\ specs.

THEN

ONESCAPE: RESTORE.FUNCTION.KEYS MAIN.MENU

;

\ Summary options

: PRINT.SUMMARY

\ Prints out the file and acquisition specs.

{SPLIT2} SCREEN.CLEAR

." <cr> when printer is ready..." BELL

." (Any other key aborts)"

KEY 13 <

IF

SUMMARY.MENU

ELSE

{DEF-1} SCREEN.CLEAR OUT>PRINTER CR CR CR

4 SPACES ." Date: " .DATE 5 SPACES ." Time: " .TIME

8 SPACES ." Operator: " OP.NAME "TYPE CR CR

4 SPACES ." Experiment name: " TITLE "TYPE CR

4 SPACES ." Experiment number: " EXP# "TYPE CR CR

4 SPACES ." Acq. Rate: " ACQ.RATE . CR

4 SPACES ." No. data points: " #SETS . CR

4 SPACES ." Gain: " ACQ.GAIN . CR CR

CONSOLE

CR ." Press any key to continue."

KEY DROP

{DEF-1} SCREEN.CLEAR

SUMMARY.MENU

THEN

;

: PRINT.DATA

\ Prints out the collected data.

{SPLIT2} SCREEN.CLEAR

." <cr> when printer is ready..." BELL

." (Any other key aborts)"

KEY 13 <

IF

SUMMARY.MENU

ELSE

{DEF-1} SCREEN.CLEAR OUT>PRINTER CR CR CR

4 SPACES ." Date: " .DATE 5 SPACES ." Time: " .TIME

8 SPACES ." Operator: " OP.NAME "TYPE CR CR

4 SPACES ." Experiment name: " TITLE "TYPE CR

4 SPACES ." Experiment number: " EXP# "TYPE CR CR



```

." X-values      Signal "
CR CR
#SETS 1 + 1 DO
    PEAK.DATA [ 1, 2 ]
    PEAK.DATA [ 1, 1 ]
    . 18 ?COL - SPACES . CR
LOOP
CONSOLE
CR ." Press any key to continue."
KEY DROP
{DEF-1} SCREEN.CLEAR
SUMMARY.MENU
THEN
;

: PLOT.SUMMARY          \ Prints out plot of data, with all relevant specs.
    SCREEN.CLEAR
    PLOT.DATA
    SHOW.ACQ
    {SPLIT1} SCREEN.CLEAR
    {SPLIT2} SCREEN.CLEAR
    {BOTLINE} SCREEN.CLEAR
    ." <cr> when printer is ready . . ." BELL
    ." (Any other key aborts) "
    KEY 13 <
    IF
        SUMMARY.MENU
    ELSE
        {SPLIT2} SCREEN.CLEAR
        SCREEN.PRINT
        CONSOLE
        CR ." Press any key to continue. "
        KEY DROP
        {DEF-1} SCREEN.CLEAR
        SUMMARY.MENU
    THEN
;

\-----

\ Saving the data in memory.

: WRITE.FILE            \ Default drive for data storage is C (Hard Drive)
    FILE.TEMPLATE
    5 COMMENTS
    INTEGER DIM[ 2 ] SUBFILE
    REAL DIM[ #SETS ] SUBFILE
    REAL DIM[ #SETS ] SUBFILE
    REAL DIM[ #SETS ] SUBFILE
END
    \
    \ Defines the format of
    \ the data file.
    \
    \

```

HOME

```

." Opening file " FILENAME "TYPE
13 EMIT FILENAME DEFER> FILE.CREATE
." Writing file " FILENAME "TYPE
13 EMIT FILENAME DEFER> FILE.OPEN

```

```

TITLE      1  >COMMENT
OP.NAME    2  >COMMENT
EXP#       3  >COMMENT
XLBL      4  >COMMENT
YLBL      5  >COMMENT

```

\ .  
\ Outputs the variables to the  
\ appropriate positions in  
\ the data file.  
\

```

#SETS HOLDIT [ 1 ] :=
MAX.IN.SET HOLDIT [ 2 ] :=
1 SUBFILE HOLDIT ARRAY>FILE
2 SUBFILE PEAK.DATA XSECT[ 1 ] SUB[ 1 , #SETS ] ARRAY>FILE
3 SUBFILE PEAK.DATA XSECT[ 2 ] SUB[ 1 , #SETS ] ARRAY>FILE
4 SUBFILE PEAK.DATA XSECT[ 3 ] SUB[ 1 , #SETS ] ARRAY>FILE
FILE.CLOSE

```

```

ONERR:                                \Error trap
." Can't open file for writing. "
." Type any key to continue." BELL KEY DROP
?FILE.OPEN IF FILE.CLOSE THEN

```

```

;
: GET.FILENAME                        \Requests name for the data file.
." Filename please ? " "INPUT
FILENAME ":=
SCREEN.CLEAR

```

```

;
: OUTPUT.DATA.FILE                    \Invokes the words above to save the data.
#SETS 0 >
IF
  SCREEN.CLEAR
  {SPLIT2} SCREEN.CLEAR ." Output "
  GET.FILENAME
  WRITE.FILE
  SHOW.SAVE
  MAIN.MENU
THEN

```

---

# \ Performing the data acquisition.

225

```

: DATA.ACQ                                \ Performs data acquisition using the Lab Master ADC.
  CHAN.0 A/D.INT                            \ Initiating the data
  {DEF-1} SCREEN.CLEAR                      \ acquisition board.
  {BOTLINE} SCREEN.CLEAR
  CR ." <cr> to start data acquisition ... " BELL
  ." (Any other key aborts) "
  KEY 13 <
  IF
    MAIN.MENU
  ELSE
    WAIT
    ACQ.RATE SYNC.PERIOD
    #SETS 1 + 1 DO
      SYNCHRONIZE                            \ Collects data at the rate
      A/D.IN>ARRAY                          \ specified by ACQ.RATE
    LOOP
      ACQ.BUF SUB[ 1 , #SETS ]              \ Stores the acquired
      PEAK.DATA XSECT[ 2 ] SUB[ 1 , #SETS ] := \ data.
      BANNER
      MAIN.MENU
      PEAK.DATA XSECT[ 2 ] SUB[ 1 , #SETS ] [] MAX
      4095 = IF
        {BOTLINE} SCREEN.CLEAR
        ." WARNING: The inputted signal has saturated the ADC."
        BELL
      ELSE
        PROMPT
      THEN
    THEN
  ;

: ACQ.PARAMETERS                          \ Prompts operator for acquisition settings.
  {DEF-1} SCREEN.CLEAR
  ." New data set:" CR CR
  ." Your name (or initials) please? " "INPUT OP.NAME " := CR CR
  ." Title of experiment? (name for data set) " "INPUT TITLE " := CR CR
  ." Experiment ident. number? " "INPUT EXP# " := CR CR
  BEGIN
    ." Number of data sets in this experiment ? " #INPUT CR CR
    IF #SETS :=
      ELSE GRAPHICS.DISPLAY {SPLIT1} HOME ." Press F1" EXIT
    THEN
      #SETS MAXSETS >
      IF ." Maximum #sets allowable is " MAXSETS
        -1 0 FIX.FORMAT MAXSETS .
        -1 4 SCI.FORMAT FALSE
      ELSE TRUE
      THEN
    UNTIL

```

```

." Data acquisition rate (msec) ?"
#INPUT ACQ.RATE :=
PEAK.DATA XSECT[ 1 ] SUB[ 1 , #SETS ] [RAMP
PEAK.DATA XSECT[ 1 ] SUB[ 1 , #SETS ] 1. -
ACQ.RATE FLOAT
1000 /
*
PEAK.DATA XSECT[ 1 ] SUB[ 1 , #SETS ] :=
CR CR ." Connect input leads to Channel 0 and Ground. "
CR ." Type any key to continue. " KEY DROP
CR CR ." Gain required ?"
CR ." 1 = 1X 2 = 10X 3 = 100X 4 = 500X "
#INPUT ACQ.GAIN :=
CR CR ." Require a " CAP.REQ [ ACQ.GAIN ] . .
." " pico-farad capacitor on the daughter board ."
ACQ.GAIN 1 - A/D.GAIN
CR ." Type any key when the capacitor is set. " KEY DROP
DATA.ACQ
;

: REPEAT.ACQ \Repeats data acquisition using the last set of conditions stored
{DEF-1} SCREEN.CLEAR
CR CR ." REPEAT ACQUISITION "
CR CR ." New experiment ident. number? " "INPUT EXP# " :=
DATA.ACQ
;

\-----

: SUMMARY.KEYS \Redefines the function keys to the summary options.
F1 FUNCTION.KEY.DOES ESCAPE
F2 FUNCTION.KEY.DOES PRINT.SUMMARY
F3 FUNCTION.KEY.DOES PRINT.DATA
F4 FUNCTION.KEY.DOES PLOT.SUMMARY
F5 FUNCTION.KEY.DOES NOP
F6 FUNCTION.KEY.DOES NOP
;

: SUMMARY
{DEF-1} SCREEN.CLEAR
STORE.FUNCTION.KEYS
SUMMARY.KEYS
SUMMARY.MENU
INTERPRET.KEYS
.
ONESCPE: RESTORE.FUNCTION.KEYS MAIN.MENU
;

\-----

```

\ Input acquisition  
 \ rate.  
 \ Filling in the  
 \ retention values in  
 \ sec into the data file

\ Input & store the  
 \ programmable  
 \ gain.  
 \ Setting low pass  
 \ filter on the ADC

```

: ACQ.QUIT                                \ Word to quit application of this program.
  SCREEN.CLEAR \ Clears prompt
  {SPLIT2} SCREEN.CLEAR BELL ." Quit (y/n)?"
  KEY DUP EMIT
  DUP 90 > IF 32 - THEN 89 =                \ Checks if response is "y" or "Y"
  IF BYE THEN
  MAIN.MENU
;

: MAIN.KEYS                                \ Sets up function keys for MAIN.PROGRAM.
  F1 FUNCTION.KEY.DOES ACQ.QUIT
  F2 FUNCTION.KEY.DOES ACQ.PARAMETERS
  F3 FUNCTION.KEY.DOES REPEAT.ACQ
  F4 FUNCTION.KEY.DOES MAIN.PLOT.DATA
  F5 FUNCTION.KEY.DOES OUTPUT.DATA.FILE
  F6 FUNCTION.KEY.DOES SUMMARY
;

: MAIN.PROGRAM
  MAIN.KEYS                                \ Defines the function keys.
  MAIN.MENU                                \ Displays the selection menu.
  INTERPRET.KEYS
;

-----
: ACQUIRE.DATA                            \ Starts the program once it has been loaded.
  CLEAR.FUNCTION.KEYS
  GRAPHICS.DISPLAY
  BANNER
  " TIME (sec) XLBL " :=
  " COUNTS YLBL " :=
  CAP.REQ @ [ 1 ] ENTER[ 0 , 0 , 1500 , 8200 ]
  7 2 FLX.FORMAT
  MAIN.PROGRAM
;

```

## Appendix C

### Segment Analysis Program

#### \ SEGMENT ANALYSIS PROGRAM

\ Program name: SEGMENT.ASY (ASYST Version 2.0)  
\ Directory: ASYST2

\ This program is a semi-automated procedure for determining the absorbances of the chloroform segments in chloroform/water segmented flow as measured using the on-tube photometric detector. The data files used herein must have been collected using the program DATACQ.ASY in order to be correctly formatted.

\ The program was tested against manual determinations of the segment absorbances. The standard deviations of each segment absorbance is printed out with the mean absorbance, and can be used as a check that the plateau absorbance was correctly determined. About 5% of the time the program will fail to properly identify the organic from the aqueous segment absorbances. In these case the array SEGMENT.MEANS must be printed out and the organic absorbances manually identified.

\ Written by: C. Lucy, 27 May 1987.  
\ ( This program is based on XYDPP.DMO shown in the ASYST  
\ Module 1 manual, pg. I-20-16 to I-20-23. )

---

#### \ Program Structure

\ This program is designed to be menu driven. Some manual operations are required in order to extract the organic segment absorbances from the on-tube detector signal.

#### \ Main Menu

- \ F1) Quit - exits operation from the acquisition program and from ASYST.
- \ F2) Plot transmittance - plots the raw data as collected by the on-tube detector. The vertical axis is auto-scaled to the signal intensity.
- \ F3) Plot absorbance - plots the absorbance as calculated using CALC.ABSORBANCE. The vertical scale must be set manually. Note, if the maximum is set too low the data is truncated at this point and the absorbances will have to be recalculated.
- \ F4) Read file - retrieves data from disk (default drive is C (Hard Disk)). The data must be in the correct format (i.e. that set by DATACQ.ASY).
- \ F5) Save file - stores the data. The filename should include the extension ".DAT".
- \ F6) Calc absorbance - allows you to manually identify the 100% transmittance and this is used to calculate the absorbances.

\ F7) Measure segments determines the mean absorbance of all the segments and then  
 \ prints out those corresponding to the organic segments.  
 \ Uses the spikes caused by the segment ends to identify the  
 \ start of a segment. The number of such spikes must be  
 \ specified (Does not have to be exact, but must err on the high  
 \ side.) Memory limitations restrict this programs to files  
 \ containing less than 60 spikes. Note the chloroform segments  
 \ are identified on the basis of its lower background absorbance

\ F8) Print screen - reproduces the contents on the screen on the printer.

\ -----  
 \ Variable declarations

INTEGER SCALAR MAXSETS

SCALAR MAX.IN.SET

SCALAR #SETS

SCALAR FIRST#

\ First data point of the peak.

SCALAR LAST#

\ Last data point of the peak.

SCALAR #SPIKES

\ Max no.of meniscus spikes in data set

SCALAR AVG.DELAY

\ Delay after spike before avg started

SCALAR #POINTS

\ Number of points averaged on plateau

SCALAR SEG.NUM

\ Counter for segments in array

SCALAR INITIAL

\ Marker for first organic segment

2056 MAXSETS :=

\ Either of these lines may be changed

3 MAX.IN.SET :=

\ to allow larger data sets to be used.

DIM[ 2 ] ARRAY HOLDIT

\ Output buffer for #SETS & MAX.IN.SETS

DIM[ 60 ] ARRAY MAXIMA.LOCATION

REAL SCALAR 100%T.MEAN

SCALAR PLOT.MAX

\*SCALAR SEG.TOTAL

DIM[ MAXSETS , MAX.IN.SET ] ARRAY PEAK.DATA \ Peak data buffer

DIM[ 60 ] ARRAY MAXIMA.INTENSITY

DIM[ 60 ] ARRAY SEGMENT.MEANS

\ Array of segment absorbances

DIM[ 60 ] ARRAY STD.DEV.SEGMENTS

\ Std. dev. of segment absorbances

DIM[ 4 ] ARRAY LIN.REG.X

DIM[ 4 ] ARRAY LIN.REG.Y

25 STRING OP.NAME

\ Operator's name.

25 STRING TITLE

\ Experiment title.

25 STRING EXP#

\ Experiment number.

25 STRING XLBL

\ X-axis label

10 STRING YLBL

\ Y-axis label

14 STRING FILENAME

1 STRING Y/N

\ -----

## **\ Window definitions**

230

**\ Divides the screen into small windows in which the plot and menus are presented.**

0 0 0 79	WINDOW (TOPLINE)	\ Top banner line across screen.
20 0 21 79	WINDOW (SPLIT2)	\ Middle window for menus.
24 0 24 79	WINDOW (BOTLINE)	\ Bottom line of screen for prompt.
1 0 24 79	WINDOW (DEF-1)	\ Excludes top banner line.

---

**: DATA.VU**                    \ Defines plotting parameters for graph..

.000 .200	VUPORT.ORIG	\ Defines the position and
1.00 .750	VUPORT.SIZE	\ size of the plot window.
HORIZONTAL	AXIS.FIT.OFF GRID.OFF	\ Removes the grids from
VERTICAL	AXIS.FIT.OFF GRID.OFF	\ the graph.
.130 .180	AXIS.ORIG	\ Sets the graph position and
.880 .820	AXIS.SIZE	\ size within the window.
.025 .008	TICK.SIZE	
.5 .8	TICK.JUST	

---

## **\ Screen Messages**

**: BANNER**                    \ Program banner

(TOPLINE)	SCREEN.CLEAR	
25 SPACES	.	" Segment Analysis Program"

;

**: SHOW.FILENAME**            \ Places the current filename in the top line on the screen.

(TOPLINE)	SCREEN.CLEAR	
35 SPACES	FILENAME	"TYPE

;

**: PROMPT**                    \ Prompt on bottom line while menu is displayed.

(BOTLINE)	SCREEN.CLEAR	.	" Your choice please "
-----------	--------------	---	------------------------

;

**: WAIT**                    \ Message that the computer is performing calculations

(BOTLINE)	SCREEN.CLEAR	.	" Please wait "
-----------	--------------	---	-----------------

;

---



```

: MAIN.MENU          \ Menu of function keys available in this program.
  (SPLIT2) HOME SCREEN.CLEAR
  ." F1)Quit      F2)Plot transmittance F3)Plot absorbance F4)Read file "
  CR
  ." F5) Save file F6)Calc absorbance F7)Measure segments F8)Print screen"
  PROMPT
  CURSOR.OFF
;

```

### Data Plotting functions

```

: DATA.VU.SET        \ Sets the axis range of the plot
  PEAK.DATA XSECT[ 1 ] SUB[ 1 , #SETS ]
  SWAP
  OVER OVER WORLD.COORDS
  []MIN/MAX DUP
  100 < IF
    DROP
    (BOTLINE) SCREEN.CLEAR HOME
    ." What is the max. absorbance of this plot?" #INPUT
    PLOT.MAX :=
    PLOT.MAX
    WAIT
    \ Cryptic check on if the data is
    \ absorbance or transmittance.
    \ Note: If this maximum is set to
    \ the data is truncated at this level.
  THEN
  VERTICAL WORLD.SET
  []MIN/MAX HORIZONTAL WORLD.SET
  []MIN SWAP []MIN SWAP WORLD.COORDS AXIS.POINT
;

```

```

: LABEL.PLOT          \ Positioning the x and y labels for the plot axes.
  NORMAL.COORDS
  .0250 .80 POSITION 270 LABEL.DIR
  YLBL LABEL
  XLBL "LEN 2. /
  .0175 * .5 SWAP -
  .05 POSITION 0 LABEL.DIR
  LABEL
  CURSOR.OFF
  \ Positioning the y label
  \ Writing the y label
  \ 1/2 the number of XLBL sets
  \ the position of the y-label
  \ Writing the x label
;

```

```

: TRANSMITTANCE.PLOT  \ Plots the raw transmittance data
  WAIT
  " COUNTS" YLBL ":="
  DATA.VU
  VUPORT.CLEAR
  PEAK.DATA XSECT[ 2 ] SUB[ 1 , #SETS ]
  DATA.VU.SET
  XY.AXIS.PLOT
  PEAK.DATA XSECT[ 1 ] SUB[ 1 , #SETS ]
  \ Setting up the
  \ axes of the graph.
  \

```

```

PEAK.DATA XSECT[ 2 ] SUB[ 1 , #SETS ] \Plotting the data
XY.DATA.PLOT
LABEL.PLOT
OUTLINE
PROMPT
;

```

```

: ABSORBANCE.PLOT \Plots the absorbances as calculated by CALC.ABSORBANCE
  WAIT
  "ABSORBANCE" YLBL ":="
  DATA.VU
  VU.PORT.CLEAR
  PEAK.DATA XSECT[ 3 ] SUB[ 1 , #SETS ]
  DATA.VU.SET
  #SETS 1 + 1 DO
    PLOT.MAX PEAK.DATA XSECT[ 3 ] [ 1 ] < IF
      PLOT.MAX PEAK.DATA XSECT[ 3 ] [ 1 ] :=
    THEN
  LOOP
  XY.AXIS.PLOT
  PEAK.DATA XSECT[ 1 ] SUB[ 1 , #SETS ]
  PEAK.DATA XSECT[ 3 ] SUB[ 1 , #SETS ]
  XY.DATA.PLOT
  LABEL.PLOT
  OUTLINE
  PROMPT
;

```

```

: PRINT.SCREEN \Dumps a copy of whatever is on screen to the printer
  {BOTLINE} SCREEN.CLEAR
  {SPLIT2} SCREEN.CLEAR
  ." <cr> if plot is on the screen and the printer is ready ..." BELL CR
  ." (Any other key aborts) "
  KEY 13 <
  IF
    MAIN.MENU
  ELSE
    {SPLIT2} SCREEN.CLEAR
    SCREEN.PRINT
    CONSOLE
    CR ." Press any key to continue. "
    PCKEY ?DROP DROP
    {DEF-1} SCREEN.CLEAR
    MAIN.MENU
  THEN
;

```

---

\Saving the data in memory.

233

```
: WRITE.FILE                                \Default drive for data storage is C (Hard Drive)
  FILE.TEMPLATE
    5 COMMENTS
    INTEGER DIM[ 2 ] SUBFILE                \
    REAL DIM[ #SETS ] SUBFILE              \Defines the format of
    REAL DIM[ #SETS ] SUBFILE              \ the data file.
    REAL DIM[ #SETS ] SUBFILE              \
    REAL DIM[ #SETS ] SUBFILE              \
  END
  HOME
  ." Opening file " FILENAME " TYPE
  13 EMIT FILENAME DEFER> FILE.CREATE
  ." Writing file " FILENAME " TYPE
  13 EMIT FILENAME DEFER> FILE.OPEN
  TITLE      1 >COMMENT                    \
  OP.NAME 2   >COMMENT                    \ Outputs the variables to the
  EXP#      3 >COMMENT                    \ appropriate positions in
  XLBL      4 >COMMENT                    \ the data file.
  YLBL      5 >COMMENT                    \
  #SETS HOLDIT [ 1 ] :=
  MAX.IN.SET HOLDIT [ 2 ] :=
  1 SUBFILE HOLDIT ARRAY>FILE
  2 SUBFILE PEAK.DATA XSECT[ 1 ] SUB[ 1 , #SETS ] ARRAY>FILE
  3 SUBFILE PEAK.DATA XSECT[ 2 ] SUB[ 1 , #SETS ] ARRAY>FILE
  4 SUBFILE PEAK.DATA XSECT[ 3 ] SUB[ 1 , #SETS ] ARRAY>FILE
  FILE.CLOSE

  ONERR:                                     \Error trap
    ." Can't open file for writing. "
    ." Type any key to continue." BELL KEY DROP
    ?FILE.OPEN IF FILE.CLOSE THEN
;

: GET.FILENAME                                \Requests name for the data file.
  (SPLIT2) SCREEN.CLEAR
  ." Filename please ? " INPUT
  FILENAME ":="
  SCREEN.CLEAR
;

: OUTPUT.DATA.FILE                            \Invokes the words above to save the data.
  #SETS 0 >
  IF
    SCREEN.CLEAR
    (SPLIT2) SCREEN.CLEAR ." Output "
    GET.FILENAME
    WRITE.FILE
    MAIN.MENU
  THEN
;
;
```

**: READ.FILE** \Retrieves a data file from disk storage (drive C is default)

```
{SPLIT2} SCREEN.CLEAR
." Reading " FILENAME DEFER> FILE.OPEN
FILENAME "TYPE 13 EMIT
1 COMMENT> TITLE ":=
2 COMMENT> OP.NAME ":=
3 COMMENT> EXP# ":=
4 COMMENT> XLBL ":=
5 COMMENT> YLBL ":=
1 SUBFILE HOLDIT FILE>ARRAY
HOLDIT [ 1 ] #SETS :=
HOLDIT [ 2 ] MAX.IN.SET :=
2 SUBFILE PEAK.DATA XSECT[ 1 ] SUB[ 1 , #SETS ] FILE>ARRAY
3 SUBFILE PEAK.DATA XSECT[ 2 ] SUB[ 1 , #SETS ] FILE>ARRAY
4 SUBFILE PEAK.DATA XSECT[ 3 ] SUB[ 1 , #SETS ] FILE>ARRAY
FILE.CLOSE
SHOW.FILENAME
```

\ Assign values from the  
data file to the  
various variables.

ONERR: \Error trap  
." Can't open file for writing. "  
." Type any key to continue." BELL KEY DROP  
?FILE.OPEN IF FILE.CLOSE THEN

**: INPUT.DATA.FILE** \ Uses the words above to request and retrieve a file

```
{DEF-1} SCREEN.CLEAR
GET.FILENAME
READ.FILE
MAIN.MENU
```

**: CALC.ABSORBANCE** \ Calculates absorbance using:  $A = \log \frac{100\%T}{\%T}$   
\ i.e. assumes no dark current.

```
{DEF-1} SCREEN.CLEAR
PEAK.DATA XSECT[ 2 ] SUB[ 1 , 100 ]
ARRAY.EDIT
{SPLIT2} SCREEN.CLEAR HOME
." First index of 100% transmittance? "
#INPUT FIRST# := CR
." Last index of 100% transmittance? "
#INPUT FIRST# - 1 + LAST# :=
PEAK.DATA XSECT[ 2 ] SUB[ FIRST# , LAST# ]
MEAN 100%T.MEAN :=
```

\ The first 100 transmittance  
points are displayed for  
manual identification of  
an organic plateau as the  
100% transmittance.

```

WAIT
STACK.CLEAR
100%T.MEAN PEAK.DATA XSECT[ 2 ] SUB[ 1 , #SETS ] .1 + / \ Calculating
LOG \ absorbance
PEAK.DATA XSECT[ 3 ] SUB[ 1 , #SETS ] := \ using above
\ equation.

GRAPHICS.DISPLAY
SHOW.FILENAME
MAIN.MENU

```

```

: MEAS.SEGMENTS \ Semi-automatic method for measuring the organic
\ segment absorbance. Tested against manual procedure.
\ Note: About 5% of the runs will not correctly identify all
\ of the organic segments as a result of a double spike due
\ to a single meniscus. In these cases you must print out
\ the array SEGMENT.MEANS and total the absorbances
\ manually.

0 SEGMENT.MEANS :=
0 STD.DEV.SEGMENTS :=
{SPLIT2} SCREEN.CLEAR HOME
." What is the maximum number of interface spikes in the data ? " #INPUT
#SPIKES := \ Note: insufficient memory for > 60
#SPIKES SET.#.OPTIMA \ Sets up conditions for the search for
3 SET.#.POINTS \ the spikes caused by the meniscus
SCREEN.CLEAR \ passing through the detector.
." Delay how many points after maximum before averaging ? " #INPUT
AVG.DELAY := \ i.e. how many points after spike
SCREEN.CLEAR \ before the plateau starts
WAIT
PEAK.DATA XSECT[ 3 ] SUB[ 1 , #SETS ] \ Search for the spikes in the
LOCAL.MAXIMA \ absorbance signal.
MAXIMA.INTENSITY SUB[ 1 , #SPIKES ] := \ Stores the intensity and
MAXIMA.LOCATION SUB[ 1 , #SPIKES ] := \ the location of the spikes
MAXIMA.LOCATION DUP [ 2 ] SWAP [ 1 ] -
.6 * #POINTS := \ Sets the number of points in plateau to be averaged.
\ Note: may have to be changed for different experimental conditions.
0 SEG.NUM :=
#SPIKES 1 + 1 DO \ Starts calculation of absorbance of all segments (org & aq)
MAXIMA.INTENSITY [ 1 ] .3 >
MAXIMA.LOCATION [ 1 ] #SETS #POINTS 4 + - < AND IF
SEG.NUM 1 + SEG.NUM :=
PEAK.DATA XSECT[ 3 ] SUB[ MAXIMA.LOCATION [ 1 ]
AVG.DELAY + , #POINTS ]
DUP
MEAN SEGMENT.MEANS [ SEG.NUM ] :=
SAMPLE.VARIANCE SQRT STD.DEV.SEGMENTS [ SEG.NUM ] :=
THEN
LOOP

```

```

1 INITIAL :=
SEGMENT.MEANS [ 1 ] .02 > IF
2 INITIAL :=
THEN
SEGMENT.MEANS [ SEG.NUM ] .02 > IF
SEG.NUM 1 - SEG.NUM :=
THEN
LIN.REG.X @[ 1 ] ENTER[ INITIAL , INITIAL
SEG.NUM 2 - , SEG.NUM ]
SEGMENT.MEANS SUB[ INITIAL , 2 , 2 ]
LIN.REG.Y SUB[ 1 , 2 ] :=
SEGMENT.MEANS SUB[ SEG.NUM 2 - , 2 , 2 ]
LIN.REG.Y SUB[ 3 , 2 ] :=
LIN.REG.X LIN.REG.Y 1 LEASTSQ.POLY.FIT
DUP
SEG.NUM REAL RAMP SWAP [ 1 ] *
SWAP [ 2 ] +
SEGMENT.MEANS SUB[ 1 , SEG.NUM ] SWAP -
SEGMENT.MEANS SUB[ 1 , SEG.NUM ] :=
0 SEG.TOTAL :=
{DEF-1} SCREEN.CLEAR OUT>PRINTER. CR CR CR
." File: " EXP# "TYPE CR CR
." Seg mean Std. Dev."
CR CR
6 4 FIX.FORMAT
SEG.NUM 1 + INITIAL DO
STD.DEV.SEGMENTS [ 1 ]
SEGMENT.MEANS [ 1 ] DUP
SEG.TOTAL + SEG.TOTAL :=
. 5 SPACES . CR
2 +LOOP
." Total = " SEG.TOTAL .
CR CR
CONSOLE
-1 3 SCI.FORMAT
CR ." Press any key to continue."
KEY DROP
{DEF-1} SCREEN.CLEAR
MAIN.MENU

```

\ Figuring out if the first absorbance  
 \ is an organic or aqueous segment.  
 \ Based on higher background  
 \ absorbance of aqueous phase.  
 \ Take every second  
 \ absorbance after  
 \ the first organic  
 \ Use first and last 3  
 \ organic segments  
 \ for linear regression  
 \ determination of  
 \ organic baseline.  
 \ Subtract the  
 \ background abs  
 \ and print out the  
 \ absorbances and  
 \ associated std.dev.  
 \ Std. dev. can be used as a check that the  
 \ segment absorbance was correctly measured.  
 \ Printing out the mean  
 \ and standard deviation  
 \ of the organic segments  
 \ Also calculate overall total  
 \ organic absorbance.

---

```

: PEAK.QUIT

```

\ Command which quits application of this program.

```

SCREEN.CLEAR
{SPLIT2} SCREEN.CLEAR BELL ." Quit ?"
KEY 89 = IF
BYE
THEN
MAIN.MENU

```

\ Checks if answer is "Y"

---

**: MAIN.KEYS**                      \Sets up function keys for MAIN.PROGRAM.

237

F1 FUNCTION.KEY.DOES PEAK.QUIT  
F2 FUNCTION.KEY.DOES TRANSMITTANCE.PLOT  
F3 FUNCTION.KEY.DOES ABSORBANCE.PLOT  
F4 FUNCTION.KEY.DOES INPUT.DATA.FILE  
F5 FUNCTION.KEY.DOES OUTPUT.DATA.FILE  
F6 FUNCTION.KEY.DOES CALC.ABSORBANCE  
F7 FUNCTION.KEY.DOES MEAS.SEGMENTS  
F8 FUNCTION.KEY.DOES PRINT.SCREEN  
F9 FUNCTION.KEY.DOES NOP  
F10 FUNCTION.KEY.DOES NOP

;

**: MAIN.PROGRAM**

MAIN.KEYS  
MAIN.MENU  
INTERPRET.KEYS

\Defines the function keys.  
\Displays the selection menu.

;

**: INIT**

\Starts the program.

CLEAR.FUNCTION.KEYS  
GRAPHICS.DISPLAY  
BANNER  
-1 3 SCI.FORMAT  
CURSOR.OFF  
MAIN.PROGRAM

;

## APPENDIX D

### Nonsteady State Extraction

It must be kept in mind during this discussion that the terms "steady state" and "nonsteady state" used herein refer to the mass transfer processes, and so are dependent on the form of the concentration gradients at the interface. Thus these terms do not have the meaning typically applied to them in discussions of chemical kinetics.

In order to treat the time lag and the accelerated extraction which occur due to the nonsteady state extraction, the related case of nonsteady state diffusion through a plane sheet will be discussed here. The sheet has a finite thickness,  $l$ . If one face,  $x=0$ , of the sheet is kept at a constant concentration,  $C_1$ , and the other face, at  $x=l$ , is at a different concentration,  $C_2$ , and the sheet is initially at a uniform concentration  $C_0$ , there is a finite interval of time before the steady-state condition (i.e. linear concentration gradient across the sheet) is established. The total amount of diffusing material  $Q_t$  which has passed through the sheet in time  $t$  is given by [158]:

$$Q_t = D_m(C_1 - C_2)\frac{t}{l} + \frac{2l}{\pi^2} \sum_{n=1}^{\infty} \frac{C_1 \cos n\pi - C_2}{n^2} \left\{ 1 - \exp\left(-D_m n^2 \pi^2 t / l^2\right) \right\} + \frac{4C_0 l}{\pi^2} \sum_{m=0}^{\infty} \frac{1}{(2m+1)^2} \left\{ 1 - \exp\left(-D_m (2m+1)^2 \pi^2 t / l^2\right) \right\} \quad (D.1)$$

where  $D_m$  is the diffusion coefficient of the substance and  $l$  is the characteristic length over which diffusion must occur, the thickness of the sheet in this case.

A solvent extraction process can be viewed most simply using the Whitman two film theory [141,142,144]. In a typical extraction, the solute is either injected into or formed within the bulk aqueous phase ( $C_1$ ), diffuses through the Nernst film whose initial concentration is zero ( $C_0=0$ ), and is then extracted into the organic phase, which for a quantitative extraction process will act as an infinite sink ( $C_2=0$ ). Under these conditions



equation D.1, written in terms of the dimensionless parameters  $Q_t/C_1l$  and  $D_mt/l^2$ , for the total amount of diffusing substance and time respectively, reduces to [158]:

$$\frac{Q_t}{C_1l} = \frac{D_mt}{l^2} - \frac{1}{6} - \frac{2}{\pi^2} \sum_{n=1}^{\infty} \frac{(-1)^n}{n^2} \exp\left(-n^2 \pi^2 \left(\frac{D_mt}{l^2}\right)\right) \quad (D.2)$$

which as  $t \rightarrow \infty$ , approaches the line [158]:

$$\frac{Q_t}{C_1l} = \frac{D_mt}{l^2} - \frac{1}{6} \quad (D.3)$$

which is the expression for the steady state approximation for the nonsteady state behavior.

In the experimental arrangement considered in Chapter 5, the concentration of iodine is initially the same in the bulk aqueous phase and in the Nernst film ( $C_0 = C_1$ ), since the reactants have had sufficient time to diffuse into this film before the iodine formation reaction occurs. As in the extraction case discussed above  $C_2$  is effectively zero since the organic phase acts as a "sink" for the extracted material (Section 4.2.2). For this case the expression is:

$$\begin{aligned} \frac{Q_t}{C_1l} = & \frac{D_mt}{l^2} + \frac{1}{3} - \frac{2}{\pi^2} \sum_{n=1}^{\infty} \frac{(-1)^n}{n^2} \exp\left(-n^2 \pi^2 \left(\frac{D_mt}{l^2}\right)\right) \\ & + \frac{4}{\pi^2} \sum_{m=0}^{\infty} \frac{1}{(2m+1)^2} \exp\left(-(2m+1)^2 \pi^2 \left(\frac{D_mt}{l^2}\right)\right) \end{aligned} \quad (D.4)$$

which as  $t \rightarrow \infty$ , yields the steady state approximation:

$$\frac{Q_t}{C_1l} = \frac{D_mt}{l^2} + \frac{1}{3} \quad (D.5)$$

A graph of  $Q_t/C_1l$  as a function of  $D_mt/l^2$  is shown in Figure D-1 for the case of  $C_0=C_2=0$  (equations D.2 and D.3) and for the case of  $C_0 = C_1$  and  $C_2 = 0$  (equations D.4

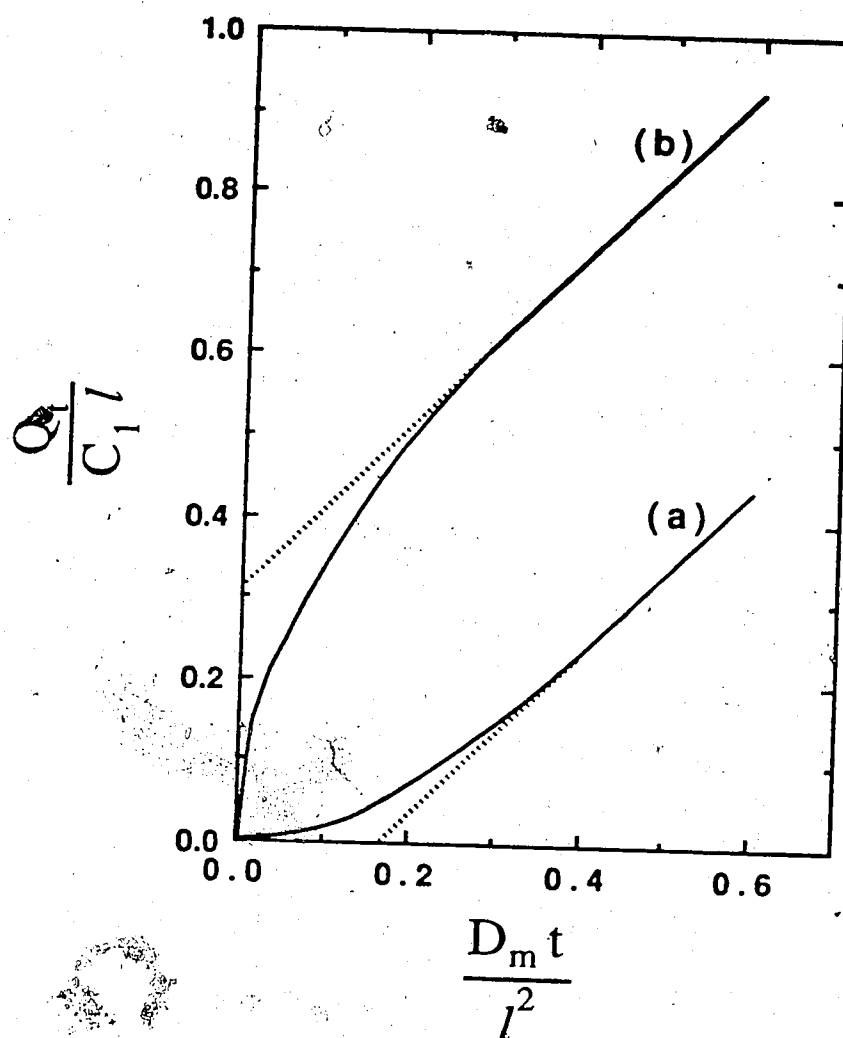


**Figure D-1** Approach to steady state diffusion through a plane sheet for the case when: (a) the initial concentration with the sheet is zero ( $C_0 = 0$ ) and (b) the initial concentration of the sheet is equal to that in one of the phases ( $C_0 = C_1$ ). These cases are plotted in terms of the dimensionless parameters  $Q_t/C_1 l$  and  $D_m t/l^2$ , for the amount of material which has passed through the sheet and the time, respectively. The solid lines reflect the true diffusion behavior and the dotted lines are the steady state approximation to this behavior.

and D.5). To within the accuracy of plotting the steady state in both cases is achieved by  $D_m t/l^2 \approx 0.4$ . At greater times than this the use of the steady state approximation accurately predicts the diffusion behavior.

In extraction studies involving a lag time[140,157], the steady state approximation has been successfully applied to the extraction data after the initial period. Thus in this work it would be appropriate to use the steady state approximation to the data collected after the initial period of rapid extraction due to the nonsteady state conditions.